

FACILITY FORM 602

N69-32694

(ACCESSION NUMBER)

(PAGES)

CR-101840

(NASA CR OR TMX OR AD NUMBER)

(THRU)

(CODE)

(CATEGORY)

DAC-63364

# RADIOISOTOPE HEATER DEVELOPMENT PROGRAM

## FINAL REPORT

by  
M. W. HULIN

**CASE FILE  
COPY**

Prepared under Contract No. NAS 9-8846

by

Donald W. Douglas Laboratories, Richland, Washington  
McDonnell Douglas Astronautics Company—Western Division

for

NATIONAL AERONAUTICS AND SPACE ADMINISTRATION

# **RADIOISOTOPE HEATER DEVELOPMENT PROGRAM**

## **FINAL REPORT**

by  
M. W. HULIN

DISTRIBUTION OF THIS REPORT IS PROVIDED IN THE INTEREST OF  
INFORMATION EXCHANGE. RESPONSIBILITY FOR THE CONTENTS  
RESIDES IN THE AUTHOR OR ORGANIZATION THAT PREPARED IT.

Prepared under Contract No. NAS 9-8846

by

Donald W. Douglas Laboratories, Richland, Washington  
McDonnell Douglas Astronautics Company—Western Division

for

NATIONAL AERONAUTICS AND SPACE ADMINISTRATION



## CONTENTS

FIGURES	vii
TABLES	x
SUMMARY	1
INTRODUCTION	2
Background	2
Program Objectives	3
Safety and Design Criteria	4
Program Approach	5
Program Results	6
SYMBOLS	8
THE USE OF THERMAL HEATERS IN MANNED SPACECRAFT APPLICATIONS	11
Approach	11
The survey	11
Evaluation	11
Conclusions	20
SAFETY AND DESIGN ANALYSIS	20
Safety Approach	20
Safety criteria	21
Mission profile and failure modes	23
Design criteria	23
Selected heater materials	23
Shape and size tradeoffs, and heater nomenclature	26
Reference designs and fabrication details	34
Reference heater mounting design	45
Cost and weight optimization	45
Design approach and tradeoff study summary and recommendations	48
Ablator Design Analysis	49
Ablator degradation in normal operation	49
Aerothermal analysis	50
Structural Analysis	63
Pressure vessel analysis	63
Impact	66
Ocean burial considerations	66
Oxidation and sea water corrosion	67



Shielding and Dose Rate Analysis	67
<sup>238</sup> Pu heater dose rates	67
<sup>147</sup> Pm heater dose rates	68
Accident and Failure Analysis	71
Launch pad explosion and fire	71
Failure modes	77
Secondary failure modes	77
Probabilistic methods	78
Radiological Consequences and Hazards	78
Release to the upper atmosphere	79
Release in a launch abort -- the maximum credible accident	80
Fresh water contamination	82
Ocean water contamination	82
HEATER MATERIALS SELECTION	85
Radioisotope Fuels	85
Primary Containment Vessel	87
Energy Absorbent Layer	88
Structural Container - Pressure Vessel <sup>238</sup> PuO <sub>2</sub>	88
Structural Container for Pm <sub>2</sub> O <sub>3</sub>	90
Oxidation Barrier	91
Thermal Insulation Layer	91
Ablator Material	91
Kinetics of Helium Release from the Plutonia Fuel Structure	93
Bibliography	96
THERMAL CONTROL OF ALSEP MISSION COMPONENTS	96
System Requirements	96
Battery Thermal Control	96
Design description	97
Lunar night operation	98
Lunar day operation	100
Self-regulating heat pipe design	101
Meeting other mission requirements	101
Central Station Thermal Control	102
Design description	103
Lunar night operation	103
Lunar day operation	105
Self-regulating heat pipe design	106
Meeting other mission requirements	106
Thermal Control Summary and Weights	106
Selection of Radioisotope Heaters	108
Battery	108
Central station	108
MANUFACTURING PROCESSES AND QUALITY ASSURANCE	108
Approach	110
Quality program	110
Quality Program Plan	110
Design and Development	113
Drawing and specification review	113
Inspection and test methods	113

Qualification testing	113
Identification and Traceability	115
Control of DWDL-Procured Material	115
Selection of procurement sources	115
Vendor source inspection	115
Receiving inspection	116
Control of Government-Furnished Material	116
Receiving	116
Storage	116
Nuclear materials control	116
Control of DWDL-Fabricated Articles	117
Nonconforming Material	117
Inspection, Measurement, and Test Equipment	117
Inspection Stamps	118
Preservation, Packaging, Handling, Storage, and Shipping	118
Training and Certification of Personnel	118
Data Reporting and Corrective Action	118
Program Documentation and Reporting	119
Manufacturing and Inspection Methods	119
 PROGRAM PLANS AND BUDGETARY COST ESTIMATES	 120
Final Detailed Design and Safety Analysis	120
Manufacturing Processes and Inspection Techniques	121
Prototype Hardware Development and Development Tests	123
General	125
Hardware tests	125
Fabrication of Test Hardware	127
Manufacture of Flight-Type Heaters	128
Documentation and Licensing	128
Qualification and Acceptance Test Programs	129
Test summary	129
Safety Analysis Report	133
Program Management and Reports	133
Reports	133
Program Plans and Schedule	134
Recommended program and options	134
Program schedule and milestones	135
Program option budgetary costs	135
 SAFETY ANALYSIS REPORT	 137
 CONCLUSIONS AND RECOMMENDATIONS	 143
Areas Requiring Additional Analyses or Tests	144
Recommendations	145
 Appendix A - HEATER DESIGN EVOLUTION	 147
 Appendix B - DRAG COEFFICIENT SUMMARY	 157
Flat-Faced Cylinder and Rounded-End Cylinder	157
Cube or Rectangular Parallelepiped	163

Appendix C - REENTRY MODEL	165
Appendix D - THERMAL ANALYSIS MODELS	167
Thermal Analyzer Program (TAP-3)	167
Charring Ablator Code, STAB 2	168
Heater Model Used for Side-On Spinning Orientation	168
Heater Model Used for Side-On Nonspinning Orientation	169
Heater Model Used for End-On Orientation	169
Heater Model Used for Charring Ablator Analysis	171
Appendix E - IMPACT STUDIES	173
Appendix F - NEUTRON AND PHOTON SPECTRA	179
Appendix G - STATISTICAL PROCEDURE	183
Appendix H - SMALL PARTICLE FALLOUT	189
Appendix I - GROUND RELEASE ANALYSIS	193
Appendix J - CALCULATION OF MAXIMUM PERMISSIBLE CONCENTRATIONS AND ISOTOPE DISPERSION IN SEAWATER	197
REFERENCES	203
BIBLIOGRAPHY	211

## FIGURES

1	Typical Reference Heater Design	3
2	Phase 1 Program Tasks	7
3	Mission Profile for Nuclear Safety and Accountability	24
4	PMC-10-2S $^{147}\text{Pm}_2\text{O}_3$ Cermet Spherical 10-W Capsule with Cubic or Cylindrical Ablator	32
5	PMC-50-2S $^{147}\text{Pm}_2\text{O}_3$ Cermet Spherical 50-W Capsule with Cubic or Cylindrical Ablator	32
6	PUC-10-4 Nominal 10-W $^{238}\text{PuO}_2$ Heater	34
7	PUC-50-4 Nominal 50-W $^{238}\text{PuO}_2$ Heater	35
8	PMC-10-2 Nominal 10-W $^{147}\text{Pm}_2\text{O}_3$ Heater	36
9	PMC-50-2 Nominal 50-W $^{147}\text{Pm}_2\text{O}_3$ Heater	37
10	PMC-5-1 Nominal 5-W. $^{147}\text{Pm}_2\text{O}_3$	38
11	PUC-5-1 Nominal 5-W $^{238}\text{PuO}_2$ Heater	39
12	PUM-10-4 Nominal 10-W $^{238}\text{PuO}_2$ Bare Microsphere	39
13	PUM-50-4 Nominal 50-W $^{238}\text{PuO}_2$ Bare Microspheres	40
14	PMC-25-1 Nominal 25-W $^{147}\text{Pm}_2\text{O}_3$ Heater	40
15	PUC-25-1 Nominal 25-W $^{238}\text{PuO}_2$ Heater	41
16	PUC-10-3 Nominal 10-W $^{238}\text{PuO}_2$ Heater	41
17	PUC-50-3 Nominal 50-W $^{238}\text{PuO}_2$ Heater	42
18	PMC-50-1S 50-W Spherical Pm Heater (WT $\cong$ 2.56 LB)	42
19	Stacked Capsule Concept	43
20	50-W Unitized Pm Heater (W $\cong$ 2.82 LB)	43
21	PUC-50-2S Spheroidal Concept 50-W $^{238}\text{PuO}_2$ Cermet	44
22	Representative Support for 50-W Heater	46
23	Heater Weight Vs Power Comparison	47
24	Earth Orbital Decay Integrated Heating for Different Designs	56
25	Cold-Wall Heating and Ablation at the Stagnation Point for 50-W Reference Design, Side-On Nonspinning on Lunar Return (For spinning capsule, multiply by 0.36)	56
26	Temperature Response of 50-W $^{147}\text{Pm}$ Heater, Reference Design Earth Orbital Decay, End-On	58
27	Temperature Response of 50-W $^{147}\text{Pm}$ Heater, Reference Design, Earth Orbital Decay, Side-On Spinning	59
28	Temperature Response of 50-W $^{147}\text{Pm}$ Heater, Reference Configuration with Charring Ablator Earth Orbital Decay, Side-On Nonspinning	59
29	Temperature Response of 10-W $^{147}\text{Pm}$ Heater, Reference Design, Earth Orbital Decay, Side-On Spinning	60
30	Temperature Response of 50-W $^{147}\text{Pm}$ Reference Heater 6-1/4° Lunar Return, Side-On Spinning	60
31	Temperature Response of 50-W $^{147}\text{Pm}$ Heater, Reference Design, 90° Lunar Return, Side-On Nonspinning	61
32	$^{238}\text{Pu}$ Dose Rates	69

33	<sup>147</sup> Pm Dose Rates	69
34	<sup>147</sup> Pm Heater Dose Rate Vs T-III Shield Thickness	70
35	<sup>147</sup> Pm Heater Dose Rate Vs Hastelloy-X Shield Thickness	70
36	Launch Pad Abort Thermal Environment	72
37	Launch Pad Abort Thermal Response	74
38	Launch Pad Debris Model	76
39	Maximum Credible Accident, 50-W Pu and Pm Heaters	81
40	Cumulative Fraction of Land Area in the United States Occupied by Open-Type Reservoirs of Capacity N or less	83
41	Exposure from 50-W Release to Sea Water	83
42	POCO Graphite Specific Heat Vs Temperature	94
43	POCO Graphite Thermal Conductivity Vs Temperature	94
44	Helium Release From Plutonia	95
45	Schematic of Self-Regulating Heat Pipe/Radiator	98
46	Battery Thermal Control Concept	99
47	Laboratory Data for Self-Regulating Heat Pipe	102
48	Central Station Thermal Control Concept	104
49	Manufacturing Program Logic	109
50	Fuel Preparation Flow Diagrams	111
51	Manufacturing Flow Diagram - Promethia- and Plutonia- Fueled Heaters	112
52	Quality Program Flow Chart	114
53	Systems Analysis Block Diagram	122
54	Test Specimen Fabrication and History Chart for Phase II Development Tests	126
55	Phases II and III Task Schedule	136
A-1	<sup>147</sup> Pm <sub>2</sub> O <sub>3</sub> Capsule, Model PMC-10-1	148
A-2	<sup>147</sup> Pm <sub>2</sub> O <sub>3</sub> Capsule, Model PMC-50-1	148
A-3	<sup>238</sup> PuO <sub>2</sub> Bare Microspheres, Model PUM-10-1	149
A-4	<sup>238</sup> PuO <sub>2</sub> Bare Microspheres, Model PUM-50-1	149
A-5	<sup>238</sup> PuO <sub>2</sub> Cermet, Model PUC-10-1	150
A-6	<sup>238</sup> PuO <sub>2</sub> Cermet, Model PUC-50-1	150
A-7	<sup>238</sup> PuO <sub>2</sub> Bare Microspheres, Model PUM-10-2	151
A-8	<sup>238</sup> PuO <sub>2</sub> Bare Microspheres, Model PUM-50-2	151
A-9	<sup>238</sup> PuO <sub>2</sub> Cermet, Model PUC-10-2	152
A-10	<sup>238</sup> PuO <sub>2</sub> Cermet, Model PUC-50-2	152
A-11	<sup>238</sup> PuO <sub>2</sub> Microspheres, Model PUM-10-3	153
A-12	<sup>238</sup> PuO <sub>2</sub> Microspheres, Model PUM-50-3	153
A-13	Spherical Heaters	154
B-1	Comparison of Drag Coefficient of Cylinder for Specular and Diffuse Reflection	158
B-2	Side-On Cylindrical Drag Vs Mach No. in Free-Molecule Flow	158
B-3	Drag Coefficient for a Cylinder in Crossflow Vs Knudsen No.	160
B-4	Transonic Drag Coefficients for Different Shapes	160
B-5	Drag Coefficient for Cylinders and Spheres Function of Reynolds No. at Low Mach Numbers	162
B-6	Drag Coefficients of Spherical Segments	162
D-1	Nodal Network to Simulate Side-On Spinning Orientation	169
D-2	Nodal Network for Side-On Nonspinning Model of 50-W <sup>147</sup> Pm Heater, Reference Design	170



D-3	Nodal Network for End-On Model of 50-W $^{147}\text{Pm}$ Heater, Reference Design	172
E-1	10-Watt Simulated Heater Impact Specimen before Assembly, Showing Graphite Insulator, T-III Shell, Ta Foam, and Bronze Fuel Simulant	175
E-2	Electron Beam Welded T-III 10 Watt Simulated Heater Impact Specimen	175
E-3	Complete Graphite Bonded 10-Watt Simulated Heater Impact Specimen	176
E-4	4-50 Watt and 10-10 Watt Simulated Heater Impact Specimens before Impact	176
E-5	Model 9 after 308 ft/sec Impact against Graphite	177
E-6	Model 6 after 417 ft/sec Impact against Graphite	177
E-7	Longitudinal Section of Model 1 after Successfully Withstanding 420 ft/sec Impact against Granite	178
E-8	Longitudinal Section of Model 8 after 505 ft/sec Impact against Granite (This Model Sustained Intergranular Cracks at the Corners of the Impacted End)	178
G-1	Normal Frequency Distribution for $Q_E$	185
H-1	Deposition Rate Vs Time	190
H-2	Tropospheric Air Concentration from a Megacurie Release to the Lower Polar Stratosphere (No radiological delay)	191
I-1	Isotope Fuel Vapor Pressures	194
I-2	Lung Dose from the Release of $1.43 \times 10^{-5}$ Ci $^{147}\text{Pm}$ Under Various Meteorological Conditions with a 1 m/sec Windspeed	195
I-3	Maximum Dose from Elevated Volume Release	195
J-1	Integrated Exposure from 100% Release to Sea Water of 50 W of Radioisotope	201

## TABLES

1	Summary of Thermal Control Applications	12
2	Heater Thermal Requirements Summary	20
3	Design Criteria	25
4	Density Values for Heater Materials	26
5	PMC Reference Heater Design Summary	28
6	Reference Plutonia Heater Design Summary	30
7	Heater Concept Comparison for Promethium Fuel	31
8	Heater Weights and Reference Designs	47
9	Summary of Mass Losses from Ablators	50
10	Ballistic Coefficient Summary	52
11	Summary of Reentry Quantities for Earth Orbital Decay Trajectories, Flat-Headed Cylindrical Capsule	54
12	Summary of Reentry Quantities for Lunar Return Trajectories, Flat-Headed Cylindrical Capsule	55
13	Alternate A Design Reentry Quantities for -5.2° Lunar Return	57
14	Temperature Results for Alternate Designs	61
15	Summary of Pressure Vessel Analysis Results for Reentry	65
16	Soil Burial Temperatures	66
17	Material Oxidation and Sea Water Corrosion Rates	68
18	Characteristics of Radioisotope Heat Sources	86
19	Fuel Form Comparison	88
20	Physical Properties of Candidate Structural Container Materials	89
21	Properties of Candidate Oxidation Barrier Materials	92
22	POCO Graphite Property Data Vs Temperature	93
23	Thermal Control Summary	107
24	Summary of Development Tests for Phase II	124
25	Summary Qualification Tests	130
26	Acceptance Tests	131
27	Phases II and III Program Milestones	135
28	Safety Analysis Report Outline	138
A-1	Heater Weight Comparison	155
E-1	Simulated Heater Impact Test	174
F-1	Photon Flux 1 Meter From $\text{Pm}^{147}$ Heater	179
F-2	Neutron Flux 1 Meter From $\text{Pu}^{238}$ Heater	180
F-3	Photon Flux 1 Meter From $^{238}\text{Pu}$ (No Aging) Heater	180
F-4	Photon Flux 1 Meter From $^{238}\text{Pu}$ (Aged 6 years) Heater	101
J-1	Adjusted Maximum Permissible Concentrations	200

# RADIOISOTOPE HEATER DEVELOPMENT PROGRAM

## PHASE I STUDY FINAL REPORT (CONTRACT NO. NAS 9-8846)

By M. W. Hulin\*

### SUMMARY

In September 1968, phase I of a three-phase program was undertaken by the Donald W. Douglas Laboratories (DWDL), a directorate of the McDonnell Douglas Astronautics Company-Western Division, to develop a family of small radioisotope heaters for use in manned spacecraft components. The technical portion of this program covered a 5-month period. Primary objectives were to: (1) Identify potential applications for small (1- to 50-W) radioisotope heaters in manned spacecraft systems; (2) develop a heater design that would meet selected safety criteria and have a high probability of being safety- and flight-qualified; (3) develop an optimum group of heaters to meet the requirements of a maximum number of applications and mission times of from 14 days to 5 years; (4) generate program plans and budget estimates for phases II and III of the program.

The study was initiated by conducting a survey of thermal requirements of current and planned manned-spacecraft components. This survey identified applications requiring between 180 and 300 thermal sources ranging in size from less than 1 to over 100 W. Detailed safety and design analyses resulted in a reference heater design that will meet the selected safety criteria and have a high probability of surviving all mission phases, operational environments, and credible accidents. Optimization analysis showed that two heater sizes, 10- and 50-W, and two isotopic fuels, promethia and plutonia, would meet the majority of identified applications and mission requirements. Also, analyses showed that it is more economical to develop uniform-size heaters for promethia and plutonia heaters of the same power level. Although some weight penalty is incurred in this approach, considerable cost savings are realized by significantly reducing the number of development and qualification tests. Based on results of the study, program plans to develop, test, fabricate, and qualify radioisotope heaters were prepared. Thus, all primary objectives were achieved in this study.

---

\*Program Manager, Projects and Systems, Donald W. Douglas Laboratories, Richland, Washington.

It is entirely feasible to develop a group of small radioisotope heaters for a large number of manned spacecraft applications. Completion of a development program will greatly reduce the time between identification of requirements and ultimate mission qualification. Also, development of flight-qualified heaters will allow systems engineers a wider choice of methods of supplying heat to space components.

Because of the favorable results of this study, DWDL recommends that phases II and III of the Radioisotope Heater Development Program be initiated and funded at the level required to produce flight-qualified heaters.

## INTRODUCTION

This final report, cataloged as MDAC Report No. DAC-63364, is submitted to the NASA Manned Spacecraft Center under Contract NAS 9-8846. The report describes technical effort from September 19, 1968 through February 18, 1969. Two important events occurred subsequent to final contract negotiations. An agreement was signed by NASA and AEC providing for technical direction by AEC of tasks 4 through 8 of the phase I study, and phases II and III. Also a NASA/MSC requirement for a radioisotope heater for the ALSEP seismic experimental package was identified. AEC/DID was given responsibility for developing the heater.

Although these events did not materially affect the phase I study, they will have a definite impact on the direction and scope of phases II and III.

## Background

The low-temperature environment in which spacecraft operate creates many heat requirements to keep components operational. In addition, life support system chemical processes need heat for closed-system operation. These requirements are currently met by electric heaters powered by solar or fuel cells; however, a potentially simpler and more reliable way to supply heat is by decay of a radioisotope. Radioisotopes have been used in spacecraft at high power levels to supply electric power, and at very low power levels for instrument dial illumination, but each power source has required an extensive safety qualification program.

Despite the attractiveness of small radioisotope thermal sources, their use has been avoided because of a lack of precise guidelines, and the expectation that an expensive and time-consuming safety test program would be required for each application. As the number, complexity, and duration of missions increase, the advantages of radioisotope sources become significant and point to the need for development of these sources as flight-qualified hardware. This study investigated a program to develop a standardized group of radioisotope heat sources that would minimize development costs and shorten the time needed to achieve the benefits of these devices.

As is current practice, thermal control problems may be solved by use of electric heaters. But there are penalties: increased primary-power requirements and thus system weight; redundant heater design (unless the heater is sufficiently reliable, because heater failure would cause total mission failure); and modification of the power control electronics to accommodate the heater. Use of radioisotope-decay heat reduces or eliminates these penalties, but the offsetting considerations are increased qualification-test costs and demonstration of the heaters' capabilities to meet safety requirements.

### Program Objectives

This report presents the results of phase I of a three-phase program to develop a group of small radioisotope heaters for manned-spacecraft component applications. The results establish the feasibility of developing an optimum group of small (1 - to 50-W) heaters that will meet mission requirements of 14 days to 5 years, with a high probability of surviving all mission phases and environments. Figure 1 shows a typical reference design developed during this study.

Materials specified in figure 1 are the best available from the standpoint of compatibility, availability, and capability to meet all mission and environmental requirements. Selection was based on data available in the literature, personal discussions with cognizant personnel, and detailed analyses.

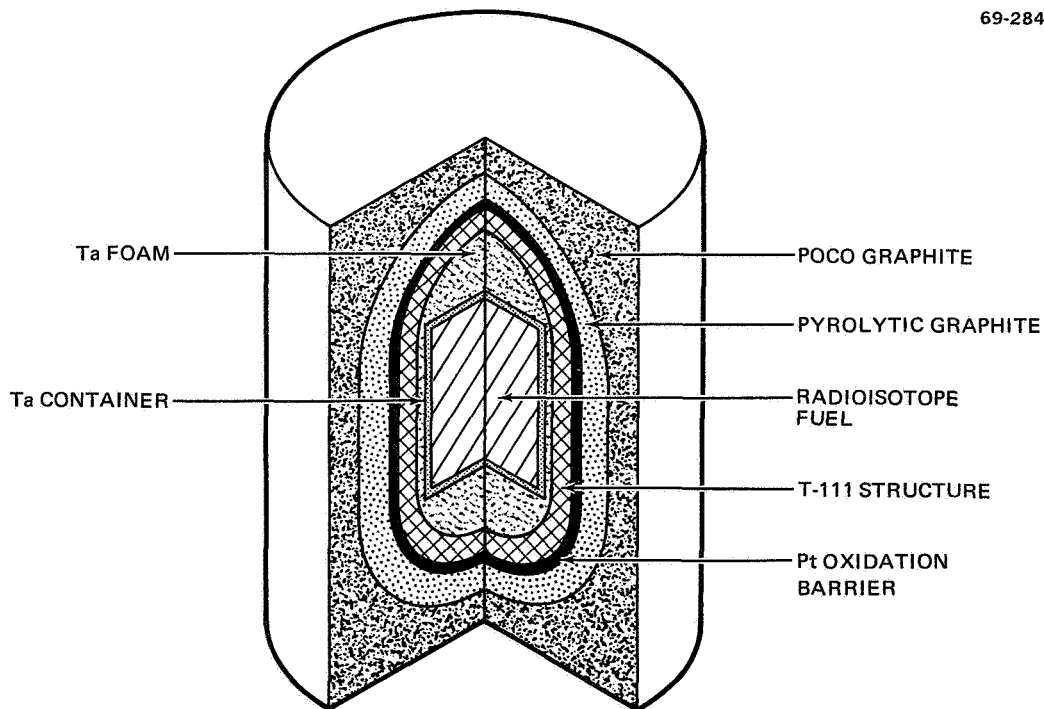


Figure 1. Typical Reference Heater Design



The phase I study program had four primary objectives:

1. To identify potential applications for small (1- to 50-W) radioisotope heaters in manned spacecraft systems.
2. To develop a heater design that would meet the selected safety criteria and have a high probability of being safety- and flight-qualified.
3. To develop an optimum group of heaters to meet the requirements of a maximum number of applications, and mission times of from 14 days to 5 years.
4. To develop program plans and budget estimates for phases II and III.

The results of the application survey, analyses, and design efforts presented in this report show that all of these objectives were met.

### Safety and Design Criteria

From the outset, it was understood that acceptance and use of radio-isotope heaters would depend on superior safety performance characteristics as well as sound engineering justifications. The heaters must be designed to present insignificant hazard resulting from anticipated mission or credible abort environments. This philosophy led to the following guidelines: there should be no danger or special requirements imposed on astronauts performing their normal duties aboard the spacecraft; there should be only an insignificant possibility of injurious radiation dose as a result of credible accidents or incorrect handling.

Using these guidelines, the following safety criteria were generated:

1. Design for industrial handling.
2. Survival in fireball, overpressure, and debris.
3. Intact reentry from lunar return, earth orbit, and suborbital abort.
4. Ocean release with less than  $10^{-2}$  maximum permissible concentration (MPC) at the surface.
5. Intact impact at terminal velocity.
6. Resistance to corrosion for 10 half-lives.
7. Integral shielding to provide protection for astronauts, ground handling crews, and inexperienced personnel.

Stable industrial handling characteristics are ensured by designing to ORNL Class C III structural and thermal stress conditions. Intact reentry is ensured by providing protection against reentry debris and ablation. Static

pressure resistance will maintain capsule integrity to depths where isotope concentration at the ocean surface will be  $<10^{-2}$  MPC. Heaters will be designed and tested for high assurance of survival after impact on granite. Since the radiation that astronauts may be exposed to must be limited to International Committee on Radiation Protection maximum occupational exposure (ICRP-MOE) levels, the integral shield is designed to limit the dose rate to 5 mr/hour at 1 meter. This will also permit ground handling with a minimum of special procedures and equipment, and the integral shield will provide significant protection from injury in the event of incorrect handling.

Using the safety criteria as well as environmental and thermal requirements as guidelines, the following heater design criteria were established:

- Thermal output-5 to 50 W after 6 months for promethia-fueled heaters and 2 years for plutonia-fueled heaters.
- Mission times - 14 days to 5 years.
- Orbital life - 20 years.
- Maximum continuous operating temperature -  $<500^{\circ}\text{F}$ .
- Intact reentry from lunar return, earth orbit, and suborbital abort.
- Launch pad abort survival from Titan IIIM, Saturn 1B, and Saturn V launch vehicle.
- Ten half-life corrosion lifetimes.
- Helium containment for 10 half-lives.
- Radiological dose rates of less than 5 mr/hour at 1 meter.
- Launch vibration load survival up to 44.9 g sinusoidal and 23.7 g random.

These criteria represent a translation of the safety criteria into workable quantities.

### Program Approach

To accomplish the objectives of the phase I study, the program was divided into 10 tasks:

1. Application studies - Review, investigate, and document potential thermal heater applications associated with crew system equipment.
2. Safety analysis - Establish safety criteria and constraints using NASA/MSC and AEC inputs, and perform detailed safety analysis.

3. Design and analysis - Characterize heater configurations, temperatures, heat transfer modes, and power levels; and identify optimum sizes and power levels to span the 1- to 50-W range.
- 3a. Specific application - Apply radioisotope heater design technology to a specific thermal control problem as specified by NASA/MSC.
4. Reference designs - Produce reference heater designs for the AEC and NASA/MSC review and selection prior to development.
5. Radioisotope fuels and encapsulating materials - Select heater fuels and materials that are compatible, meet all operational and environmental conditions, and are state-of-the art or near term state-of-the art.
6. Manufacturing processes and inspection techniques - Define fabrication and inspection techniques required to manufacture the heaters.
7. Coordination with the AEC - Confirm safety and design criteria and design approaches with AEC.
8. Program plans and budget estimates for phases II and III - Prepare program plans and budgetary cost estimates for phases II and III, and present program options for production of flight-qualified hardware.
9. Preliminary safety analysis report description - Prepare a preliminary description of a typical safety analysis report.
10. Program management and reports - Prepare monthly reports and presentation material on tasks 1 through 9; prepare a summary and a final report on the phase I study; and provide direction required to achieve program objectives.

The interrelationship of these tasks is shown in figure 2. Tasks 1, 2, and 5 were inputs to task 3. Task 3 results were used to establish reference designs (task 4) from which detailed designs and specifications can be made. Data and results from tasks 1 through 5 are inputs to task 6. These later tasks have an important bearing on phases II and III because they describe in detail the plan for developing and qualifying the heaters.

Task 7 provided for review and comment by AEC on the safety and design criteria, reference designs, materials selection, manufacturing program logic, and program plans and budgetary cost estimates for phases II and III.

### Program Results

The results of this program shows that two heater sizes, 10 and 50 W, and two fuels, promethia cermet and plutonia bare microspheres or cermet, will meet the majority of identified applications having power levels of from 5

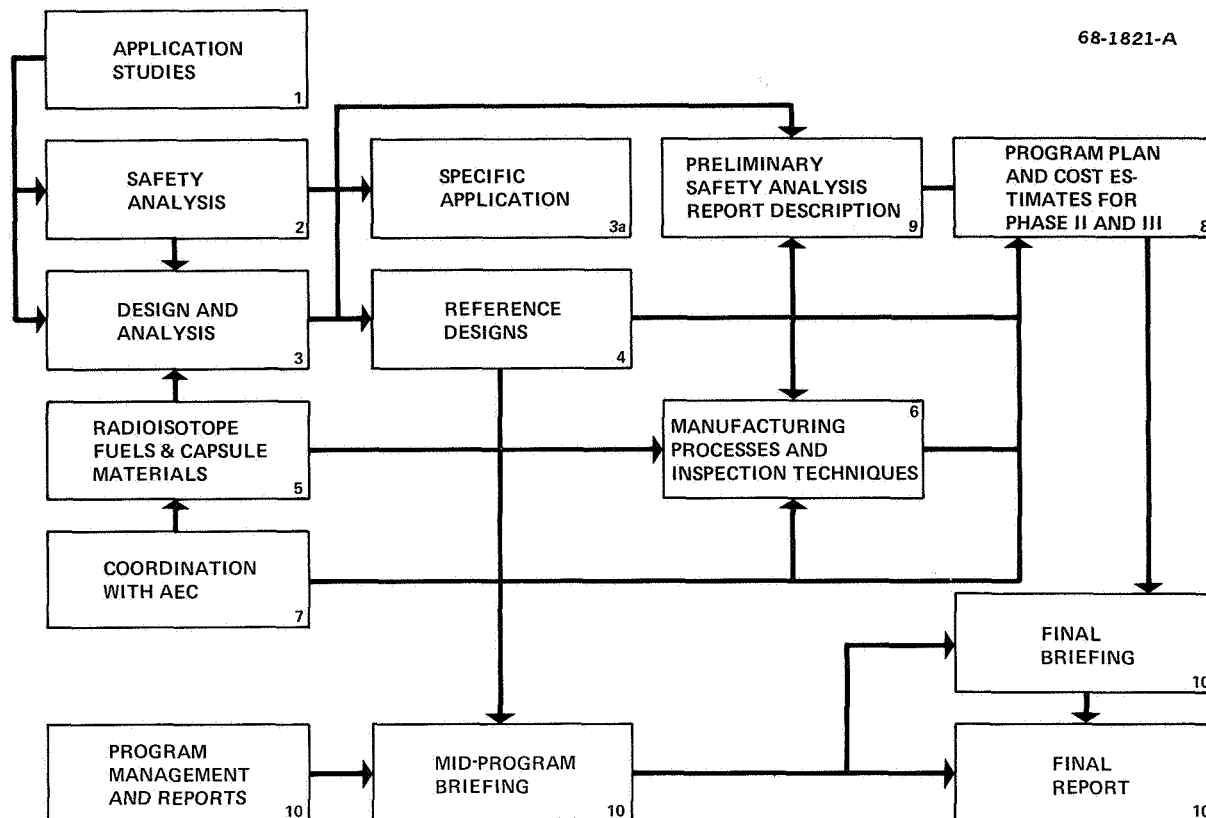


Figure 2. Phase I Program Tasks

to 50 W and mission times of 14 days to 5 years. The designs evolved from this study have a high probability of survival under all mission phases, operating conditions, and environments.

Materials and fabrication techniques selected are state-of-the art or near state-of-the art. The heaters are designed to maintain a margin of safety under all probable conditions and situations, but are not overly conservative. As part of an independent research and development program at DWDL, limited impact testing was performed on simulated reference heater designs. These initial tests, while not conclusive, confirm the validity of the design approach. Since this was a study program, extensive tests of materials and hardware will be required during phase II to completely validate the designs and to qualify the heaters as flight hardware. These tests are discussed later in this report.

## SYMBOLS

$A$	-	Diffusion velocity (m/sec).
$A_c$	-	Cross-sectional area of heater exposed to debris fragments ( $\text{ft}^2$ ).
$A_E$	-	End-on area of heater ( $\text{ft}^2$ ).
$A_F$	-	End-on area of debris fragment ( $\text{ft}^2$ ).
$A_i$	-	Influence coefficient.
$A_s$	-	Side-on area of heater ( $\text{ft}^2$ ).
$C$	-	Capacitance of a given node (a small volume of the heater).
$C_D$	-	Drag coefficient.
$C_p$	-	Peak concentration of radioisotope ( $C_i/\text{m}^2$ ).
$C_i$	-	Curie.
$D$	-	Radiation dose or depth (m).
$F$	-	Radioisotope concentration factor.
$f_2$	-	Fraction of the body burden in the organ.
$f_w$	-	Fraction of $\dot{I}$ deposited in the organ of interest.
$H_s$	-	Air enthalpy at the stagnation temperature.
$H_{540}$	-	Air enthalpy at 540 °R.
$I_b$	-	Amount of radioactive carrier material in the body at any given time.
$I_e$	-	Radioactive carrier concentration in the ocean.
$\dot{I}$	-	Quantity of radioactive carrier material taken into the body each day.
$k$	-	Total number of failure modes.
$K_s$	-	Soil thermal conductivity (Btu/hr-ft- °F).



KE	-	Kenetic energy (ft-lb/sec).
L	-	Capsule length (ft).
MPC <sub>a</sub>	-	Maximum permissible concentration in air.
MPC <sub>s</sub>	-	Maximum permissible concentration in sea water.
MPC <sub>w</sub>	-	Maximum permissible concentration in drinking water.
n	-	Capsule length-to-diameter ratio.
N <sub>d</sub>	-	Fraction of permissible dose attributed to sea water contamination.
N <sub>p</sub>	-	Correction factor to account for sources of protein in the diet other than the sea.
N <sub>s</sub>	-	Fraction of the total ocean contamination attributed to a particular source.
P	-	Probability of nonfailure.
P <sub>i</sub>	-	Nonfailure probability for a particular failure mode i ( $1 \leq i \leq k$ ).
P <sub>tot</sub>	-	Probability of overall nonfailure.
Q	-	Capsule power (Btu/hr) or rate of release of radioactivity (Ci/sec).
q	-	Quantity of airborne radioactive material inhaled per unit time.
q'	-	Maximum permissible organ burden.
Q <sub>A</sub>	-	Point of failure based on analytical model of capsule behavior and environment.
q <sub>cw</sub>	-	Cold wall heat rate (Btu/hr).
Q <sub>E</sub>	-	Difference between Q <sub>F</sub> and Q <sub>A</sub> (must be > 0 in order that failure not occur).
Q <sub>F</sub>	-	Calculated point of failure for a given heater design.
R	-	Radioactivity (Ci) per gram of carrier or distance from release point, (meters).
T <sub>B</sub>	-	Biological half-life.
T <sub>e</sub>	-	Effective half-life.
TID	-	Total integrated dose (Ci/m <sup>3</sup> ).

$T_S$	-	Capsule surface temperature ( $^{\circ}\text{F}$ ).
$u$	-	Windspeed (m/sec).
$V_e$	-	Velocity of entering body when crossing 400 000-ft tangent line.
$V_p$	-	Volume of protein consumed.
$V_w$	-	Volume of water consumed.
$X$	-	Concentration of airborne radioactivity in the downwind or x direction ( $\text{Ci}/\text{m}^3$ ).
$Y$	-	Concentration of airborne radioactivity in the crosswind or y direction ( $\text{Ci}/\text{m}^3$ ).
$Y_i$	-	Admittance of the heat-flow paths by which a given node is connected to other nodes in the network.
$Z$	-	Concentration of airborne activity in the vertical or z direction. ( $\text{Ci}/\text{m}^3$ ).
$\gamma_e$	-	Angle between capsule trajectory and tangent to the earth at 400 000-ft altitude.
$\lambda_b$	-	Biological elimination (decay) constant.
$\lambda_e$	-	Effective decay constant ( $\lambda_b + \lambda_R$ ).
$\lambda_R$	-	Radiological decay constant.
$\nu$	-	Frequency of nonfailure.
$\sigma_e$	-	Stress at a particular time/temperature/pressure condition.
$\sigma_E$	-	Overall standard deviation for $Q_E$ .
$\sigma_F$	-	Overall standard deviation for $Q_F$ .
$\sigma_i$	-	Principal stresses, or standard deviation about point i.
$\sigma_y$	-	Yield stress in simple tension or standard deviation in crosswind.
$\sigma_z$	-	Standard deviation in vertical direction.

## THE USE OF THERMAL HEATERS IN MANNED SPACECRAFT APPLICATIONS

### Approach

A survey of current or planned uses of radioisotope heat sources for thermal control of manned spacecraft components (task 1) was initiated by written requests for information from program directors involved in manned spacecraft programs. This was followed by direct discussions with cognizant program personnel. Finally, identified applications were evaluated and divided into four groups according to operation, availability of data, complexity, and heater size.

The survey.- A letter describing the objectives of the Radioisotope Heater Development Program and the purpose of the survey was sent to manned spacecraft and launch vehicle program directors within the McDonnell Douglas Astronautics Company (MDAC). Program managers at the NASA Manned Spacecraft Center were contacted through the program technical monitors. MDAC program offices to whom letters were sent were (1) Space Laboratories, (2) Saturn/Workshop, (3) Launch Vehicles, (4) Manned Orbital Laboratory, (5) Advanced Manned Orbital Laboratory, (6) Gemini, and (7) Big "G" (Gemini).

The letters were followed by direct discussions with approximately 36 cognizant program personnel. Questionnaires had been prepared in advance covering such items as (1) description of application, (2) operating temperature range, (3) thermal power profile, (4) number of heaters required per application, (5) environmental and/or application requirements or constraints, and (6) drawings and descriptive material.

Evaluation.- Evaluation of data and information obtained from the survey was conducted by dividing the identified applications into four groups. Group A lists applications where constant heat is required. Group B lists applications where some type of thermal control is necessary, such as an on-off switch or thermostat (the largest number of applications fall within this group). Those areas where applications have been identified, but details concerning power profile and temperature requirements are not available, are listed under group C. Finally, applications where isotopes would probably not be considered because of size or complexity are listed in group D.

This information is summarized in table 1. Using the data from groups A and B, the numbers of heaters required were grouped by power level. The result is shown in table 2. Data shown in tables 1 and 2 indicate that there are relatively few applications below 5 and above 50 W.

TABLE 1  
SUMMARY OF THERMAL CONTROL APPLICATIONS  
Group A - Continuous Thermal Requirement

Description	Power requirement (W)	Thermal requirement	No. per vehicle	Total No. required	Remarks
1. Waste water dump systems	3-1/2 to 10	50° to 100°F	3 to 5	9 to 15	Urine dump, fuel cell water dump, experiment effluent dump, wash water dump, humidity condensate dump (EOSL, MOL, Saturn/Workshop)
2. Fecal dehydration	~20 per man	200° to 300°F	1 to 6	3 to 18	EOSL, MOL, Saturn/Workshop
3. Air-evaporator preheater	~100 per man	100° to 150°	1	1	Heats air to increase capacity to evaporate urine (EOSL)
4. View ports	~4 per man	Above dew point	1 per viewport	1 per viewport	Prevents condensation on viewport viewing surfaces (all vehicles)
5. Structural cold spots	~40	60°F	2 to 4	4 to 8	Needed at interface between dome ends and cylindrical surface on crew compartment (EOSL, MOL)
6. H <sub>2</sub> and O <sub>2</sub> purge lines	~10 per line	Above freezing point	8	8	MOL
7. Standby fuel cell heat	10 to 20 per cell	70°F	3	3	Values are estimated; standby fuel cell must be available at all times and be in condition for immediate loading (MOL)
8. Cool panels	~60	-	1	1	MOL thermal control system
9. Heat for base thermal requirements	>50	-	1 (min.)	3 (min.)	Temperature requirement depends on specific applications; provide minimum heat requirement; variable loads/peaks supplied by electric heaters; number required depends on physical interface requirements (a requirement on all vehicles)

TABLE 1. - Continued  
SUMMARY OF THERMAL CONTROL APPLICATIONS  
Group B - Applications Requiring a Controllable or On-Off System

Description	Power requirement (W)	Thermal requirement	No. per vehicle	Total No. required	Remarks
1. Guidance and control	50 to 75	70° to 75°C	6	6	Must be controlled to $\pm 1^\circ\text{C}$ (EOSL)
2. Airlock module pressure wall	57 to 250	>32°F	1	1	57 W peak prelaunch; 197 W peak preactivation; 250 W continuous orbit storage (Saturn/Workshop)
3. Hot water control	~140 to 150	<180°F max at 7 psia	2 to 4	6 to 12	Potable water accumulator needs heat to prevent bacteria growth (EOSL, MOL, Saturn/Workshop)
4. Battery temperature control	~10 to 50	60° to 80°F	1 per onboard battery	1 per onboard battery	Heat required during standby mode; power required depends on battery size; one battery in four is a standby which is required to be available at all times and be in condition for immediate loading
5. Large electronic assemblies	~5	-35° to 85°C	20	20	To provide heat during storage and/or quiescent periods to prevent thermal shock and mechanical deformation upon activation (EOSL)
6. Engine valve heater	<50	48° to 140°F	4 to 8	12 to 24	Thermal profile is function of vehicle orientation, but cyclic operation is required (EOSL, MOL, Saturn/Workshop)
7. Engine catalyst heater	Not known	>140°F	4 to 8	12 to 24	140°F must be maintained at engine valve. Thermal profile is a function of vehicle orientation. Cyclic operation is required (EOSL, MOL, Saturn/Workshop)

TABLE I. - Continued  
SUMMARY OF THERMAL CONTROL APPLICATIONS  
Group B (Continued)

Description	Power requirement	Thermal requirement	No. per vehicle	Total No. required	Remarks
8. Cryogenic heat exchanger	Variable; depends on cryogenic use rate (~10 to 50)	Liquid H <sub>2</sub> O <sub>2</sub> , and N <sub>2</sub> temp. to near room-temp.	1	3	Supplies heat to warm stored cryogenics to temperatures suitable for use (EOSL, MOL, Saturn/Workshop)
9. Saturn 1B/S-IVB lifetime extension					Depends on number of stages to be launched
a. Sequencer assem.	40	-65° to 155° F	1		The present Saturn 1 B/IU combination has a relatively short orbital lifetime; increasing this lifetime to 72 hours would provide the desired flexibility for dual launch missions coupled with a greater rendezvous capability; power profile is cyclic in nature (ref. 1)
b. Switch selector	5	-13° to 155° F	1		
c. Multiplexers	5	-4° to 185° F	4		
d. Attitude control relay	10	-260° to 260° F	1		
e. Signal conditioning assembly	25	-65° to 155° F	3		
f. 5 vdc excitation module	5	-65° to 155° F	1		
g. Attitude control relay	5	-65° to 260° F	1		
h. 28-V power distribution assembly	40	-65° to 155° F	1		
i. Signal conditioning assem.	10	-65° to 155° F	1		
j. Oxidizer tank	30	>20° F	2		
k. Fuel tank	~30	>20° F	2		
l. Oxidizer line	10	>20° F	2		
m. Helium quadruple check valve	10	>20° F	2		

TABLE 1. - Continued  
SUMMARY OF THERMAL CONTROL APPLICATIONS  
Group B (Continued)

Description	Power requirement	Thermal requirement	No. per vehicle	Total No. required	Remarks
10. Workshop attitude control system (WACS) electronics and sensors heating requirement				Depends on number of stages to be launched	
a. Vehicle control system					Required heater power based on low emissivity ( $\epsilon$ ) surface on panel outboard surface (ref. 2)
(1) Gyro package	9 to 11	-67° to 131°F	10		
(2) Horizon sensor system (conical scan)					
(a) Heads	21 to 24	0° to 130°F	4		Total power required would be 42 W for operational and 48 W for nonoperational because only two units require power
(b) Electronics	16	0° to 130°F	1		Because of smaller area involved, much less power is required than for the horizon sensors
(3) Sun sensors	7	-67° to 212°F	1		
(4) Control computer	40	-4° to 185°F	1		
(5) Horizon sensor system (static)					Total power required would be 56 and 48 W for operational and nonoperational, respectively, because only two locations (2 units) require power
(a) Heads	24 to 28	0° to 130°F	4		
(b) Electronics	16	0° to 130°F	1		
b. Control system instrumentation multiplexers	40	-20° to 160°F	3		

TABLE 1. - Continued  
SUMMARY OF THERMAL CONTROL APPLICATIONS  
Group B (Continued)

Description	Power requirement	Thermal requirement	No. per vehicle	Total No. required	Remarks
11. Saturn V/S-IVB stage synchronous orbit electrical components					Additional heat requirements for synchronous orbit capability (ref. 3)
a. Switch selector	15	>-13°F	1		
b. Remote analog submultiplexer	15	>-13°F	2		
c. Remote digital submultiplexer	15	>-4°F	1		
d. Multiplexer assem.	15	>-4°F	4		
e. 50-amp motor-driven switch	5	>-30°F	4		
12. WACS electronics (attitude control relays only)	10 to 30	0° to 155°F	2	2	
13. Workshop telemetry system	60 per panel	Variable	4 (4 panels)	2	Temperature requirements vary; -65° to 155°F for some modules; 0° to 155°F and -130° to 155°F for others; during storage, power requirements could be less; 1-year mission requires 3 month operation, 6 month storage followed by 3 month operation
14. Helium bottles	1 to 1.5	-	2 per system	6 (min)	(EOSL, MOL, Saturn/Workshop)



TABLE 1. Continued  
SUMMARY OF THERMAL CONTROL APPLICATIONS  
Group B (Continued)

Description	Power requirement	Thermal requirement	No. per vehicle	Total No. required	Remarks
15. Mars Lander thermal control	120	0° to 125°F	1	1	Isotope may be one or several; must be compatible with onboard equipment and experiments
16. a. Desorption of molecular sieve bed		350°F desorption 55° to 70°F adsorption (40 min each)	3	3	Four operating beds per space station (2 pairs) 1 spare, non-operating. Power requirements are high and intermittent (EOSL)
b. Desorption of silica gel beds		250°F desorption 50° to 60°F adsorption (40 min each)			

TABLE 1. - Continued  
 SUMMARY OF THERMAL CONTROL APPLICATIONS  
 Group C - Identified Applications But No Data Available

Description	Power requirement 300 Btu/hr	Thermal requirement	No. per vehicle	Total No. required	Remarks
1. Heat supply to Gemini B					Heat must be supplied by MOL as heat is not available onboard Gemini B; power requirements not available (MOL)
2. Nozzle heat for vaporization of LH <sub>2</sub>					Heat is required to vaporize LH <sub>2</sub> ; H <sub>2</sub> is used to spin up turbine and operate O <sub>2</sub> pump; a "bootstrap" method; residual heat in the engine bell is currently used to start system (space startup of stages)
3. Hydraulic systems heat					Heat is required to maintain hydraulic fluid at the proper viscosity
4. Small solid retro rockets					Heat is required to prevent condensation
5. Igniters					Cesium wire igniters have a problem when extremely cold; ordnance used for component separation and solid engine destruction
6. Food preparation					Some type of oven is desired; present method of using hot water is not satisfactory because adding cold food to hot water results in a lukewarm product

TABLE 1. - Concluded  
SUMMARY OF THERMAL CONTROL APPLICATIONS  
Group D - Applications where Isotope Heaters Would Probably Not be Used

Description	Power requirement	Thermal requirement	No. per vehicle	Total No. required	Remarks
1. Film magazine and file storage	5	60° - 80°F	1 - 2	1 - 2	Potential film fogging would probably preclude the use of radioisotopes (EOSL)
2. Cryogenic tanks to provide tank pressure			1 per propellant tank	-	Use of isotope heaters would require an extensive R&D effort; this application is probably best accomplished with electric heat
3. Electrical and electronic junction temperatures	1		Not known	-	Requires small, thermal, statically controlled heater with a 25% duty cycle
4. Gas manifolds and feed lines	Generally >1				Presently supplied by small electrical strap heaters; 50% duty cycle
5. Fuel transfer lines	1	20° to 120°F	20	20	Heaters imbedded in line; 20 heaters/line on WACS
6. Gemini-type RCS components	1 to 1.5 per application	25° to 160°F	32	32	There are a total of 16 thrusters on the Gemini vehicle; there is no communication between components; therefore, each thruster must be supplied with heat; new space vehicle designs utilizing system analysis and heat pipes for thermal balance or thermal control could probably eliminate most of the electric heater requirements

TABLE 2  
HEATER THERMAL REQUIREMENTS SUMMARY  
(Groups A and B)

Thermal requirement (W)	Approximate number required
< 5	20
5 - 10	50
10 - 20	50
20 - 30	15
30 - 40	50
40 - 50	25
> 50	<u>30</u>
Total	240

### Conclusions

The survey shows that some type of thermal control is required for a large number of space components and systems. Over 37 applications were identified requiring approximately 180 to 300 heaters ranging in size from less than 1 to over 100 W. It is obvious that radioisotope heaters will not be considered for all of these applications, either because they offer no advantages over electric heaters or because of complexity and/or size. Realistically, the first application will be where radioisotope heaters are clearly superior, or where an experiment or mission could not be performed (or would be greatly curtailed) if they were not available. However, radioisotope heaters would have been considered for applications such as vehicle view ports, heat for base thermal requirements, structural cold spots, and standby fuel cell heat had they been available.

### SAFETY AND DESIGN ANALYSIS

The objectives of the safety and design analyses (tasks 2 and 3) were to produce reference designs and associated safety criteria for a group of radioisotope heaters suitable for a broad range of manned spacecraft thermal control applications. The approach was to determine suitable safety criteria, combine these with mission integration requirements (minimum weight and size), and establish design criteria. Design analysis was then performed to optimize the capsule configuration.

#### Safety Approach

Acceptance and use of the radioisotope heaters depend on their superior safety and performance characteristics as well as sound engineering justifications, reduced weight, and high reliability. They must be designed to present

insignificant hazards in anticipated mission or credible abort environments. Safety criteria were based on:

1. Mission integration - No danger or special requirements for astronauts such as modification of duty cycles to reduce radiation dose.
2. Public safety - Insignificant possibility of injurious radiation dose as a result of credible accidents or improper handling.

The safety approach consists of:

1. Definition of accident environments based on applications, missions, and probability analysis.
2. Establishment of safety criteria, and joint review with AEC.
3. Selection and evaluation of designs and materials that meet the criteria.
4. Analysis of failure modes, effects, and possible hazards.
5. Application of probabilistic methods to design for probable and/or severe conditions, and estimate realistic risks and hazards.

Safety Criteria.- Safety criteria developed to ensure compliance with the safety philosophy are defined below.

Design for industrial handling - ORNL-CIII minimum standards (ref. 4): The heaters must withstand industrial hazards associated with transportation, handling, and installation. In view of the excellent record established by industry in the use of multicurie radioisotope sources, it is logical to use established standards for their design to ensure suitable performance for the heaters. ORNL has established a source classification system and has determined that most industrial capsules fall in the classification range of BII to CIII. Heater design, analysis, and qualification tests will assure a minimum of CIII levels.

Launch abort environment survival: The heater together with the heater mounting assembly must be designed to survive the overpressure, blast debris, thermal and chemical environments of the launch vehicles during manned missions. Thermal environment will be as described by the liquid fuel and abort model of Kitt and Bader. (ref. 5 ). The blast debris and overpressure models will be those given for SNAP 27 (ref. 6 ) appropriately scaled for launch vehicle variation. The chemical environment model will be based on published TRW data (ref. 7 ).

Reentry debris protection and intact reentry from lunar return ( $\gamma_e = 6.25^\circ, 90^\circ, V_e = 36\ 300\text{ ft/sec}$ ), earth orbit ( $\gamma_e = 0^\circ, 30^\circ, V_e = 25\ 600\text{ ft/sec}$ ), and suborbital abort ( $\gamma_e = 10^\circ, V_e = 22\ 000\text{ ft/sec}$ ): An ablation protection system will be designed which ensures (with a safety factor) intact reentry for the above trajectories and all capsule reentry orientations. Resistance to reentry debris collision will be provided by the heater mounting assembly. The debris model will be formulated using available Air Force radar launch vehicle tracking data.

Formulation of the debris model and design analysis of the mounting structure are phase II efforts. The trajectories specified are not necessarily the worst. Phase II will consider the entire  $V_e$ ,  $\gamma_e$  envelope and determine the most severe conditions. Entry angle  $\gamma_e$  is defined as the angle between the capsule trajectory and a tangent to the earth at 400 000 ft altitude. Entry velocity is the capsule velocity when crossing the 400 000-ft tangent line.

Resist water immersion static overpressure to a depth sufficient to limit ocean surface contamination below  $10^{-2}$  maximum permissible concentration (MPC): The depths at which significant quantities of  $^{147}\text{Pm}$  and  $^{238}\text{Pu}$  will yield  $10^{-2}$  MPC at the ocean surface will be based on point instantaneous release. MPC for sea water will be evaluated for each radioisotope based on the assumptions that (1) the total protein diet of those exposed consists of sea-food which has fully concentrated the radionuclide, and (2) maximum allowable exposures are based on ICRP-MPBB values.

Intact terminal velocity impact on granite: The capsule will remain intact at terminal velocity impact on granite. Verification will be by impact test. Testing is required at maximum impact terminal velocities and impact temperatures predicted by aerothermal analysis. This will be done in phase II.

Ten half-life resistance to corrosion in air, soil, and sea water: A design goal for the heaters will be 10 half-life corrosion containment in burial and immersion environments. This analysis will be based on the following assumptions: Highest reported corrosion rates (including galvanic couple data; no credit for helium retention in plutonia fuel; and no credit for materials other than the structural shell and oxidation barrier. Testing will be directed at identifying rates of corrosion and corrosion-resistant materials and configurations.

Ten half-life radioactive materials containment under ambient burial conditions: Long term containment of  $^{238}\text{Pu}$  fuel will be based on time-dependent stress-strain analysis of the structural vessel. The analysis will include the following assumptions: Stress level safety factor = 2; no credit for helium retention in plutonia fuel; Larson-Miller stress-rupture-temperature-time relationship; no credit for materials other than structural shell; and burial 1 year after encapsulation.

Twenty-year reentry: The structural vessel will be designed for the temperature-internal pressure spike associated with  $^{238}\text{Pu}$  fuel. The analysis will include the following assumptions: 20-year helium accumulation; no credit for helium retention in plutonia fuel; and credit only for the structural vessel.

Integral shielding: Provision will be made for the following safeguards: Astronaut dose limited to ICRP-MOE levels; ground handling consistent with occupational exposure practices; and minimum possibility of severe radiation doses as a result of incorrect handling.

Mission profile and failure modes. - A mission profile chart is presented in figure 3. From this chart and preliminary safety analyses, the following critical events are identified:

1. Critical failure modes
  - Uncontrolled reentry environment.
  - Land impact on unyielding surface.
  - Launch pad explosion and fire.
2. Secondary failure modes
  - Functional failure during mission phase.
  - Water impact.
  - Ground burial.
  - Accidents during prelaunch phase.

Results of the analyses directed at each of the above failure modes are presented in this report under Accident and Failure Analysis, and Radiological Consequences and Hazards.

### Design Approach and Tradeoff Study

Since the potential requirement for radioisotope heaters was established, the remainder of the study concentrated on meeting the remaining two technical objectives. Results are discussed in the following paragraphs.

Design criteria. - The design philosophy governing the analysis which led to proposed heater configurations was to provide for containment of fuel under all normal and abort conditions while fulfilling the requirements for a reliable heat source of minimum weight, volume, and cost for a maximum number of missions.

The specific design criteria summarized in table 3 are a translation of the safety criteria, mission power requirements, and cost-weight minimization into workable quantities. Heater power levels selected are consistent with the list of power requirements determined by means of the applications survey, and with mission life requirements of 14 days to 5 years.

A maximum orbital life of 20 years was used in connection with the safety constraints. Normal heater operating temperatures were determined to be considerably less than 500°F. The heaters were then designed to ensure containment of fuel under conditions set forth in table 3, and to provide a high probability of fuel containment in the event of terminal velocity impact or launch pad abort.

Selected heater materials. - The radioisotope fuel forms and the materials used in the heater designs were selected to provide maximum safety consistent with minimum cost and weight. Detailed discussions of candidate fuel forms and heater materials are presented in the heater materials selection of this report, together with the rationale used in the final selection. The selected fuel forms and materials are listed below.





TABLE 3  
DESIGN CRITERIA

Thermal output:

$^{147}\text{Pm}_2\text{O}_3$  at encapsulation: 5.7, 11.4, 28.5, and 57.0 W at BOL\*  
(6-month shelf life)

$^{238}\text{PuO}_2$  at encapsulation: 5.1, 10.1, 25.3, and 50.5 W at BOL\* (2-year  
shelf life)

Mission time: 14 days to 5 years

Orbital life: 20 years

Normal heater operating temperatures:  $<500^\circ\text{F}$

Ambient temperature range (lunar surface):  $-300^\circ\text{F}$  to  $+250^\circ\text{F}$

Intact reentry

Lunar return:  $\gamma_e = 6.25^\circ$ ;  $V_e = 90^\circ$

Earth orbit:  $\gamma_e = 0^\circ$ ;  $V_e = 30^\circ$

Suborbital abort

Launch pad abort containment for Titan IIIM, Saturn IB, and Saturn V vehicles

Design for static overpressure to a depth sufficient to limit ocean surface contamination below  $10^{-2}$  MPC.

Corrosion lifetime (soil and sea water)

$^{147}\text{Pm}_2\text{O}_3$ : 26 years

$^{238}\text{PuO}_2$ : 870 years

Helium containment lifetime (burial conditions): 870 years

Radiological dose rate:  $<5$  mr/hr at 1 meter

Vibration

Sinusoidal vibration load: 44.9 g (ref. 8)

Random vibration load: 23.7 g

All designs to meet standard shipping and launch pad environments

\*This allows for nominal 5, 10, 25, and 50 W after 6 months shelf life for promethia and 2 years for plutonia.

Fuel form: promethia -  $^{147}\text{Pm}_2\text{O}_3$  - W cermet; and plutonia -  $^{238}\text{PuO}_2$  bare microspheres or  $^{238}\text{PuO}_2$  - Mo cermet

Primary containment vessel: Ta

Impact energy absorption layer: Ta foam

Structural container: T-111

Oxidation barrier: Pt

Thermal insulation layer: pyrolytic graphite

Ablator material: POCO graphite

Density values used in determining the weight of the materials are presented in table 4.

TABLE 4  
DENSITY VALUES FOR HEATER MATERIALS

Material	Density (lb/in <sup>3</sup> )	Density (lb/ft <sup>3</sup> )	Density (gm/cm <sup>3</sup> )
$\text{Pm}_2\text{O}_3$ cermet	0.330	570	9.14
$\text{PuO}_2$ cermet	0.366	632	10.13
$\text{PuO}_2$ microspheres	0.246	425	6.81
Ta	0.60	1038	16.7
T-111	0.604	1043	16.8
Platinum	0.775	1340	21.45
Ta foam (30 v/o Ta)	0.1812	313	5.02
Pyrolytic graphite	0.070	121	1.94
POCO graphite	0.0738	127.5	2.04

Shape and size tradeoffs, and heater nomenclature. - In order to avoid confusion and positively identify each specific design, a code numbering system was developed as shown below:

- Example 1:
 

Radioisotope  
↓  
Fuel Form  
↓  
PMC-10-1 ← series  
↑  
Thermal power

(This refers to a 10-W  $^{147}\text{Pm}_2\text{O}_3$  cermet fuel and is series 1.)

2. Example 2: PUM-50-4

(This refers to a 50-W  $^{238}\text{PuO}_2$  bare microsphere fuel and is series 4.)

3. Example 3: PUC-50-1S

(This refers to a 50-W  $^{238}\text{PuO}_2$  cermet fuel and is series 1. The "S" means that the fuel capsule has a spherical shape; no letter at the end of the code number means that the fuel capsule is a cylinder.)

For the tradeoff studies, a reference set of designs for each power level (5, 10, 25 and 50 W, nominal) and fuel form (promethia cermet, plutonia cermet, and plutonia microspheres) was selected and analyzed to form a basis for comparison.

After selecting the materials, the next considerations were shape, thicknesses, and arrangement. Since promethia cermets are largest, PMC capsules were considered first.

PMC sizes listed in table 5 are based on a specific power of 71.6 W/lb at time of encapsulation and a density of 0.33 lb/in.<sup>3</sup>. Power levels at time of encapsulation are 5.7, 11.4, 28.5, and 57.0 W which result in nominal levels of 5, 10, 25, and 50 W, respectively, 6 months after encapsulation.

The basic shape selected for the reference capsules is cylindrical. This choice was made largely on the basis of state-of-the-art fabrication experience. A fuel capsule L/D (length to diameter) ratio of unity was selected on the basis of previous independent research and development analytical work and on consideration of the reentry heating characteristics (a slender cylinder tends to ablate more rapidly than a thicker one).

A thin wall (0.020 in.) of Ta cladding around the fuel is provided for containment during fabrication. This in turn is centered within the T-111 structural shell which has oblate spheroidal ends. End caps made of 30 v/o tantalum foam are provided between the elliptical shell and the flat ends of the cladding. The thickness of the protective shell was set at 0.060 in. for the 5- and 10-W sizes and 0.120 in. for the larger sizes. These thicknesses were based on radiation shielding requirements, and on structural strength requirements (impact, crush, etc.).

The platinum oxidation barrier surrounds the T-111 shell and eliminates T-111-graphite compatibility problems; 0.020 in. for each size appears sufficient, based on corrosion and oxidation rate considerations.

For POCO/pyrolytic graphite ablator/insulator combinations, a 0.25-in. thickness of each material was selected for all capsule sizes, based on existing reentry data and preliminary integrated heat load computations for the capsules during reentry. The 0.25-in. pyrolytic graphite layer between the outer POCO graphite ablator and the platinum is oriented with the low thermal

TABLE 5  
PMC REFERENCE HEATER DESIGN SUMMARY

Layer	Material	Density (lb/in. <sup>3</sup> )	Weight (lb)			
			5 W PMC-5-1	10 W PMC-10-2	25 W PMC-25-1	50 W PMC-50-2
Fuel	<sup>147</sup> Pm <sub>2</sub> O <sub>3</sub> -20 v/o W	0.330	0.080	0.163	0.396	0.790
Cladding	20 mils Ta	0.60	0.028	0.044	0.078	0.123
2 end caps	30 v/o Ta foam	0.181	0.018	0.034	0.080	0.157
Structural shell	60 or 120 mils T-111	0.604	0.111	0.169	0.512	0.955
Oxidation barrier	20 mils platinum	0.775	0.056	0.082	0.152	0.234
Insulation	1/4 in. pyro- lytic graphite	0.070	0.101	0.138	0.230	0.336
Outer ablator	1/4 in. (min.) POCO graphite	0.074	0.303	0.384	0.588	0.815
Total capsule weight (lb)			0.697	1.014	2.036	3.410
Total capsule volume (in. <sup>3</sup> )			6.19	8.70	14.07	21.41
Total surface area (in. <sup>2</sup> )			18.7	23.1	32.4	43.2
Overall diameter (in.)			1.877	2.056	2.432	2.770
Overall length (in.)			2.237	2.544	3.028	3.556
Frontal area, end-on (in. <sup>2</sup> )			2.767	3.319	4.645	6.026
W/A, end-on (lb/ft <sup>2</sup> )			36.25	43.99	63.12	81.49
Frontal area, side-on (in. <sup>2</sup> )			4.198	5.230	7.364	9.840
W/A, side-on (lb/ft <sup>2</sup> )			23.89	27.93	39.81	49.90
Specific power, (W/lb)			7.19	9.86	12.39	14.66

conductivity plane in the radial direction. This limits heat conduction into the interior and reduces thermal gradients and stresses in the POCO graphite.

A comprehensive breakdown of reference PMC capsule weights and dimensions is given in table 5. Note that the outer POCO graphite, T-111 structural shell, and fuel are the heaviest parts of the designs. Also, total heater weight/watt of power decreases by a factor of 2 from the 5- to 50-W sizes.

The plutonia heaters are based on a fuel form specific power of 181.6 W/lb and bulk densities of 0.366 lb/in.<sup>3</sup> for the cermet (PUC) and 0.246 lb/in.<sup>3</sup> for the PuO<sub>2</sub> microspheres (PUM). Resulting fuel sizes are smaller than corresponding PMC sizes. Provision for helium expansion is made by using 30 v/o Ta foam around the Ta cladding and within the structural shell. Two cases were considered: First, a void-to-fuel ratio near unity was assumed, including end cap void space, and thicknesses of surrounding layers were assumed to be the same as for PMC heaters. The results are presented in table 6. Since the plutonia heater sizes were found to be smaller than the PMC sizes, a second case was considered in which the structural shell and surrounding layers were assumed to have the same dimensions as the PMC designs. The resulting void-to-fuel ratios are about 1.9 for the PUC heaters and about 3.1 for the PUM heaters. Total heater weights for the two cases are compared in table 6. A cost and weight analysis and comparison of minimal vs uniform plutonia heaters are presented under Cost and Weight Optimization later in this report.

Heater configuration tradeoff studies were performed to determine (1) the best ablator shape for protection against aerodynamic heating and earth impact; and (2) the best fuel and pressure shell shape for structural strength and impact resistance. Five ablator shapes were considered: spherical, cylindrical with flat ends (reference case), cylindrical with oblate spheroidal ends, cubic, and rectangular parallelepiped. Of the five, only the reference case and spherical shape were studied in detail.

Six combinations of ablator and fuel capsule shape were analyzed:

1. Reference design - Cylindrical fuel capsule and flat-ended cylindrical ablator.
2. Alternate A - Spherical fuel capsule and cubic ablator.
3. Alternate B - Cylindrical fuel capsule and rectangular parallelepiped ablator.
4. Alternate C - Spherical fuel capsule and flat-ended cylindrical ablator.
5. Alternate D - Cylindrical fuel capsule and cylindrical ablator with oblate spherical ends.
6. Alternate E - Spherical fuel capsule and spherical ablator.

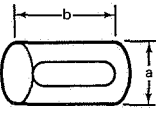
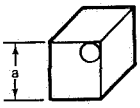
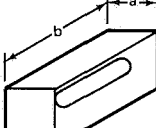
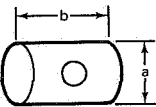
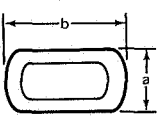
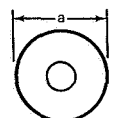
TABLE 6  
REFERENCE PLUTONIA HEATER DESIGN SUMMARY

	5 W PUC-5-1	PuO <sub>2</sub> cermet 10 W PUC-10-3	25 W PUC-25-1	50 W PUC-50-3	PuO <sub>2</sub> microspheres 10 W PUM-10-4	50 W PUM-50-4
	Minimal-size heaters					
Total weight (lb)	0.530	0.740	1.524	2.423	0.674	2.098
Total volume (in. <sup>3</sup> )	5.04	6.58	11.35	16.27	6.45	15.88
Total surface area (in. <sup>2</sup> )	16.3	19.5	28.1	35.7	18.8	35.2
Overall diam (in.)	1.763	1.952	2.275	2.550	1.902	2.530
Overall length (in.)	2.065	2.388	2.793	3.224	2.272	3.156
W/A, end-on (lb/ft <sup>2</sup> )	31.10	37.02	53.84	68.18	34.15	60.10
W/A, side-on (lb/ft <sup>2</sup> )	20.86	24.29	34.44	42.86	23.21	37.85
Specific power (W/lb)	9.44	13.52	16.40	20.65	14.83	23.83
	Uniform reference heaters					
	PUC-5-2	PUC-10-4	PUC-25-2	PUC-50-4	PUM-10-5	PUM-50-5
Total weight (lb)	0.663	0.964	1.915	3.205	0.941	3.080
Total volume (in. <sup>3</sup> )	6.19	8.70	14.07	21.41		
Total surface area (in. <sup>2</sup> )	18.7	23.1	32.4	43.2	Same as	
Overall diam (in.)	1.877	2.056	2.432	2.770	for cermet	
Overall length (in.)	2.237	2.544	3.028	3.556		
W/A, end-on (lb/ft <sup>2</sup> )	34.50	41.82	59.37	76.59	40.83	73.60
W/A, side-on (lb/ft <sup>2</sup> )	22.74	26.75	37.45	46.95	26.32	45.55
Specific power (W/lb)	7.55	10.38	13.06	15.60	10.63	16.25

Note that these represent the pertinent combinations-- a cylindrical fuel capsule within a cylindrical, rectangular, or rounded-end cylindrical ablator and a spherical fuel capsule within a cylindrical, spherical, or cubic ablator. The six combinations are shown in table 7.

The equivalent spherical fuel capsules for promethia cermet fuel are illustrated in figures 4 and 5. These were designed on the basis of the same fuel volume and structural layer thicknesses as in the equivalent reference designs. Although outer dimensions of the spherical layers are slightly larger than in the reference case, layer weights are less. Total weight of the bare spherical capsule plus pyrolytic graphite (also spherical) is about 19% less for both power levels. Note that no Ta foam is shown; in practice, some Ta foam would probably be required.

TABLE 7  
HEATER CONCEPT COMPARISON FOR PROMETHIUM FUEL

Capsule shape Ablator shape	Cylindrical cyl. (flat-end)	Spherical cubical	Cylindrical rect. faced	Cylindrical cyl. (flat-end)	Cylindrical cyl. (rounded ends)	Spherical Spherical
	 Reference Design	 Alternate A	 Alternate B	 Alternate C	 Alternate D	 Alternate E
Weight summary (lb)	10W 50W	10W 50W	10W 50W	10W 50W	10W 50W	10W 50W
Bare capsule	0.49 2.26	0.40 1.84	0.49 2.26	0.40 1.84	0.49 2.26	0.40 1.84
Pyrographite	0.14 0.34	0.11 .28	0.14 0.34	0.11 0.28	0.14 0.34	0.11 0.28
POCOgraphite	0.38 0.81	0.58 1.36	0.55 1.24	0.42 0.94	0.25 0.51	0.22 0.43
Total wt	1.01 3.41	1.09 3.48	1.18 3.84	0.93 3.06	.88 3.11	0.73 2.55
Dimensions (in.)						
a	2.06 2.77	2.18 2.98	2.06 2.77	2.18 2.98	2.06 2.77	2.18 2.98
b	2.54 3.56	--- ---	2.50 3.52	2.18 2.98	2.50 3.52	--- ---
Total vol (in. <sup>3</sup> )	8.70 21.41	10.36 26.46	10.57 26.97	8.14 20.78	6.53 17.11	5.43 13.86
Impact velocity (ft/sec)						
End-on	245 333	178 232	196 262	221 293	382 532	423 578
Edge or side on	329 438	131 171	178 233	328 435	330 448	
W/A lb/ft <sup>2</sup>						
End-on	44.0 81.5	33.2 56.4	40.2 72.1	35.9 63.2	38.3 74.3	28.2 52.6
Edge or side on	27.9 49.9	23.5 39.9	33.2 56.7	28.2 49.6	28.7 52.5	

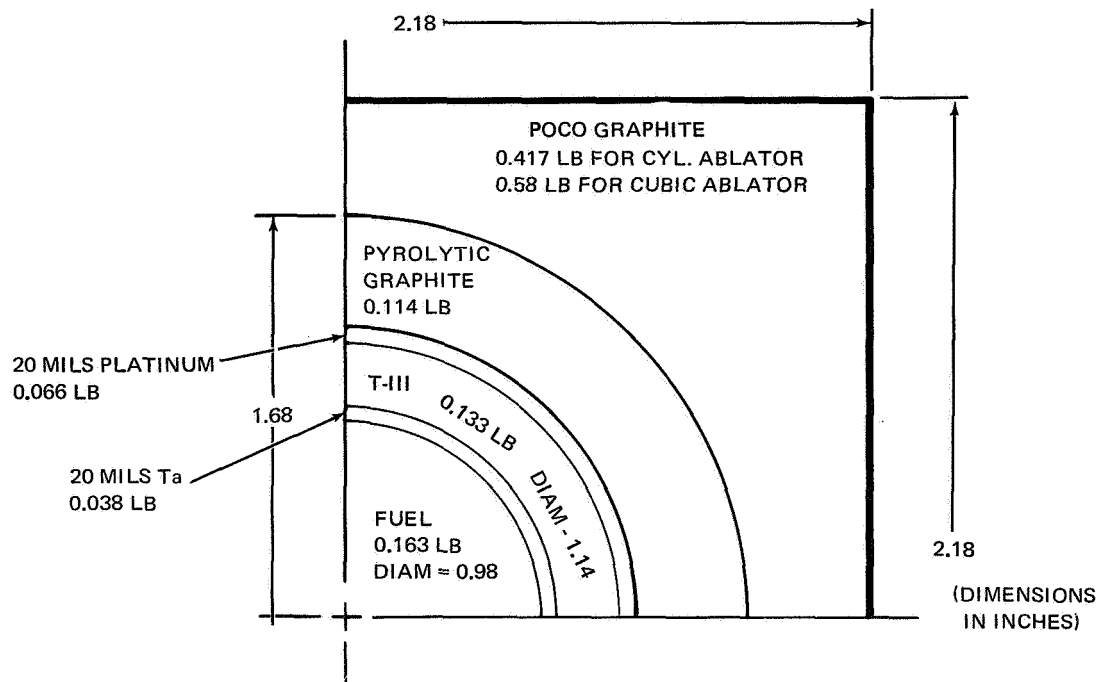


Figure 4. PMC-10-2S  $^{147}\text{Pm}_2\text{O}_3$  Cermet Spherical 10-W Capsule with Cubic or Cylindrical Ablator

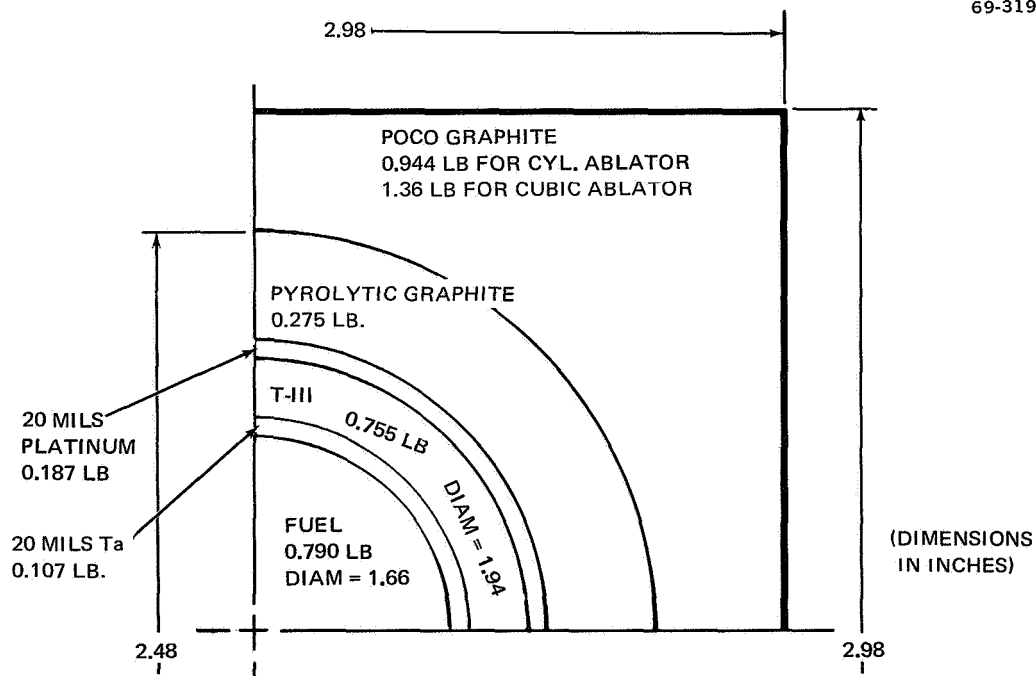


Figure 5. PMC-50-2S  $^{147}\text{Pm}_2\text{O}_3$  Cermet Spherical 50-W Capsule with Cubic or Cylindrical Ablator



Part of this weight advantage is lost in encasing the spherical capsule in a flat-ended cylinder or parallelepiped. An overall weight summary of promethia-fueled capsules is presented in table 7 for the six designs. For the same outer ablator shape, whether a parallelepiped or cylinder, overall weights for spherical capsule designs are about 10% lower than for cylindrical inner capsules.

Although the spherical fuel design results in a significant weight reduction for promethia capsules, comparative weights for plutonia capsules are more nearly equal, assuming a fixed void-to-fuel ratio. This is because cylindrical capsules can utilize void space in the end caps for helium expansion, while spherical capsules have no corresponding volume. The end caps, therefore, create a small weight penalty for promethia fuel; but for plutonia capsules, end caps can be used effectively. On the other hand, a spherical vessel is theoretically stronger for the same internal pressure (volume). Neglecting fabrication and welding considerations, a spherical plutonia capsule with the same internal volume as the reference case is equivalent from an internal pressure standpoint--but superior from a containment standpoint.

Data shown in table 7 indicate that a cubic or rectangular shape results in the heaviest ablator, while a spherical or cylindrical shape with rounded ends is lightest; the reference flat end cylindrical shape is in between. The same trend holds for total volumes and surface areas.

Reentry heating and impact characteristics of design alternatives are discussed in the Design Analysis section of this report; the results are reviewed here and related to the design.

In reentry heating, two considerations are of prime importance: the ballistic coefficient and the heating ratios. Weight/area values for the different designs are listed in table 7 for two basic orientations. Note that heater designs with spherical fuel capsules have the lowest weight/area value for any given ablator shape. Corresponding stagnation-point heating is less, and since the heating ratios are the same, integrated heating is also less. Despite the lower surface-heating, designs with spherical fuel capsules attain temperatures equivalent to those of designs using cylindrical capsules because heat is more readily conducted inward. Therefore, there is no significant difference in internal temperatures of the two fuel-capsule shapes.

Reentry heating, however, is strongly dependent on the shape of the outer ablator. Cubic and rectangular-faced designs have the lowest total surface heating as determined by ballistic coefficient and heating ratio effects. The sphere and the round-end cylinder have the greatest surface heating. Flat-ended cylindrical ablator designs fall in between.

The reentry impact velocity calculations are summarized in table 7. Note the significantly lower velocities for cubic and rectangular-faced shapes. Round shapes are again the worst case, and flat-ended cylinders fall in between.

Reference Designs and Fabrication Details. - figures 6 and 7 show typical design details of the 10- and 50-W reference heater designs. Primary containment of the fuel is provided by a Ta capsule. The cylindrical section of the capsule is a tube with a 0.020 in. -thick wall; the ends are identical in shape and are machined from 0.040-in. Ta sheet. Fabrication of the primary containment starts with the welding of an end into the tubular section. A standing lip weld is provided for and can be tungsten-inert-gas (TIG) welded or electron-beam (EB) welded. Since the primary container is not designed as a pressure vessel, welding the ends requires only that they be leak-tight until the capsule is sealed into the heater's structural shell.

After the fuel form is placed in the primary container, a disk of 0.010-in. -thick Ta is placed over the fuel as a spacer to prevent volatilization of the isotope during closure welding.

The structural shell consists of a tubular central section and ends formed in the shape of an oblate spheroid. The material chosen is a Ta alloy, T-111, which contains tungsten and hafnium.

Assembly of the structural shell begins with the EB welding of one end to the tubular section. In the case of a plutonium-fueled capsule, Ta foam is used around the capsule as well as at both ends to center the fuel within the T-111 structure. The structural shell is closed by EB-welding the other

69-320

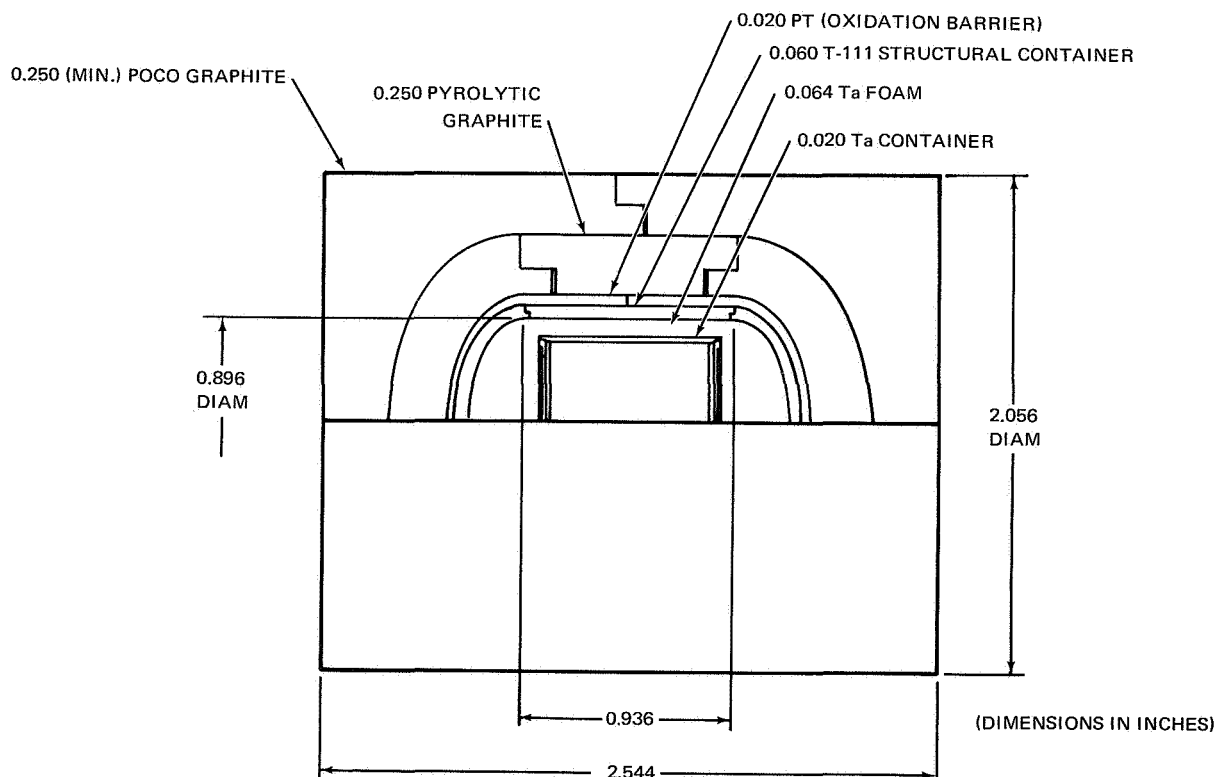


Figure 6. PUC-10-4 Nominal 10-W  $^{238}\text{PuO}_2$  Heater

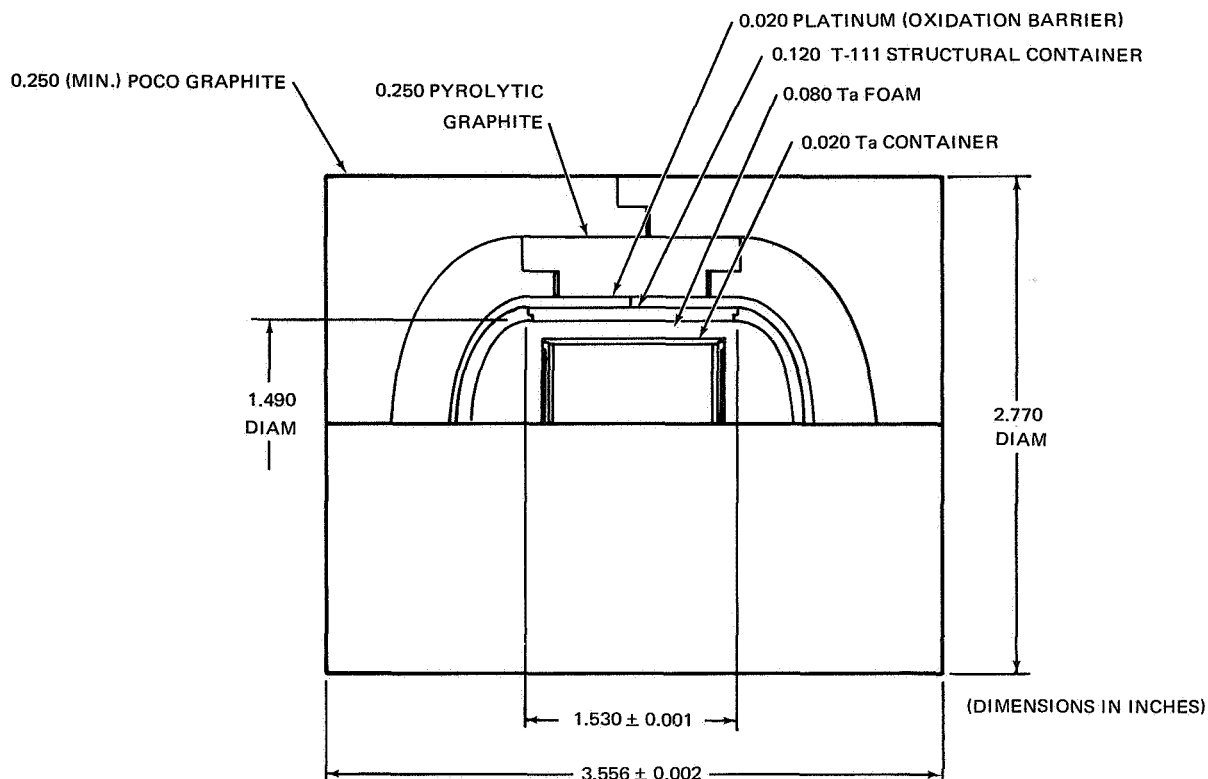


Figure 7. PUC-50-4 Nominal 50-W  $^{238}\text{PuO}_2$  Heater

end to the tubular section. All structural welds are inspected with an ultrasonic nondestructive test device to ensure against voids or inclusions in the welds, and 100% penetration.

Since T-111 is a refractory metal alloy subject to oxidation at elevated temperatures, a barrier against degradation is provided by a 0.020-in.-thick platinum shell. Identical halves are butt-welded to form a complete cover over the structural shell.

Protection to ensure survival of the capsules during reentry is provided by an outer shell of POCO graphite as an ablator and an insulating shell of pyrolytic graphite with the AB plane concentric to the structural shell. The pyrolytic graphite is composed of three pieces; two identical ends and one tubular section. (It may be possible to form the pyrolytic graphite in only two pieces, using a common mandrel, and machining the ends to fit as a male/female joint.) The POCO graphite ablator is formed into cylindrical billets; machined; and the two halves bonded together. Bonding of the pyrolytic graphite is probably not required.

Uniform heater designs: Figures 6 through 9 illustrate the details and dimensions of typical designs and sizes for the nominal 10- and 50-W heaters using  $^{147}\text{Pm}_2\text{O}_3$  or  $^{238}\text{PuO}_2$ . All thicknesses and sizes from the structural

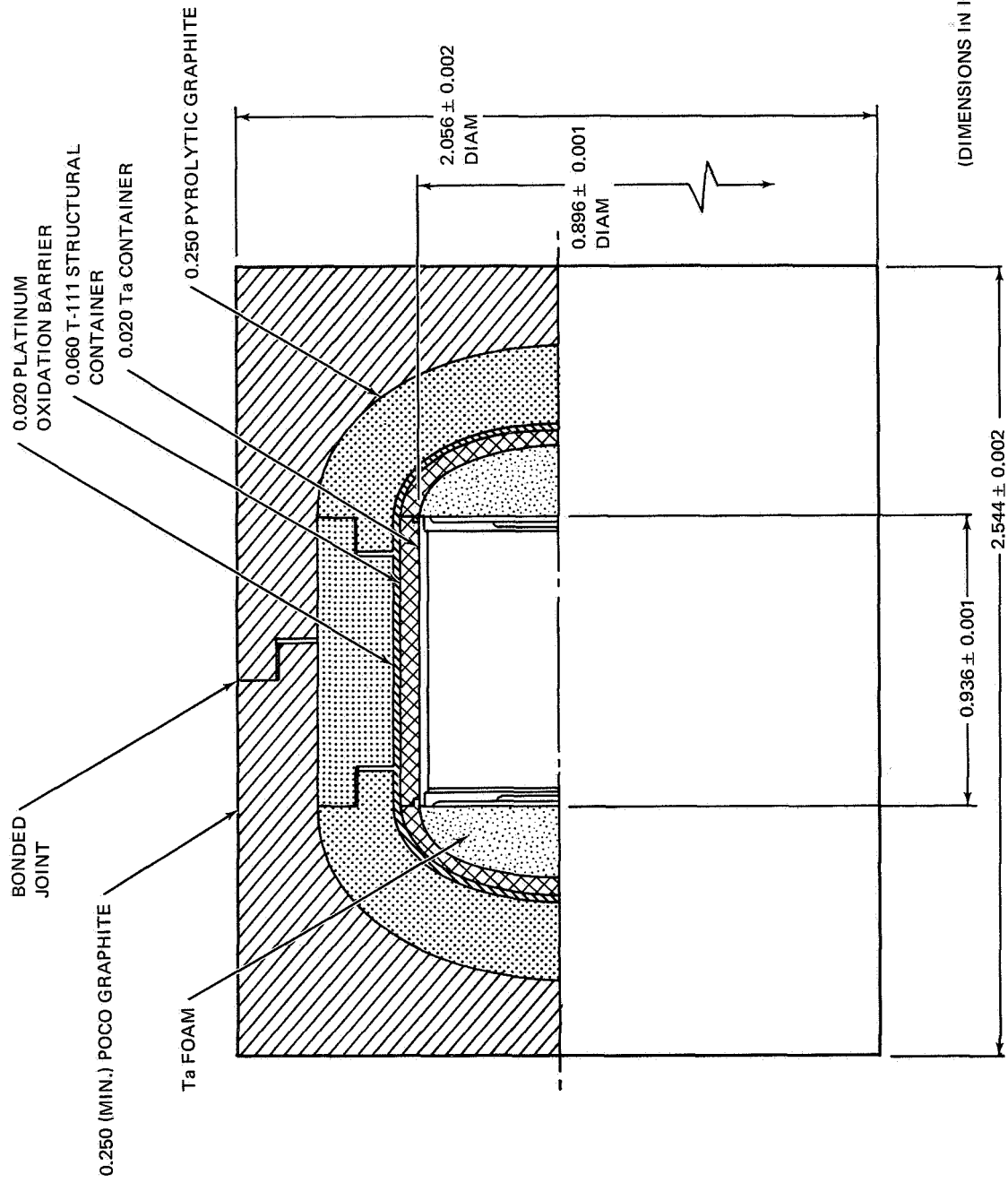


Figure 8. PMC-10-2 Nominal 10-W  $^{147}\text{Pm}_2\text{O}_3$  Heater

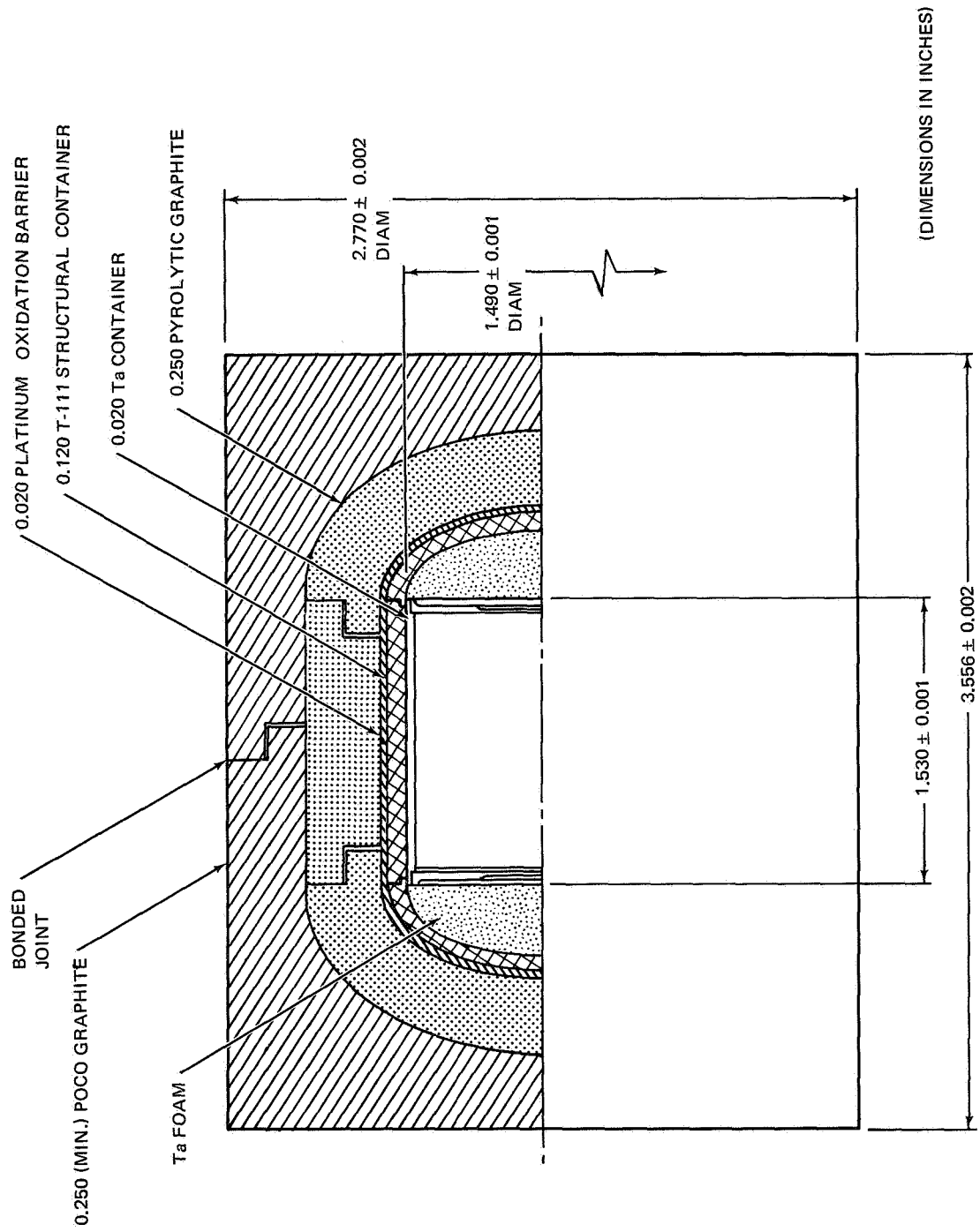


Figure 9. PMC-50-2 Nominal 50-W  $^{147}\text{Pm}_2\text{O}_3$  Heater

shell outward are the same for similar power levels. Use of identical parts wherever possible reduces the equipment required and simplifies fabrication.

Other reference designs: Figures 10 through 17 complete the list of reference heater designs developed during this study. All use the same materials and retain the flat-ended cylinder configuration for the ablator. Figures 12 and 13 illustrate a concept that uses  $^{238}\text{PuO}_2$  bare microspheres for fuel. These heaters are slightly smaller and lighter in weight than their counterparts using the cermet fuel form.

Alternate heater concepts: Although the flat-ended cylindrical configuration was selected for the reference designs, several alternate configurations were considered. Three of these are shown in figures 18 through 20. All refer to Pm fuel, but Pu can be used in the spherical and stacked design concepts as well.

The types of materials used for the spherical geometry are identical to those for the reference cylindrical design. An advantage of this design is the potential reduction in fabrication costs once the techniques have been developed. However, impact velocity is high (table 7) and it may be more difficult to integrate with a component and to stack or group the heaters.

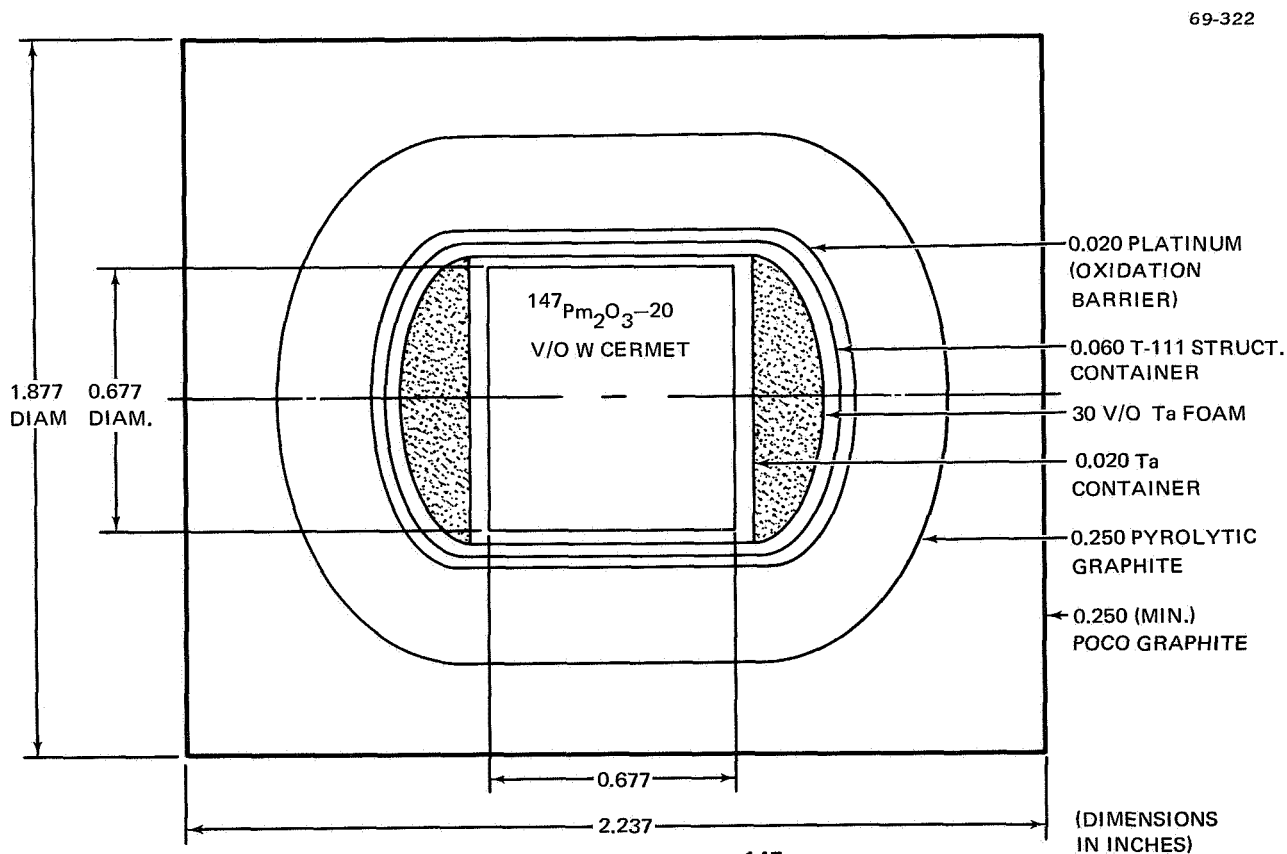


Figure 10. PMC-5-1 Nominal 5-W.  $^{147}\text{Pm}_2\text{O}_3$  Heater

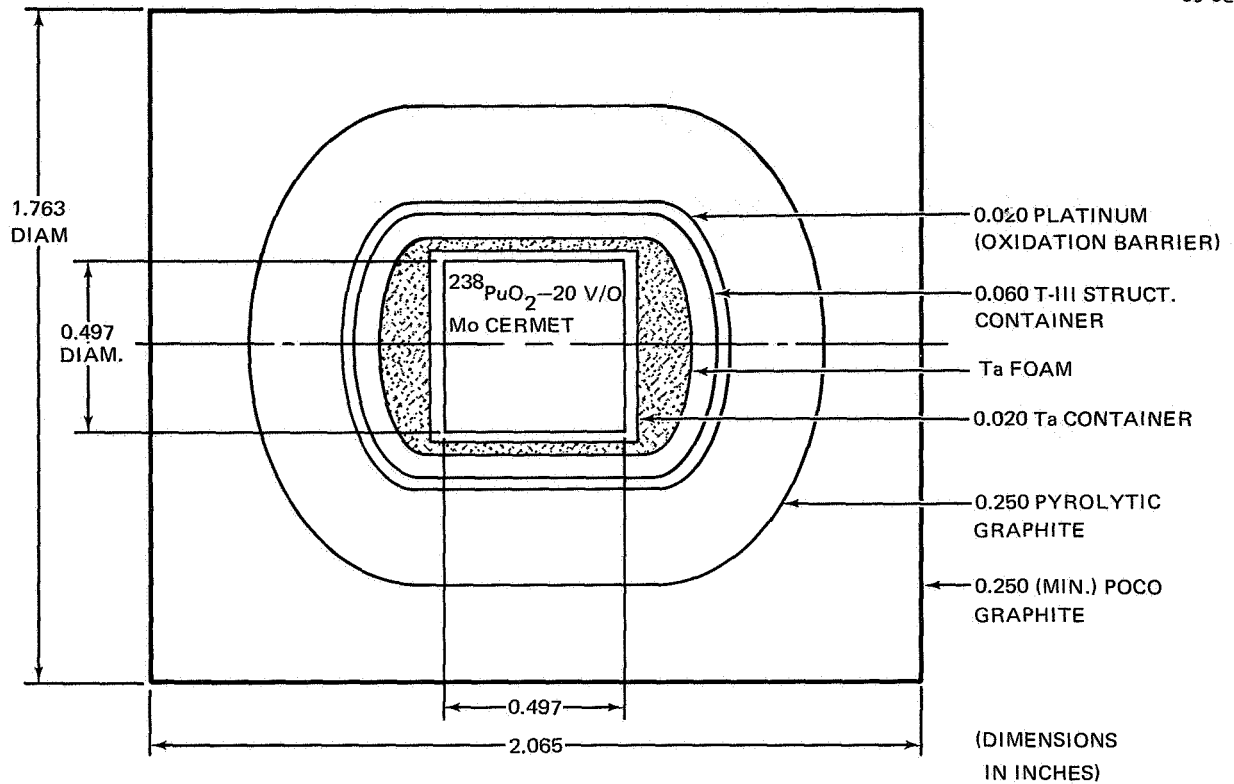


Figure 11. PUC-5-1 Nominal 5-W  $^{238}\text{PuO}_2$  Heater

69-775

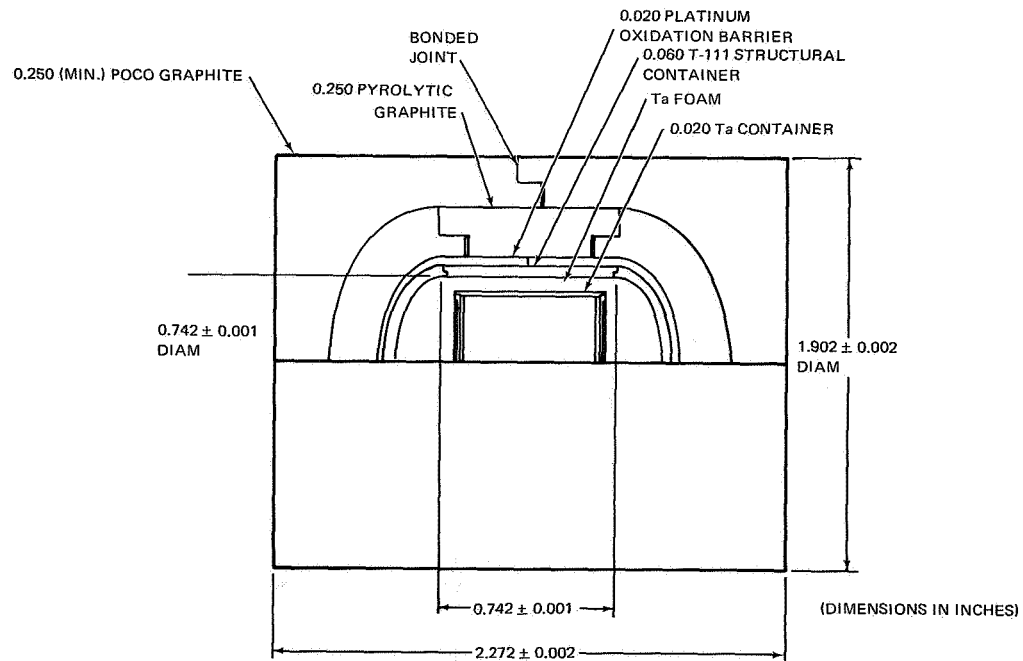


Figure 12. PUM-10-4 Nominal 10-W  $^{238}\text{PuO}_2$  Bare Microsphere

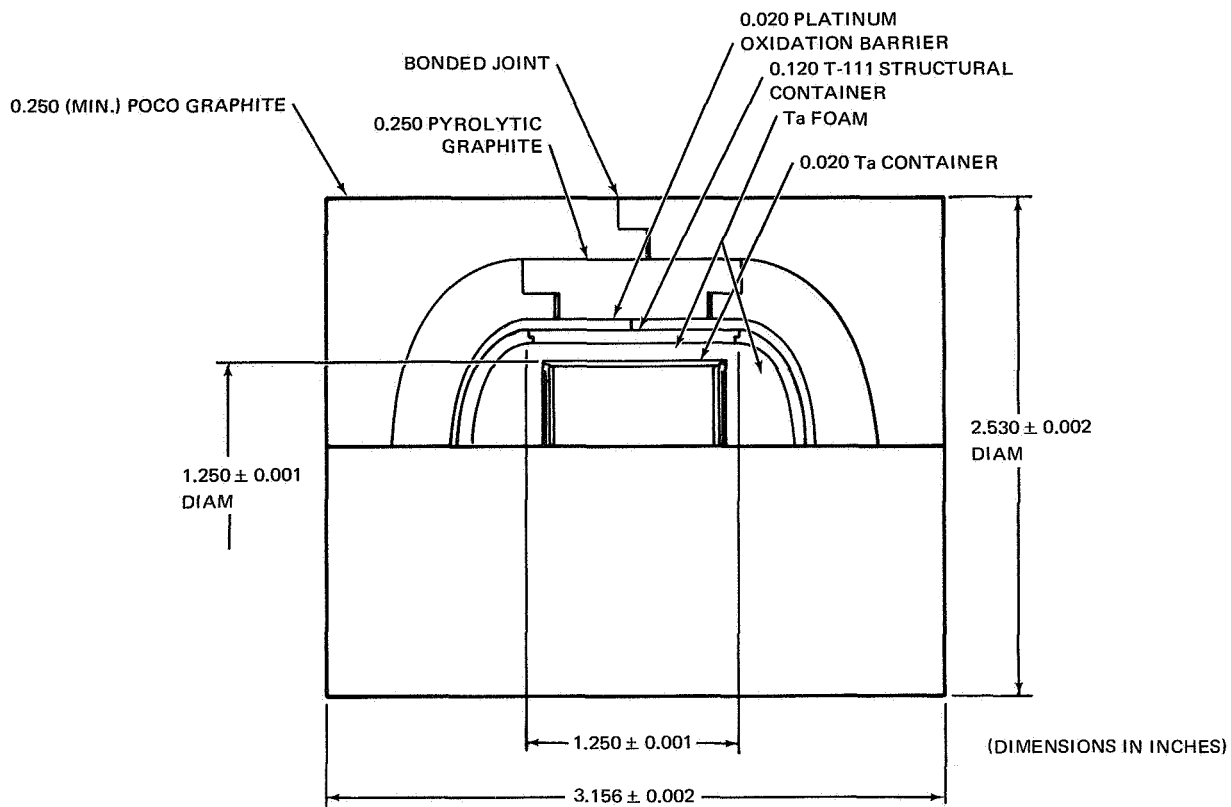


Figure 13. PUM-50-4 Nominal 50-W  $^{238}\text{PuO}_2$  Bare Microspheres

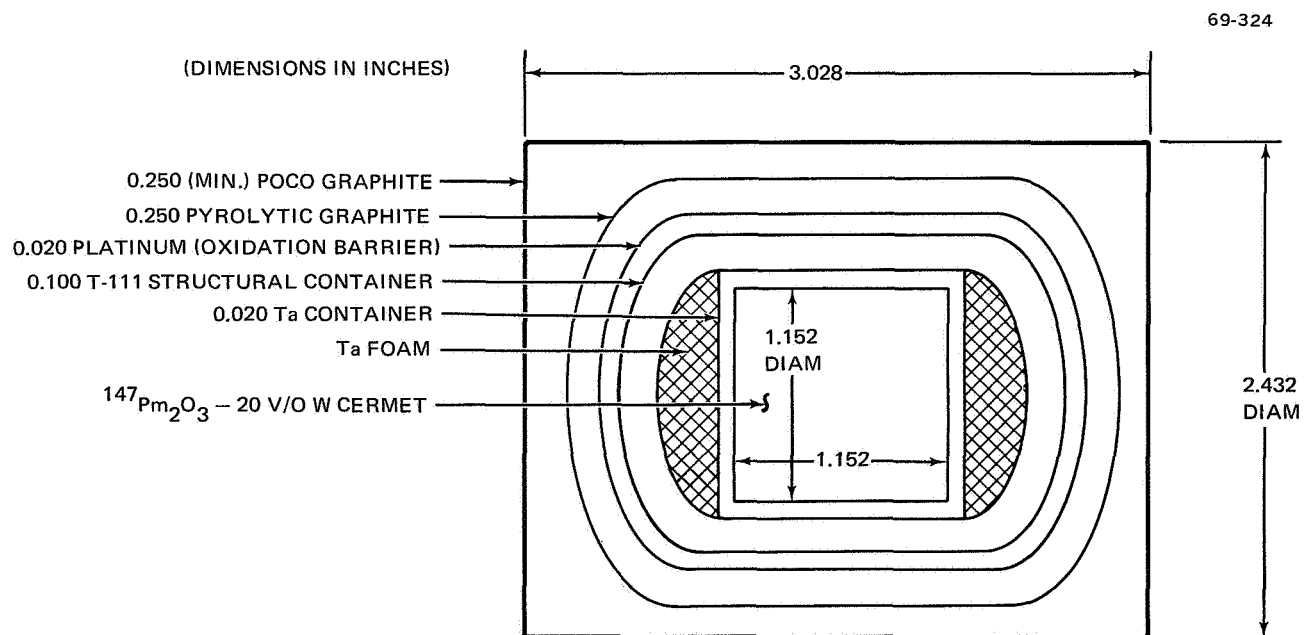


Figure 14. PMC-25-1 Nominal 25-W  $^{147}\text{Pm}_2\text{O}_3$  Heater



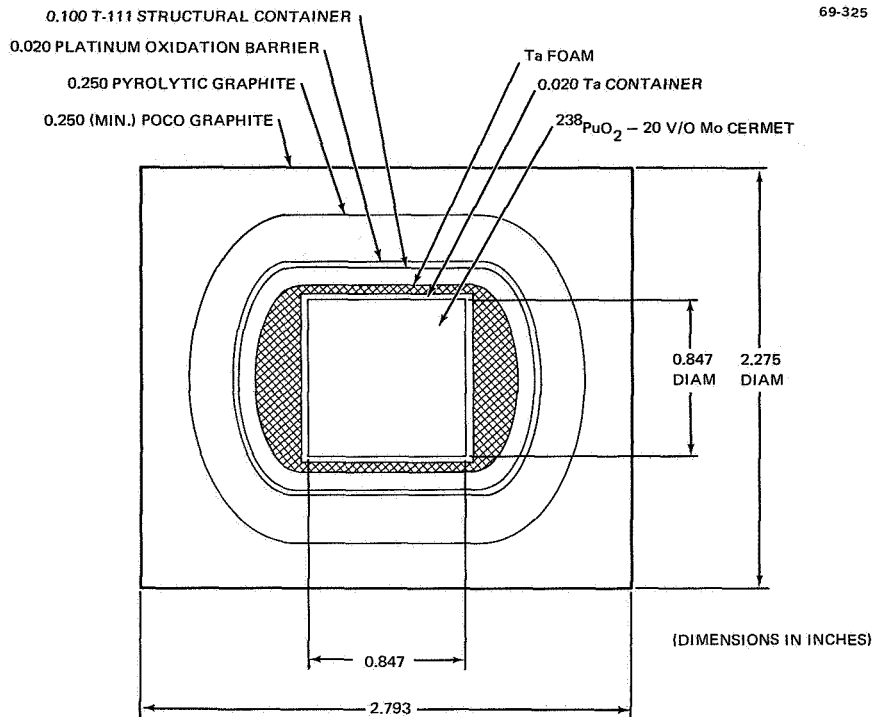


Figure 15. PUC-25-1 Nominal 25-W  $^{238}\text{PuO}_2$  Heater

(DIMENSIONS IN INCHES)

69-326

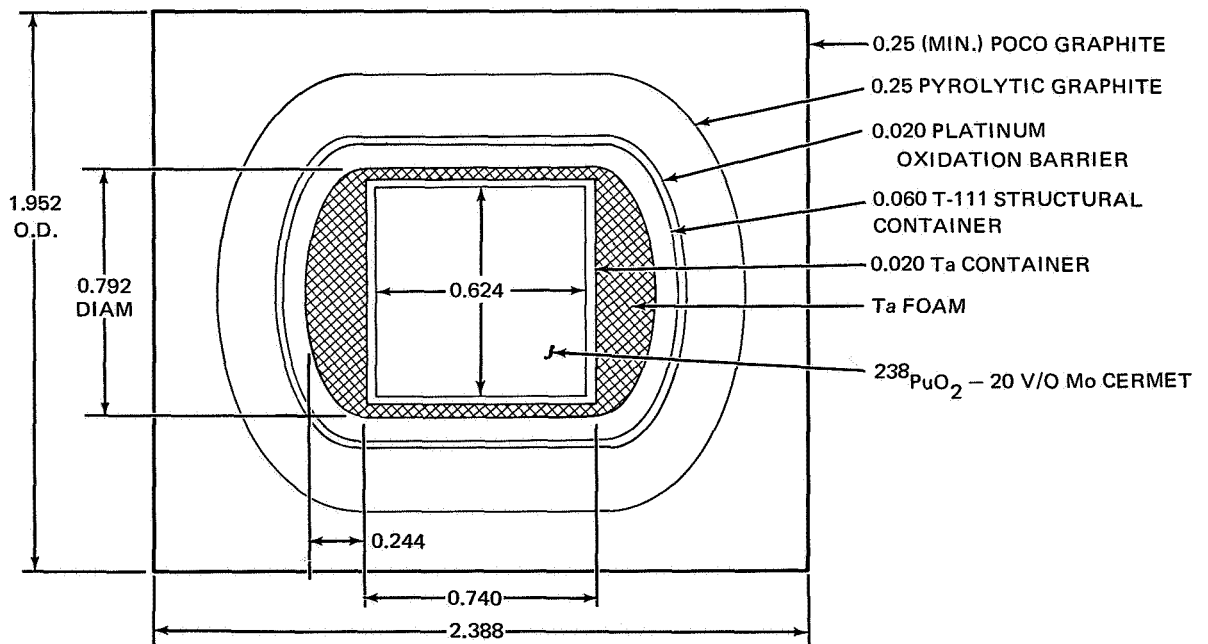


Figure 16. PUC-10-3 Nominal 10-W  $^{238}\text{PuO}_2$  Heater

(DIMENSIONS IN INCHES)

69-327

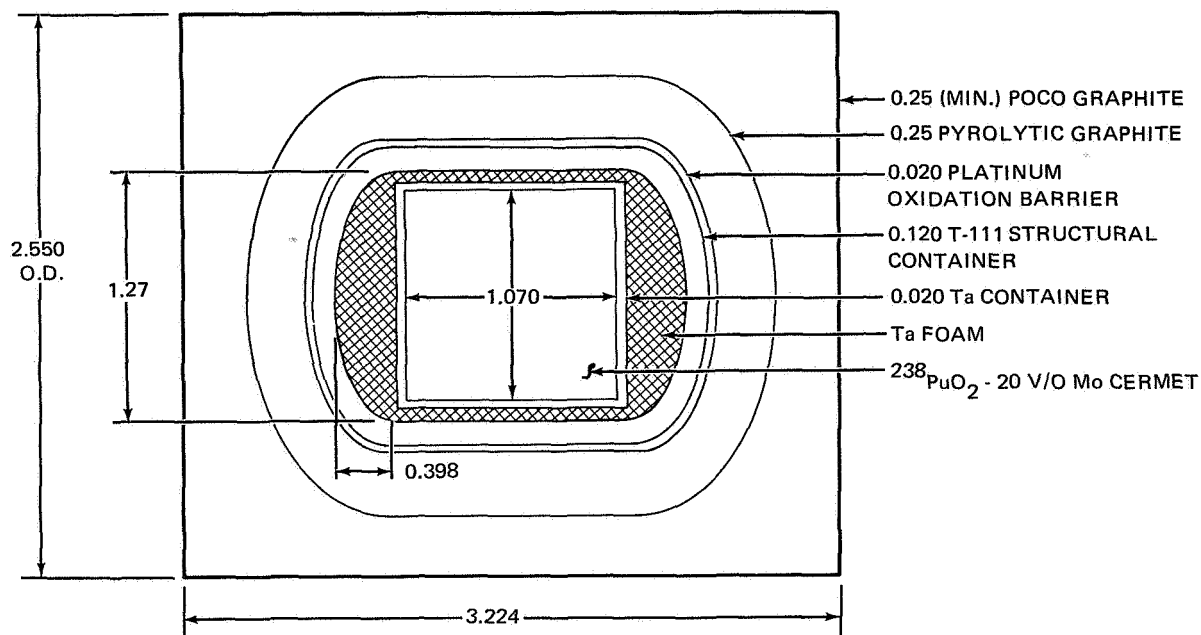


Figure 17. PUC-50-3 Nominal 50-W  $^{238}\text{PuO}_2$  Heater

69-328

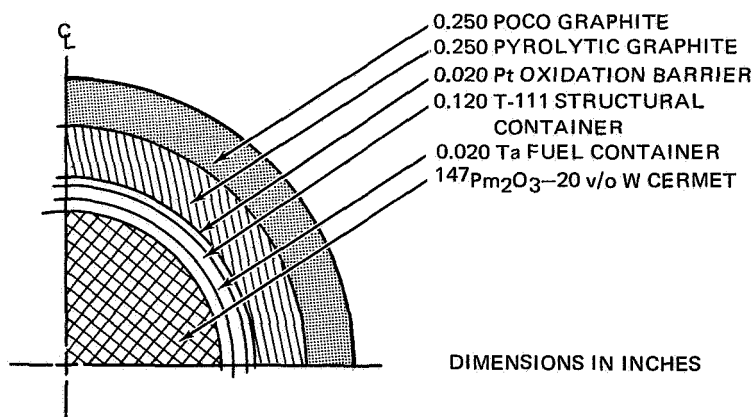


Figure 18. PMC-50-1S 50-W Spherical Pm Heater (WT  $\cong$  2.56 LB)

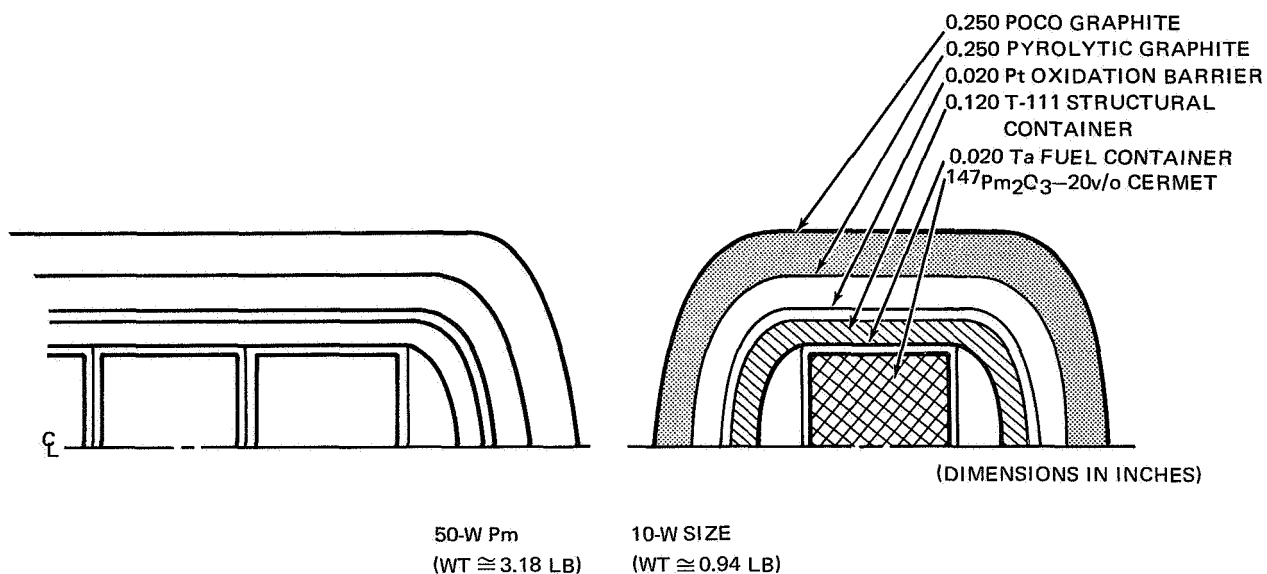
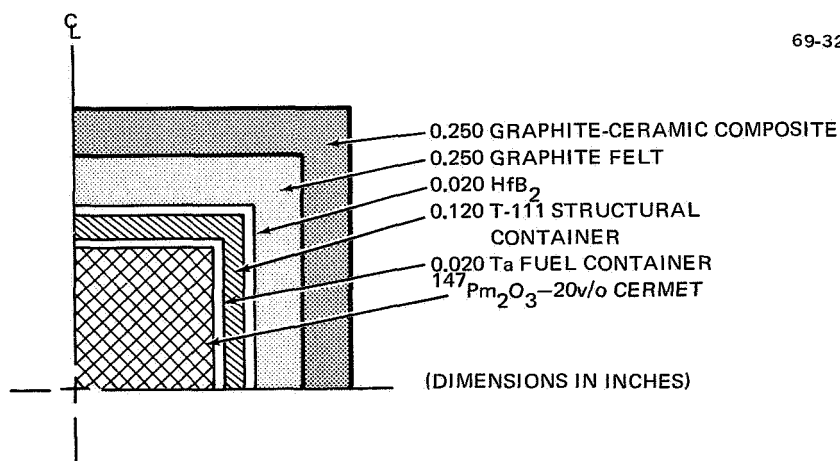


Figure 19. Stacked Capsule Concept

Figure 20. 50-W Unitized Pm Heater (W  $\approx$  2.82 LB)

The stacked capsule concept (fig. 19) used a baseline 10-W capsule. This capsule is identical to the 10-W baseline cylindrical design except that the T-111 structure thickness is 120 mils rather than 60 mils; this is necessary to provide adequate shielding when a number of capsules are stacked together. The major advantage of this design is that it standardizes capsule sizes and thus reduces fabrication costs. But qualification costs would be higher because each size would have to be tested separately; and the design does incur a weight penalty.

The third concept (fig. 20) is the promethia unitized design. It departs from the other design concepts in a number of important areas: (1)  $\text{HfB}_2$  replaces Pt for the oxidation barrier, (2) graphite felt is used in place of pyrolytic graphite for thermal insulation, (3) a graphite ceramic,  $\text{HfB}_2\text{-WSi}_2\text{-C}$  or  $\text{TiB}_2\text{-WSi}_2\text{-C}$ , replaces POCO graphite for the ablator. Using these materials (which are under development at DWDL), the ablator insulator can be pressed around the fuel capsule in a one-step process. DWDL has fabricated approximately 12 radioisotope heaters using this process and stand-in fuels. Recently, one promethia-fueled capsule was also fabricated by this process. Examination of the stand-in fueled capsules has shown that no fuel penetrated the Ta container on any of the capsules. A program is currently underway at DWDL to determine the physical and mechanical properties of the graphite-ceramic. This method cannot be used with Pu at the present time because of the need for a void within the capsule.

Figure 21 illustrates a spherical capsule in a cube-shaped ablator. This concept is slightly larger than the reference design in overall dimensions

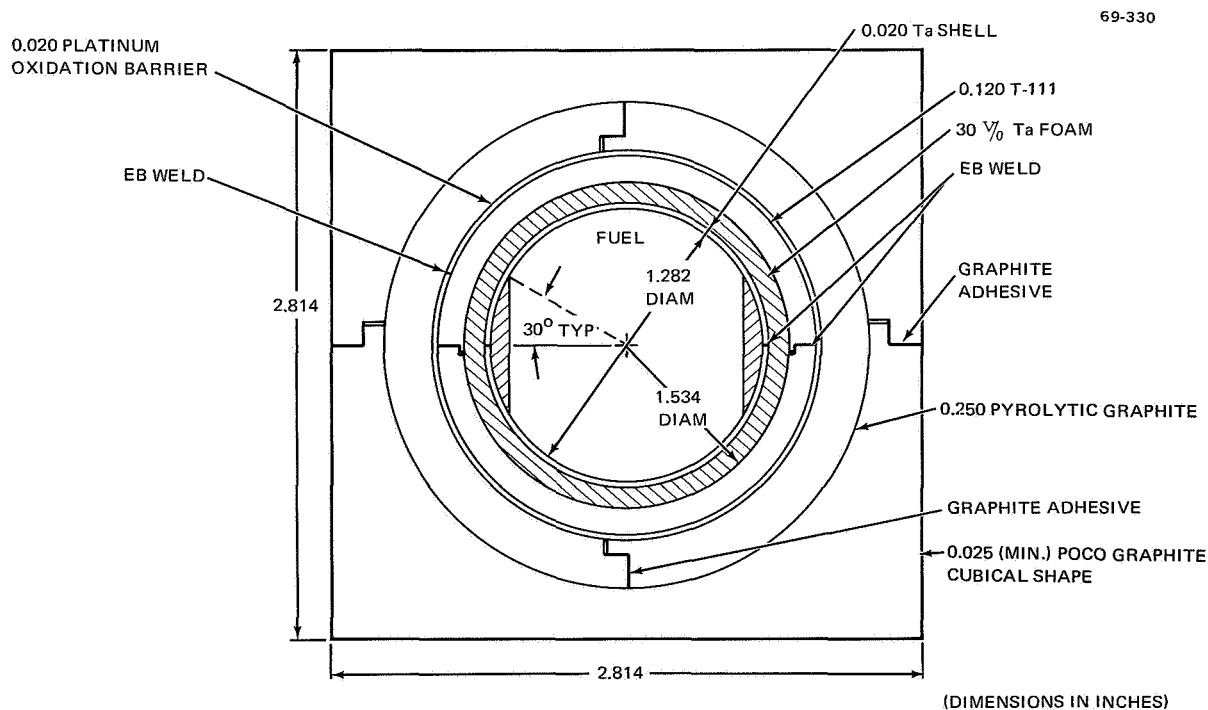


Figure 21. PUC-50-2S Spheroidal Concept 50-W  $^{238}\text{PuO}_2$  Cermet

and it weighs slightly more. Its chief advantage over the reference design is a significant reduction in impact velocity. The primary disadvantage at present is the high development cost required to produce a spherical cermet-fueled capsule, and the lack of experience in forming cubic shapes.

A number of heater configurations were considered before selecting the flat-ended cylinder as the reference design. These are presented in appendix A.

Reference heater mounting design. - The heater mounting system serves other purposes in addition to correct positioning of the thermal energy source. The mounting must provide low thermal resistance so that heater operating temperatures will not exceed design limits. In addition, a systems approach takes into account the fact that an appropriately designed support furnishes protection to the heater from blast debris. To design the heater to withstand debris without some protection by the mounting assembly would unduly penalize the heater from a weight, volume, and cost standpoint.

Figure 22 illustrates a representative design for a support system in which the heater is attached to the exterior of the unit requiring heat. The illustration shows a design employing a sheet metal housing, a saddle block, and an aluminum cover plate. Bolts and locknuts are used to hold the cover in place. The mount is attached to the component with bolts inserted into reinforced threaded holes. The saddle block accommodates the curved surface of the heater and furnishes a good thermal conduction path to the component.

Cost and weight optimization. - The survey of thermal requirements aboard manned spacecraft established 37 different application areas requiring between 180 and 300 heaters. A survey of unmanned spacecraft applications would substantially add to these estimates; there is also the likelihood of additional applications evolving during hardware testing phases. It therefore seems logical to assume that all power levels in the 1- to 50-W range are equally probable. This rationale should serve as the basis for power level selection until such time as a better assumption may be substantiated.

Weight optimization: Table 8 gives the weights of the 5-, 10-, 25-, and 50-W Pu and Pm cermet reference heaters. Figure 23 presents weight vs power level for combinations of the same and different heater sizes. This curve is based on Pm heater weights; however, the same conclusions would be valid for Pu. The number(s) in each power level interval represents the lightest heater or combination of heaters that satisfies the power requirements of that interval.

From figure 23 it is seen that the weight differences between the lightest and the next heaviest heater or combinations which satisfy the given thermal requirement are small (generally < 1 lb). The important point is that all of the applications can be satisfied without incurring a significant weight penalty by using 10- and 50-W heaters either individually or by stacking and/or diluting.

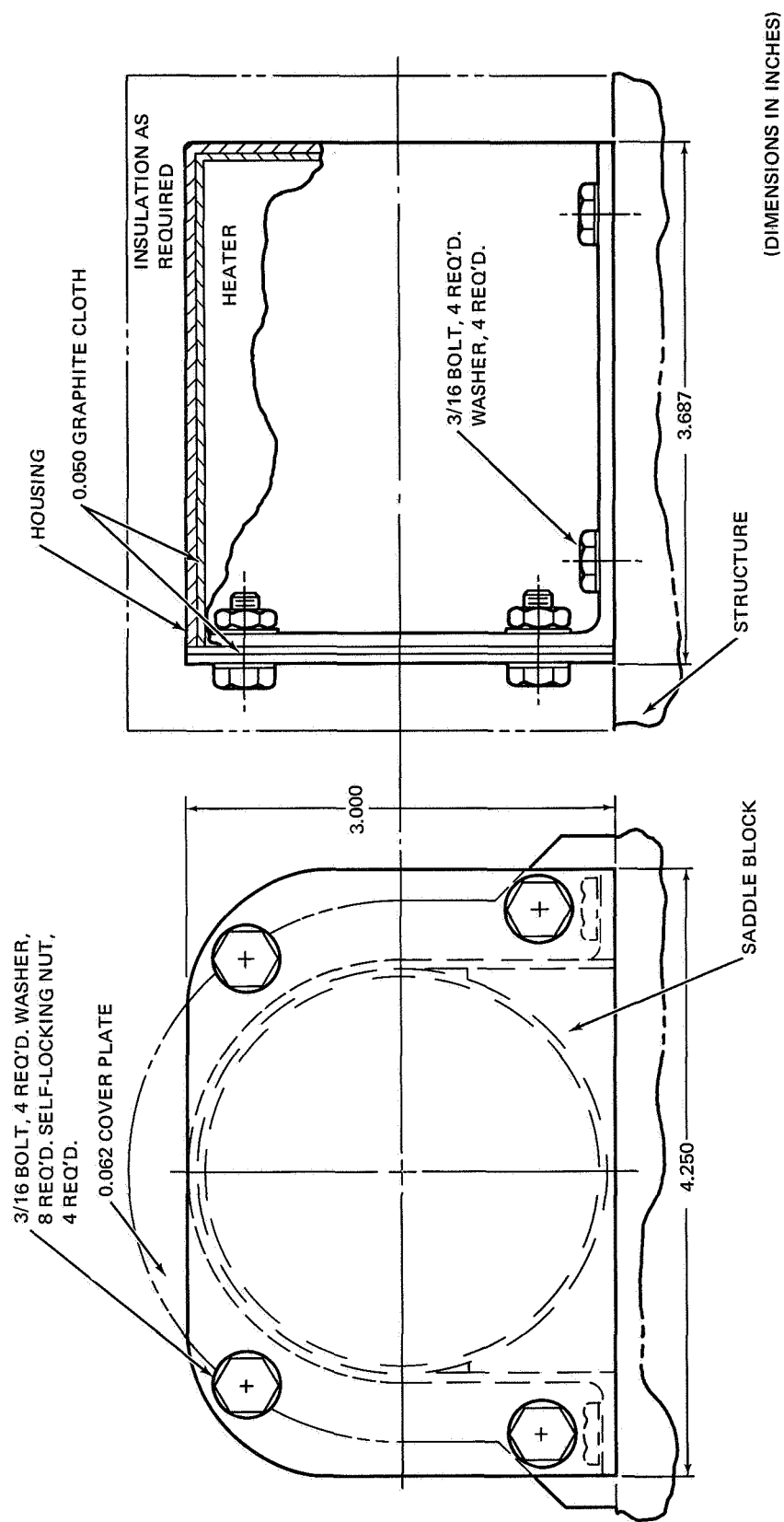


Figure 22. Representative Support for 50-W Heater

TABLE 8  
HEATER WEIGHTS AND REFERENCE DESIGNS

Pm <sub>2</sub> O <sub>3</sub> cermet	Weight (lb)
PMC-5-1	0.697
PMC-10-2	1.014
PMC-25-1	2.036
PMC-50-2	3.410
PuO <sub>2</sub> cermet (minimal size)	
PUC-5-1	0.530
PUC-10-3	0.740
PUC-25-1	1.524
PUC-50-3	2.423
PuO <sub>2</sub> cermet (uniform size)*	
PUC-10-4	0.964
PUC-50-4	3.205

\*All dimensions and material thicknesses of structural shell out to and including POCO graphite ablator are identical to the PMC heater designs.

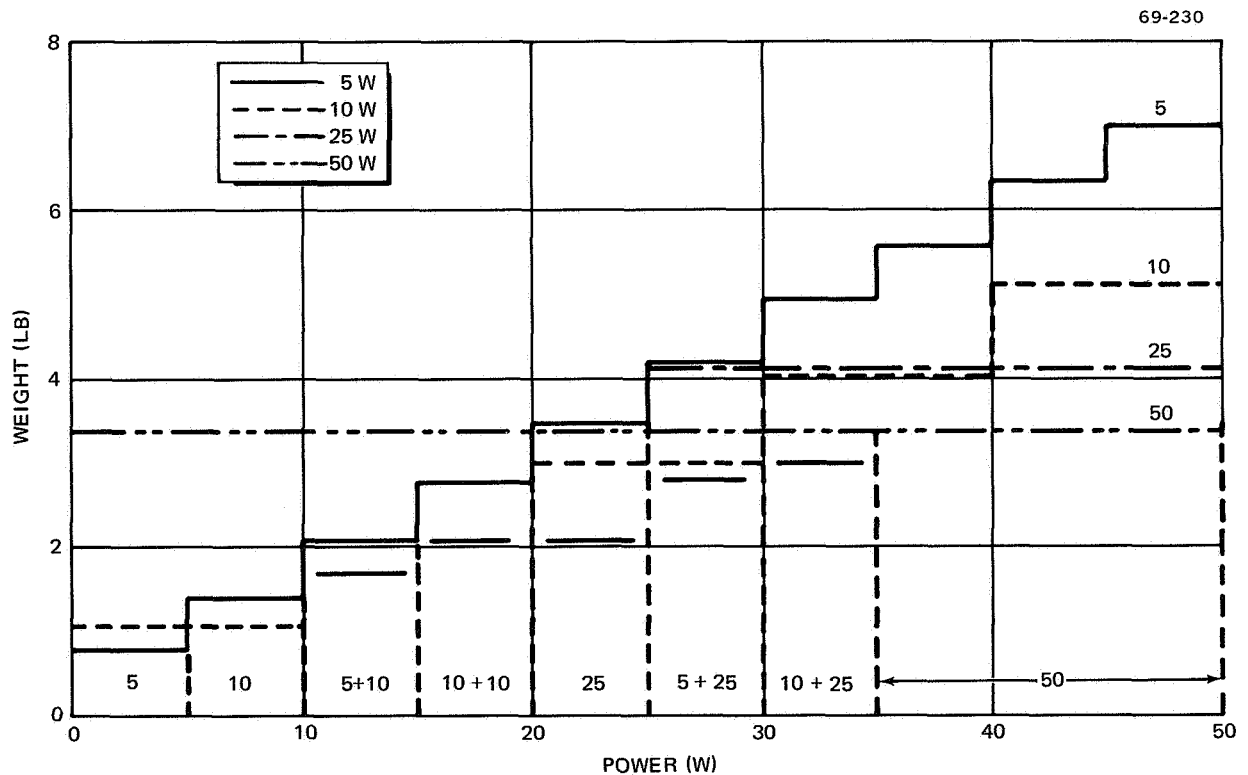


Figure 23. Heater Weight vs Power Comparison

Cost considerations for additional heater power levels: A cost-effective program requires a minimum number of different size heaters while adhering to minimal weight guidelines. Estimated development and qualification costs for a third heater size, if the 10- and 50-W heaters were previously developed and qualified, are \$150 000 to \$200 000. If a payload penalty of \$2000/lb is assumed, and if the small weight differences between heater combinations are considered, a large number of heater applications must exist in order to amortize the cost of producing an additional heater size. From figure 23 it is seen that the largest weight penalty incurred by producing only 10- and 50-W heaters occurs in the 20- to 25-W interval where three 10-W heaters weigh about 1 lb more than one 25-W size. It would require approximately 100 applications in the 20- to 25-W interval to justify production of a third heater size. For any other power interval, the number of applications required for amortization would be significantly higher since typical weight differences are a few tenths of a pound. However, if the payload penalty is on the order of \$50 000/lb because of launch vehicle and/or mission constraints, the development of a specific-sized heater would be justified.

Cost considerations for minimal vs uniform heater sizes: The Pm and Pu uniform-size heaters have the same outer dimensions and all material thicknesses are the same from the structural shell outward. From table 8, it is seen that the 10-W Pu cermet minimal heater size is 0.224 lb lighter than the uniform size, while the 50-W Pu heater is 0.781 lb lighter than the Pu uniform size. The uniform Pu heater provides a greater void/fuel volume ratio than does the minimal size and, thus, provides a greater margin of safety in terms of internal helium buildup.

The additional cost of fabricating and qualifying two different heater sizes for one power level is approximately \$80 000 to \$100 000. Many of the qualification tests such as ablation, impact, vibration, launch abort debris, etc., could be performed with only one heater size for each power level selected if the uniform-size series were chosen over the minimum-size series.

Engineering analyses and manufacturing development costs would also be reduced with a uniform heater size approach. Due to the relatively small weight differences (0.224 to 0.781 lb), it would appear difficult to justify the minimal size approach when considering the great number of heaters required to amortize the development costs of two different heater sizes for one power level. Finally, the uniform size approach permits interchangeability of Pm and Pu heaters since only one mounting arrangement is required for each power level.

Design approach and tradeoff study summary and recommendations. - Results of the design approach and tradeoff studies are summarized below; reference design recommendations are also presented.

Summary of results: Spherical capsules based on internal capsule volume equal to that for the reference designs weigh slightly less than the reference designs but are theoretically stronger in relation to internal pressure. The primary disadvantage at present is the high development cost required to



produce the spherical cermet-fueled capsule; as far as can be determined, no cermet-fueled spherical capsule has been fabricated to date.

Flat-ended cylindrical heaters with spherical fuel capsules will result in a net weight saving of about 10% while the cubic heater configuration results in a net increase of about 10% compared to the reference designs.

Use of a squared-off ablator such as a cube or rectangular parallelepiped results in substantially lower impact velocities, even considering possible rounding of the corners during reentry heating. In addition, the total heat load is less during reentry. Spheres and elliptical-ended cylinders are worst from the standpoint of heating and impact. Flat-ended cylinders fall in between. Some penalty is incurred regarding weight, volume, and surface area using the squared-off ablators. The amounts are shown in table 7. The cubic heater with the spherical fuel capsule (alternate A, table 7) is the best design from the standpoint of reentry and impact velocities.

Safety and design analysis and limited impact testing indicate that the reference heater designs meet established safety criteria and have a high probability of surviving all mission phases and environments.

Two reference design sizes, the 10- and the 50-W, will span the power range from 1 to 50 W without incurring significant weight penalties. Only in special situations would the development of a third size be warranted.

Use of uniform or standardized sizes for Pu- and Pm-fueled heaters incurs a small weight penalty when compared to the additional development, qualification, and production costs for minimum-size heaters.

Recommendations: The phase II safety analysis, design, and development should concentrate on the reference design. If budget and schedule permit, alternates A, B, and C (table 7) should be further analyzed and tested.

Only two heater sizes should be considered for development - the 10- and 50-W sizes. Pu and Pm heaters of the same nominal power level should be standardized. The spherical and rounded-end cylindrical ablator designs are not competitive in terms of reentry and impact velocities, although they are the lightest designs. It is recommended that these not be considered further.

Several additional criteria for final selection of the optimum shape have been identified. These areas, many of which do not submit to quantitative evaluation, require additional consideration; where possible, analyses and/or testing should be undertaken. A partial list of such areas include fabrication complexity; costs of development, qualification, and production; flexibility; and component and mission evaluations.

### Ablator Design Analysis

Ablator degradation in normal operation - The surface temperature of a radioisotope heater in normal operation will be determined by the heat balance relationship with the environment. Typical values range from 100° to

400°F. These temperatures may be maintained for a period of several years depending upon the length of the mission.

At these moderately elevated temperatures, long term degradation of certain ablation materials may result prior to reentry, thereby reducing the thermal performance of the ablator. An investigation was conducted to locate data pertaining to long term degradation of several characteristic ablator materials at temperatures corresponding to those experienced during normal operation. Types of degradation considered were sublimation, evaporation of the material itself or a volatile component in high vacuum, breakdown such as thermal rupture of polymer bonding, and oxidation. At elevated temperatures, these effects often result in significant changes in the properties of the material and in the reentry performance of the ablator. Data shown in table 9 (refs. 9 through 23) furnish general indications of material breakdown temperatures and are useful mainly for comparisons rather than for absolute values. Note that there is some disagreement among the various sources quoted; in particular, data concerning the various phenolics are quite incomplete.

TABLE 9  
SUMMARY OF MASS LOSSES FROM ABLATORS

Material	Sublimation, degassing, etc (%/yr)	Oxidation (mil/yr)	Temp (°F)
Graphites	<0.1	--	572
	--	c. 0.6	450
Pyrolytic graphite	Negligible	--	3000
	--	<0.001	450
Phenolics	On the order of 10	--	270
	Rapid decomposition	--	~400
Teflon	1.5 to 3.0	--	600

These data indicate that the phenolics will experience significant degradation, depending on operating temperature and mission life. Pyrolytic graphite appears to undergo negligible degradation, and the graphites and teflon appear to be little affected unless the temperatures involved are near 400°F and the mission lives are beyond 5 years.

Aerothermal analysis. - Aerodynamic characteristics of the heater designs are important; two critical areas of safety are protection from reentry heating and containment after earth impact. For both of these areas, ablator design, ablative material chosen, and its shape and thickness are prime factors. In this section, the designs are studied for independent reentry for lunar return and earth orbital decay trajectories. Basic phenomena involved and factors affecting the results are discussed and related to the designs.

Initial conditions: Initial flight characteristics are referenced to a 400 000-ft altitude over the North Pole. This is the normal atmosphere starting point since at this altitude, orbiting bodies of the type considered will not make a complete orbit before they fall to earth (the North Pole is taken only as a convenient point of reference).

The initial surface temperature of the heaters was calculated to be 240°F based on a space equilibrium condition. The internal temperatures were only a few degrees higher.

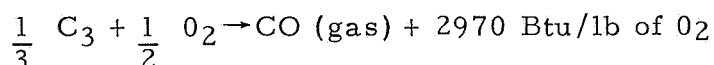
Initial velocities were assumed to be 25 694 ft/sec (circular velocity) for orbital decay and 36 300 ft/sec (corresponding to the Apollo velocity) for lunar return. Several selected flight angles for lunar return were considered from -90° to skip trajectories. A worst-case 0° flight angle for orbital decay was assumed.

The initial weights, projected areas, and weight-to-area ratios for the reference and alternate designs have been discussed. Detailed analysis of drag coefficients for different shapes and flow regimes is presented in appendix B, including a summary of drag coefficients used in trajectory calculations. The corresponding ballistic coefficients ( $W/C_D A$ ) for the various designs in different flight orientations are shown in table 10 for free molecule (upper atmosphere) flow, continuum hypersonic (heating) regime, and subsonic (impact) velocities.

Reentry environment: Using these initial conditions as input, trajectory calculations were made for the different designs at lunar reentry angles of -5.2°, -6.25° and -90.0°\*. In addition, trajectories for -20° and -38° lunar return angles were calculated for the reference 50-W Pm design. \*

The trajectory calculations were made using the differential equations of motion for a point mass relative to a rotating oblate earth. Variation of the drag coefficient through the various flow regimes was included. Throughout the trajectory, actual (corrected for body radius) heating rates were calculated using the Detra and Hidalgo correlations of the Fay and Riddell equations. Details of this code are given in appendix C.

Graphite ablation is calculated including combustion and sublimation, if any. The amount oxidized is computed assuming an oxygen diffusion controlled process and using the Reynolds analogy for boundary layer flow (mass flow proportional to heat flow). The oxygen flux is multiplied by the heat of combustion, assuming the reaction






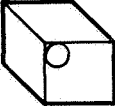
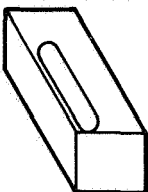
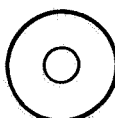
Dividing by the graphite density then gives the depth of graphite ablated.

The amount of graphite sublimated was computed by (1) assuming a sublimation temperature of 6000°F; (2) calculating the radiation heat loss at

---

\*Additional reentry angles were added to supplement those specified in the design criteria. A more comprehensive evaluation of trajectory conditions is required in phase II to ensure that all critical design conditions have been included.

TABLE 10  
BALLISTIC COEFFICIENT SUMMARY

Flow regime							Flight orientation							
	10-W	50-W	10-W	50-W	10-W	50-W	Side-on	Edge-on	10-W	50-W	10-W	50-W	10-W	50-W
fm*	10	18	10	18	10	19			12	20	16	28	14	26
Cont** (ave)	19	34	19	33	19	35			23	40	33	57	31	57
Sub***	113	202	113	198	115	210			18	31	26	44	188	351
fm*	22	41	18	32	19	37	End-on	Flat face first	17	28	20	36		
Cont** (ave)	24	45	20	35	32	62			18	31	22	40		
Sub***	63	116	51	90	153	297			33	56	40	72		
fm*	14	26	14	24	14	26	Random tumbling		17	28	20	36		
Cont** (ave)	24	43	20	35	26	48			18	31	22	40		
Sub***	109	197	107	190	148	274			33	56	40	72		
fm*	16	29	16	27	16	29	End-over-end tumbling							
Cont** (ave)	25	45	21	36	28	52								
Sub***	95	174	90	162	154	290								

\* molecular flow

\*\* continuum flow

\*\*\*subsonic flow

6000°F (495 Btu/ft<sup>2</sup> sec); (3) estimating the time period in which the heating will exceed 495 Btu/ft<sup>2</sup>-sec; and (4) taking a simple surface heat balance, neglecting oxidation heating, transpiration cooling, and heat transfer to the interior, but including re-radiation, aerodynamic heating, and sublimation.

Detailed results for the reference designs in an earth orbital decay trajectory are shown in table 11. The corresponding integrated heating results for the design alternatives are illustrated in figure 24 and compared with the reference design results. The heating rates are found to be too low to cause significant graphite sublimation regardless of orientation or stabilization. Therefore, the amount of graphite removal is small, and based only on diffusion-controlled oxidation. Some temperature results are shown in table 11; these calculations are discussed in detail in the next section.

Note in figure 24 that integrated heating at the stagnation point is nearly the same for the reference design oriented side-on and end-on. The effect of rounding the ends of the cylindrical ablator is evident by comparing the results for end-on for alternate D with the reference design. The flat-faced cylinder design of alternate C has lower heating end-on because of the decreased weight (table 7). Side-on, all cylindrical ablator designs have similar heating (alternate D has slightly higher heating).

In spite of its light weight, the sphere has very high integrated heating because of its lower drag coefficient. Lowest heating is attained by the cubic ablator design (alternate A). The rectangular-faced design (alternate B) falls in between alternate A and the reference case. These results emphasize the heating advantage of a high-drag flat-face ablator over the normal rounded shape.

A summary of lunar return trajectory quantities for the Pm<sub>2</sub>O<sub>3</sub> reference design is presented in table 12. Calculations are for the 50-W heater. Extreme reentry angles are -5.2° and -90°, the minimum and maximum angle return for an Apollo mission.

In addition, calculations were made for the 50-W reference heater for reentry angles of -20° and -38°. The integrated heating and corresponding graphite ablation for the 50-W heater oriented side-on and nonspinning is plotted in figure 25 as a function of lunar return angle. The sharp increase in integrated heating for small reentry angles is noteworthy. The worst case regarding heating of the capsule is the -5.2° trajectory resulting in 115 000 Btu/ft<sup>2</sup> at the stagnation point. Lower angles result in skip trajectories, and, although the total combined heating is greater, the amount at each pass is less than for -5.2°. The time between passes would cool the capsule. For example, at -5.0° the integrated heating for the first pass is 65 500 Btu/ft<sup>2</sup> and 70 100 Btu/ft<sup>2</sup> for the return. The time between first pass and return is about 3-1/4 hours, which is sufficient to cool the capsule. Even at 5.10°, the return time is 1-3/4 hours after first pass.

The skip trajectories, however, can result in more graphite removal. At -5.2°, the amount of graphite ablated for the nonspinning 50-W capsule is 0.34 in.; 0.16 in. is oxidized and 0.18 in. is sublimated. At -5.0° on the

SUMMARY OF REENTRY QUANTITIES FOR EARTH ORBITAL  
DECAY TRAJECTORIES, FLAT-HEADED CYLINDRICAL CAPSULE

Heater	Flight orien- tation	T-111 max temp (°F)	Peak heating rate (Btu/ft <sup>2</sup> -sec)	Time to peak heating rate (sec)	Integrated heating (Btu/ft <sup>2</sup> )	Time to impact velocity	Ablator thickness removed	
50-W Pm <sub>2</sub> O <sub>3</sub> reference design	End-on	2058	202 *	1630	49 000 *	1855	333	0.12 *
	Side-on non- spinning	1961	249 *	1385	50 300 *	1650	438	0.13 *
	Side-on spinning	2111	90	1385	18 100	1650	438	0.65
50-W Pm <sub>2</sub> O <sub>3</sub> reference with charring ablator	Side-on non- spinning	1572	249 *	1385	50 300 *	1650	438	0.134 *
10-W Pm <sub>2</sub> O <sub>3</sub> reference design	Side-on spinning	2150	78	1220	14 040	1557	329	0.03
5-W Pm <sub>2</sub> O <sub>3</sub> reference design	Side-on spinning	2180	77	1180	13 000	1537	302	0.03
25-W Pm <sub>2</sub> O <sub>3</sub> reference design	Side-on spinning	2132	86	1315	16 400	1596	390	0.04

\* At stagnation point

\* At stagnation point

TABLE 12

SUMMARY OF REENTRY QUANTITIES FOR LUNAR RETURN  
TRAJECTORIES, FLAT-HEADED CYLINDRICAL CAPSULE

Heater and trajectory	Flight orien- tation	T-111 max temp (°F)	Peak heating rate (Btu/ft <sup>2</sup> -sec)	Time to peak heating rate (sec)	Integrated heating (Btu/ft <sup>2</sup> )	Time to impact (sec)	Impact velocity (ft/sec)	Ablator thickness removed
50-W Pm <sub>2</sub> O <sub>3</sub> reference design								
6-1/4° lunar	End-on	1645	888 *	75	53 045 *	308	333	0.11 *
6-1/4° lunar	Side-on non- spinning	1574	1140 *	70	63 430 *	350	438	0.22 *
6-1/4° lunar	Side-on spinning	1683	411	70	22 800	350	438	0.04
90° lunar	End-on	797	4355 *	8	14 532*	88	333	0.03 *
90° lunar	Side-on non- spinning	826	5040 *	7	15 960*	136	438	0.06 *
90° lunar	Side-on spinning	947	1810	7	5740	136	438	0.02
5.2° lunar	Side-on spinning	2496	273	90	41 200	587	438	0.06
10-W Pm <sub>2</sub> O <sub>3</sub> reference design								
5.2° lunar	Side-on spinning	2315	270	90	26 500	497	329	0.04
* At stagnation point								

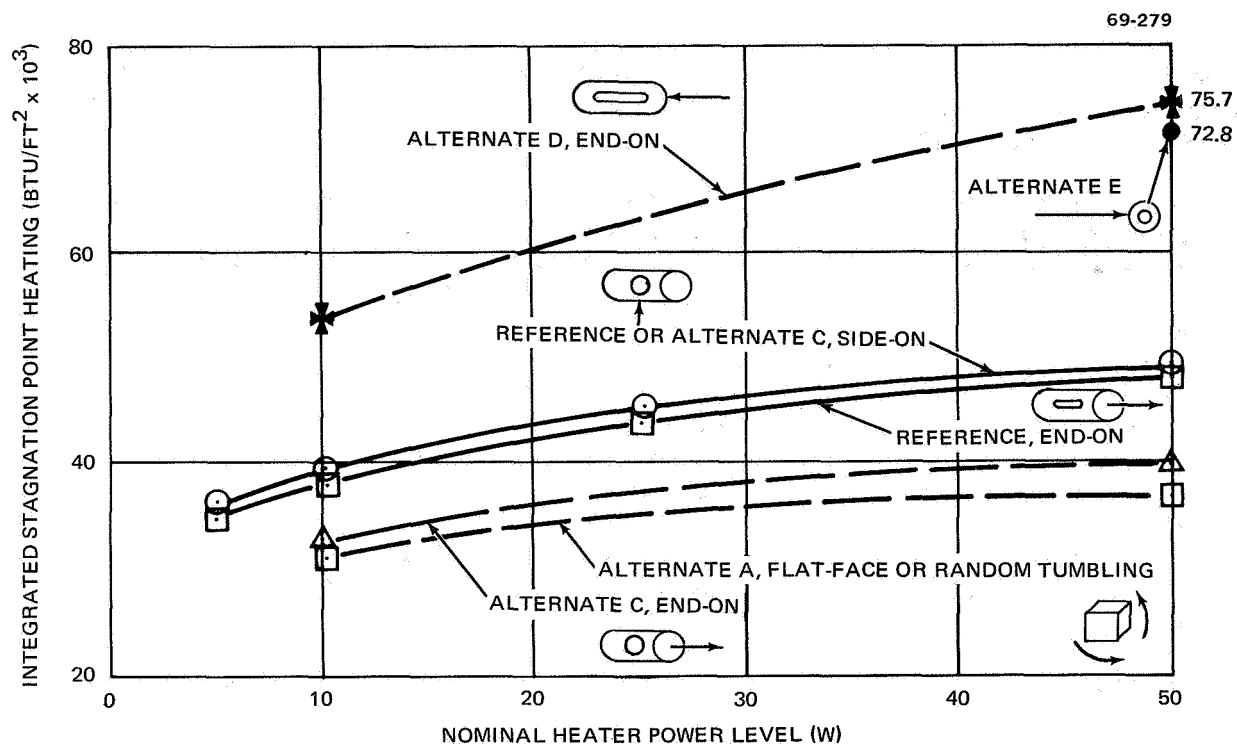


Figure 24. Earth Orbital Decay Integrated Heating for Different Designs

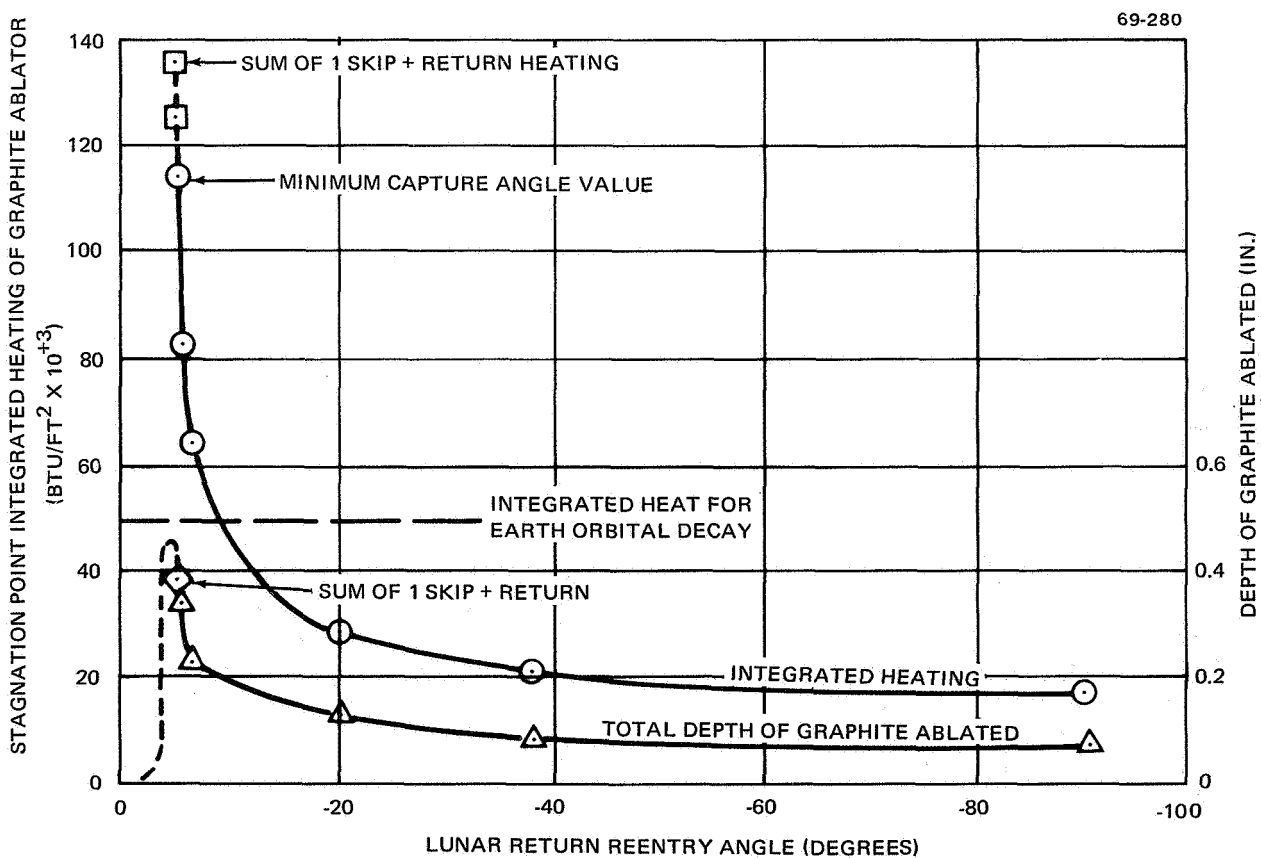


Figure 25. Cold-Wall Heating and Ablation at the Stagnation Point for 50-W Reference Design, Side-On Nonspinning on Lunar Return (For spinning capsule, multiply by 0.36)



first pass, 0.04 in. is oxidized and 0.09 in. is sublimated. On the return reentry, 0.13 in. is oxidized and 0.11 is sublimated. A total removal at  $-5.0^\circ$  is therefore about 0.37 in.

At angles lower than  $-5.0^\circ$ , the heating rates become too low to cause significant sublimation. For example, the peak heating rate at  $-4.0^\circ$  is about 134 Btu/ft<sup>2</sup>-sec, the integrated heating is 8710 Btu/ft<sup>2</sup>, and the amount of graphite oxidized is less than 0.0047 in. for the first pass. However, the number of orbits increases sharply for lower angles until a critical angle is achieved where, for practical purposes, the heater never returns. H. R. Spahr at Sandia has estimated (for a similar body) a lifetime of about 65 orbits for an initial reentry angle of approximately  $-4^\circ$ . The method of calculation was probably conservative, depending on the relative position of the moon at the particular time. Although velocity decreases with each orbit, the orbit becomes more circular and the body lingers longer in the atmosphere. Ablation is likely to increase somewhat with each orbit. Assuming an average ablation depth of 1.5 times the depth ablated on the first pass, and taking 65 orbits at  $-4.0^\circ$ , the total depth of graphite ablated is about 0.45 in. This should be close to the worst case since the angle of no return is approximately  $-3.0^\circ$ .

Calculations were also made for alternate A, the cubic design with the lowest heating, for a  $-5.2^\circ$  lunar return trajectory. Results for both the 10- and 50-W heater are shown in table 13.

TABLE 13  
ALTERNATE A DESIGN REENTRY QUANTITIES FOR  $-5.2^\circ$  LUNAR RETURN

	Flight orient.	T-111 max temp (°F)	Peak heat- ing rate (Btu/ft <sup>2</sup> -sec)	Time to peak heat- ing (sec)	Integrated heating (Btu/ft <sup>2</sup> )	Time to impact (sec)	Graphite ablated (in.)
50 W	random	2226	504 *	90	68 600	566	0.11 *
10 W	random	----	505 *	90	49 800	538	0.09 *
* At stagnation point							

Note the significantly lower heating and amount of graphite ablation for this design compared with the results in figure 25 for the reference design. The cubic ablator does not generally sublimate at the stagnation point, although a small amount of sublimation will occur at the edges. The amount of sublimation is not enough to alter the basic shape. The cubic ablator appears to offer a greater advantage at these severe conditions than it does in earth orbital decay, assuming that the outer ablator material is graphite or a material with a high heat of ablation where the basic cubic shape remains unchanged.

Thermal response: The previously computed trajectory and heating parameters were used as inputs to the heat transfer and ablation programs

to determine the thermal response in various regions of the capsule during reentry. These time-dependent parameters included velocity, stagnation enthalpy, cold-wall heat flux, and oxygen flux to the surface. In addition, the time-to-impact and impact velocity were determined.

These parameters served as inputs to the TAP-3 and STAB-2 codes for subliming and charring ablators, respectively. The complete nodal systems used in the models for the various flight orientations are given in appendix D.

For several reference heater trajectories and flight orientations, the temperatures obtained for (1) the ablator surface, (2) the T-111 layer, and (3) the fuel center are presented in figures 26 through 31 as functions of time. For the side-on, nonspinning, and end-on flight orientations, these points were chosen at stagnation point of the capsule to reflect the maximum temperatures reached in each layer of the multilayered capsules.

The critical T-111 peak temperatures for all cases analyzed appear in tables 11 and 12. Because of the large number of combinations of fuel and fuel form, capsule geometry, capsule power level, type of ablator, trajectory, and flight orientation parameters, the total number of possible reentry cases is several hundred. Only those situations which represent either worst or critical cases were analyzed. The results are shown in tables 11 and 12.

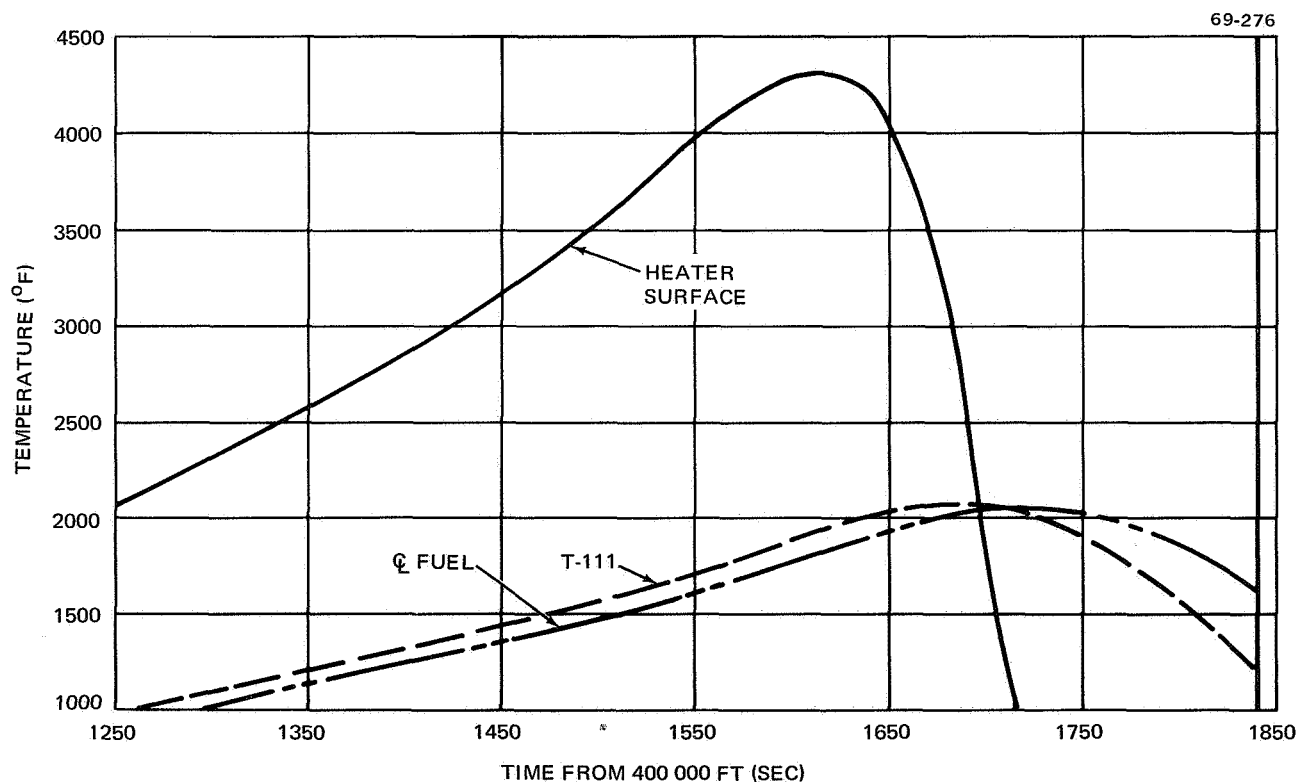


Figure 26. Temperature Response of 50-W  $^{147}\text{Pm}$  Heater, Reference Design Earth Orbital Decay, End-On

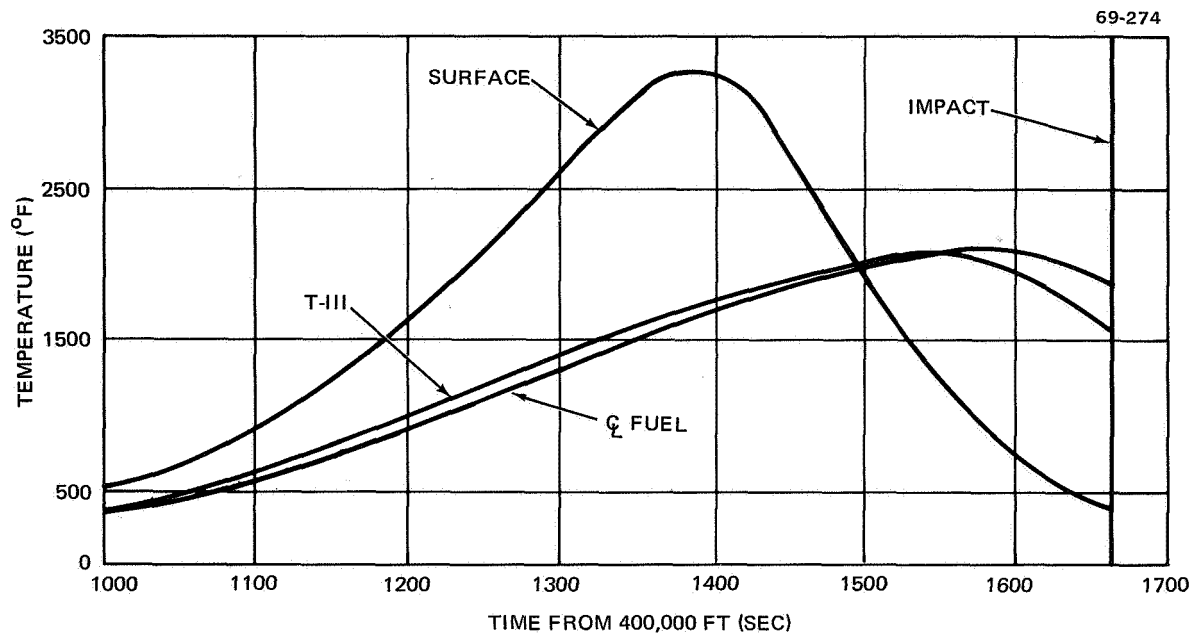


Figure 27. Temperature Response of 50-W  $^{147}\text{Pm}$  Heater, Reference Design, Earth Orbital Decay, Side-On Spinning

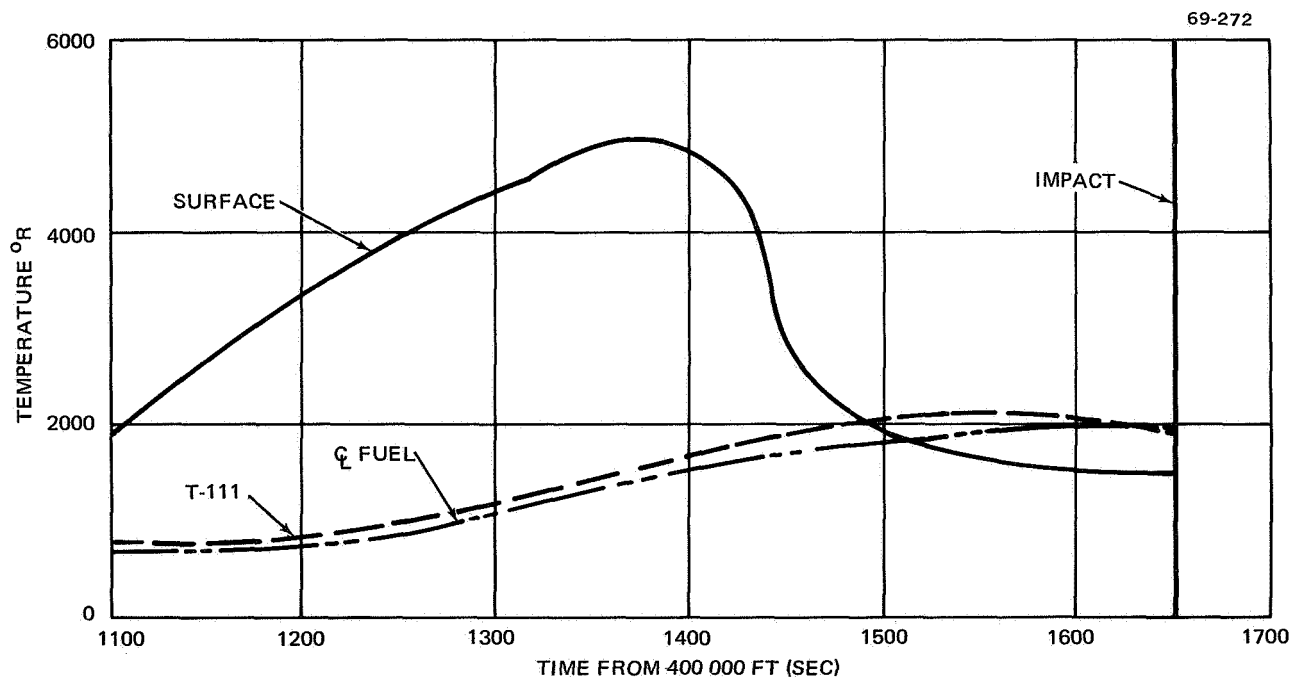


Figure 28. Temperature Response of 50-W  $^{147}\text{Pm}$  Heater, Reference Configuration with Charring Ablator Earth Orbital Decay, Side-On Nonspinning

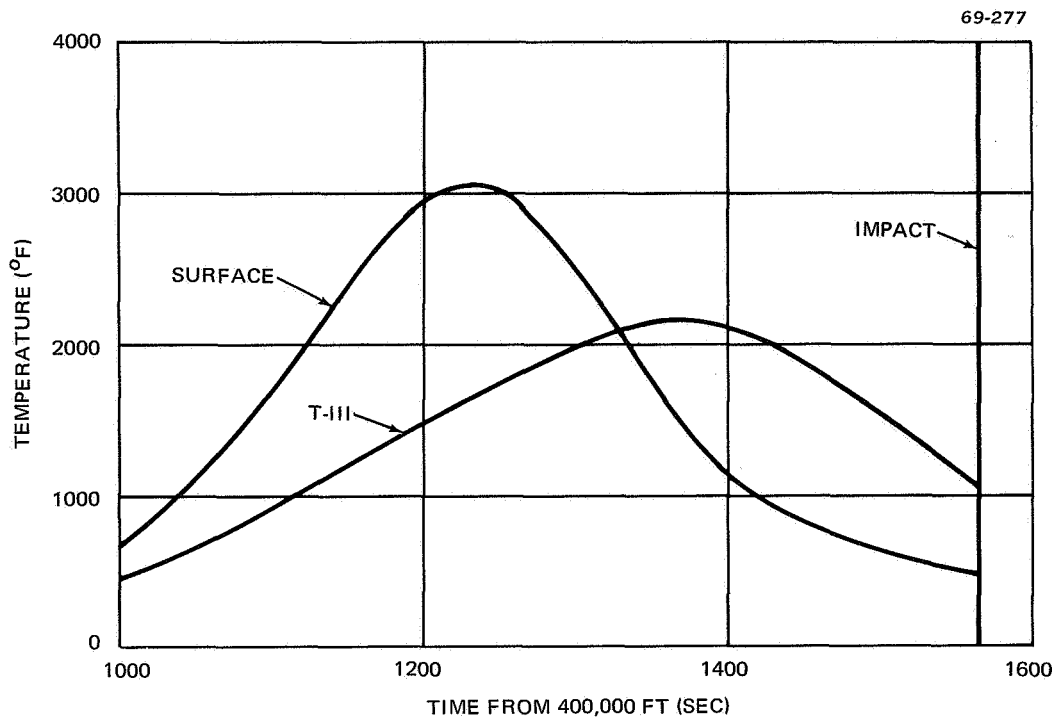


Figure 29. Temperature Response of 10-W  $^{147}\text{Pm}$  Heater, Reference Design, Earth Orbital Decay, Side-On Spinning

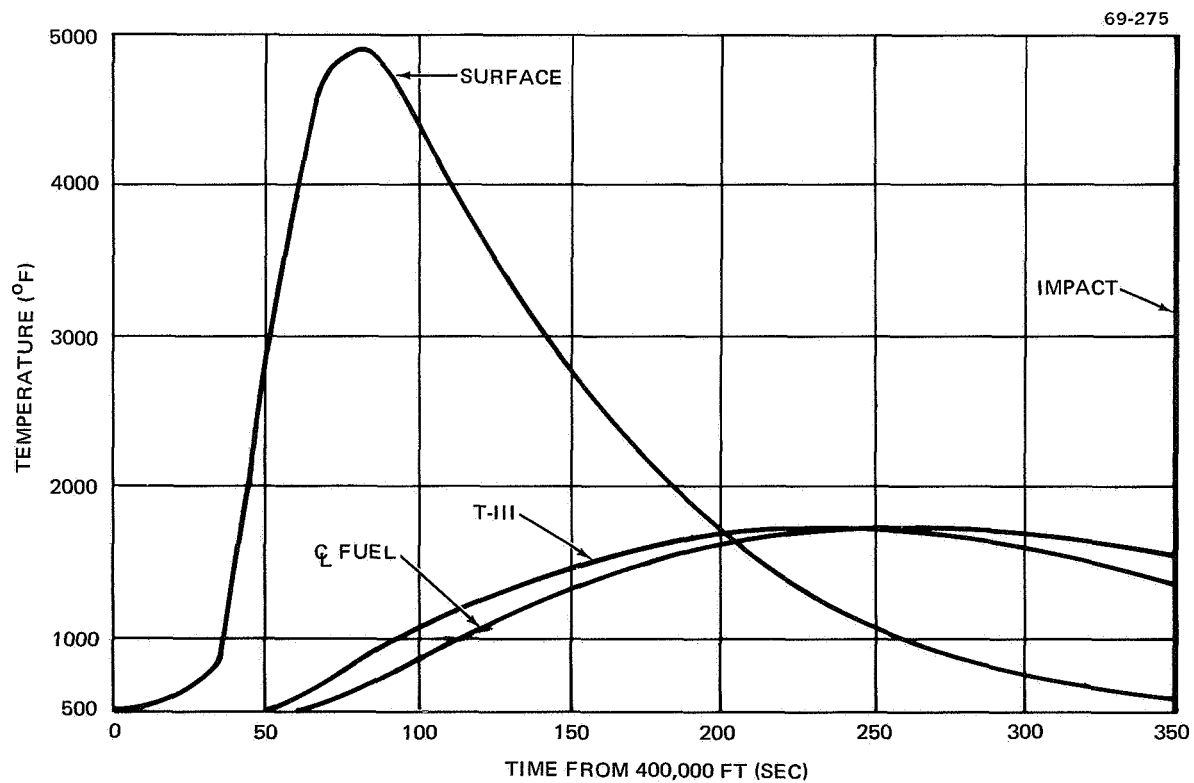


Figure 30. Temperature Response of 50-W  $^{147}\text{Pm}$  Reference Heater  $6\frac{1}{4}^\circ$  Lunar Return, Side-On Spinning

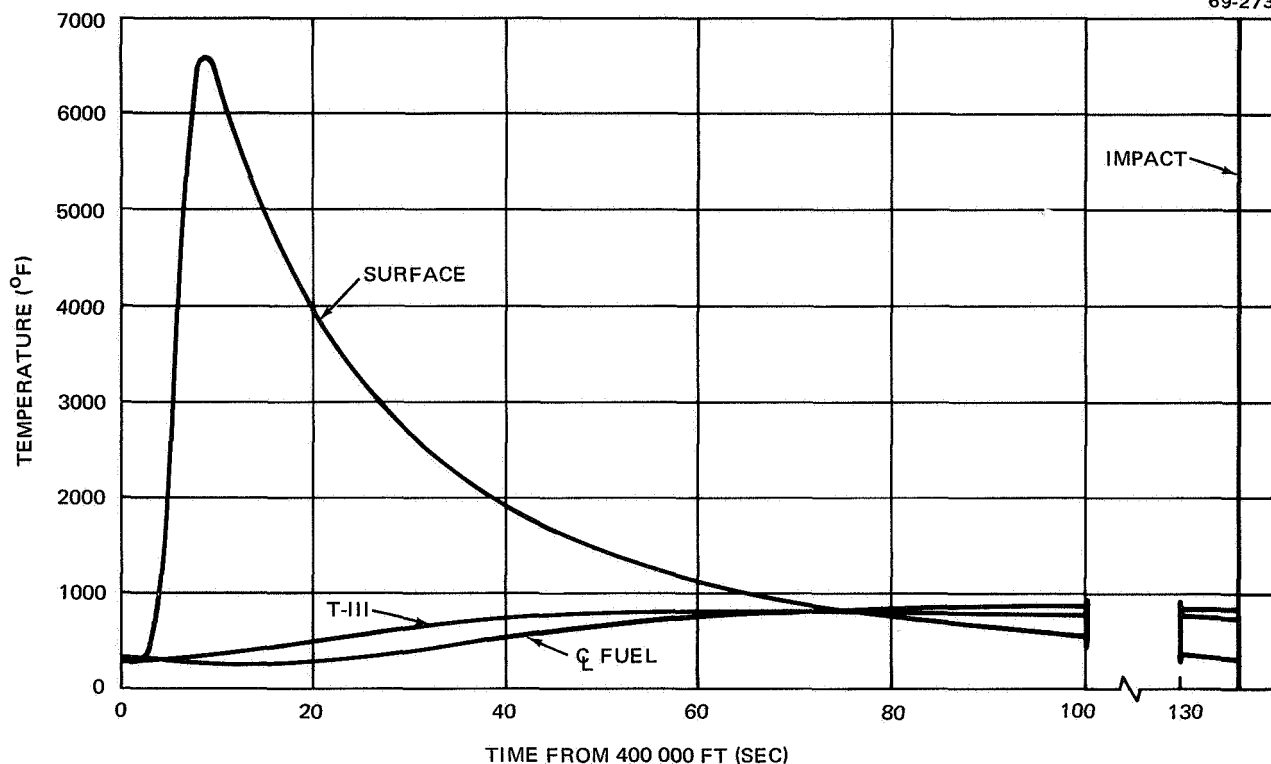


Figure 31. Temperature Response of 50-W  $^{147}\text{Pm}$  Heater, Reference Design,  $90^\circ$  Lunar Return, Side-On Nonspinning

In addition to the results for the reference design, thermal response calculations were performed for the cubic ablator (alternate A) design. The results are presented in table 14. Calculations were made assuming uniform heating on the surface for a random tumbling mode and using a one-dimensional spherical TAP-3 model. Although local heating effects will occur at the cube edges, uniform temperatures inside the insulation appears to be a reasonable assumption in view of anisotropic thermal conduction characteristics of pyrolytic graphite. An average-to-stagnation-point heating factor of 0.30 was assumed for the cubic shape in a tumbling mode.

TABLE 14  
TEMPERATURE RESULTS FOR ALTERNATE DESIGNS

Design	Trajectory	Orientation	Peak average surface temp ( $^\circ\text{F}$ )	Peak T-111 temp ( $^\circ\text{F}$ )
50-W cu. (alt. A)	Earth orbital decay	Random tumbling	2700	2058
50-W cu. (alt. A)	$-5.2^\circ$ lunar return	Random tumbling	2226	3556

**Thermal stress:** A thermal stress analysis of the 50-W, side-on, non-spinning earth orbital reentry case indicated low stress levels. Maximum thermal gradients occur for a  $-90^\circ$  lunar return trajectory. The surface temperature rises quickly to  $6000^\circ\text{F}$  while the internal temperature is approximately  $1000^\circ\text{F}$ . A difference of several thousand degrees exists from front face to back if no rotation occurs. The highest temperature differential across the 1/4-in. -thick POCO layer was found to be about  $2000^\circ\text{F}$  while the maximum gradient across the insulating pyrolytic graphite was  $3000^\circ\text{F}$ . Detailed thermal stress analyses should be performed for this critical condition when more accurate temperature profiles become available during phase II of the program.

The dynamic pressure forces are also greatest at  $-90^\circ$  lunar return. As the capsule reenters the dense atmosphere, decelerations up to  $363\text{ g's}$  are encountered. This occurs just after peak heating. The stagnation enthalpy, which is about  $26\,000\text{ Btu/lb}$  at high altitudes during the lunar return trajectory, averages about  $10\,000\text{ Btu/lb}$  at the time of peak stagnation pressure.

Test information regarding the capability of POCO graphite to withstand mechanical failure or erosion at these conditions is encouraging if not conclusive. POCO graphite was developed to provide outstanding thermal stress characteristics and mechanical properties. It was extensively tested as a nose cone candidate material under extreme reentry conditions in the RESEP (ref. 24) program conducted by MDAC. The range of aerodynamic test conditions exceeded those for  $-90^\circ$  lunar return. Ablation rates of the POCO specimens compared closely with those for thermochemical ablation alone at conditions of interest. Thermal stress failure was never observed at any of the test conditions. Detailed analysis is required to compare the test thermal stress with that occurring in flight.

**Alternate ablators:** The analysis presented above delineates the capability of the 1/2-in. -thick POCO-pyrolytic graphite ablator/insulator design to withstand heating and ablation during reentry. The ablator shape has a significant bearing on aerodynamic heating and, therefore, on internal temperatures. The block ablator (cubic or rectangular-faced) results in the lowest heating and temperatures, particularly in the critical area of shallow-angle lunar return.

The flat-ended cylinder design results in tolerable internal temperatures and graphite ablation depths for all reentry trajectories with the possible exception of lunar return at angles less than about  $-6^\circ$ . In the critical area, the ablation depth could be as great as  $0.45\text{ in.}$ , but only for a very narrow range of critical angles and only for nonspinning side-on orientation. This means that the POCO graphite could conceivably be completely stripped away and, assuming that the pyrolytic graphite layer is mechanically strong enough so that no spalling occurs, only  $0.050\text{ in.}$  of pyrolytic graphite would remain. Obviously, internal temperatures for this case would be prohibitive. The cylindrical ablator design, therefore, meets safety needs for protection from reentry heating for the great number of missions involving earth orbital reentry and for lunar missions where return trajectories preclude angles less than about  $-6^\circ$ . Additional ablator requirements are needed for missions where the

critical area cannot be precluded. The design was not changed to include these requirements since this would unnecessarily penalize the majority of applications involving only earth orbital return.

On the other hand, analysis indicates that design alternate A (cubic ablator) meets all reentry protection requirements, even at critical angle conditions. There are two main reasons for this: (1) Reentry heating is so low that no appreciable graphite sublimation occurs, and (2) graphite removed by oxidation comes primarily from the edges where the thickness is greatest. Further analysis at the critical lunar return angles is recommended for this design.

It is clear from the results presented in this report that, where possible, shapes such as spherical and rounded ends for cylinders should be avoided in order to reduce aerodynamic heating and impact velocity.

The graphite materials were found to exceed the performance of alternate ablator materials such as Teflon, glassy materials such as quartz, and charring ablators. The Teflon ablator thickness which would be required for the 50-W reference capsule on lunar return at  $6\text{-}1/4^\circ$  was calculated to be about 2 in. The result for quartz was about  $1\text{-}1/2$  in. These thicknesses result in a severe weight penalty.

As expected, only charring-ablator composites composed mostly of graphite or carbon were found to have heats of ablation on a level of that for pure graphite. In particular, Narmco 4047 was analyzed and compared. This phenolic graphite material has a low density ( $74\text{ lb/ft}^3$  compared with  $127.5\text{ lb/ft}^3$  for POCO) and a heat of ablation equivalent to graphite. The plastic pyrolyzes at intermediate temperatures, thereby reducing incoming heat and leaving a low density of carbonaceous char.

Narmco 4047 was found to compare well with POCO for reentry transients with long soak periods. This is shown in table 11 where the amounts of ablation are similar and the backface temperature for the charring ablator is several hundred degrees less. Aside from questions of material degradation, there remains the question of whether the low-density graphite char can withstand the dynamic pressure loading and thermal stresses of steep-angle reentry.

## Structural Analysis

Pressure vessel analysis. - A limit which is imposed on the capsule design is the requirement that the T-111 structure contain the internal helium buildup from plutonium fuels for a 20-year orbital life. The reference capsule designs were analyzed to ensure that this requirement was satisfied. The T-111 pressure vessel walls were considered to be 0.120 in. thick for the 50-W heaters and 0.060 in. thick for the 10-W heaters, in the shape of a circular cylinder with semiellipsoidal heads. No credit was taken for the strength of the platinum oxidation barrier; and a conservative assumption of 100% release of helium from the fuel was made. Longtime T-111 creep was not analyzed because the capsules are at maximum temperature for only a

few minutes during reentry. Reentry and earth burial are the only conditions where significant pressure stress occurs.

a. Reentry after 20-year orbital life: The amount of helium generated is solely dependent on the amount of  $^{238}\text{Pu}$  undergoing transmutations. However, the amount of helium released from the interstitial volumes of the fuel is a complex process dependent on temperature, pressure history, and fuel form. For the design case where 100% of the helium is released, the ideal gas equation may be combined with the expression for radioactive decay to determine the pressure within the T-111 structure, 20 years after encapsulation, as a function of the absolute temperature of the gas and of the void-to-fuel-volume ratio of the capsule. The gas temperature was conservatively taken to be equal to the T-111 temperature.

The stresses were computed for a right circular cylinder having semi-ellipsoidal ends. The discontinuity stresses at cylinder-ellipsoid junctions were included in the analysis (ref. 25 ).

Several methods of predicting failures in materials are amenable to hand calculations, notably the maximum stress theory, maximum strain theory, and Von Mises' theory. Of these, Von Mises' theory gives perhaps the best agreement with experimental results for ductile materials such as T-111 (refs. 26, 27, and 29). This method predicts yielding if

$$\sigma_e \equiv \sqrt{\frac{(\sigma_1 - \sigma_2)^2 + (\sigma_2 - \sigma_3)^2 + (\sigma_3 - \sigma_1)^2}{2}} \geq \sigma_y \quad (1)$$

where the  $\sigma_i$  are principal stresses and  $\sigma_y$  is the yield strength in simple tension. The quantity,  $\sigma_y$ , is temperature-dependent--strongly so at higher temperatures. Values of  $\sigma_y/\sigma_e$  were computed for several capsules and flight orientations for the earth orbital decay trajectory, which produces the highest T-111 temperature during the heating transient.

Table 15 presents flight orientation, peak temperatures, corresponding pressures within the T-111 structural shell, and the quotient  $\sigma_y/\sigma_e$ , which is a type of safety factor. The results indicate that, within the accuracy of the Von Mises' yield theory, there should be no difficulty caused by helium pressure buildup for the T-111 thicknesses selected in the reference designs, although the PUC-10-3 T-111 structure may undergo some yielding if it reenters in the side-on spinning mode.

b. Earth burial temperature and pressure: Helium containment after earth impact is also of concern since safety criteria dictate a containment period of 10 half-lives. Soil burial may produce capsule heat significantly above normal operating temperatures and thereby lead to increased helium pressure.

Capsule surface temperatures for soil burial were determined for a cylindrical, stationary (non-self-burying) capsule in a homogeneous, infinite



TABLE 15  
SUMMARY OF PRESSURE VESSEL ANALYSIS  
RESULTS FOR REENTRY

Heater designation	Flight orientation	Ratio void/fuel	T-111 temperature (°F)	Pressure (psi)	$\sigma_y / \sigma_e$
PUC-10-3	Side-on spinning	1.065	2150	8178	0.96
PUC-10-4	Side-on spinning	2.01	2150	4333	1.54
PUC-50-3	End-on	1.04	2058	8079	1.26
PUC-50-4	Side-on	1.82	2111	4714	1.76

medium (depth below soil surface greater than about 10 capsule diameters). Soil thermal conductivities ranging from 0.22 to 0.24 Btu/hr-ft-°F were used, based on unpublished data from J. B. Boyd, Sandia. These values are lower than the thermal conductivity of approximately 70% of the earth's land surface. The equation relating capsule heat generation and capsule surface temperature for soil burial is:

$$T_s = \frac{Q \ln(n + \sqrt{1 + n^2})}{2\pi K_s L} \quad (\text{ref. 29}) \quad (2)$$

where  $T_s$  = capsule surface temperature above soil temperature (°F)  
 $Q$  = capsule power (Btu/hr)  
 $n$  = capsule length/diameter ratio  
 $K_s$  = soil thermal conductivity (Btu/hr-ft-°F)  
 $L$  = capsule length (ft)

Burial temperatures above soil ambient for 10- and 50-W capsules, with and without ablators, are shown in table 16 for the promethia cermet, plutonia cermet, and plutonia bare microsphere fuel forms, at the power levels at which maximum temperatures are produced.

The highest burial temperature would occur for a heater with ablator and insulator removed. Assuming this condition, maximum pressure during burial may be determined by differentiation of the pressure-time relationship. The resulting maximum pressure for the PUC-50-3 heater was found to be 11 909 psi and the T-111 temperature at that time was 174°F. Since the T-111 strength is quite high at such a low temperature, the value of the safety factor,  $\sigma_y / \sigma_e$ , was higher than during reentry: 1.90 vs 1.26.

As in reentry, no credit was taken for helium retention by the fuel. While data for this phenomenon are uncertain, it is quite possible that, at

TABLE 16  
SOIL BURIAL TEMPERATURES

Fuel form	Nominal power level (W)	Capsule surface temperature above soil ambient (°F)	
		With ablator	Without ablator
Promethia cermet	10	144	257
	50	477	724
Plutonia cermet	10	138	263
	50	460	729
Plutonia bare microspheres	10	140	271
	50	473	762

temperatures experienced during burial, a significant portion of the helium would be retained in the fuel.

Impact. - Analytical methods for determining material failure due to impact loading are not sufficiently developed to guarantee safety. Therefore, DWDL has a continuing Independent Research and Development program for impact testing of simulated design configurations.

The most recent test specimens simulated 10- and 50-W heaters. Tests showed that T-111 in the 10-W reference design configuration (no platinum or graphite present) can withstand impact against granite at 420 ft/sec.

The majority of the specimens showed major deformation after impact, but appeared to provide complete fuel containment. Subsequent helium leak measurements showed, however, that in many cases, small cracks were present in the T-111 shell. These were caused by a combination of oxidation on the outer surface and intergranular attack on the T-111 by the fuel simulant on the inside surface at the corners where maximum stress occurs. Subsequent impact tests will use a fuel simulant more nearly representative of the radioisotope fuel.

The design used in the test specimens allowed a weld penetration of 2/3 of the T-111 structural shell and resulted in increased deformation of the shell in the impact area. The weld area was redesigned to give greater penetration and, thus, reduce shell deformation.

Photographs, impact test conditions, and results are included in appendix E.

Ocean burial considerations. - Calculations for a cylindrical container indicate that for burial at a depth of 17 000 ft, the value for the measure of safety,  $\sigma/\sigma_a$ , is 2.61 for the PMC-50-2 capsule and 2.27 for the PMC-10-2

capsule. The 17 000-ft depth exceeds that of approximately 85% of the ocean floor. Note that the safety factor is based on structural vessel yield strength. Because of inner structure support, no buckling is expected.

The heater will meet the ocean depth static overpressure criterion of  $10^{-2}$  MPC at the ocean surface. Assuming no vertical mixing limit and hemispherical dispersion, the depth at which a point release will produce  $10^{-2}$  MPC at the surface is 11 500 ft for  $^{238}\text{Pu}$  and 5200 ft for  $^{147}\text{Pm}$  (see discussion under Ocean Water Contamination in this report).

Ocean burial temperatures were calculated based on natural convection from a cylindrical capsule in a horizontal orientation. Capsule surface temperatures would be less than  $5^{\circ}\text{F}$  above ocean ambient temperatures for all heater designs.

Oxidation and sea water corrosion. - Although 0.020-in. -thick platinum had been tentatively selected for an oxidation- and corrosion-resistant cladding, investigation of other materials was undertaken. A literature search was conducted for data indicating the behavior of several candidate materials in the following environments; sea water at temperatures of  $80^{\circ}$  to  $200^{\circ}\text{F}$  and soil at  $100^{\circ}$  to  $1500^{\circ}\text{F}$ . The materials included nickel, cobalt, Hastelloy C, Hastelloy X, Haynes 25, T-111, and Pt.

Published data were found to disagree by orders of magnitude. However, a summary is presented in table 17 of representative oxidation and sea water corrosion rates in mils/year for the different materials at various temperatures (refs. 30 through 43). It is generally assumed that oxidation is the main corrosion mechanism when capsules are buried in common soils (ref. 30).

The listings in table 17 confirm the selection of platinum. Nickel and cobalt apparently will not meet the sea water and soil corrosion requirements associated with 10-half-life fuel containment. The melting points of Hastelloy C, Hastelloy X, and Haynes 25 are in the neighborhood of  $2300^{\circ}$  to  $2500^{\circ}\text{F}$ , which is only slightly above the temperatures reached during reentry. Platinum and T-111 have melting points well above the maximum temperatures expected during reentry. The T-111 structural container also has excellent resistance to sea water corrosion and oxidation at moderate temperatures.

### Shielding and Dose Rate Analysis

Dose rates at 1 meter from the Pu and Pm heaters were calculated considering heater power, shield material, and shield thickness as parameters. Pertinent results are presented in figures 32 through 35.

$^{238}\text{Pu}$  heater dose rates. - The reference design 10- and 50-W Pu-fueled heaters will produce 0.6 and 2.8 mrem/hr (respectively) at beginning of life at 1 meter from source center. This dose rate will increase slightly with age to 0.7 and 3.3 mrem/hr 6 years after encapsulation. These results and the relationships between heater power, shield material thickness, capsule age, and radioisotope purity are shown in figure 32.

TABLE 17

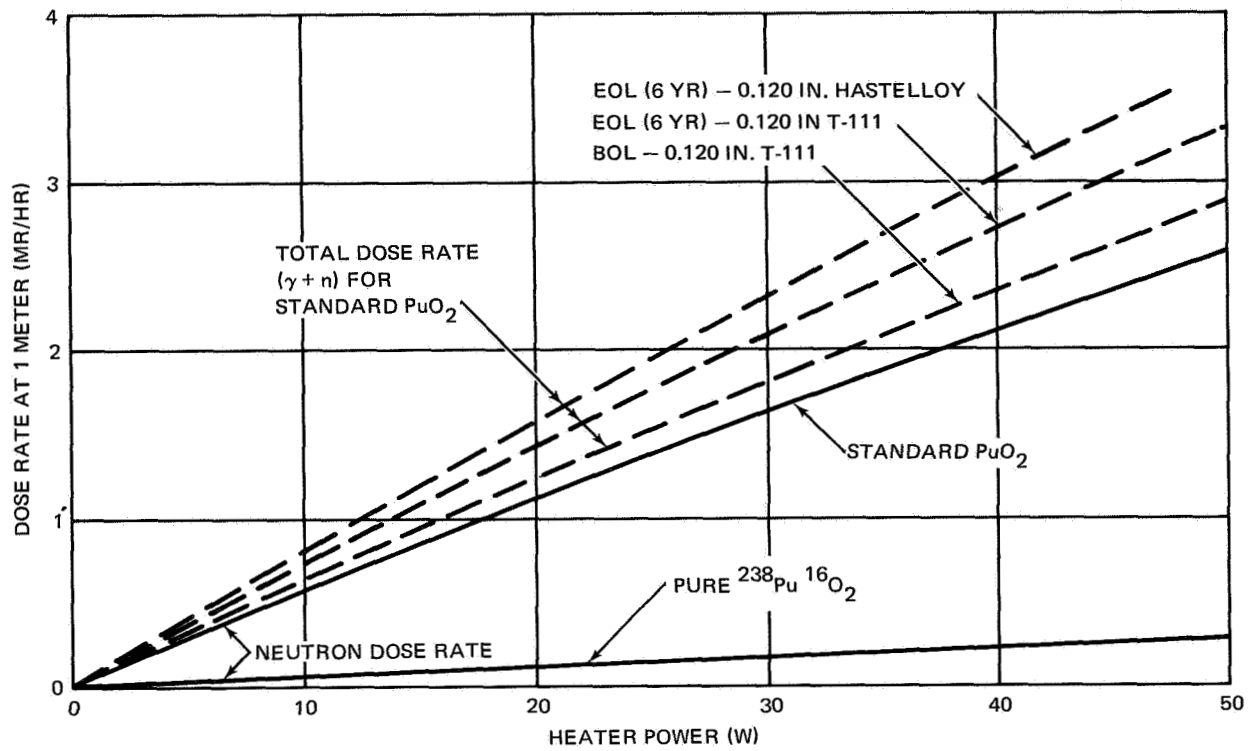
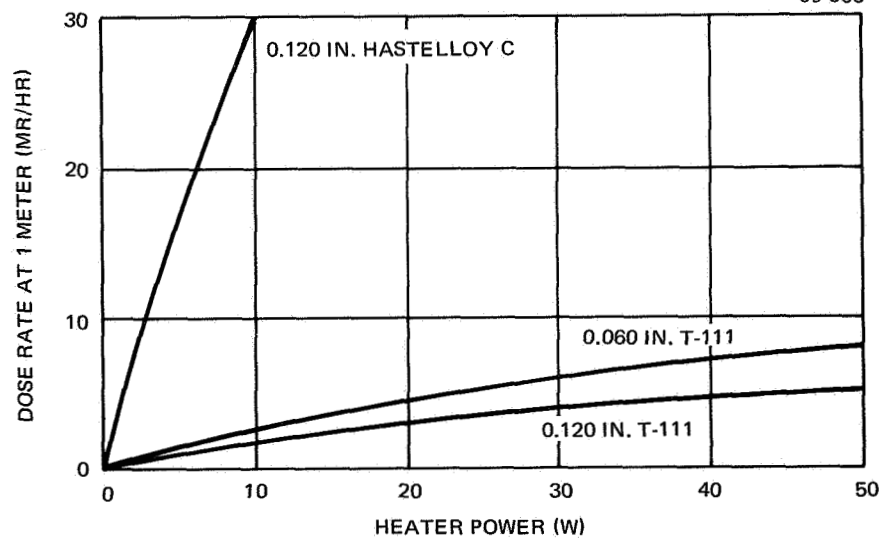
## MATERIAL OXIDATION AND SEA WATER CORROSION RATES

Material	Oxidation (m/yr)	Sea water corrosion (m/yr)	Temp(°F)
Platinum	<0.001	--	1200
	--	0.001-0.005	room
Nickel	negligible	--	1470
	--	0.5-1 (bad pitting also)	room
Cobalt	0.6	--	750
	--	0.18 (distilled water)	77
Hastelloy C	~0.1	--	up to 800
	--	< 0.05	up to 400
Hastelloy X	~0.1	--	up to 800
	--	< 0.05	up to 400
	--	0.09 (steam)	1022
Haynes 25	~0.1	--	up to 800
	--	<0.0035	up to 400
T-111	<0.035	--	536
	--	~ 0.001-0.005	room

External dose rate from  $^{238}\text{Pu}$  heaters consists of neutron and gamma ray contributions. Neutrons come from spontaneous fission of  $^{238}\text{Pu}$  and from  $(\alpha, \eta)$  reactions with light element contaminants (if present). Gamma rays come from decay of  $^{238}\text{Pu}$  and from decay of the daughter products of other Pu isotopes. At beginning of life, the principal gamma ray source is  $^{238}\text{Pu}$ , while after several years, decay products of  $^{236}\text{Pu}$  (principally  $^{208}\text{Tl}$ ) become dominant.  $^{236}\text{Pu}$  is initially present at 1 ppm.

Neutron dose rates are based on neutron emissions of  $3 \times 10^4$  and  $2.2 \times 10^3$  n/sec/gm- $^{238}\text{Pu}$  respectively (refs. 44 and 45) for standard and purified  $^{238}\text{PuO}_2$ . Purification of  $\text{PuO}_2$  assumes removal of all light-element contaminants and preparation of  $\text{PuO}_2$  with enriched  $\text{O}^{16}$ . The beginning-of-life gamma dose is shown added to the standard  $\text{PuO}_2$  neutron dose to give total beginning-of-life dose rates between 0.6 and 2.7 mrem/hr for 10- to 50-W capsules containing 0.120 in. of T-111. End-of-life dose rates for both T-111 and superalloy capsules are shown. Note that the use of superalloy shielding is permissible for Pu.

$^{147}\text{Pm}$  heater dose rates. - The reference 10- and 50-W Pm-fueled heaters will have external dose rates of 3 and 5 mrem/hr (respectively) at

Figure 32.  $^{238}\text{Pu}$  Dose RatesFigure 33.  $^{147}\text{Pm}$  Dose Rates

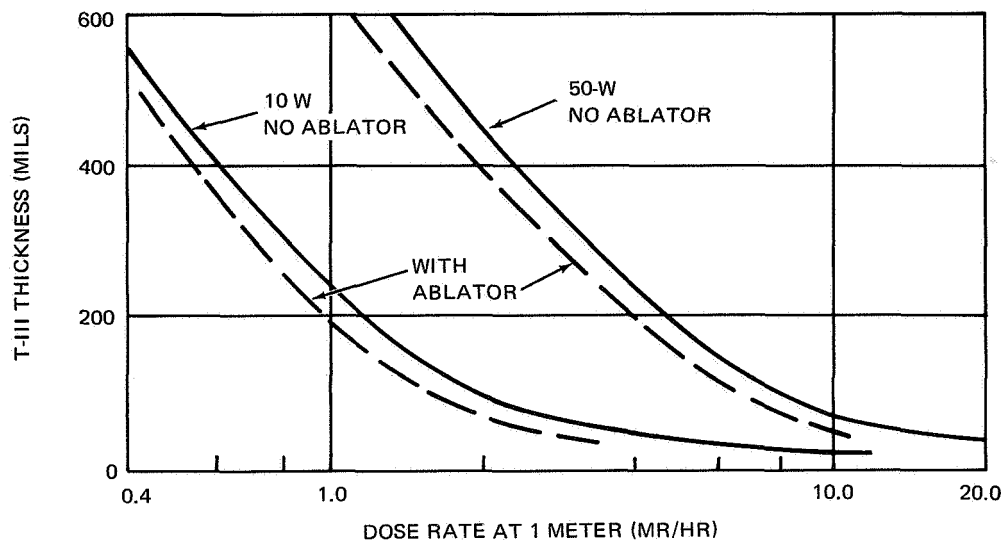


Figure 34.  $^{147}\text{Pm}$  Heater Dose Rate Vs T-111 Shield Thickness

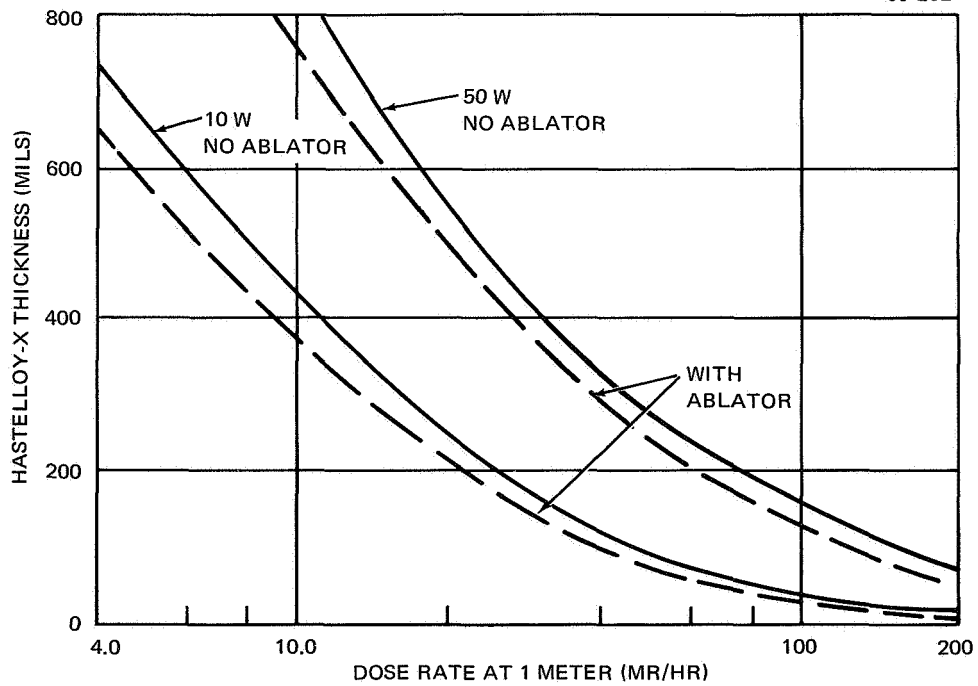


Figure 35.  $^{147}\text{Pm}$  Heater Dose Rate Vs Hastelloy-X Shield Thickness

1 meter. The design criterion of 5 mrem/hr at 1 meter was used to size the thickness for the 50-W capsule. Other design criteria established the 0.060-in. T-111 thickness for the 10-W capsule.

Capsule dose rate as a function of heater power for capsules containing 0.060 and 0.120 in. (total) of cladding is shown in figure 33; 0.060 to 0.120 in. of T-111 or other heavy metal (depending on heater power) will shield to the design criteria. However, note that 0.120 in. of superalloy is grossly insufficient. Thus, use of a superalloy for structural radioisotope containment would necessitate use of an auxiliary heavy metal shield or a substantial increase in the wall thickness. Both are undesirable design modifications.

$^{147}\text{Pm}$  heaters will have an external dose rate consisting of bremsstrahlung and gamma rays. Bremsstrahlung (0.06 to 0.15 MeV) is produced by  $^{147}\text{Pm}$  beta decay. Gamma rays (0.45 and 0.75 MeV) come from the  $^{146}\text{Pm}$  contaminant which is present at approximately 0.25 ppm. Bremsstrahlung is relatively easy to shield; consequently, the shield curve for Pm has the characteristic shapes shown in figures 34 and 35.

The first layers of shield material drastically reduce the external dose rate by shielding the low-energy bremsstrahlung. The dose rate is then controlled by passage of higher-energy  $^{146}\text{Pm}$  gamma rays which are more difficult to shield. Comparing figure 34 to figure 35, the bremsstrahlung is much more sensitive to heavy metal shielding. The incentive to use the more dense T-111 for the structure material is clear.

Gamma ray and neutron spectra from the 10- and 50-W Pm and Pu heaters at 1 meter were calculated and are given in appendix F. Gamma ray analysis for both fuels was performed with the computer program ISOSHLTD (ref. 46). The neutron dose contribution from plutonia was hand-calculated based on fast neutron tissue dose response and point source geometry.

### Accident and Failure Analysis

Critical and secondary failure modes were identified earlier in this report. Each was analyzed to the extent consistent with the phase I effort.

Launch pad explosion and fire. - A critical design condition results from an abort consisting of launch vehicle destruction and total consumption of the rocket fuel on the launch pad. The capsule may be subjected to any combination of temperature, corrosive environment, blast pressure, and debris associated with the pad abort fireball and residual fire.

Four launch vehicles identified in the applications study as prime candidates for manned missions using radioisotope heaters are: (1) Intermediate 20 (S-IC and S-IVB stages), (2) Intermediate 21 (S-IC and S-II stages), (3) Saturn 1B, and (4) Titan III M.

Intermediates 20 and 21 are two-stage earth orbital versions of the Saturn V where either the S-II or S-IVB stage is removed. The complete Saturn V lunar launch vehicle is made up of three booster stages, the lunar

excursion module (LEM), and the command module (Apollo spacecraft). The three booster stages are:

<u>Stage</u>	<u>Propellant</u>	<u>Propellant weight (lb)</u>
S-IC	LO <sub>2</sub> /RP	4 555 000
S-II	LO <sub>2</sub> /H <sub>2</sub>	970 280
S-IVB	LO <sub>2</sub> /H <sub>2</sub>	234 000

The Saturn 1B vehicle consists of a 1B first stage and an S-IVB second stage. The first stage contains about 200 000 lb of LO<sub>2</sub>/RP fuel.

The Titan III M vehicle contains about 200 000 lb of liquid fuel, N<sub>2</sub>O<sub>4</sub>/N<sub>2</sub>H<sub>4</sub>-UDMH, and 1 000 000 lb of solid fuel, NH<sub>4</sub>Cl<sub>4</sub>/PBA.

Thermal environment: The thermal environment for the various launch vehicles is presented in figure 36.

The Saturn V, the Intermediates (combination of vehicle stages), the Saturn 1B, and the first 2.5 sec of the Titan III M abort thermal profiles are based on Kite and Bader's model (ref. 47) adjusted for the fuel-load characteristics of each vehicle. The Titan fuel mixture (N<sub>2</sub>O<sub>4</sub>/N<sub>2</sub>H<sub>4</sub>-UDMH) reacts and burns (ref. 48) at roughly the rate and temperature associated with the

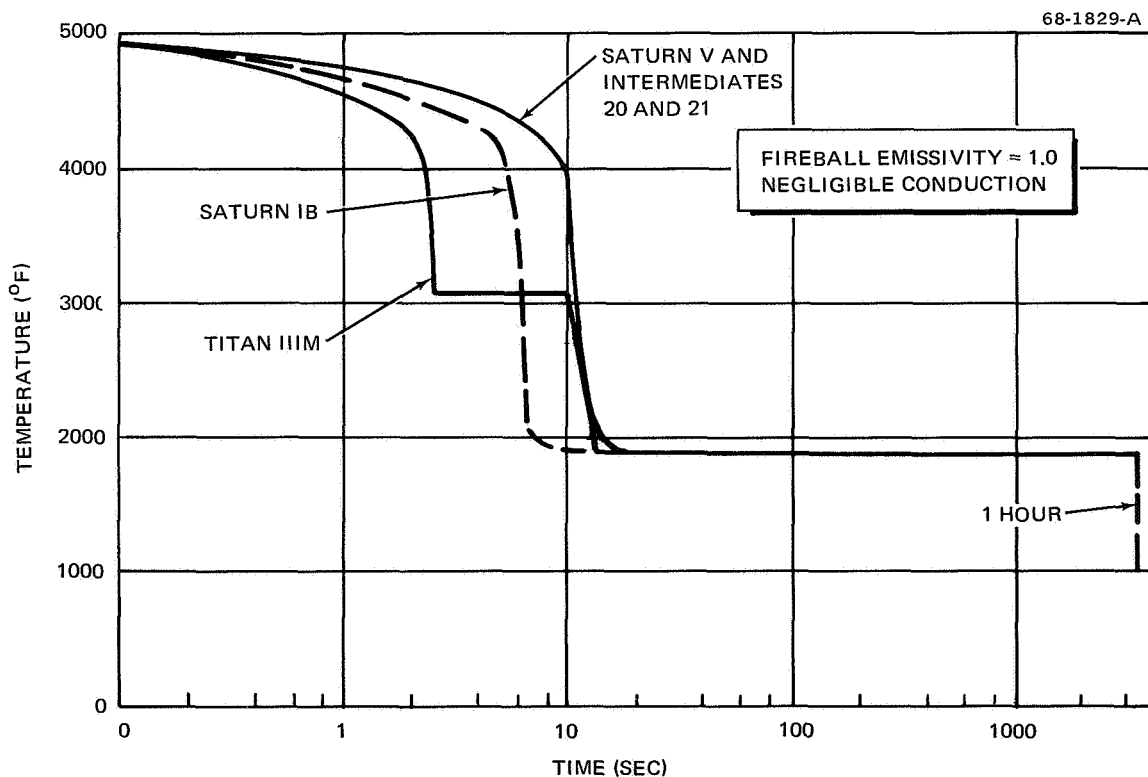


Figure 36. Launch Pad Abort Thermal Environment



LO<sub>2</sub>/RP, LH<sub>2</sub> fuels of the Saturn vehicles. The Titan 3000°F heat pulse between 2.5 and 10 sec is characteristic of the burning temperature of the solid fuels at the overpressures associated with the fireball. \* Residual fire is due to remaining solid fuel burning at atmospheric pressure. The thermal profiles are used under the assumption of radiative heating with fireball emissivity of unity. Convection and conduction are considered negligible.

A limited amount of experimental data is now available on the burning temperature of Titan III M solid fuel. \*\* At the time of this writing, Isotopes, Inc. has just completed a test series involving burning samples of Titan III M (UTC-3001) and Scout (Algol IIB) solid fuels. Various isotope capsule test samples were subjected to the fuel fires.

Isotopes, Inc. pyrometer tests indicate burning fuel surface temperatures of 3350°F; a calorimeter in contact with fuel indicates approximately 50 Btu/ft<sup>2</sup> sec heat flux; a calorimeter in proximity (not touching) between two blocks indicates 75 Btu/ft<sup>2</sup> sec heat flux. Converting the proximity heat flux to radiative temperature with  $\epsilon = 1$ , 3180°F temperature is obtained confirming the model of figure 36. However, true emissivity is better given as  $\epsilon = 0.4$  (alumina) corresponding to 4000°F. The test also indicated burning times of several minutes, depending on block size. SANDIA is currently extending the work of Isotopes, Inc. in an attempt to define a worst-case solid fuels fire test.

The combination of actual fire temperature and duration could invalidate the model used. Thus, the phase II effort will establish a new Titan III M thermal model.

More important than fire temperature are the results of the tests involving capsules. It was observed that graphite will protect the capsule providing the substrate doesn't melt. In this regard, the graphite-protected refractory/platinum capsules were generally intact. Refractory/platinum capsules without graphite contained the bulk of fuel material, but showed slight cracks. Superalloy capsules with graphite typically melted within the graphite shell (providing the graphite remained intact); superalloy capsules without graphite protection disappeared.

The graphite was observed to be immediately coated with molten alumina (from the fuel). The graphite survives because of its high melting point, and is totally protected from oxidation. A practical solution for this fire condition appears to be a design employing a mechanically resilient graphite outer structure.

The worst launch-abort thermal environment currently identified is that produced by various combinations of the Saturn V stages (fig. 36). Thus, the

---

\*Personal Communication, Dr. E. Walden, United Technology

\*\*Personal Communication, Nelson Rose, Isotopes, Inc. and Dr. R. D. Hardee, Sandia Laboratories

reference capsules were subjected to a time-dependent thermal analysis using the Saturn V time-temperature environment.

Figure 37 shows the transient temperature response of the platinum oxidation layer of the 10- and 50-W  $^{147}\text{Pm}$  cermet capsules. Cases are shown for the 50- and 10-W capsules respectively, assuming the ablator (emissivity = 0.8) intact. Temperatures in the 50-W capsule rise more slowly because of the higher total heat capacity. Cases are also shown for the 10-W capsule with ablator removed by blast debris. The surface emissivities considered were 0.2 and 0.5; 0.2 represents the highest measured emissivity for strip platinum, while 0.5 is a conservative estimate of the maximum emissivity of the platinum surface after removal of the ablator. Actual surface temperatures will fall somewhere in between. However, the maximum temperature for the worst case is conservatively 450°F lower than the melting point of platinum.

Blast debris environment: The only detailed launch pad debris study to date has been performed for the SNAP 27 Radioisotope Thermoelectric Generator (RTG) (ref. 49). This study has resulted in a fragment size and velocity distribution model which is currently being used as a guide for impact

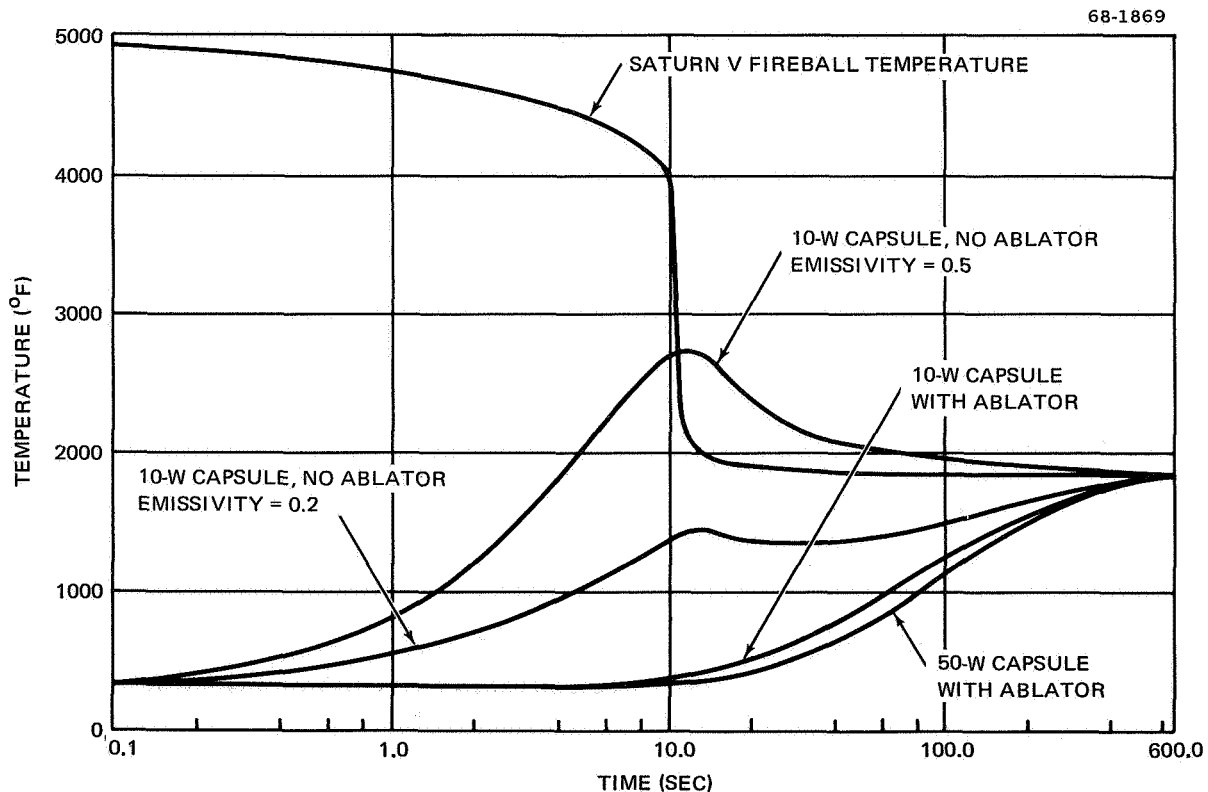


Figure 37. Launch Pad Abort Thermal Response

testing. The model has been generalized to other launch vehicles according to the following assumptions:

1. The capsule is located 35 ft from source of projectiles.
2. Pertinent projectiles come from the top dome of the launch stage closest to the capsules (for the Saturn V, this is the S-IVB stage).
3. The fragments are 0.060-in.-thick, type 2014 aluminum plate characteristic of the S-IVB top dome. Capsule impingement occurs with the debris face-on.
4. Debris production for top stage vehicles other than S-IVB is proportional to S-IVB by ratio of end areas.
5. The burst pattern is  $2 \pi r^2$  (uniform particle distribution throughout a hemisphere).
6. Collision probability is  $\frac{1/2 (\text{bulkhead area})}{2 \pi r^2}$ .
7. Collision energy available for transfer to the fuel capsule is  $\frac{KE A_C}{A_F} + \text{shear energy of punchout}$ .

where:

KE = kinetic energy of the fragment.  
 $A_C$  = cross-sectional area of the capsule.  
 $A_F$  = flat-face area of the fragment.

This model is shown in figure 38 and is intended for correlation to capsule impact test results. Available impact energy is shown for the three types of launch vehicles as a function of capsule collision probability. A few tentative conclusions can be drawn:

1. Results of the impact test program indicate that the heaters with design improvements will reliably survive impact against granite with impact energies to about 10 000 ft-lb. The debris is aluminum plate which readily yields, so survival impact energies probably can be considerably higher. This appears to be borne out by current SNAP 27 debris collision test results and provides confidence that the capsules will survive debris collision.
2. The assumptions are conservative with regard to capsule distance from debris source and no credit for structural material between the capsule position and debris source. Thus, collision probabilities are smaller than those shown, and must be evaluated during vehicle integration.
3. Impact testing appears to be the only practical approach to design for the debris environment.

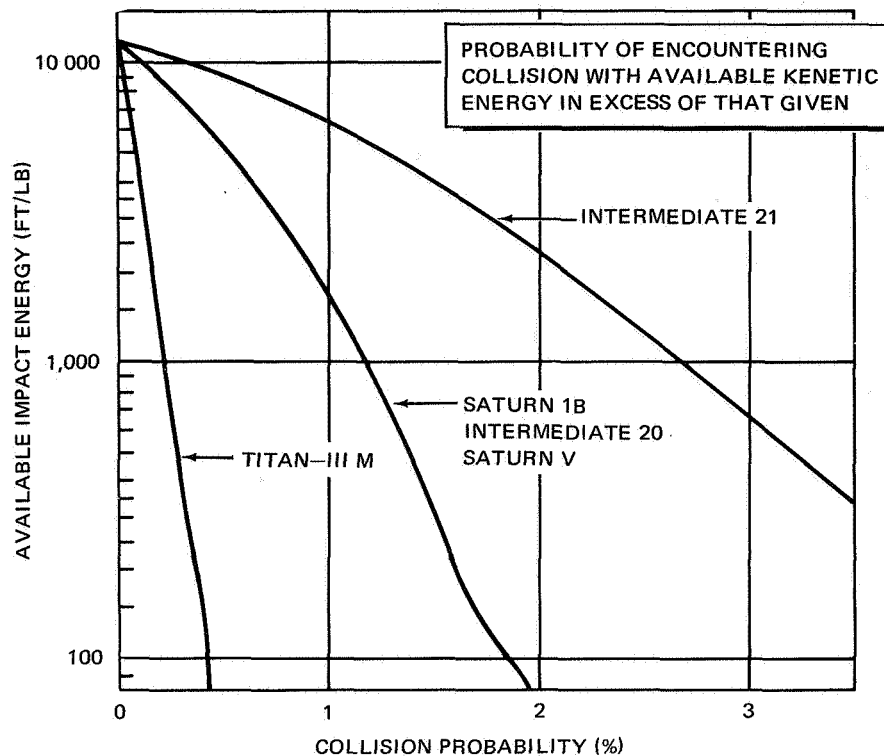


Figure 38. Launch Pad Debris Model

It is intended to design and test for a standard impact condition during phase II. However, the mounting bracket design is an integral part of debris protection. Design details will be firmed subsequent to vehicle integration identification. In specific cases where debris environment is more severe than that evaluated in phases II and III, special tests may be required.

**Overpressure environment:** Capsule integrity during external pressure loading was examined earlier in this report. It was found that the capsules will resist static overpressure in excess of 20 000 psi. This substantially exceeds any static overpressures identified in the SNAP 27 design. Testing during phase II is required to substantiate the dynamic overpressure response and is identified for the phase II effort.

The reference capsule materials and configurations were examined from the standpoint of chemical integrity (refs. 50 and 51). The materials system will provide absolute protection against the chemical environment, providing the platinum oxidation barrier remains intact. The platinum layer will undergo negligible attack from the chemical environment. Mechanical damage presents the only potential means of breaching the platinum; this must be evaluated experimentally during phase II of the program.

As previously discussed, the thermal environment will not cause failure of the platinum.

Failure modes. - The heaters have been designed to satisfy all safety and design criteria specified earlier in this report. However, it is useful to identify potential failure modes so that the analysis and testing required in phases II and III may be identified.

Ablator failure: The ablator and capsule may fail because of:

1. Too little ablator thickness or nonoptimum material to withstand thermochemical heating and ablation.
2. Too little insulation to protect inner capsule (thermal conductivity too high or thickness too small).
3. Insufficient ablator mechanical strength to withstand combined steep-angle deceleration forces and thermal stresses.
4. Accidental removal of ablator prior to reentry.

Impact failure: The capsule may fail on impact because of:

1. Velocity too high for capsule design (capsule size, shape, and layer thicknesses).
2. Unfavorable angle of impact.
3. Unfavorable temperature at impact.
4. Unfavorable internal pressure at impact
5. Partial chemical degradation of structure.
6. Inappropriate material for structural containment considering ductility, density, mechanical strength, and manufacture.
7. Potential weakness due to welding and fabrication.

Secondary failure modes. - Failures other than those identified would be one or a combination of types listed below:

1. Functional failure during mission phase:
  - a. Shortened containment life due to irradiation.
  - b. Shortened containment life due to thermal cycling.
  - c. Shortened containment life due to vibration or mechanical shocks.
2. Water impact:
  - a. Thermal stresses on impact of the hot reentering capsule with the colder water.

- b. Long-term corrosion of the protective oxidation and structural layers.
- 3. Ground burial:
  - a. Rupture from internal pressure due to excessive temperatures.
  - b. Corrosion of the oxidation and structural liners.
- 4. Accidents during prelaunch phase:
  - a. Vibration or mechanical shock.
  - b. Chemical attack or corrosion.
  - c. Melting or yield of containment material due to high temperatures or thermal stresses.

Each case does not appear credible based on analysis. The development testing program described later in this report is designed to simulate the above conditions and uncover any potential weaknesses in the design.

Radioisotope heat sources designed and qualified to resist ORNL Class C III (ref. 4) test conditions will resist destruction by virtually any handling or transportation accident. This can be shown by analysis and by reviewing the history of medical and industrial use of radioisotope capsules.

Disposal by nonrecovery is entirely realistic. The majority of heaters (~70%) will have ocean burial. Design analysis shows that heaters in sea water will resist corrosion for long time periods. Release of measurable activity at any time is very unlikely. The remaining heaters (30%) will land, for the most part, in soft soil, in some cases partially buried; most will never be found intentionally or accidentally. Design analysis shows that the heaters will last for long time periods in a soil/air environment and release of measurable activity at any time is very unlikely.

Probabilistic methods. - A safety analysis subtask was to develop an application of probabilistic methods for estimating risks and hazards of heater failure. This scheme is described in appendix G. The method is appropriate for a digital computer program which should be written and applied as part of the phase II analysis effort. The code will follow through the probabilistic fault tree of figure 3, providing the probability of occurrence and an assessment of the hazard resulting from failure. Note in appendix G that the individual (event) performance models use statistical deviation of the materials properties and accident environment data. Related probability models will also be incorporated from the work of Anno and Schoutens (ref. 52).

### Radiological Consequences and Hazards

Safety problems associated with a radioisotope heater are much less difficult than those associated with the larger radioisotope electrical power

source. This is due to the smaller inventory, lower temperature, and design simplicity of the heaters.

The heaters and the power source both experience the same sequence of events in use and therefore could be exposed to the same accident conditions. The use of either will involve fabrication, testing, transport, prelaunch handling, launch, orbital operation, and postmission disposal. The consequences of a mishap in these stages is entirely different for the heater and the power source.

A 50-W heater contains about 1.47 K Ci of  $^{238}\text{Pu}$  compared to the SNAP 9A inventory of 16.2 K Ci and the SNAP 27 inventory of 45 K Ci. Thus, in the unlikely event of a major release, the power sources would be 10 to 30 times more hazardous. Even so, the inventory difference is much less important than the difference in operating temperatures.

A radioisotope power source must operate at temperatures in excess of  $1000^{\circ}\text{F}$  if electricity is to be generated with reasonable efficiency. Generally, the operating temperature is limited by material capability; consequently, melting is the immediate consequence of loss of coolant. The reference heaters, on the other hand, operate at low temperatures. Most applications are below  $150^{\circ}\text{F}$ . A 50-W heater in  $100^{\circ}\text{F}$  air, with no cooling system, will reach a temperature of only  $370^{\circ}\text{F}$ . At this temperature, fuel vapor pressure is negligible. It follows that a heater can experience serious accidents without a major release of radioactive material.

Design simplicity also minimizes hazards from a radioisotope heater. The containing structures and ablation protection are integral parts of the heater. The structure can provide the small amount of shielding needed; design compromise to allow for integration of a cooling and/or power conversion system is not required.

The heaters are designed for at least a 10 half-life fuel containment. Pm heaters can be expected to last considerably longer (probably an order of magnitude). At the end of 10 half-lives, inventories of 50-W Pm and Pu heaters are 121 and 1.44 Ci respectively. At 20 half-lives, inventories are reduced to 0.117 and 0.0014 Ci--an insignificant value.

Loss of thermal power with age is an additional consideration. After normal deployment (5 to 10 years), the Pu heater will still produce nearly its initial heat. However, the Pm heater output will be substantially reduced. Reduction of thermal power reduces air and soil burial temperatures approximately in proportion to power loss. Thus, after 2 half-lives, temperature falls to near ambient. Corrosion rates for the capsule at ambient air and soil conditions are negligible.

Release to the upper atmosphere. - It is conceivable, but highly improbable, that a series of events could destroy the reentry protection, and the heater could be subjected to upper atmosphere dispersal. Although this eventuality must be considered, it can be shown that such a release does not constitute a significant hazard.

Analysis of reentry burnup and dispersion of the radioisotope is normally considered in several ways: (1) high-altitude burnup (250 000 ft) resulting in particles of less than about  $10\mu$  diameter, (2) high-altitude burnup resulting in particles greater than about  $10\mu$ , and (3) partial burnup resulting in low-altitude dispersal of particles as well as reentry of intact or nearly intact heaters.

Radioisotope material reduced to particulate form by aerodynamic forces are transported to the earth's surface by atmospheric processes and gravity. Large, dense particles fall out quickly, but even light, gaseous material reach the biosphere. Both large-particle (local) and small-particle (worldwide) fallout are considered.

Small particle fallout: For burnup of a 50-W heater, the peak  $\text{Ci}/\text{m}^3$  concentrations during release to the mesosphere (approximately 200 000 ft) are  $C_p = 8.2 \times 10^{-18}$  ( $^{238}\text{Pu}$ ) or  $7 \times 10^{-16}$  ( $^{147}\text{Pm}$ ). To the lower polar stratosphere (30 000 to 80 000 ft),  $C_p = 1.5 \times 10^{-16}$  ( $^{238}\text{Pu}$ ) or  $1.25 \times 10^{-14}$  ( $^{147}\text{Pm}$ ).

The maximum permissible  $\text{Ci}/\text{m}^3$  concentrations for continuous exposure of populations\* are  $\text{MPC}_p^p = 2 \times 10^{-14}$  (soluble  $^{238}\text{Pu}$ ),  $3 \times 10^{-13}$  (insoluble  $^{238}\text{Pu}$ ),  $3 \times 10^{-10}$  (soluble  $^{147}\text{Pm}$ ), and  $1 \times 10^{-9}$  (insoluble  $^{147}\text{Pm}$ ).

Thus, maximum concentrations from a 50-W release are below the permissible values by factors of  $C_p/\text{MPC}_p^p = 0.007$  (soluble  $^{238}\text{Pu}$ ) or  $4 \times 10^{-5}$  (soluble  $^{147}\text{Pm}$ ). The analysis leading to the above conclusions is presented in appendix H.

Large-particle fallout: Much less conclusive results can be drawn regarding large particle fallout because (1) existing data are inadequate to rigorously calculate fallout from high altitude, and (2) for large particles, the hazard results from potential angle particle radiation exposure and/or through the ecological chain.

Large-particle fallout will be more localized; in fact, the limiting severity (i.e. highest possible dose) is given in the following discussion concerning maximum credible land and water releases. In general, a small fraction of the earth surface would be involved. Doses to individuals would not be injurious--in all but exceptional cases, less than MPD.

Release in a launch abort--the maximum credible accident. - The most severe accident associated with use of radioisotope heaters would be a large release of radioactive material due to a launch abort. The heater will be designed to survive such a conflagration. Nevertheless, because the probability cannot be reduced to zero, the consequences warrant consideration.

The effects of instantaneous forced release of 50 W of  $^{147}\text{Pm}$  and  $^{238}\text{Pu}$  to air is shown in figure 39. Simple release could not produce these effects

---

\* Based on the 1959 ICRP recommendations; in each case, the nonoccupational  $\text{MPC}_a$  is higher by a factor of 3.



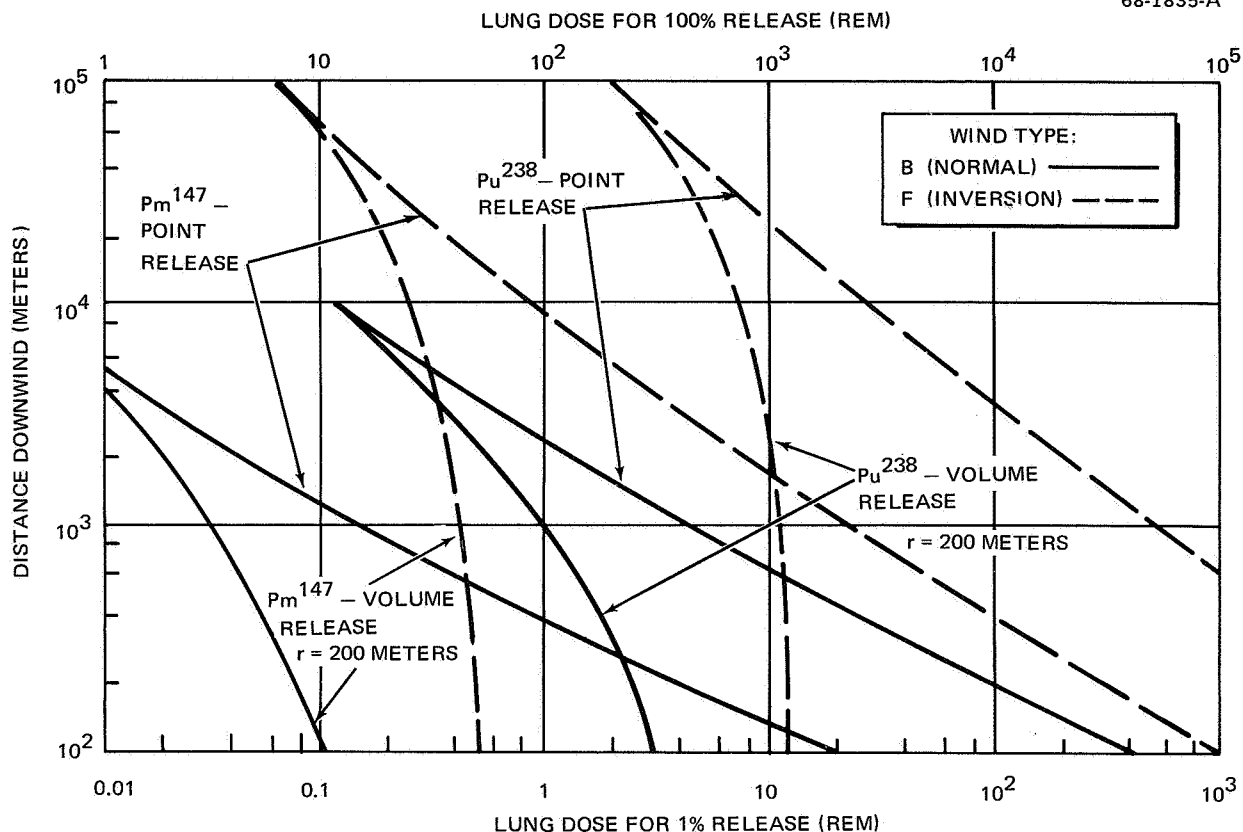


Figure 39. Maximum Credible Accident, 50-W Pu and Pm Heaters

because a large amount of energy is required to vaporize or atomize the fuel. It has been shown (ref. 53) that 40%, 6%, and 0.5% of bare  $PuO_2$  microspheres may volatilize if exposed to the Saturn V fireball at 0, 5, and 10 sec respectively after launch pad abort initiation. However,  $PuO_2$  and  $Pm_2O_3$  cermet release less than  $10^{-2}\%$  fuel inventory when exposed to the entire fireball.

Weather conditions have significant effects on downwind airborne radioactivity. Type B wind (3m/sec, unstable) conditions are used in hazards analysis as typical; Type F (1m/sec, thermal inversion) are improbable conditions which represent a worst case. Thus, the solid curves read on the left ordinate (1% release) represent a credible but highly improbable accident. The dashed curves are given for information but cannot be correlated with a realistic accident probability. The right-hand ordinate is applicable only to  $^{238}PuO_2$  bare microspheres or  $^{147}Pm_2O_3$  powder fuel forms, assuming total fuel inventory volatilization at the instant of abort initiation. Additional conservative assumptions include no credit for vertical dispersion and 100% retention of radioactive material that enters the respiratory system. On the basis of the 1% release model, it can be concluded that dose rates exterior to the controlled areas are within tolerable limits.

Note that point and volume release curves are given. Fireball release will be represented by fireball volume dilution. The point release case represents the maximum concentration release and would be typical in any ground accident (not necessarily from a launch abort) where the fuel is quickly vaporized but not dispersed by the vaporizing medium. Further results, including the effect of fireball rise and various other wind conditions, and the analytical approach used in this ground release analysis are given in appendix I.

Fresh water contamination. - A heater could fall into fresh water. In the United States, fresh-water lakes, reservoirs, and rivers cover some  $4 \times 10^4$  sq miles (about 1% of the total area).

Hazard studies to date have concentrated on reservoir contamination because the path to man is shortest in this case. In the United States (for which data are available), one-half of the fresh water area consists of reservoirs, where the term "reservoir" includes man-made lakes such as Lake Mead.

Especially in large communities, reservoir systems are complex. The initial source is generally a large, open, impounding reservoir. From this source, the water is transferred to smaller reservoirs as "raw" water at a water-treatment plant. After filtering and chlorinization, the water is stored in closed tanks to prevent contamination prior to entering the distribution mains in the municipality.

The delay time and the cleanup actions can greatly reduce doses from reservoir contaminants. These factors usually are not taken into account in safety studies because they are different for each reservoir complex.

A 50-W heater contains enough radioactive material to contaminate about  $1.6 \times 10^{11}$  gal ( $^{147}\text{Pm}$ ) or  $8 \times 10^{10}$  gal ( $^{238}\text{Pu}$ ). As shown in figure 40, the probability is only  $4 \times 10^{-4}$  that a capsule landing in the United States would hit a drinking water reservoir no larger than this.

USNRDL data (ref. 54) indicates that about  $1.2 \times 10^{-4}\%$  per day of a promethia sample may go into solution in sea water. For a 50-W heater, this is 0.15 Ci/day or 55 Ci/year. This will contaminate approximately  $7.5 \times 10^5$  gal to  $\text{MPC}_w$ . As indicated by figure 41, the probability of impacting in a reservoir which contains less than  $10^7$  gal is vanishingly small. Since the turnover rate in reservoirs is relatively high, the probability of a reservoir's being contaminated to  $\text{MPC}_w$  levels by a heater, either  $^{147}\text{Pm}$  or  $^{238}\text{Pu}$ , is quite small.

Ocean water contamination. - Sea water contamination is an inherently complex problem because it can take many forms, and involves an elaborate and little understood ecological system.

Intact heaters in the ocean constitute no hazard; corrosion rates are so low that containment integrity will be maintained indefinitely. The heaters will probably withstand pressures of the greatest depths, and even in the

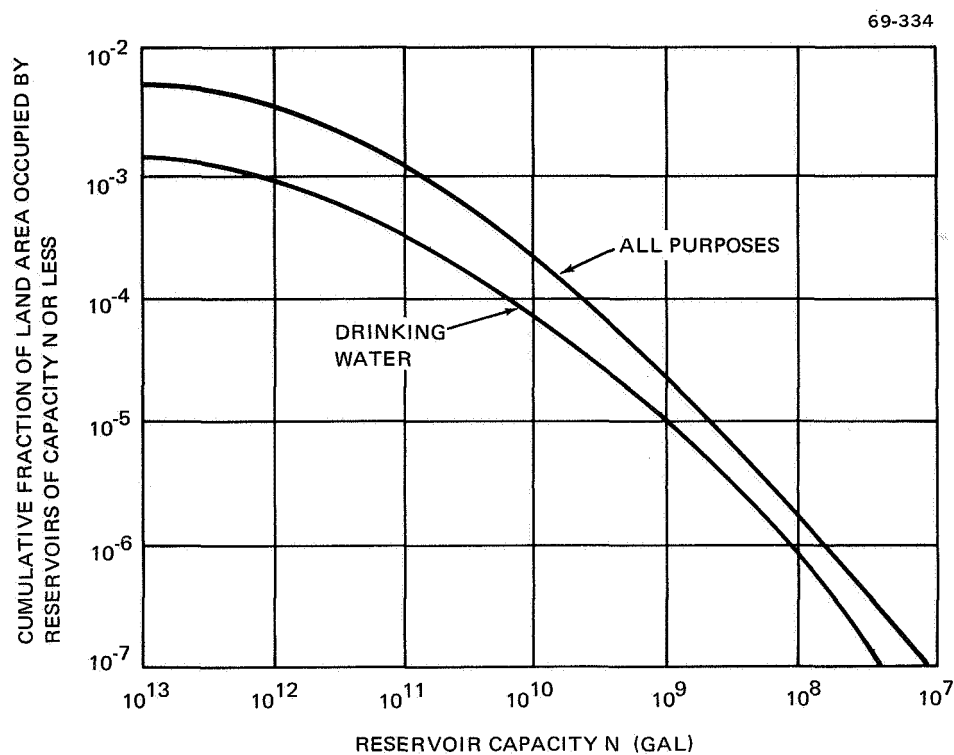


Figure 40. Cumulative Fraction of Land Area in the United States Occupied by Open-Type Reservoirs of Capacity  $N$  or Less

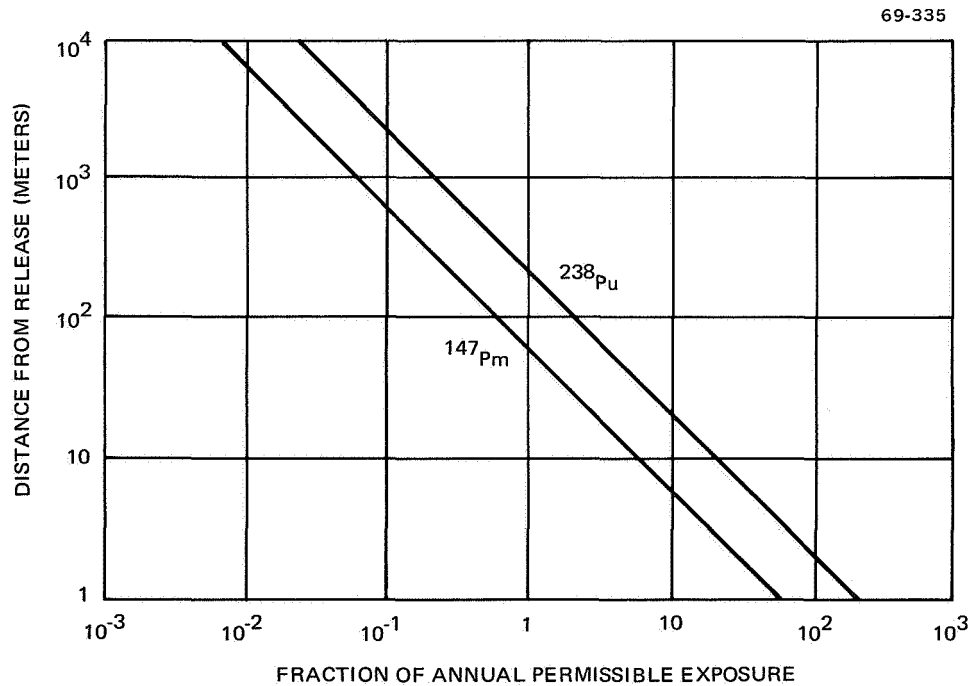


Figure 41. Exposure from 50-W Release to Sea Water

event of release, the fuel would create little or no hazard because there is little exchange between the ocean's layers.

If a damaged or faulty capsule were dropped into the ocean, the radioactive material would be released quite slowly because the fuel forms are relatively insoluble. The low rate of release greatly reduces potential hazards.

Radioisotopic fuel could be released to sea water much more rapidly if the heater were damaged by reentry forces, and if ablation of the fuel created large particles. But even these particles would be dispersed over a large area which would effectively reduce hazards.

While release to sea water could occur only slowly and/or over a wide area, it is instructive to consider the potential consequences of a rapid release in a small volume. Even in this extreme and improbable case, the hazard is acceptably small. A concentration in sea water is not related in any direct way to dose to humans. The maximum permissible concentration in sea water is obtained by assuming that all protein in the diet of the people of interest consists of seafood which has fully concentrated the radioactive material. Using these assumptions, exposure for 1 year at MPC<sub>s</sub> corresponds to 15 rem to the gastrointestinal tract or 30 rem to the bone, the respective critical organs for <sup>147</sup>Pm and <sup>238</sup>Pu. Denoting these values as emergency integrated Ci-sec/m<sup>3</sup> exposures, TID<sub>E1</sub> = 2 Ci-sec/m<sup>3</sup> for <sup>238</sup>Pu, and TID<sub>E2</sub> = 600 Ci-sec/m<sup>3</sup> for <sup>147</sup>Pm.

In these terms, integrated exposures to 100% release from a 50-W heater, based on a diffusion velocity of 0.01 m/sec and a 75-meter mixing depth, is TID<sub>1</sub>/TID<sub>E1</sub> = 200/R for <sup>238</sup>Pu, and TID<sub>2</sub>/TID<sub>E2</sub> = 60/R for <sup>147</sup>Pm. This is illustrated in figure 41. It is evident that high integrated exposures can exist only in a small area. The basis of these results are given in appendix J.

Actually, the sea water contamination problem is less serious than these calculations suggest. First, full biological concentration of these radioisotopes, a factor of 10<sup>3</sup>, cannot occur instantaneously because this requires several steps in the food chain. Second, higher concentrations are associated with the fish at shallow depths that normally feed over a large area compared to the area of high concentration. Further, humans who live largely on seafood do not confine their attention to such small areas. Thus, it can be concluded that release to the open ocean will not result in overexposures.

Data in figure 41 can be modified to consider surface concentration from breached, deeply submerged capsules. Assuming no vertical mixing limit, hemispherical dispersion, and instantaneous total release of the isotope inventory, the depth at which surface concentration would be 10<sup>-2</sup> MPC is 11 500 ft for Pu<sup>238</sup> and 5200 ft for Pm<sup>147</sup>.

## HEATER MATERIALS SELECTION

The radioisotope heater for use in space vehicles is a heterogeneous combination of materials that provide maximum operating performance and safety. The materials must be compatible under all environments and temperature conditions encountered during the complete mission profile from launch to reentry, impact, and possible burial.

In this section, candidate materials are discussed along with the rationale used in the final selection.

### Radioisotope Fuels

Several radioisotope fuels that have been investigated as potential heat sources are shown in table 18. Of these,  $^{147}\text{Pm}$  and  $^{238}\text{Pu}$  were selected for the reference heater designs primarily because, together, they cover the required mission times of from 14 days to 5 years; their cermet fuel forms are inherently safe; their emitted radiations can be easily shielded; and they are readily available. Cobalt 60, while available, requires very heavy shielding and is not suitable for small sources;  $^{90}\text{Sr}$  has been used in several land-based applications, but, due to its energetic beta decay which results in penetrating bremsstrahlung, heavy shielding is required which eliminates it from consideration for a small heat source. Rubidium also requires heavy shielding and is not readily available. Cesium has a relatively short half-life and requires heavy shielding. Thulium suffers on two counts: it has a relatively short half-life and requires moderate shielding. Polonium has been proposed for space applications because of its high power density. But the main difficulty with polonium is the high vapor pressure of its compounds, which makes them quite unstable. Polonium also has a relatively short half-life. Curium-242 has a very high power density, but like  $^{210}\text{Po}$  it has a relatively short half-life. Curium-244 is being considered as a possible supplement to  $^{238}\text{Pu}$  as it has a moderate power density and half-life but at the present time it is not readily available and requires considerably more shielding than does  $^{238}\text{Pu}$ . Tritium ( $^3\text{H}$ ) and thulium-171 have also been suggested as potential heat sources. However,  $^3\text{H}$  has no stable high-temperature fuel form and  $^{171}\text{Tm}$  suffers from the contaminant,  $^{170}\text{Tm}$ , which requires moderate shielding.

The  $^{147}\text{Pm}$  and  $^{238}\text{Pu}$  fuel forms chosen for detailed analysis based on half-life, shielding, impact, availability, cost, compatibility, and state of development, were the  $^{147}\text{Pm}_2\text{O}_3\text{-W}$  cermet,  $^{238}\text{PuO}_2$  microspheres (plasma-fired or sol-gel), and  $^{238}\text{PuO}_2$  cermet. Final selection will depend on the mission time requirement and the fuel form state of the art at time of fabrication.

$^{238}\text{Pu}$  and  $^{147}\text{Pm}$  have stable high-temperature fuel forms which have been extensively studied with regard to fuel immobilization, vapor pressure, impact characteristics, and release to the biosphere.

## CHARACTERISTICS OF RADIOISOTOPIC HEAT SOURCES\*

	<sup>60</sup> Co	<sup>90</sup> Sr	<sup>106</sup> Ru	<sup>137</sup> Cs	<sup>144</sup> Ce	<sup>147</sup> Pm	<sup>170</sup> Tm	<sup>210</sup> Po	<sup>238</sup> Pu	<sup>242</sup> Cm	<sup>244</sup> Cm
1. Half-life (yrs)	5.24	28	1.0	30	0.78	2.6	0.35	0.38	87.4	0.45	18.1
2. Compound form	Metal	SrTiO <sub>3</sub>	Metal	CsCl	Ce <sub>2</sub> O <sub>3</sub>	Pm <sub>2</sub> O <sub>3</sub>	Tm <sub>2</sub> O <sub>3</sub>	Metal	PuO <sub>2</sub>	Cm <sub>2</sub> O <sub>3</sub>	Cm <sub>2</sub> O <sub>3</sub>
3. Melting point of compound (°C)	1480	1910	2310	646	2190	2130	2375	255	2250	1950	1950
4. Density of compound (g/cm <sup>3</sup> , actual or 90% TD)	8.8	4.6	12.4	3.2	6.2	6.6	8.0	9.3	10.0	9.0	9.0
5. Power density, (W/cm <sup>3</sup> compound)	15.8	1.01	13.7	0.38	6.2	1.8	9.6	1210	3.9	882	20.4
6. Availability	Avail.	Avail.	Poten. avail.	Avail.	Avail.	Avail.	Avail.	Avail.	Avail.	Poten. avail.	Avail.
7. Type of radiation (major)**	γβ	βχ	γβχ	βγχ	βγχ	β	β	α	α	αγ	αγ
8. Shielding required	Heavy	Heavy	Heavy	Heavy	Heavy	Minor	Moderate	Minor	Minor	Minor	Moderate
9. Biological hazard, (MPC, air)	3x10 <sup>-9</sup>	10 <sup>-10</sup>	2x10 <sup>-9</sup>	5x10 <sup>-9</sup>	2x10 <sup>-9</sup>	2x10 <sup>-8</sup>	10 <sup>-8</sup>	7x10 <sup>-11</sup>	7x10 <sup>-13</sup>	4x10 <sup>-11</sup>	3x10 <sup>-12</sup>

\* Reference 55.

\*\* α Alpha  
β Beta  
γ Gamma  
η Neutron  
χ Penetrating bremsstrahlung

The best fuel form identified for missions of over 2 years' duration is the  $^{238}\text{PuO}_2$ -Mo cermet. It is currently under development at the Battelle Memorial Institute (refs. 56 and 57). This fuel form promises more radioisotope immobilization than other available or potentially available Pu forms for credible abort environments. The next-best potential fuel form is the  $\text{PuO}_2$ - $\text{ZrO}_2$  solid solution under development at the Los Alamos Scientific Laboratory (refs. 58 through 61). It has been fabricated and subjected to limited testing. More testing is required to fully qualify its performance.  $\text{PuO}_2$  microspheres are the only plutonia fuel form presently available, fully qualified, and thus, suitable for immediate use in radioisotope heaters. All three Pu fuel forms are satisfactory; the advanced fuel forms only provide a higher degree of fuel immobilization in the event of capsule breach.

For missions of 2 years or less, the  $^{147}\text{Pm}_2\text{O}_3$ -W cermet is recommended. This fuel is highly desirable from the standpoint of safety, and there is no helium generation; thus, design for pressure containment is not required. The fuel decays fast enough to eliminate long term hazards from loss of encapsulation. Biologically, it is considerably less hazardous than most other radioisotopes.

DWDL has developed  $\text{Pm}_2\text{O}_3$ -W cermet technology to the point where fabrication of small sources ( $\approx 10$  W) is within the state of the art. No technical limitation is expected for fabrication of 50-W and larger sizes. The cermet has demonstrated impact superiority over bare microspheres and a hot-pressed ceramic compact (ref. 62). In addition to basic resistance to fragmentation, the cermet provides microencapsulation of the fuel, which prevents excessive exposure of  $^{147}\text{Pm}_2\text{O}_3$  to the biosphere in the improbable event of a breach in the structural shell. Table 19 presents a comparison of promethia and plutonia fuel forms.

An interesting point is that, from the data shown in table 19, it appears that the power density of plutonia fuels is approximately double that of promethia. However, because of the requirement to maintain a void-to-fuel ratio approximately equal to one, actual power densities for plutonia fuels are nearly the same as for promethia fuel. Thus, fuel capsules of plutonia and promethia can be made interchangeable within the structure container.

### Primary Containment Vessel

Arc-cast tantalum has been chosen for the primary containment vessel (the layer that immediately surrounds the radioisotope fuel) over other refractory metals and superalloys because of its high melting point, ready availability in many shapes, ease of fabrication (particularly TIG welding), and compatibility. The only function of the primary containment vessel is to allow handling outside of radiation control gloveboxes and/or hot cells. This will allow subsequent assembly procedures to be accomplished more economically.

TABLE 19  
FUEL FORM COMPARISON

	$^{147}\text{Pm}_2\text{O}_3$ -20v/o W cermet	$^{238}\text{PuO}_2$ -20v/o Mo cermet	$^{238}\text{PuO}_2$ -20m/o $\text{ZrO}_2$ solid solution	$^{238}\text{PuO}_2$ bare microspheres (62.5% packing fraction)
Power density	1.4 W/cc	3.66 W/cc	3.5 W/cc	2.86 W/cc
Specific gravity fuel form	9.13 g/cc	10.12 g/cc	9.65 g/cc	6.31 g/cc
Helium release	No He; $\beta$ -emitter	Not known; est. less than solid solution or microspheres	Estimated to be similar to microspheres	Estimated 5% to 20% at 2100°F for 5 min.
Impact resistance	Excellent	Excellent results with W matrix	Poor	Poor
Half-life	2.62 yr	87.4 yr	87.4 yr	87.4 yr

Superalloys such as L605 (HS25), Inconel X750, and Hastelloy X are actually more difficult to fabricate than tantalum. Other refractory metals and alloys were considered, but none were as ductile when welded, as readily formed, and as readily available as pure tantalum.

#### Energy Absorbent Layer

Tantalum foam was selected as the shock absorbent material around the primary containment capsule. However, other material such as Ta wool may be considerably less expensive and just as adequate for shock attenuation. This material provides void spaces for helium retention and absorbs energy from impact.

#### Structural Container - Pressure Vessel $^{238}\text{PuO}_2$

Physical properties of candidate materials for the heater structure container are presented in table 20. T-111 was selected for this component because the elevated-temperature strength of T-111 is comparable to T-222 and Ta-10W, and its ductility is greater than Ta-10W. Lower initial cost,



TABLE 20

## PHYSICAL PROPERTIES OF CANDIDATE STRUCTURAL CONTAINER MATERIALS

Property	T-111	Ta	Ta-10W	T-222	Hastelloy X	HS 25	Mo	TZM
Melting range (°F)	5400	5425	5495	5406	2300-2450	2425-2570	4730	4730
Density (lb/in <sup>3</sup> )	0.604	0.60	0.608	0.604	0.297	0.33	0.37	0.37
$\alpha$ , in./in. °F x 10 <sup>6</sup> at T (°F)	4.0 2500F	~4.56 2400	4.0 2000	est 4.0 2500	9.2-19 1800	9.41 (avg) 1800	3.0 2400	3.0 2400
Stress to produce rupture at 2400°F (10 hr), x 10 <sup>3</sup> psi	25	13	25	>32	0	0	12-18	40-80
Ultimate strength at 2400°F, x 10 <sup>5</sup> psi	43	11.5	60	53	0	3	18	55
Elongation (% in 2 in. at room temperature)	29	25	24-25.3	30	41-46	58-64	16-49T* 20-58L*	9-13T* 36-40L*
800°F	>15	18	<3	>15	44	74	---	---
2400°F	28	>48	14-19	20	Does not apply	6	---	14-16* 29-40L*
Oxidation at 2200°F	---	Scaling occurs above 950°F	Oxida- tion rate approx- imately 2/3 that of un- alloyed Ta	---	250 wt gain, spalls at 1000 hr	250 wt loss	Oxidizes rapidly above 1300°F	

\*T = transverse rolling direction; L = with rolling direction.

greater ease of fabrication, and comparative availability also make T-111 a logical choice over T-222. The high-temperature strength of T-111 is superior to Ta. The following additional rationale was used for selection of T-111.

1. The peak temperature (2100°F) reached during reentry comes within 200°F of the melting point of Co and Ni superalloys such as L605 (HZ25) and Hastelloy X.

2. The material must have high energy absorption characteristics; i.e. the area under its stress strain curve should be large and its modulus of elasticity should be moderate. Refractory alloys T-111 and T-222 and W-Re are superior to Mo and Nb alloys.

3. The material must be compatible with other components of the heater and not force serious compromise in cost or performance of adjacent components (inner container,  $^{238}\text{PuO}_2$ , and Ta foam).

4. The material must be available; readily weldable, preferably by TIG techniques (although EB welding is possible); ductile in the as-welded condition; and not prohibitively expensive.

5. The thicknesses of T-111 selected for the Pu heaters, 0.060 in. for the 10-W and 0.120 in. for the 50-W, are dictated by the 20-year orbital life temperature/pressure requirements.

#### Structural Container for $\text{Pm}_2\text{O}_3$

The same rationale used to select T-111 for the structural  $\text{PuO}_2$  container applies for  $\text{Pm}_2\text{O}_3$  heaters except that the shell thickness is determined by shielding requirements--not temperature/pressure history considerations. Analysis indicates that thicknesses in either case are about the same. A high-Z atomic weight material is superior to a material with low Z for radiation shielding. Molybdenum and niobium alloys are not as effective radiation shields as the W and Ta alloys. All superalloys have relatively low attenuation efficiencies. For shielding, the Pm 10-W heater with a 0.060 in. -thick T-111 structural shell will keep the dose rate within 5 mr/hr at 1 m. For the same requirements, 0.63 in. of Hastelloy-X is needed. Hastelloy-X heater weight would be 4.059 lb compared to 1.011 for the 10-W heater with a T-111 shell. For the 50-W heater, the structural shell thicknesses are 0.120 in. for T-111, and 1.13 in. for Hastelloy-X; and the corresponding weights are 3.410 lb and 16.68 lb respectively. Consequently, for purposes of standardization, the thickness of the T-111 structural container is identical for both  $\text{PuO}_2$  and  $\text{Pm}_2\text{O}_3$  heaters of the same power level. The fact that reentry and impact requirements are comparable for either heater is additional support for this design selection.

The shielding and thermal requirements for the structure container virtually rule out the use of superalloys unless excessive thicknesses are used and/or the thermal insulation is significantly thickened.

## Oxidation Barrier

Platinum was selected as the oxidation/corrosion-resistant layer because of its excellent resistance to sea water corrosion and oxidation, and because of its high melting point. Pt, Ir, Rh, Co, Ni, their alloys, and the refractory borides were considered. The best oxidation barrier and resistant to general corrosion is Ir; however, Pt is also excellent, and far more available and economical than Ir. Table 21 lists the properties of these materials.  $\text{TiB}_2$  and  $\text{HfB}_2$  show promise and should be considered further.

$\text{TiB}_2$  and  $\text{HfB}_2$  would prevent diffusion of carbon from the insulation layer into the Ta, thereby preventing embrittlement by carburization. Cobalt, nickel, and their alloys are of questionable value because of their low melting points and interaction with carbon.

## Thermal Insulation Layer

Pyrolytic graphite was chosen for thermal insulation because of its very favorable values of thermal conductivity in both "a" and "c" directions. The low value of thermal conductivity in the "c" direction inhibits heat flow into the capsule structure. The relatively high value of thermal conductivity in the "a" direction helps produce uniform heating for capsule reentry orientations such as end-on and side-on nonspinning. Chemical vapor deposition (CVD) techniques will be used for forming the pyrolytic graphite.

Other materials and techniques for the insulation layer are being investigated at DWDL under Independent Research and Development programs. One program is investigating thornel fibre-reinforced pyrolytic graphite and expanded pyrolytic graphite. Another program is developing techniques for integrating the ablator with the insulation and structural container using graphite ceramic composite materials.

## Ablator Material

POCO graphite is considered the prime candidate for ablative reentry protection. MDAC has found this material to have high survival capability at heating rates considerably above those predicted for the radioisotope heaters undergoing a 90° lunar return trajectory. Physical and thermal data are presented in table 22 and figures 42 and 43.

A carbon-fiber-reinforced phenolic charring ablator material (Narmco 4028) was investigated analytically. First indications are that the reentry thermal protection provided is good; however, long term degradation of phenolic ablators at normal operating temperatures up to 400° to 500°F may be serious. In addition, reliable and reproducible performance data are scarce.

Reinforced pyrolytic graphite was considered as a combination ablator/insulator. However, this material varies somewhat from one batch to another and reliable thermal performance data are not available.

TABLE 21  
PROPERTIES OF CANDIDATE OXIDATION BARRIER MATERIALS\*

Property	Rh	Pt	Ir	Pt-10Rh	Hastelloy X	HS25 (L605)
Melting point	3371	3217	4450	3362	~2350	~2500
Spectral emissivity at 2400°F	0.17	0.27	0.29 (3100°F)			
Cp (Btu/lb-°F)	0.0317 (441°F)	0.042 (2400°F)	0.032 (531°F)		0.10 (70°-212°F)	0.09 (80°-212°F)
Thermal conductivity (K, Btu/hr-ft-°F)	82.2 <sup>3</sup> (2400°F)	38.2- 61.7 (2400°F)	48.4 (2400°F)		12.0 (1100°F)	13.1 (1300°F)
Elongation in 2 in. (%)		30-40 annealed 2.5-3.5 cold-worked			43(R. T.) 45(1000°F) 33.5(1500°F) 45(1800°F)	64(R. T.) 30(1600°F)
Ultimate tensile strength at rm temp (10 <sup>3</sup> psi)	61.2	18-28	32		114 22.5(1800°F)	146 47(1600°F)
Density (lb/in <sup>3</sup> )	0.447	0.755	0.813	0.722	0.297	0.33
Young's Modulus, (10 <sup>3</sup> psi)	41.2	22.0	74			
Oxidation at 2400°F, (mg/dm <sup>2</sup> /day)	(Fair)	50(wt loss) (excellent)	(excellent)	40(wt loss) (excellent)	250(wt gain) (spalls at 1000 hr)	250(wt loss)
Formability	Poor	Good	Poor	More difficult than Pt		
Cost	Not readily available in sheet form	\$295/oz	High	\$375-400/oz		

\*All data are from references 63 through 69.

TABLE 22  
POCO GRAPHITE PROPERTY DATA VS TEMPERATURE

	Grade AXF-5Q		
	75°F	1500°F	3000°F
Density range (gms/cm <sup>3</sup> )	1.80 - 1.88	N/A	N/A
Tensile strength (psi)	10 000	11 000	12 000
Compressive strength (psi)	20 000	N/A	N/A
Flexural strength (psi)	10 500	10 900	12 300
Modulus of elasticity (psi x 10 <sup>6</sup> )	1.68	1.84	2.08
Strain to failure (% elongation)	0.95	0.90	1.00
Poisson's ratio	0.15	0.18	0.22
Hardness (Rockwell B)	120	N/A	N/A
Thermal conductivity (Btu/ft-hr-°F)	65	28	17
Coefficient of thermal expansion (in./in./°F x 10 <sup>-6</sup> )	4.8	4.3	4.9
Specific heat (Btu/lb-°F)	0.20	0.42	0.50
Purity (average total ash-ppm)	200	N/A	N/A

Under an MDAC Independent Research and Development program, physical and thermal property data for graphite-ceramic composites such as HfB<sub>2</sub> • WSi<sub>2</sub> • C are being compiled. Preliminary thermal protection test results, while encouraging, are inconclusive.

#### Kinetics of Helium Release from the Plutonia Fuel Structure

It is generally known that, under certain conditions, not all of the helium produced by  $\alpha$  decay is released from the plutonium fuel structure. Helium release rates are dependent on such variables as temperature, pressure, temperature history, pressure history, size, and surface roughness of the fuel form. However, total release has been assumed for safety and design calculations presented here because of the present lack of reliable experimental substantiation for less conservative assumptions.

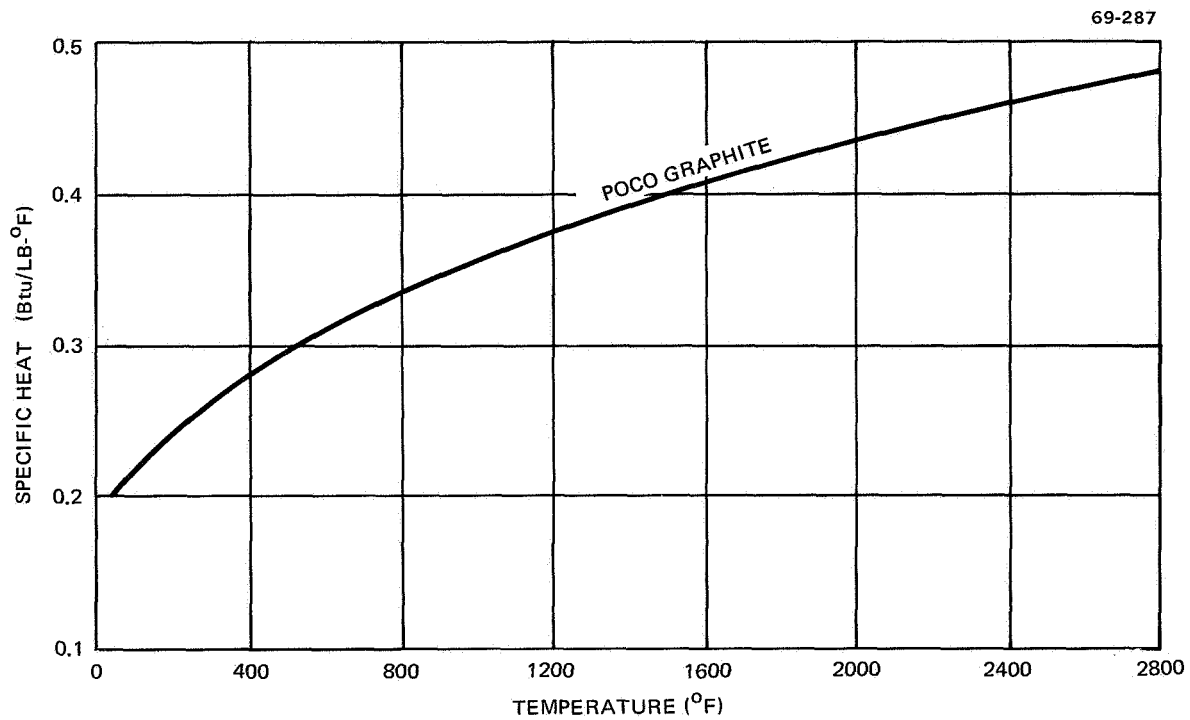


Figure 42. POCO Graphite Specific Heat Vs Temperature

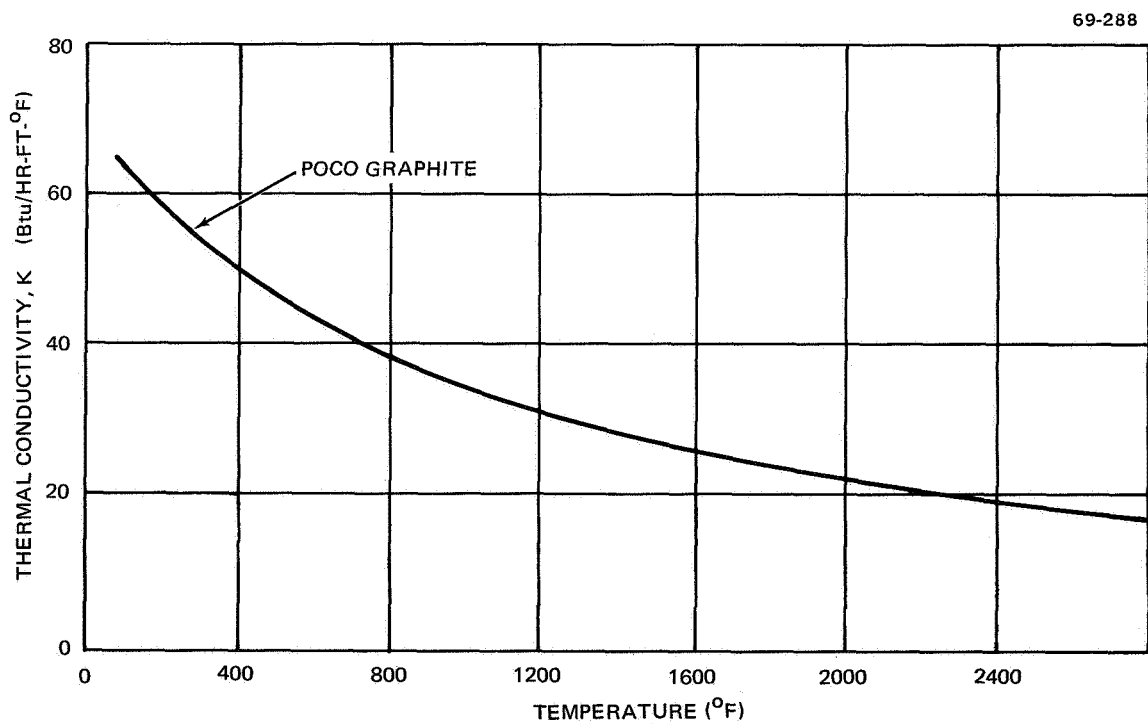


Figure 43. POCO Graphite Thermal Conductivity vs Temperature

At DWDL, an approximate mathematical model was developed which is qualitatively similar to those being developed by investigators in this field and which employs empirical constants chosen to produce agreement with unpublished microsphere data obtained from C. J. Northup, Jr. of Sandia Corporation. This model was produced in order to anticipate whether less than 100% helium release could result for the time-temperature values encountered during reentry heating. If such were the case, this would constitute an additional safety margin in the pressure vessel design. When helium release becomes better understood, the thickness of the pressure vessel walls could be reduced and a weight reduction achieved.

Figure 44 presents a rough guideline for helium release estimates. Helium release times are given as a function of temperature. At normal operating temperatures for most applications ( $<400^{\circ}\text{F}$ ), there is, essentially, complete helium retention. For the time-temperature coordinates corresponding to reentry of the capsules, the guideline indicates that considerably less than 100% helium release would occur. For a period of 200 to 300 sec at  $2000^{\circ}$  to  $2100^{\circ}\text{F}$  (as during an earth orbital decay trajectory) the model indicates that less than 25% of the available He would be released from the microsphere-fuel structure.

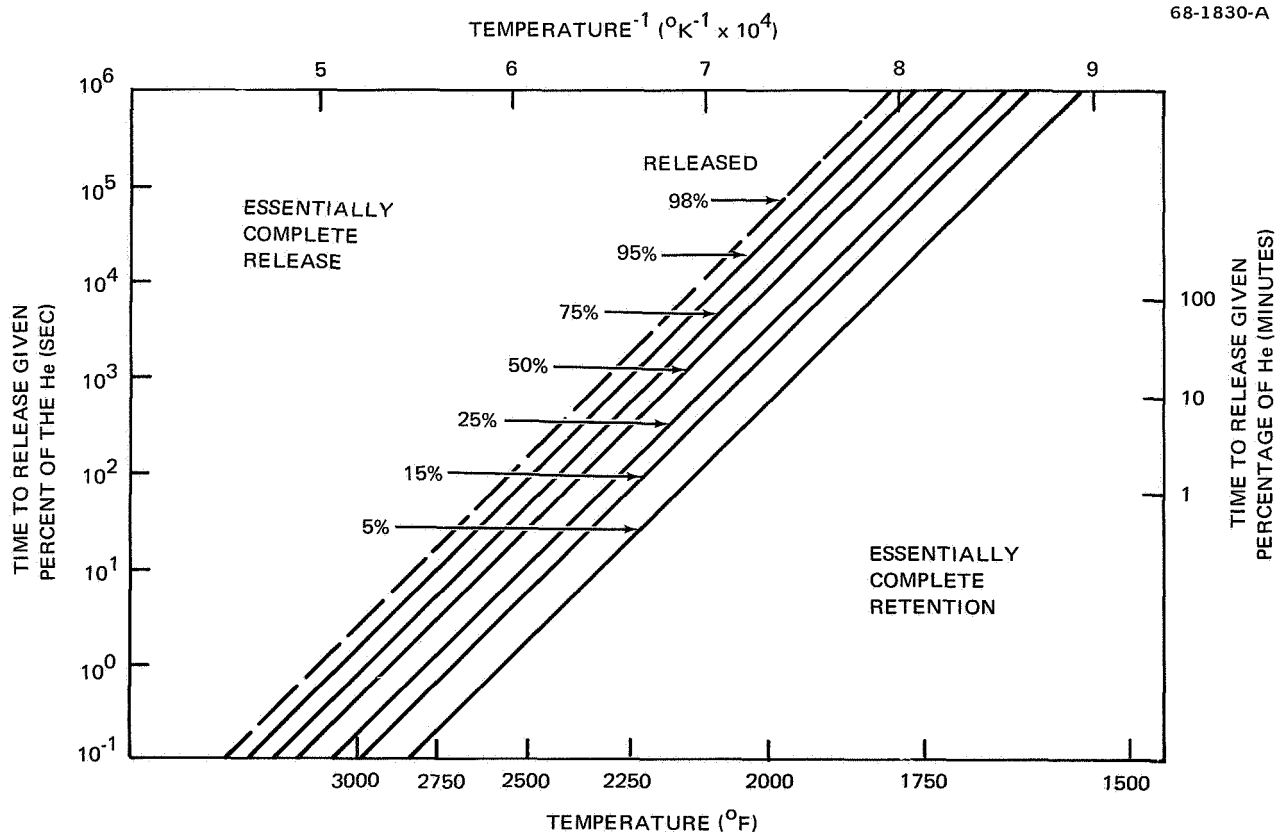


Figure 44. Helium Release from Plutonia

## Bibliography

Considerable data and references are available in the literature concerning candidate materials for heater designs. Typical sources are given in the bibliography at the end of this report.

## THERMAL CONTROL OF ALSEP MISSION COMPONENTS

At the request of NASA/MSC, the Solar Power Subsystem (SPS) designed by the Bendix Corporation (ref. 8 ) was reviewed. Preliminary designs of thermal control systems have been prepared for the central station and battery packages which utilize the reference heater designs developed under this contract, and a controllable heat pipe developed independently by DWDL. The SPS was originally designed as a backup to the SNAP-27, Radioisotope Thermoelectric Generator (RTG) of the Apollo Lunar Surface Experiments Package (ALSEP).

### System Requirements

Thermal control of the ALSEP central station and battery packages must meet the following mission requirements:

1. Compatibility during preflight storage of up to 2 years.
2. Compatibility with handling, mounting, and storage envelopes imposed by the Apollo lunar module.
3. No interfering electrical or magnetic fields.
4. Compatibility with launch and translunar flight requirements.
5. Capability of maintaining the equipment package within specific temperature limits for 1 year on the lunar surface.

With these requirements in mind, a design study was conducted; DWDL heat pipe technology was applied in conjunction with radioisotope heater capability to meet specific thermal control requirements of each equipment package as well as the mission requirements. Results show that small radioisotope heaters with self-regulating heat pipe/radiators will meet the requirements without the use of sensitive second-surface mirror-type radiators.

### Battery Thermal Control

In addition to the general mission requirements, the following data were applied to the battery thermal control mechanism:

1. Battery temperature limits: 40° to 100°F.
2. Electrical heat input: 3.0 W daytime (battery and charge controller), 1.9 W night (battery and converter).



3. Lunar surface temperature limits: +250°F daytime, -300°F night.
4. Multilayer insulation bag:

$$K_{\text{eff}} = 4.38 \times 10^{-4} \frac{\text{Btu}}{\text{hr/ft/}^\circ\text{F}} \cdot \quad (3)$$

The following requirements, developed during the analysis, will be discussed later in this report:

5. White paint radiator:  $\alpha = 0.2$ ,  $\epsilon = 0.9$  (Z93 Apollo coating).
6. Radiator area: 83 in.<sup>2</sup> with 93% fin effectiveness.
7. Maximum radiator temperature: 90°F.
8. Heat pipe: 3/8 in. OD x 0.016-in. -wall stainless steel.

Design description. - The wide temperature swing of the lunar environment and the need to dissipate the largest electrical heat load during the day require that the thermal control system be a variable heat rejection device. Sufficient heat must also be supplied to compensate for heat leaks through the multilayer insulation structure of the package for minimum lunar temperature conditions.

Small radioisotope heaters in combination with a self-regulating heat pipe/radiator will perform the required functions without moving parts or electrical power consumption.

The self-regulating heat pipe/radiator is a special adaptation of the heat pipe principle for thermal control purposes. Heat pipes are capable of transporting considerable heat with only a small temperature drop. When inert gas is included in an operating heat pipe, the gas and vapor of the working fluid separate into two distinct regions. The region of the working vapor is an active heat pipe and is nearly isothermal. The region of the inert gas is thermally inactive, and heat is transferred by conduction along the tube. With a thin-wall, low-conductivity tube, a large temperature gradient can be sustained in the inactive section with only a small heat leak.

As a variable thermal conductance device, the self-regulating heat pipe provides a conductance or turndown ratio of several thousand. For example, thermal conductance along the wall of a stainless steel heat pipe is on the order of  $1 \times 10^{-3} \text{ W/}^\circ\text{C}$  in the inert gas region. In the region of the working vapor, a conductance of  $10 \text{ W/}^\circ\text{C}$  can easily be attained. Thus, the turndown ratio is  $10/10^{-3} = 10\,000/1$ .

By proper design of the self-regulating heat pipe, the length of the active (isothermal) region will vary with the temperature of the evaporator (heat input region) of the heat pipe. This is depicted in figure 45.

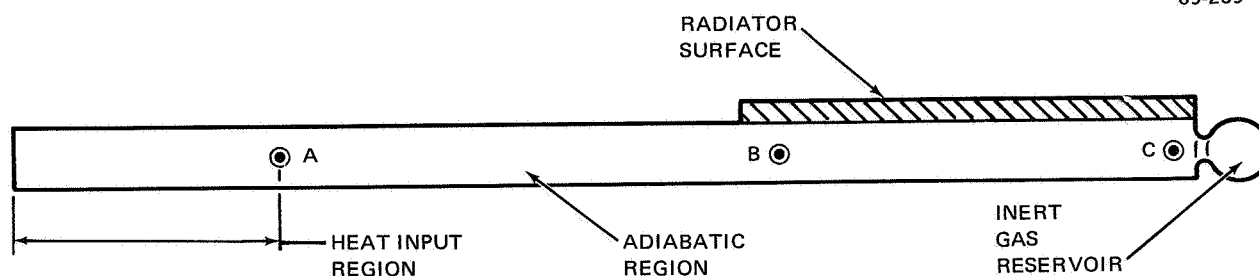


Figure 45. Schematic of Self-Regulating Heat Pipe/Radiator

For minimum heat input, the inert-gas vapor interface is at point A, and the heat leak to the radiator is by conduction along the tube wall. With intermediate heat input, the heat input region temperature increases slightly and the inert-gas vapor interface moves to B and activates some radiator surface. For maximum heat rejection, the interface moves to C; the entire radiator is active and is held nearly isothermal with the heat input region by heat pipe action. Movement of the interface results from the large change of vapor pressure of the working fluid with relatively small changes in fluid temperature. As vapor pressure increases, the inert gas is compressed to a small volume and the active radiator area increases to attain a new thermal equilibrium.

The self-regulating heat pipe/radiator as applied to the battery package is shown in figure 46. The heat pipe is formed into a Z shape with the lower bar attached to the battery heat transfer plate and the upper bar attached to the radiator. The gas interface is near the lower bar during lunar night but moves up into the radiator region as the battery warms during the day and heat rejection is necessary. A small reservoir on the upper bar of the "Z" receives the inert gas when the radiator is in full operation. The center leg of the "Z" necessarily results in a penetration of the insulation bag, but the size of the penetration and heat leak is small compared to other variable-conductance devices.

Analysis of the thermal control system involves solving a night heat balance to find the minimum heating required to compensate for leaks; a day heat balance to determine radiator size or maximum allowable heating; and a heat pipe design to determine the proper inert gas volume.

Lunar night operation. - The following heat balance must be satisfied for the lunar night condition:

$$Q_{\text{isotope}} + Q_{\text{batt. \& conv.}} = Q_{\text{bag leak}} + Q_{\text{H.P. leak}} \quad (4)$$

This equation is solved to find the required radioisotope heating to make up for losses.

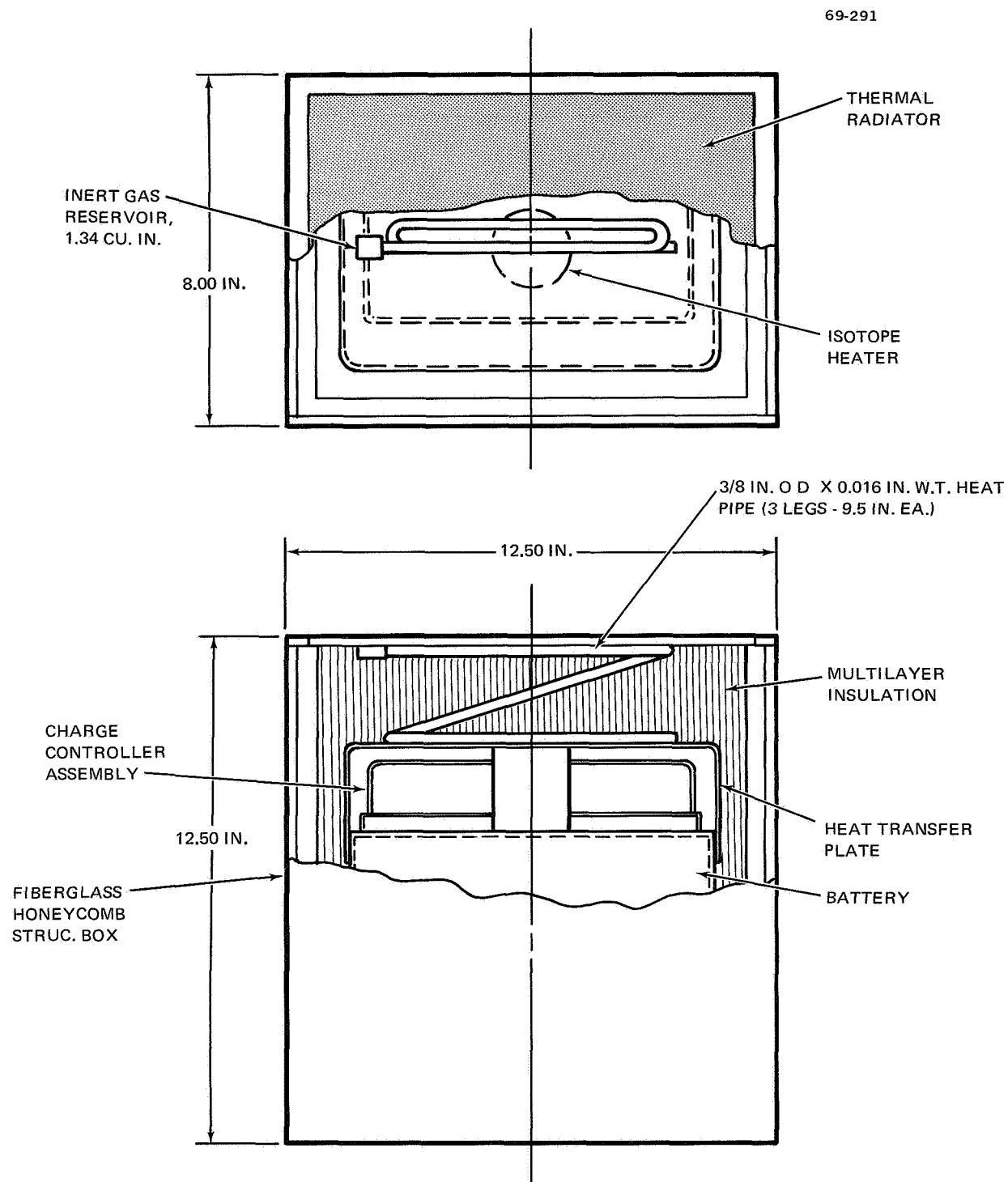


Figure 46. Battery Thermal Control Concept

The insulation bag leak was calculated for a bag thermal conductivity of  $K = \beta \times 1.75 \times 10^{-5}$  Btu/hr ft °F. With  $\beta = 25$ , the bag thickness is 0.67 in. and the bag area is 4.95 ft<sup>2</sup>.

$$Q_{\text{bag leak}} = \frac{KA\Delta T}{\Delta X} = 13.16 \text{ Btu/hr} = 3.85 \text{ W} \quad (5)$$

"Open circuit" conductance, or heat leak along the heat pipe, was calculated to be 0.15 W. Heat input from battery and converter at night was given as 1.9 W.

Minimum radioisotope heating to maintain the battery pack at 40°F or warmer would be:

$$Q_{\text{isotope}} = 3.85 + 0.15 - 1.9 = 2.1 \text{ W.} \quad (6)$$

The heat pipe leak contributes only a small fraction of the heat leak.

$$\left( \frac{0.15}{4.00} \right) (100) = 3.75\% \quad (7)$$

Therefore, isotope heating requirements are governed by the efficiency of the multilayer insulation bag.

Lunar day operation. - The daytime heat balance, solved for lunar noon conditions, would be:

$$Q_{\text{isotope (max)}} = Q_{\text{radiated}} - Q_{\text{absorbed}} - Q_{\text{batt. \& charger}} - Q_{\text{leak in}} \quad (8)$$

This heat balance gives the maximum allowable radioisotope heat which could be accommodated by the radiator system.

The heat leak through the insulation bag was calculated to be 1.5 W using the same K and  $\beta$  values as for night,  $\Delta T$  of 250°-100°F, and an area of 4.36 sq ft (the radiator surface was excluded). Heat absorbed by the 83-sq-in. radiator is calculated to be 13.84 W.

If a 10°F drop from the battery to the radiator is allowed, the radiator can dissipate 22.04 W.

The battery and charger will generate 3.0 W of heat. Solving for the maximum radioisotope heat,

$$Q_{\text{isotope (max)}} = 22.04 - 13.84 - 1.5 - 3.0 = 3.7 \text{ W} \quad (9)$$

This shows that the 83-sq-in. radiator can dissipate the required heat load at lunar noon with up to 3.7 W of radioisotope heating. The radiator, which is a white paint coating on 0.050-in. -thick aluminum, was sized somewhat arbitrarily to stay within the perimeter of the battery package's upper surface.

The above calculations indicate a minimum (2.1 W) and maximum (3.7 W) of isotope heat which would be compatible with the self-regulating heat pipe/radiator and the allowed temperature range of the battery pack. Any amount of radioisotope heat within this range could be selected to compensate for different insulation-bag properties or degradation, different radiator area or surface conditions, or decay of radioisotope. For example, a 3.7-W  $^{147}\text{Pm}$  heater would decay to 2.8 W after 1 year. It would fall within the day/night heat requirements at the beginning and end of the 1-year mission and still leave 33% margin for uncertainties in the insulation bag values.

Self-regulating heat pipe design. - The inert gas reservoir is sized by using the ideal gas law and the vapor pressure curve for the working fluid. The reservoir volume must be capable of holding all the inert gas when the radiator is fully operative (as during lunar day). Pressure on the inert gas is then equal to the vapor pressure of the working fluid at 100°F, maximum battery temperature. The inert gas temperature is about equal to the radiator temperature, or 90°F. When the battery cools, the inert gas interface must move down near the battery. Then the pressure is equal to the vapor pressure at 40°F and the gas temperature is intermediate between the cold radiator temperature and the 40°F battery.

Equations have been developed at DWDL for relating these gas volumes and properly sizing the reservoir. Using methyl alcohol as the working fluid, a volume of 1.34 in.<sup>3</sup> would be adequate. An undersize reservoir would allow the battery to fall below the 40°F limit before the inert gas interface moves to the heat input region. Providing a reservoir which is slightly larger than calculated provides closer temperature control over a given power input range. This is illustrated by data from an early laboratory-model self-regulating or controllable heat pipe as shown in figure 47.

Flight-qualified heat pipes using ammonia as the working fluid and helium as the inert gas have been delivered by DWDL for use on the NASA/GSFC ATS-E satellite. The heat pipes equalize and control the temperature around the periphery of the solar-cell mounting panels. Thermal-vacuum acceptance tests showed that the heat pipes performed according to predictions; the satellite with working heat pipes is scheduled for launch in mid-1969. Other heat pipes have been flown on satellites, one in April 1967 as a zero-g operation demonstration, and another with two heat pipes performing electronics compartment thermal equalization. Three laboratory demonstrations of self-regulating heat pipes have been designed and conducted at DWDL. This technology is ready for application to thermal control problems, and procedures for producing flight-qualified hardware are presently available.

Meeting other mission requirements. - The capability of the self-regulating heat pipe/radiator to meet launch and translunar flight requirements should not differ significantly from the results found for the thermal control design using the Surveyor-type bimetallic thermal switch described in the Bendix Corporation Report BSR-2228 (ref. 8). The heat pipe will function properly in the zero-g environment and maintain thermal control if the radiator is allowed to function.

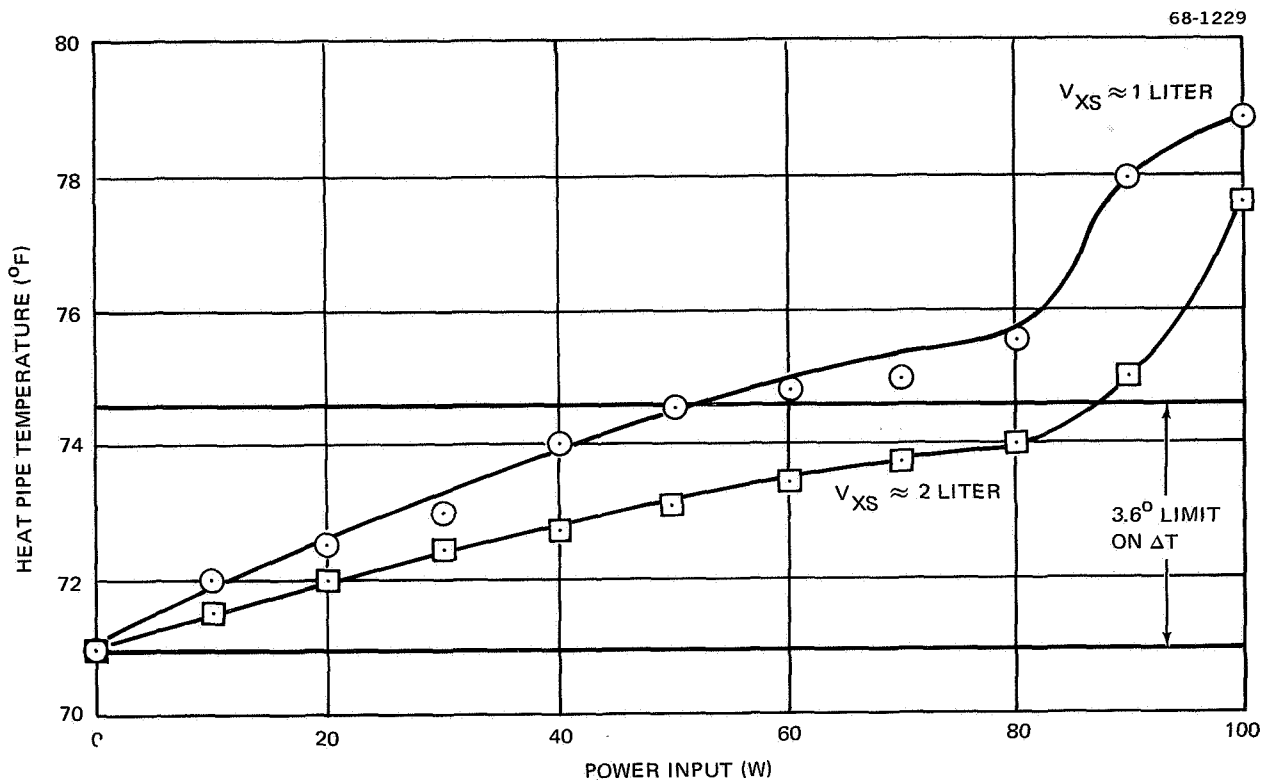


Figure 47. Laboratory Data for Self-Regulating Heat Pipe

Life tests of ammonia-helium-aluminum heat pipes have shown no thermal performance degradation when operated at over 3-year equivalent orbital heat loads. Other fluid-container combinations can be selected to meet specific requirements such as the low thermal conductance of the present design. The 2-year storage life of the heat pipe would not constitute a problem; the radiator surface could be fitted with protective covers during storage.

The heater would be installed in the battery package a relatively short time prior to launch operations. During the interim period, natural convection air-cooling of the radiator would maintain the battery at about  $20^\circ\text{F}$  above ambient air temperature. Orientation of the heat pipe/radiator would be controlled during this time so that capillary pumping action of the heat pipe would not have to overcome a large gravity head.

#### Central Station Thermal Control

The central station electronics are to be controlled to the following conditions:

1. Electronics temperature limits:  $+30^\circ$  to  $120^\circ\text{F}$ . Note that this is more stringent than the  $-22^\circ$  to  $+148^\circ\text{F}$  given in BSR-2228 by the Bendix Corporation (ref. 8).

2. Electrical heat generation: 33 W, day; 0 W, night.
3. Lunar surface temperature limits: +250°F, day; -300°F, night.
4. Multilayer insulation bag:
 
$$K_{\text{eff}} = 4.38 \times 10^{-4} \text{ Btu/hr ft } ^\circ\text{F (thickness} = 0.67 \text{ in.)} \quad (10)$$
5. Maximum radiator temperature: 110°F.
6. White paint radiator surface:  $\alpha = 0.2$ ,  $\varepsilon = 0.9$ .
7. No sunshields.
8. Radiator area: 2.7 ft<sup>2</sup> with 93% fin effectiveness.
9. Two heat pipes: 3/8 in. OD x 0.016-in. -wall stainless steel.

Design description. - The variable heat-rejection requirements for the central station electronics will be met by using self-regulating heat pipe/radiators and supplying the minimum heat requirements to meet heat leaks by a radioisotope heater. Figure 48 depicts this arrangement. To obtain a high radiator-fin effectiveness without excessive heat-pipe bending, two heat pipes are utilized. Each heat pipe will serve one-half the radiator surface. The heat pipes will be attached to the radiator and to the electronics mounting plate which will act as a transfer path for heat removal. A cup attached to the mounting plate receives the radioisotope heater, and an insulating cap reduces direct heat loss from the heater. Insertion of the heater will be an astronaut function. The mounting structure will be designed to carry the heater outside the lunar module during translunar flight and to minimize the heater temperature during this time.

Thermal analysis involves the same three steps as for the battery package: (1) find the minimum heat to make up night losses, (2) find the maximum allowable heat within reasonable radiation constraints, and (3) determine the inert-gas reservoir requirements of the heat pipes. The analysis indicates that the temperatures of the electronics package can be controlled within much tighter limits than either the baseline Bendix ALSEP design using mechanically decoupled radioisotope heaters, or the alternate design using the passive heater with a second surface-mirror-type radiator. In addition, radioisotope heat requirements are lower.

Lunar night operation. - At night, the radioisotope must supply heat equal to the insulation bag and "open circuit" heat pipe leak:

$$Q_{\text{isotope}} = Q_{\text{bag leak}} + Q_{\text{H. P. leak}} \quad (11)$$

With the heat pipe inoperative at night, the radiator will be very cold and the effective central station surface area will be 13.0 ft<sup>2</sup>. Calculation of the insulation bag leak yields 9.88 W. This is for -300°F on the central station

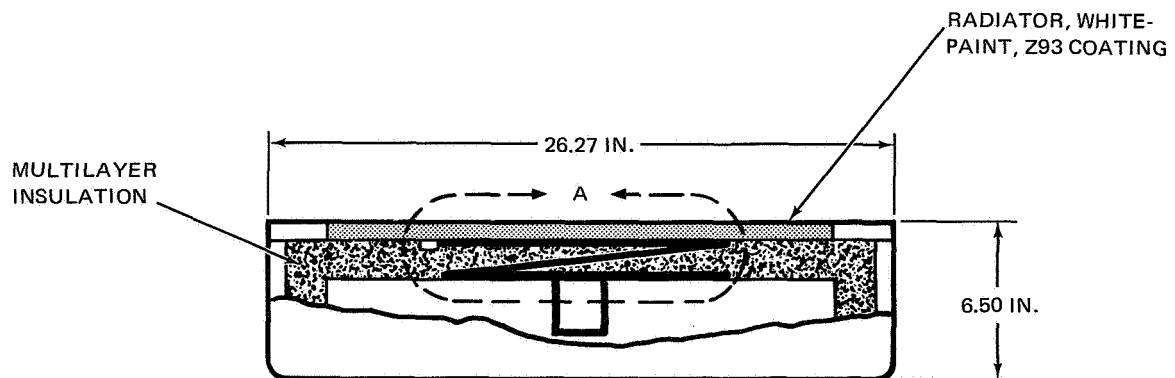
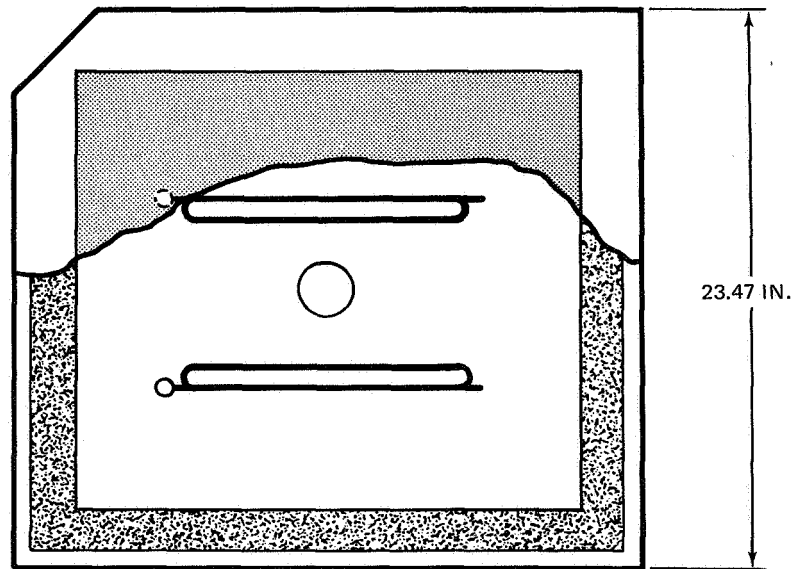
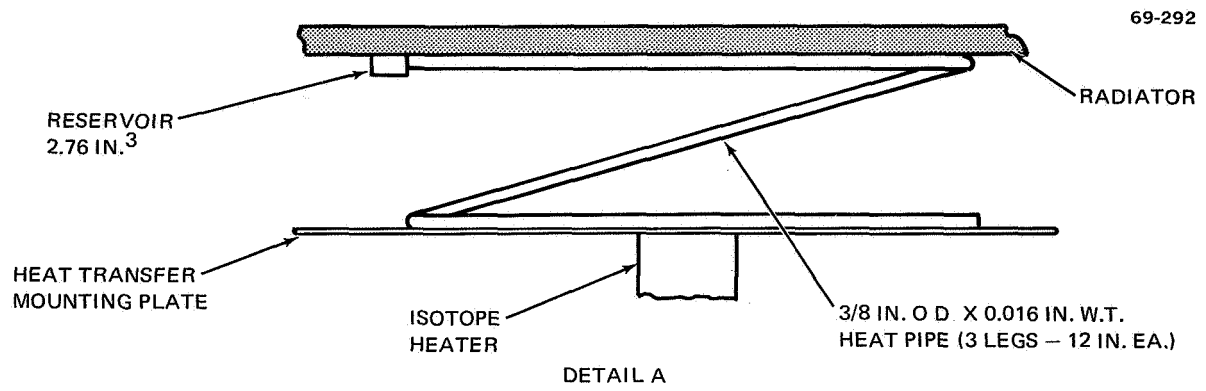


Figure 48. Central Station Thermal Control Concept



surfaces. The radiator temperature will be about the same. For two heat pipes with 10.5-in. adiabatic lengths, the heat pipe leak becomes 0.22 W. The isotope heater requirement is then

$$Q_{\text{isotope}} = 9.88 + 0.22 = 10.10 \text{ W} \quad (12)$$

and the heat pipe leak is

$$\frac{(100)(0.22)}{10.10} = 2.2\% \quad (13)$$

of the total heat loss.

The reason that the heating requirement is low--compared to the Bendix alternate design which used a passive heater--is that the radiator is thermally uncoupled from the radioisotope and electronics at night.

Lunar day operation. - The radiator could be sized to fit the heat dissipation requirements during daytime while using the 10.10-W heater. A more flexible design results by choosing a suitable radiator size to fit on the top of the central station equipment package, and then calculating the upper limit of radioisotope and/or electrical power which can be dissipated. Then,

$$Q_{\text{isotope (max)}} = Q_{\text{radiated}} - Q_{\text{absorbed}} - Q_{\text{elect}} - Q_{\text{leak in}} \quad (14)$$

A 2.7-ft<sup>2</sup> radiator will easily fit on top of the central station. For 0.063-in. -thick aluminum and the two heat pipes, a radiator effectiveness of approximately 0.93 will result. A white paint coating with  $\alpha = 0.02$  and  $\epsilon = 0.9$  will be used. The radiator capabilities become

$$Q_{\text{absorbed}} = 64.8 \text{ W} \quad (15)$$

If a maximum radiator temperature of 110°F is allowed (this corresponds to a maximum electronic temperature of approximately 120°F),

$$Q_{\text{radiated}} = 119.4 \text{ W} \quad (16)$$

Calculation of the heat leak in through the insulation bag yields  $Q_{\text{leak in}} = 3.4 \text{ W}$ . This is conservatively high because it assumes that the entire surface of the central station (except the radiator) reaches 250°F (the lunar surface temperature). By proper coating of the surfaces, this temperature could be reduced and heat leak-in reduced proportionately.

With electrical power of 33.0 W, the daytime heat balance yields

$$Q_{\text{isotope (max)}} = 119.4 - 64.8 - 33.0 - 3.4 = 18.2 \text{ W} \quad (17)$$

Thus, an isotope heater in the range 10.1 to 18.2 W would meet the criteria, and the electronics would be controlled between +30° and +120°F.

With a  $^{238}\text{Pu}$ -fueled capsule, decrease in heat output during 1 year would be negligible. With a  $^{147}\text{Pm}$  heater (originally at 18.0 W, for example), the heat output after 1 year would be about 13.8 W. This is still above the 10.10-W minimum power required and would allow for 36% uncertainty in the heat leakage term. No sunshields are required over the white paint radiator surface.

Heat pipes would be required to handle a maximum of only 51 W, or about 25 W each. Heat pipes of the size used could easily handle 100 W each if the radiator area were provided. A  $10^\circ\text{F}$  temperature drop has been allowed between the heat pipe evaporator (heat input) region and the radiator; this is conservatively high.

The greatest uncertainty of this design is the calculation of heat leaks through the insulation bag. But the self-regulating heat/radiator provides the flexibility to accommodate variations or degradation of insulation and still maintain thermal control.

Self-regulating heat pipe design. - The two heat pipes for the central station will be similar to the one used for battery thermal control. Thin stainless steel tubing is used to reduce axial conduction during night operation.

During daytime operation, the inert gas will be contained by the gas reservoir at  $110^\circ\text{F}$ , the radiator temperature. At night, the gas will expand to fill the radiator and adiabatic sections of the heat pipe, and will be at an average temperature of about  $200^\circ\text{R}$  ( $-260^\circ\text{F}$ ). By use of the ideal gas relationship, the inert gas reservoir size can be determined as a function of the working fluid used.

Meeting other mission requirements. - The other mission requirements will be met by the self-regulating heat pipe/radiator. The 2-year storage life will not be a problem if the radiator coating is protected. The capsule will be inserted in the central station by the astronaut while on the lunar surface. Temperature control of the electronics and the heater during trans-lunar flight will be accomplished by appropriate positioning of these items within and on the lunar module.

### Thermal Control Summary and Weights

The principle parameters involved in the thermal control system design are presented in table 23. Weights were calculated for the three components of each system. These weights do not include the multilayer insulation bag weight or equipment mounting/heat-transfer plates. The insulation bags should not differ significantly from those described in the Bendix Corporation design, but the heat transfer mounting plates might decrease in weight slightly since the heat pipe traverses a longer path for heat collection. Results show that the battery pack thermal control system would weigh 1.52 lb, and the central station system would weigh 5.02 lb.

TABLE 23  
THERMAL CONTROL SUMMARY

Radiator - (Al sheet with white surface coating $\alpha/\epsilon = 0.2/0.9$ )	Battery	Central station
Area (ft <sup>2</sup> )	0.61	2.70
Thickness (in.)	0.050	0.063
Effectiveness	0.93	0.93
Thermal dissipation (W, net maximum)	8.2	54.6
Max temp (°F)	90	110
Min temp (°F)	-300	-300
Heat pipes - stainless steel		
Number	1	2
Size (in.)	0.375-OD x 0.016-wall	0.735-OD x 0.016-wall
Length (in.)	28.5	72
Max heat transport (W)	8.2	27.3/pipe
Max temp (°F)	100	120
Min temp (°F)	40	30
Reservoir volume (in. <sup>3</sup> for methanol)	1.34	0.34
Radioisotope capsule		
Number	1	1
Max power (W)	3.7	18.2
Min power (W)	2.1	10.1
Diameter (in.)	1.913	2.275
Length (in.)	2.289	2.793
Weights (lb)		
Radiator	0.43	2.4
Heat pipes	0.35	1.1
Isotope heater (plutonium fuel)	<u>0.74</u>	<u>1.52</u>
Total	1.52	5.02

## Selection of Radioisotope Heaters

Sizes and power levels of small radioisotope heaters being studied at DWDL are compatible with the space and power requirements of thermal control systems for both the battery and central station.

Battery. - The required power level for thermal control of the battery is a minimum of 2.1 and a maximum of 3.7 W. The 10-W heaters using promethium or plutonium fuel would be appropriate for this application if the fuel were diluted sufficiently to result in the desired power level. An initial power level of 3.6 W using promethium would result in an output of 2.76 W--well above the minimum--at 1-year mission termination. For a plutonium-fueled capsule, originally at 3.6 W, the decrease in output over 1 year of operation would be negligible.

The 10-W cylindrical heaters have the following weights and outer dimensions:

<u>Fuel</u>	<u>Weight</u>	<u>Diameter</u>	<u>Height</u>
Pm	1.014 lb	2.056 in.	2.544 in.
Pu	0.740 lb	1.952 in.	2.388 in.

Dilution of  $\text{Pm}_2\text{O}_3$  by  $\text{Sm}_2\text{O}_3$  and of  $\text{PuO}_2$  by  $\text{UO}_2$  would result in negligible changes in capsule weights. Outer dimensions of the 10-W capsules are compatible with the available volume for the heater as shown in figure 46.

Central station. - Thermal control requirements of the central station indicate a minimum heater output of 10.1 and a maximum of 18.2 W. A 25-W heater using promethium or plutonium fuel would meet these requirements if the fuel were suitably diluted by  $\text{Sm}_2\text{O}_3$  or  $\text{UO}_2$ , respectively. An initial power level of 18.0 W, using promethium, would result in an output of 13.8 W--well above the 10.0-W minimum--after 1 year of operation. Power flattening of plutonium-fueled capsules would be negligible. A 25-W cylindrical heater has the following weights and outer dimensions:

<u>Fuel</u>	<u>Weight</u>	<u>Diameter</u>	<u>Height</u>
Pm	2.04 lb	2.432 in.	3.028 in.
Pu	1.52 lb	2.275 in.	2.793 in.

Fuel dilution would have a negligible effect on capsule weights. The outer dimensions of the 25-W capsules are compatible with the available volume for the heater as shown in figure 48.

## MANUFACTURING PROCESSES AND QUALITY ASSURANCE

DWDL's current appraisal of activity required to manufacture radioisotope heaters is shown in figure 49. Fuel preparation flow diagrams are

**Figure 49. Manufacturing Program Logic**

shown in figure 50 for both promethia and plutonia. Manufacture flow diagrams for assembly, inspection, and delivery of promethia- or plutonia-fueled heaters are shown in figure 51. Standard McDonnell Douglas procedures form the basis for the manufacturing processes and quality assurance plan discussed below.

### Approach

The intent of this plan is to meet the requirements of the Interagency Safety Evaluation Panel and the Space Council. It is consistent with NASA publications NPC 200-2 and NPC 250-1 as applicable to the Radioisotope Heater Development Program to design, develop, test, fabricate, and qualify small radioisotope heaters for manned spacecraft thermal control applications.

Established McDonnell Douglas Astronautics Company operating policies and procedures provide guidance, disciplines, and assessments to all phases of the program--from design through testing and delivery of flight-qualified products.

Additions and revisions to MDAC policies and procedures are audited for conformance to this plan; appropriate support is provided to ensure that the manufacturing and quality level attained is commensurate with contractual requirements.

Quality Program. - DWDL will organize phases II and III of the program in a manner that assures that quality requirements are determined and satisfied in all phases of contract performance. DWDL will make product changes as required to enhance heater component performance and reliability at the earliest possible point in development and fabrication. This plan provides timely prevention and detection methods, corrective actions, and documentation of all nonconformances. Objective evidence of conformance, including applicable records of inspections and test results, will be readily available to the contractor or designated representative.

The DWDL quality assurance and manufacturing policy and objectives are established by MDAC standard practice bulletins and implemented by standard practice memoranda. By working with customers, subcontractors, industry, and the contractor, the highest standards of product quality are developed and maintained.

### Quality Program Plan

Quality Assurance program plans are prepared consistent with the basic format and requirements of NPC 200-2. These include establishment and maintenance of an effective quality assurance program from design concept through delivery.

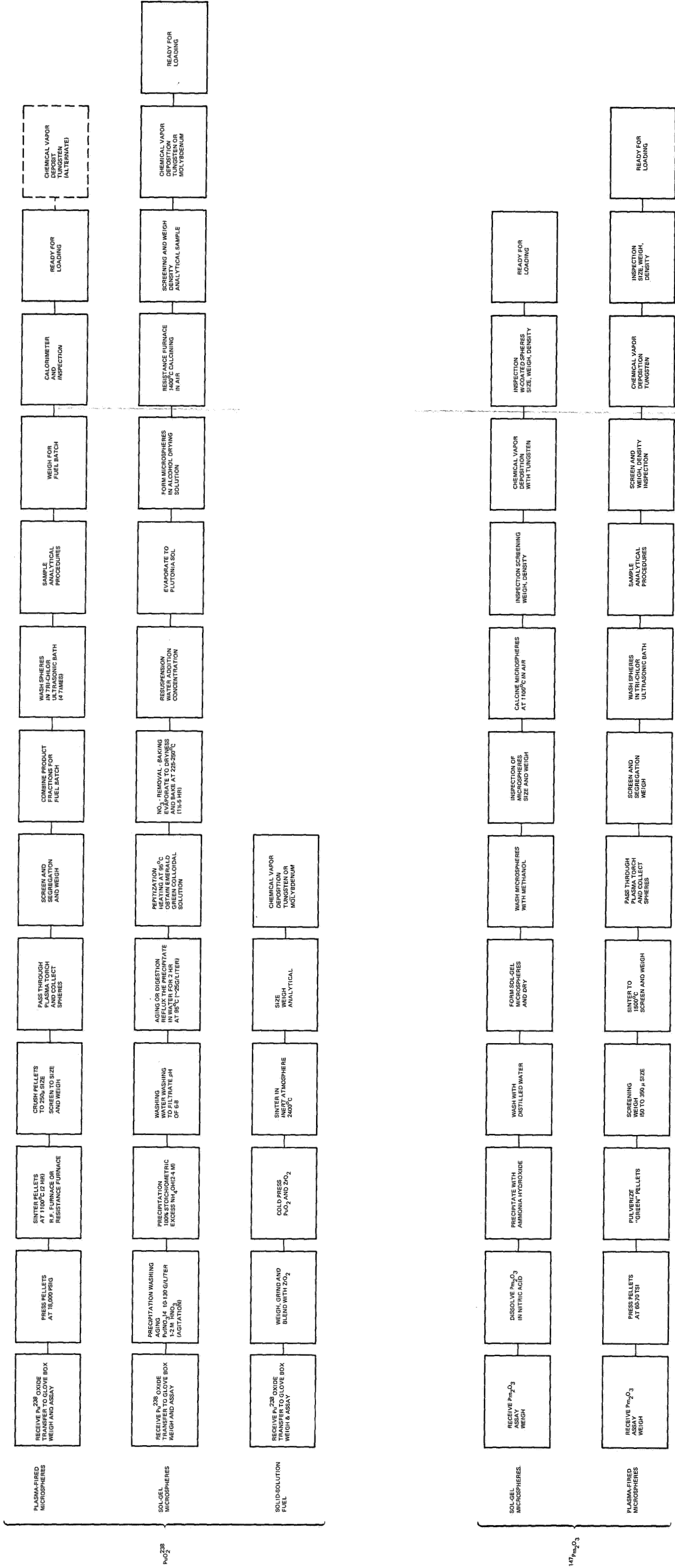


Figure 50. Fuel Preparation Flow Diagrams

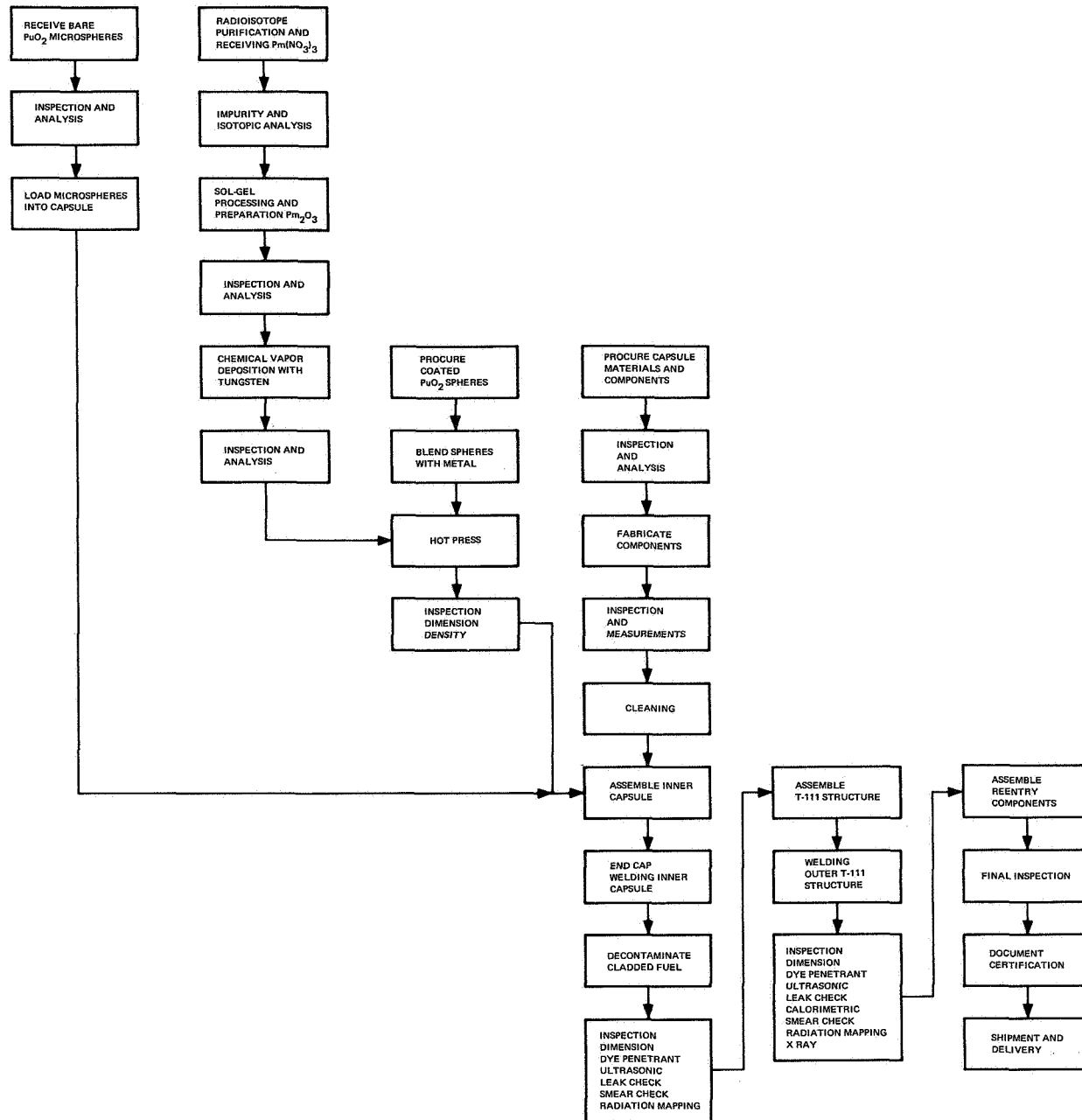


Figure 51. Manufacturing Flow Diagram – Promethia- and Plutonia-Fueled Heaters



Quality Assurance personnel have organizational freedom to identify and assess quality problems; and the responsibility to recommend and/or initiate solutions.

A simplified flow chart of the total quality program is shown in figure 52.

### Design and Development

Phases II and III will be organized in a manner to provide close coordination between the various functions at DWDL. Product quality is the prime consideration in the development of the quality program plan.

Drawing and specification review. - The MDAC Engineering Drafting Manual and drawing release systems ensure that all Development Engineering documents released for manufacture, processing, or procurement contain adequate requirements for determining and controlling quality. This control is applied to completely definitive drawings that provide design, development, and fabrication direction; to procurement drawings that provide design and development direction and guidance to vendors and subcontractors, and establish hardware acceptance criteria; and to specification drawings that control the procurement and processing of material.

Inspection and test methods. - Inspection methods are established by Reliability Assurance through a review of Development Engineering drawing releases. For items of DWDL manufacture the inspection methods are documented on the appropriate Fabrication Outline (FO) or Assembly Outline (AO) to ensure control of manufacturing processes. For supplier items, the inspection methods are documented on Inspection Operation Sheets (IOS) for use in source or receiving inspection.

All test requirements, except for government or industry standard parts, are released by Development Engineering.

Qualification testing. - Qualification tests are discussed in the Qualification Test Plan section of this report. Specific qualification criteria, and number and quantities of radioisotope capsules and stand-in capsules are included.

Prior to conducting the qualification tests, and following rework, repair, or disassembly of the test specimen, the hardware is inspected for conformance to Development Engineering drawing requirements, and submitted for functional acceptance tests. Instrumentation and measurement equipment used in qualification tests are verified to be within calibration time limits by Reliability Assurance. Hardware failures occurring during qualification testing are documented on Failure and Rejection Reports by Reliability Assurance as requested by Development Engineering.

Formal qualification or acceptance tests demonstrate that the radioisotope heaters meet established requirements under various combinations of service environments. The Test Control Drawing (TCD) for the qualification test is the controlling document and will comply with the tests specified by the Inter-agency Safety Evaluation Panel. Test environments and test levels for formal qualification or acceptance do not exceed those for the companion qualification tests.

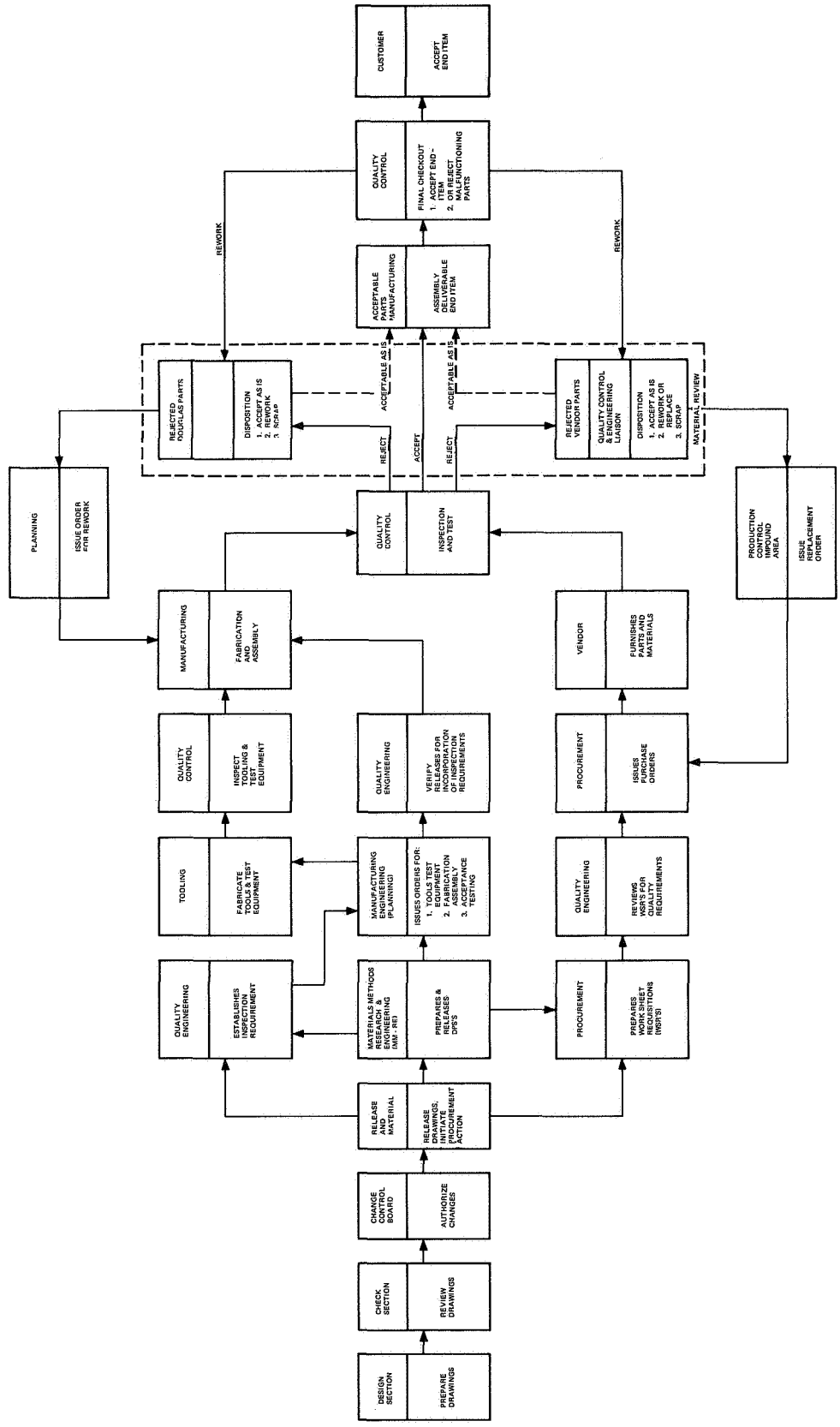


Figure 52. Quality Program Flow Chart

Data submittal requirements for formal qualification tests specify that drawings, specifications, test plans, TCD's, and procedures are to be submitted to the customer prior to the scheduled test start date. The tests are conducted under DWDL direction and control. Tests are witnessed by Reliability Assurance and the technical monitor or his designated representative.

### Identification and Traceability

All items (parts, components, or assemblies), both fabricated and procured, are subject to review by Engineering for identification (serial numbers, lot code, or date code) and traceability requirements. The final determination and effectivity of these requirements is subject to review by the customer or designated representative.

The purpose of identification is to correlate records and documentation with the associated hardware. Identification is accomplished by application of a serial number, lot code, or date code to selected parts, components, subassemblies, and end-items.

The purpose of traceability is to provide the capability to retrieve receiving, fabrication, assembly, installation, and test records of selected items of hardware relative to end-item use. Traceability is accomplished by application of the serial number, lot code, or date code to selected hardware items, and generation of continuous records through all applicable phases of procurement, manufacture, end-item installation, and checkout.

### Control of DWDL-Procured Material

DWDL is responsible for the adequacy and quality of all procured items and services unless otherwise directed in writing by the customer. Reliability Assurance verifies and attests to the conformance to specified Engineering requirements of all purchased materials and articles.

Selection of procurement sources. - The selection of procurement sources is based upon the supplier's historical records or survey reports. Reliability Assurance reviews and provides comments on the adequacy of all procurement sources.

Purchase orders and subcontract documents include basic technical requirements, government source inspection requirements, vendor source inspection requirements, source inspection statements, subcontractor quality program requirements, raw materials specifications, and identification, preservation, and packaging specifications.

Vendor source inspection. - Products are required to be in strict conformance to the requirements of the procurement documents. Reliability Assurance may elect to use the supplier's objective evidence in lieu of duplicating the inspection effort when validity of such evidence has been verified.

Receiving inspection. - DWDL receiving inspections ensure that:

1. All articles have been properly qualified in accordance with requirements of the applicable specifications; are designated for qualification testing, or that omission of specific tests has been justified and approved by the appropriate Development Engineering Section and recorded on the Design Review List.
2. All hardware has been inspected by the supplier in accordance with the purchase order requirements, and satisfactory evidence of inspection is submitted with each article or subassembly.
3. No apparent damage has occurred in transit. Items not inspected at the source by DWDL are inspected and tested upon receipt.
4. Nonconforming material is rejected and submitted to Material Review (refer to discussion under Nonconforming Material). Incomplete and nonconforming materials are returned to the supplier unless accepted by Material Review action.
5. Physical separation of raw material and purchased fabricated articles is accomplished.

#### Control of Government-Furnished Material

DWDL maintains accountability records of receipt, storage, issuance, records control, and transfer of all government-furnished material.

Receiving. - Quantity and identity of incoming shipments are verified as specified on the government shipping documents. Receiving inspections are made to ensure identity, evidence of government inspection acceptance, packaging and preservation, required documentation, obvious damage, omissions, and oversights.

Storage. - Material is stored by contract number in bonded storage to ensure protection and preservation in conformance with sound industrial practices and applicable contractual requirements. Appropriate storage inspection is made to assure that quality and storage conditions conform to specifications.

Nuclear materials control. - Government-furnished radioisotope fuels (special nuclear and/or byproduct materials) is controlled from receipt through final assembly according to applicable AEC requirements. Adequate safeguards are provided under federal regulations, at DWDL's nuclear facilities. Responsibility for accountability and control of nuclear material has been established and is maintained by the DWDL Nuclear Safety Officer in accordance with AEC regulations.

## Control of DWDL-Fabricated Articles

Reliability Assurance inspects and tests (or verifies testing of) the product for conformance to applicable engineering drawings, test procedures specifications, and other documents. These inspections and tests ensure that the reliability inherent in the design is maintained during manufacture of radioisotope-fueled capsules. Complete records of these inspections and tests are maintained.

Engineering drawings are sufficiently comprehensive that they can be used for inspection of the product. Supplementary instructions are test procedures prepared by Manufacturing Engineering and process directions prepared by Methods and Materials.

Prior to implementation, Reliability Assurance reviews the planning of tests and inspections, and generates required Inspection Operation Sheets, standard parts test specifications, and other instructions as required. Inspection and test planning commences with manufacturing and extends through final end-item tests. Review of manufacturing and test planning ensures that the documents provide adequate inspection points and special documentation records.

## Nonconforming Material

Reliability Assurance is responsible for the detection and reporting of nonconforming materials. Upon detection, all nonconforming material is promptly removed from the manufacturing system and impounded, if practical, for disposition and for completion of the Failure and Rejection Report.

The Material Review Board (MRB) is a formal DWDL board established to determine the disposition of minor nonconforming material and recommend disposition of major nonconforming material. Members of the board may call upon other government or MDAC personnel to act in an advisory or consultant capacity; such personnel will have no vote in board decisions.

## Inspection, Measurement, and Test Equipment

Reliability Assurance, in coordination with Manufacturing Engineering, Facilities, and Engineering Laboratories and Services, provides for selection, evaluation, approval, maintenance, and control of inspection standards, gauges, and measuring and test equipment necessary to ensure conformance with specifications, drawing, and contract requirements. This includes production tools and automated equipment incorporating an inspection, measuring, or test function. All equipment is used in an environment and a manner that ensures continued uniformly accurate measurements. Reliability Assurance supervises the maintenance of records of recalibration status, condition, and correction or repair of inspection, measuring and test equipment.

## Inspection Stamps

DWDL's inspection stamp control system includes, but is not limited to:

1. Stamps, decals, seals, and methods of application to identify items as they undergo in-process inspection, partial inspection, final subassembly inspection, functional tests, and final end-item inspection.
2. Records that provide traceability of each stamp to the individual responsible for its use.
3. Affixing of stamps on conforming items, indicating that inspections have been performed (if this is impractical because of a physical limitation, or when stamps will compromise quality, they are applied to tags, cards, or labels and attached to the individual items).

Stamp designs do not resemble Government inspection stamps.

## Preservation, Packaging, Handling, Storage, and Shipping

DWDL has current AEC licenses for special nuclear source material and byproduct materials. These licenses permit possession, processing, transfer, and shipment of any or all of the licensed materials to any point within the continental limits of the United States by common carrier in ICC-approved shipping containers or ICC-Specification containers in compliance with the regulations in Title 10, Part 70 of the Code of Federal Regulation and other applicable government regulations. The AEC has established safety standards for the packaging of radioactive and fissile materials (AEC Manual, Chapter 0529) for transportation from facilities not subject to 10 CFR Part 71, and to establish responsibilities for issuing AEC certificates of approval for such packages.

## Training and Certification of Personnel

Certain specified functions and operations are performed by trained and certified employees to ensure the integrity of the end-product or to comply with contractual requirements. Engineering and Manufacturing Engineering identify affected functions and operations which must be performed by trained certified employees. Continuous training provides an adequate number of qualified personnel able to perform in specific critical skill areas. The MDAC Industrial Training Program provides current training courses that support Reliability Assurance, Manufacturing, and other groups responsible for product quality. Skill levels are verified and expanded concurrent with technology advances.

## Data Reporting and Corrective Action

Procedures and responsibilities are established by DWDL for collection and analysis of failure and quality data resulting from testing, inspection, and

use of procured and produced articles. Procedures and assigned responsibilities include effective followup to ensure timely and adequate corrective action on reported deficiencies throughout the manufacturing and test program by DWDL and subcontractors. Data are collected and updated by Reliability Assurance.

### Program Documentation and Reporting

DWDL will develop the defined documentation for the Radioisotope Heater Development Program. Documents requiring customer review and/or approval are submitted prior to implementation and according to contractual requirements.

Inspection procedures for fabrication, assembly, and test operations are an integral part of the manufacturing document, and assembly and fabrication outlines. These documents are reviewed prior to implementation to ensure adequate coverage by Reliability Assurance. Special inspection procedures are issued when required.

Test procedures are written by Engineering. Manufacturing Engineering is responsible for issuing fabrication orders and assembly outlines, as applicable, for performance of required acceptance tests in accordance with test procedures.

Manufacturing and operating instructions are controlled through these activities. Detailed manufacturing documents are updated to reflect the Engineering Order.

### Manufacturing and Inspection Methods

Program management at DWDL assures rigid control of radioisotope heater manufacture and inspection methods through the use of a variety of specifications prepared to specific requirements established by the work authorizations and engineering release system. Specifications are prepared by Engineering with review and/or contributions from Manufacturing, Reliability Engineering, Purchasing, Safety, Materials, and Research. Where required, customer review and approval is obtained.

## PROGRAM PLANS AND BUDGETARY COST ESTIMATES

This section discusses the program plan and presents budgetary cost estimates for accomplishing the final design, hardware development and fabrication, and inspections and tests necessary to qualify a selected group of heaters.

The phase I program was structured into tasks covering the major technical areas of design and safety analysis, materials selection, manufacturing, and quality assurance. One output of these individual tasks was a detailed description and statement of the phase II and phase III work required to successfully fabricate and qualify heaters. Phase II will be initiated by performing a detailed design evaluation based on the phase I reference designs, the materials selected, and the development test program. The types of tests are specified and preliminary test conditions defined. Based on this information, Manufacturing and Quality Assurance can formulate plans and estimates for fabrication and inspection of the heaters. Similarly, Test Engineering will determine the requirements for development and qualification test programs.

Close liaison with the customer concerning definition of the required safety test program will be necessary in order to prepare for Interagency Safety Evaluation Panel and Space Council approvals for ultimate flight application. Fuel delivery requirements and lead times will be established to ensure availability of the radioisotopes when needed. Coordination of the planning activity with the customer will minimize the elapsed time from phase I completion to initiation of the subsequent phases.

Program plans, cost estimates, and program schedules are presented for a total program consisting of 10- and 50-W reference designs for both plutonia bare microspheres and promethium cermet fuels. The total program includes not only safety and design engineering costs but also development and qualification, facility, materials, and fabrication costs. In addition, optional programs are presented as alternate methods of approaching the goal of flight-qualified radioisotope heaters.

### Final Detailed Design and Safety Analysis

During phase II, a final detailed design, based on the reference designs and data produced in phase I, will be prepared to incorporate changes and recommendations specified by the customer and user agencies. Detailed materials specifications and manufacturing process standards will be prepared for customer approval as required, and incorporated in the working drawings together with the requirements for quality assurance.

During manufacture and assembly of representative heater components, continuous liaison will be maintained with Quality Assurance to maintain working drawings to represent the "as-built" condition of the completed heater. Quality Assurance will be responsible for ensuring that the manufacturing process and quality assurance plan outlined in the previous section is being adhered to.



The safety analysis initiated during phase I and continued in phase II will be finalized by completing the following documentation and analyses:

1. Interim revisions of the reference design, accident model, and safety analysis reports will be prepared. These documents will contain all analytical and experimental phase II results.
2. A probabilistic accident model will be formulated which includes mission constraints as variables. Accident probabilities as well as probable severity vs mission use will be determined.
3. Requirements of the safety analysis report necessary for flight safety approval will be outlined.

During the phase I program, a systems approach to the safety and design analysis problem was developed. This approach, shown in block diagram form in figure 53, will be continued in the phase II and phase III programs. Parallel tests and analyses will be conducted during phase II. This is an iterative process requiring test results to be constantly reviewed and the mathematical models and heater designs appropriately modified. This process will result in a final design that meets the stringent safety criteria and has a high probability of being safe under all credible conditions and environments. Finally, this analysis will be completed during phase III on the flight-qualified heaters and will form the basis for the safety analysis report.

#### Manufacturing Processes and Inspection Techniques

Based on the manufacturing processes and quality assurance plan previously outlined, detailed manufacturing processes and inspection techniques will be developed for manufacture of the heaters to minimize leadtimes for flight-item procurement and manufacture. The basic manufacturing plan will include the latest proven processes and inspection, quality assurance, and qualification techniques. Specifications will be prepared to establish and cover the requirements and procedures involved from initial material procurement to final assembly and delivery. In-process control will be made for complete reliability and traceability of parts. Formal documentation and recordkeeping will be maintained to ensure reproducibility of fully qualified fueled heaters. Specific objectives will be to:

1. Incorporate phase I results to simplify fabrication and minimize development costs without altering the functional reliability of the capsules.
2. Design adequate tooling and fixtures for the program.
3. Determine the validity of fabrication and testing procedures.
4. Prepare specifications for materials procurement and fabrication procedures.
5. Demonstrate the feasibility of manufacturing radioisotope-fueled capsules of the reference designs to rigid specifications and high-quality standards.

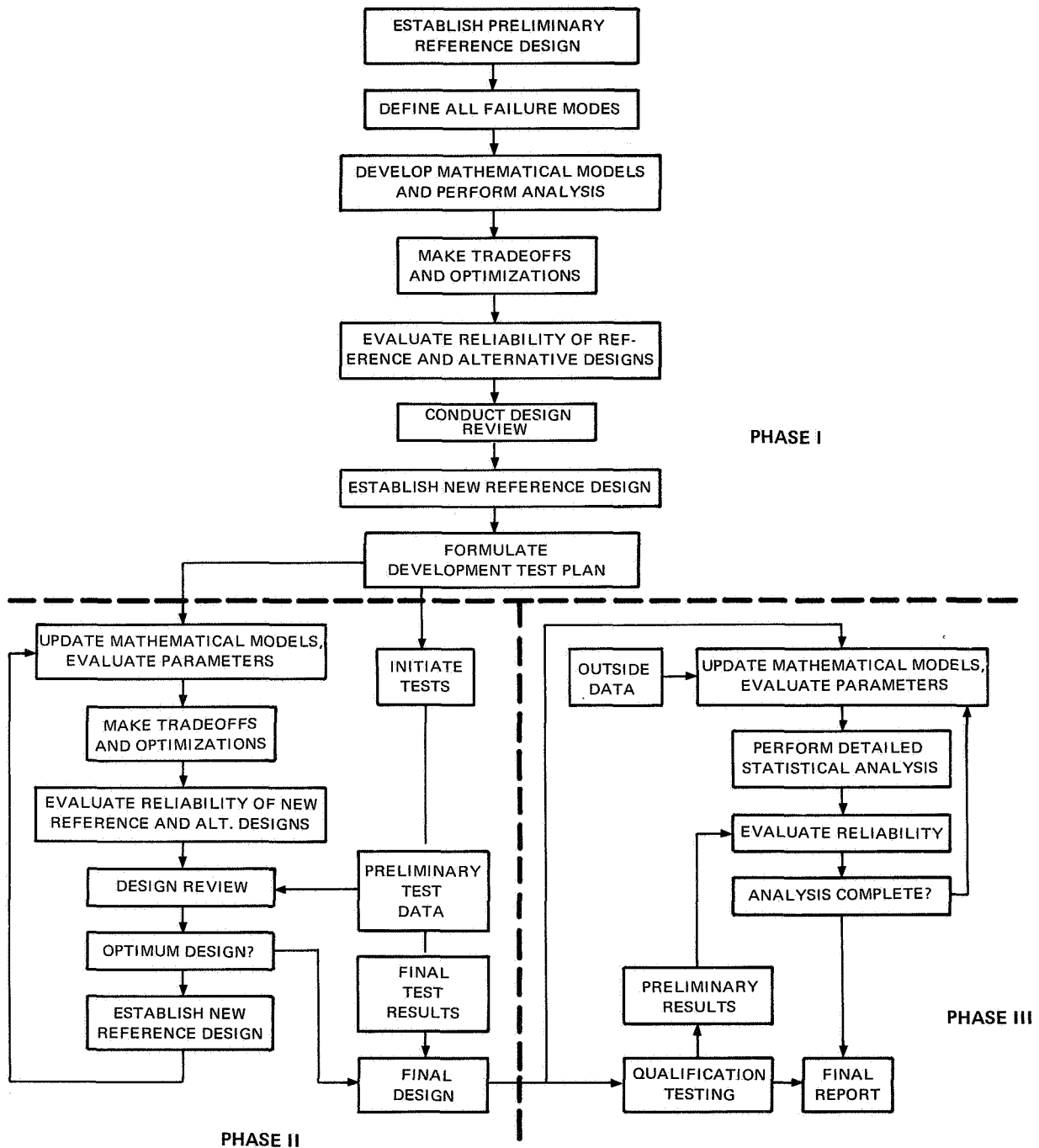


Figure 53. Systems Analysis Block Diagram

6. Evaluate new processes and process modifications for applicability to fueled capsules.

7. Apply advances in technology to minimize time and cost.

Inspection techniques will be used to ensure reliable flight-type hardware. Inspections to be performed, and points in the fabrication sequence where these inspections are required, will be carefully followed. Current techniques will be reviewed and modified as necessary. New methods of measuring the required parameters will be developed as needed and incorporated into the fabrication process. In-process control will be followed for complete reliability and traceability.

#### Prototype Hardware Development and Development Tests

A detailed plan for development and testing of heater hardware and prototype heaters has been developed. Each component of a heater will be tested individually and/or in combination with related components. Development testing and design will be an iterative process.

A summary of the development tests identified for phase II is shown in table 24. The table includes a complete development test program for both the 10- and 50-W heaters using promethia and plutonia fuels; it describes the test objectives, requirements, materials, numbers and sizes of specimens, equipment, and facilities where the tests can be performed.

It is recognized that because of schedule and/or budget constraints, it may not be possible to perform all of these tests. The following tests, however, are considered the minimum required to ensure development of flight-qualified hardware:

1. Vibration
2. Thermal shock
3. Thermal cycling
4. Dynamic pressure loading and thermal stress
5. Steep-angle reentry heating
6. Gliding reentry heating
7. Launch explosion
8. Reentry impact tests (series I)
9. Reentry impact tests (series II)
10. High-temperature burst

TABLE 24  
SUMMARY OF DEVELOPMENT TESTS FOR PHASE II

TEST DESCRIPTION	PRIMARY TEST OBJECTIVES	SECONDARY TEST OBJECTIVES	REQUIREMENTS FOR TESTS	FUEL FORM	ABLATOR	TEST SPECIMENS	FACILITY	SPECIAL INSTRUMENTATION AND/OR EQUIPMENT
1 MATERIAL PROPERTIES	EMISSIVITY OF ABLATOR, THERMAL CONDUCTIVITY OF INSULATION MECHANICAL PROPERTIES OF PROTECTIVE SHELL	THERMOPHYSICAL AND MECHANICAL PROPERTIES OF ALL STRUCTURAL LAYERS AND FUEL FORMS	SUBSEQUENT TO ANALYTICAL COMPILATION AND CORRELATION OF EXISTING DATA, SPOT CHECK & BRIDGE MISSING GAPS TO 3000°C OR HIGHER	NONE	NONE	WELDED SAMPLES OF EACH COMPONENT MATERIAL	DWDL	DROP CALORIMETER HIGH & LOW TEMP DILATOMETER THERMAL COND. MEASURING
2 CORROSION TESTS	CORROSION RATE DATA FOR SEVERAL POSSIBLE SHELL MATERIALS IN SEAWATER.	CORROSION RATE DATA UNDER STRESS IN SALT SPRAY AND BURNING PROPELLANTS	TEST WELDED STRUCTURAL SHELL AND OXIDATION BARRIER FOR SELECTED PERIODS OF TIME.	NONE	3 - NONE 3 - REFERENCE	6 TOTAL, 3 FOR 10-WATT SIZE AND 3 FOR 50-WATT SIZE	DWDL OR MDAC ENVIRONMENTAL LAB, SANTA MONICA	RESISTANCE STRAIN GAGES SALT SPRAY CHAMBER
3 RADIATION TESTS	DOSE RATE AS A FCT OF DISTANCE AND SHIELDING THICKNESS	EFFECTS OF FUEL AGE AND IMPURITIES	MAKE BETA AND GAMMA AND NEUTRON EMISSION MEASUREMENTS AT SELECTED DISTANCES AND AGES.	$Pm_{2}O_{3}$ AND $PuO_{2}$	REFERENCE	ONE 10-WATT AND ONE 50-WATT HEATER FOR EACH FUEL FORM	DWDL	THERMAL LUMINESCENCE DOSIMETERS
4 ACCELERATED LIFE TESTS	EFFECT OF POTENTIAL SWELLING AND PRESSURE BUILD-UP (ESP. FOR $PuO_{2}$ )	COMPATIBILITY OF MATERIALS AND THERMAL DEGRADATION OF ABLATOR	TEST AT STEPPED ELEVATED TEMPERATURES IN A VACUUM TO SIMULATE ACTUAL 20-YEAR THERMAL HISTORY	$Pm_{2}O_{3}$ AND $PuO_{2}$	REFERENCE	SAME CAPSULES AS ABOVE	DWDL	GRAPHITE RESISTANCE OR INDUCTION HEATING FURNACE
5 VIBRATION TESTS	VERIFICATION OF CAPSULE AND ABLATOR INTEGRITY IN LAUNCH AND SHIPPING ENVIRONMENTS.		PERFORM THREE-AXIS RANDOM AND SINUSOIDAL SWEEP TESTS, SCAN FREQUENCY SPECTRUM & NOTE RESONANCES	$UO_{2}$ MICROSPHERE STAND-IN	REFERENCE	ONE 10-WATT AND ONE 50-WATT	MDAC ENVIRONMENTAL LAB SANTA MONICA	VIBRAPHOR
6 THERMAL SHOCK TESTS	EXTERNAL ABLATOR, SHELL, AND BOND STRENGTH ON REENTRY IMPACT IN WATER.	SIMULATE QUENCH OF HEATERS FROM A LAUNCH PAD FIRE TO CRYOGENIC FUEL	HEAT WITH RF PLASMA TORCH TO REENTRY TEMP. AND QUENCH IN WATER ALSO, QUENCH FROM 1800°F TO $Li_{2}$	$UO_{2}$ MICROSPHERE STAND-IN	REFERENCE	SAME CAPSULES AS ABOVE	DWDL	RF PLASMA TORCH, INDUCTION HEATING FURNACE
7 THERMOCYCLING TESTS	CLADDING AND PROTECTIVE SHELL BOND INTEGRITY DURING EXTREME MISSION OPERATING TEMPERATURES		CYCLE FROM -180 TO 180°C FOR 6 MONTHS AT 12 CYCLES PER DAY (LUNAR EXTREMES)	$UO_{2}$ MICROSPHERE STAND-IN	REFERENCE	SAME CAPSULES AS ABOVE	DWDL	TUBE FURNACES AND VACUUM PUMP
8 AERODYNAMIC DRAG TESTS	SUBSONIC DRAG COEFFICIENTS FOR POSSIBLE ABLATOR SHAPES WITH ROUNDED CORNERS AT VARIOUS ANGLES OF ATTACK		TEST IN WIND TUNNEL ALUMINUM SPECIMENS IN VARIOUS ORIENTATIONS FOR REYNOLDS NUMBERS FROM $10^5$ TO $10^6$ .	NONE	ALUMINUM SHELL	2 - 10 WATT, 2 - 50 WATT FOR EACH ABLATOR SHAPE - ONE WITH SLIGHTLY ROUNDED CORNERS & ONE WITH LARGE ROUNDED CORNERS	MDAC AEROPHYSICS FACILITIES	STRAIN GAGE BALANCE
9 DYNAMIC PRESSURE LOADING AND THERMAL STRESS TESTS	ABLATOR INTEGRITY UNDER SIMULTANEOUS THERMAL STRESS AND DYNAMIC PRESSURE LOADING CHARACTERISTIC OF STEEP ANGLE REENTRY		HOLD SPECIMENS STATIONARY AT SELECTED ORIENTATIONS IN WIND TUNNEL AT PRESSURES UP TO 12 ATM. TYPICAL HEATING	$UO_{2}$ MICROSPHERE STAND-IN	REFERENCE AND ALTERNATIVE MATERIAL	TWO 50-WATT AND TWO 10-WATT FOR EACH ABLATOR MATERIAL	ARNOLD ENGINEERING DEVELOPMENT CENTER	PYROMETRY AND MOTION PICTURE COVERAGE
10 STEEP ANGLE REENTRY HEATING TESTS	THERMOCHEMICAL ABLATION OF OUTER ABLATOR (OXIDATION AND SUBLIMATION).	THERMAL CONDUCTION INTO CAPSULE	SUBJECT SPECIMENS TO HEAT FLUX AND PRESSURE LEVELS CHARACTERISTIC OF 90° LUNAR RETURN	$UO_{2}$ MICROSPHERE STAND-IN	REFERENCE	2 - 50 WATT, 2 - 10 WATT FOR EACH ABLATOR MATERIAL	ARNOLD ENGINEERING DEVELOPMENT CENTER	THERMOCOUPLES, PYROMETRY AND MOTION PICTURE COVERAGE
11 GLIDING REENTRY HEATING TESTS	THERMAL CONDUCTION INTO CAPSULE FOR SEVERAL ORIENTATIONS	ABLATION OF OUTER ABLATOR	TEST SPECIMENS IN ARC PLASMA FOR HEAT FLUX, PRESSURE, AND ENTHALPY LEVELS CHARACTERISTIC OF LOW ANGLE REENTRY.	$UO_{2}$ MICROSPHERE STAND-IN	REFERENCE	9 - 10 WATT, 8 - 50 WATT	MDAC/ST. LOUIS OR NASA/AMES.	SAME AS ABOVE
12 LAUNCH EXPLOSION TESTS	INTEGRITY OF OXIDATION BARRIER AND PROTECTIVE SHELL IN A LAUNCH PAD EXPLOSION	INTEGRITY OF ABLATOR	SUBJECT SPECIMENS TO DEBRIS FROM TNT EXPLOSION; IMPACT SPECIMENS WITH PARTICLES AT KNOWN VELOCITY	$UO_{2}$ MICROSPHERE STAND-IN	REFERENCE	2 - 10 WATT, 2 - 50 WATT	TNT EXPLOSIVE TEST FACILITY; MDAC AEROPHYSICS LAB EL SEGUNDO.	LIGHT GAS GUN FOR CONTROLLED IMPACT
13 REENTRY IMPACT TESTS SERIES I	FUEL CONTAINMENT AT TERMINAL IMPACT VELOCITY	EFFECT OF DIFFERENT SHELL MATERIALS, SHAPES, AND ANGLES OF IMPACT	IMPACT AT TERMINAL VELOCITIES ON GRANITE AT REENTRY IMPACT TEMPERATURE	$UO_{2}$ MICROSPHERE AND $Sm_{2}O_{3}$ CERMET STAND-IN	REFERENCE	8 - 10 WATT, 10 - 50 WATT WITH SHAPE VARIATIONS	MDAC AEROPHYSICS LAB EL SEGUNDO	LIGHT GAS GUN, MOTION PICTURE COVERAGE
14 REENTRY IMPACT TESTS SERIES II	SAME AS ABOVE	EFFECT OF ABLATOR, TEMPERATURE AND VELOCITY.	SAME AS ABOVE	$UO_{2}$ CERMET AND $Sm_{2}O_{3}$ CERMET	ALTERNATE MATERIAL	7 - 10 WATT, 10 - 50 WATT WITH DIFFERENT ABLATOR	SAME AS ABOVE	SAME AS ABOVE
15 REENTRY IMPACT TESTS SERIES III	SAME AS ABOVE	EFFECT OF FABRICATION (WELDS, ETC) AND VELOCITY.	SAME AS ABOVE	$UO_{2}$ AND $Sm_{2}O_{3}$ STAND-IN	REFERENCE	4 - 10 WATT, 6 - 50 WATT	SAME AS ABOVE	SAME AS ABOVE
16 HIGH-TEMPERATURE BURST TESTS	INTEGRITY OF CONTAINMENT UNDER LAUNCH PAD ABORT AND REENTRY HEATING CONDITIONS.	POINT OF FAILURE FROM INTERNAL PRESSURE FOR POSSIBLE SHELL MATERIALS.	SUBJECT WELDED SHELLS TO ENVIRONMENTAL PRESSURE AND THEN TO POINT OF FAILURE.	NONE	NONE	2 - 50 WATT SIZE FOR T-III SHELL MATERIAL	DWDL	TUNGSTEN ELEMENT ION PUMP VACUUM FURNACE

A somewhat higher risk is involved in this limited test program, but these risks could be offset by a more conservative design approach.

The interrelationship and sequence of the development tests discussed in table 24 are shown in figure 54. The rectangular blocks represent the tests described in the table. This figure shows that some tests can be conducted independently, while other tests are dependent on the results of a number of preceding tests.

General. - Certain tests are more closely related to materials and their environment than to a particular design. These tests, to be initiated early in phase II, are discussed below.

Material properties: One-hour, maximum-vacuum, creep-rupture tests will be performed on a refractory alloy pressure vessel to determine its capability to retain helium. The tests will be performed at temperatures up to 1320°C (2408°F) at various pressures.

Thermal conductivity of the insulation and ablation materials used will be measured in vacuum at temperatures to 2500°C (4532°F) where data are not currently available. Consideration will be given to testing at temperatures from 2500° to 3000° C (4532° to 5432°F), but this is currently beyond the limits of existing facilities.

Coefficient of thermal expansion (CTE) measurements will be made on pressure vessel, insulation, and reentry ablation materials over their temperature range of operation where data are not available.

Heat capacities (Cp) of materials for the capsule will be measured over their temperature range of operation to establish curves of Cp vs temperature.

Hardware tests. - Other tests outlined below must be performed on complete heaters, heater shells, heaters with stand-in fuel, etc., to evaluate materials compatibility. These may be defined as combined environmental tests.

1. High-temperature burst - Two unfueled capsules with a heavy-wall tube added to one end (to facilitate pressurization) will be placed in an induction furnace for 10 minutes under specific pressures and at a surface temperature of 3000°C (5432°F) as measured with an optical pyrometer.

2. Vibration - Heaters, complete in every respect except for fuel, will be hard-mounted and vibration-tested in three orthogonal axes. The frequency spectrum will be scanned and any resonances noted. Tests will be run at each resonance peak for 1 hour.

3. Mechanical shock - Reentry impact tests will be performed as required on completed stand-in capsules at the three principle axes and one intermediate angle at temperatures and velocities considered by analysis to be most severe.

Complete stand-in capsules will be subjected to impact from metal particles to simulate impingement of rocket debris on the capsule.

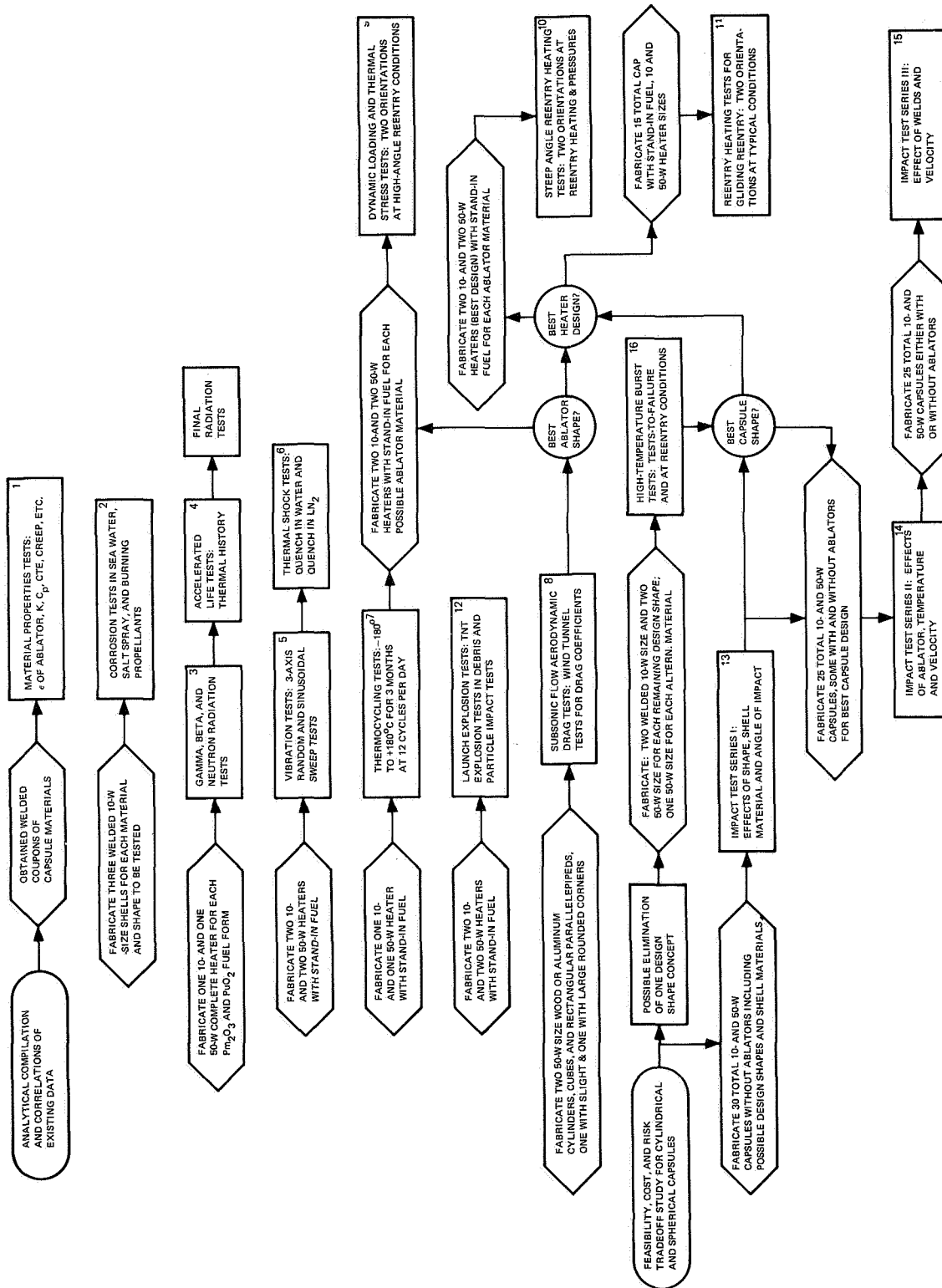


Figure 54. Test Specimen Fabrication and History Chart for Phase II Development Tests

4. Thermal shock - For the reentry case, stand-in heaters will be heated rapidly in the RF plasma torch to maximum reentry surface temperature of 3300°C (5972°F). The heating rate will be reduced to allow the capsule surface to cool to impact temperature, and the capsule will be water-quenched in a 100-gal tank of brine.

For the launch pad abort case, specimens will be placed in an air-atmosphere furnace for 15 minutes at 980°C (1796°F) (launch-pad fire temperature) and quenched in LN<sub>2</sub> to simulate quench from fire temperature by cryogenic fuel.

5. Reentry heating - Stand-in heaters will be tested in an arc plasma using gas enthalpy, gas composition, and integrated heat flux computed for representative trajectories. The trajectories considered will include a shallow angle ( $< 0.1^\circ$ ); high-integrated heat pulse representing reentry from a decaying orbit; a superorbital velocity earth-return trajectory ( $6.25^\circ$ - $90^\circ$ ); and a high-angle earth reentry representing the worst orbital abort cases ( $90^\circ$ ).

6. Accelerated life test (compatibility of all materials layers with actual fuel) - One 10- and one 50-W Pm<sub>2</sub>O<sub>3</sub> heater, and one 10- and one 50-W PuO<sub>2</sub> heater will be held at 1000°C for a specified period of time to simulate an actual 20-year thermal history of a typical capsule, as determined by analysis. A time-vs-temperature Arrhenius relationship will be utilized to determine the time for the accelerated test.

7. Thermal cycling - One 10- and one 50-W heater, using stand-in fuels, will undergo tests simulating temperature cycling that might occur on the lunar surface. The heaters will be thermal-cycled between -180° and +180°C (-292°F and +356°F) at the rate of 12 cycles/day for 6 months.

8. Radiation dosimetry profiles - These will be made for each of the 10- and 50-W Pm<sub>2</sub>O<sub>3</sub> and PuO<sub>2</sub> heaters.

9. Aerodynamic drag - Drag coefficients at several angles of attack will be determined for selected heater configurations, using aluminum models.

10. Dynamic pressure loading and thermal stress - Ten- and 50-W heaters, using stand-in fuels, will be subjected to pressures up to 12 atm under typical thermal conditions. These tests will simulate thermal stresses and dynamic loads characteristic of steep-angle reentry.

11. Corrosion tests - Three capsules for each power level will be tested in sea water and salt-spray environments at elevated temperatures to simulate a 10 half-life history for both Pm<sub>2</sub>O<sub>3</sub> and PuO<sub>2</sub> fuel forms. Capsules, with and without ablator installed, will be subjected to burning propellants to evaluate oxidation barrier protection.

#### Fabrication of Test Hardware

In accordance with the approved manufacturing program plan, a specified

number of each size of test capsule will be fabricated. Complete checkout of fabrication and assembly equipment will be performed. Complete quality control and documentation encompassing the approved manufacturing processes and quality assurance program plan will be followed. The manufacture of test hardware will encompass the same program requirements as flight-type hardware.

### Manufacture of Flight-Type Heaters

Using approved and released material specifications, quality control procedures, approved engineering drawings, and the results of the development tests, a representative group of flight-type heaters will be manufactured for delivery to the customer. Complete checkout of fabrication and assembly equipment will be performed. Complete quality control and documentation encompassing the approved Quality Control Program Plan will be followed. The manufacture of qualified flight-type hardware will entail all program requirements from delivery and handling of radioactive materials, parts configuration and control, final assembly and inspections, to delivery of complete certified heaters.

### Documentation and Licensing

The contractor will obtain the special permit necessary for shipment of the heaters; perform the hazards analysis; and complete the license application, with the conditions defined, to fulfill the requirements of the AEC and State licensing agencies for a specified number of locations. Consultation necessary to provide understanding of test conditions will be provided to the agencies.

The following tasks will be performed to implement licensing of the locations and facilities to handle radioactive materials defined in the contract. These procedures are identical to those completed by DWDL in obtaining the license for its nuclear laboratory in Richland, Washington.

1. Work to be performed involving radioactive material will be defined.
2. Location where the work will be performed with radioactive material including finished heaters will be specified.
3. Facilities and equipment to be used will be defined; how these facilities and equipment will permit safe handling and control of radioactive materials will be described.
4. Technical capability and training of personnel involved in work with radioactive material will be documented.
5. Administrative organization, showing the method of implementing the radiation control program, will be listed.
6. A hazard analysis will be made for each work site where radioactive material is to be handled. The site will be examined and its atmospheric con-



ditions reviewed. A worst credible accident will be postulated and the consequences determined with respect to civilian population and the atmospheric condition considered most detrimental, yet occurring at the location with reasonable frequency.

7. Batch size that would release sufficient material to cause maximum allowable emergency dose to the civilian population at the site boundary will be calculated.

8. Batch sizes below this quantity will be acceptable, or the facility will be improved to reduce potential hazard to the public.

9. Procedures will be provided to control the inventory of radioactive material and dispersment to the work location to ensure safe handling and accountability. A radiation control program will be established, including the necessary procedural control and dose measurement program to ensure safe working conditions for personnel.

10. A file of all correspondence with licensing agencies will be maintained. Response to questions asked by the licensing agency either by telephone or letter will be documented.

#### Qualification and Acceptance Test Programs

Qualification and acceptance tests will be performed on heaters fabricated in accordance with the approved manufacturing program described earlier in this report. A set of qualification tests similar to the development tests previously outlined has been prepared and is summarized in table 25. The acceptance tests are described in table 26.

The primary objective of the qualification and acceptance testing program is to establish design and safety reliability of the final reference heater design throughout a specified mission profile. Based partly on the results of the applications study in phase I, environmental conditions common to all or at least a majority of missions are selected. These conditions include the critical safety environments of reentry heating, impact, earth or sea water burial, and vibration and shock which encompass current boosters. Qualification tests based on these conditions are guided by the preliminary safety analysis.

All temperatures, velocities, chemical environments, etc., are selected to represent the most severe case for normal operation and credible accident situations. Except for the accelerated life tests, qualification tests will be performed on simulated heaters or primary capsules using nonradioactive  $\text{UO}_2$  or  $\text{Sm}_2\text{O}_3$  as stand-in materials for  $^{238}\text{PuO}_2$  or  $^{147}\text{Pm}_2\text{O}_3$  respectively.

All tests will be performed using control drawings, specifications, quality control procedures, and approved manufacturing processes.

Test summary. - A summary of test objectives and requirements for the qualification and acceptance tests to be performed in phase III is presented below.

TABLE 25  
SUMMARY QUALIFICATION TESTS

TEST DESCRIPTION	OBJECTIVES	REQUIREMENTS	FUEL FORM	SPECIMENS	FACILITY	SPECIAL INSTRUMENTATION
1 PUNCTURE TEST	SIMULATE PURCHASE HANDLING ACCIDENT	IMPACT AT 31 lbs ONTO 1/8-IN. DIAM PIN	UO <sub>2</sub> MICROSPHERE STAND-IN	ONE 10-W, ONE 50-W T111 SHELL ONLY	DWDL	NONE
2 CRUSH TEST	SIMULATE CRUSH HANDLING ACCIDENT	LOAD AT 2000 LB FOR 1 HOUR	UO <sub>2</sub> MICROSPHERE STAND-IN	ONE 10-W, ONE 50-W T111 SHELL ONLY	DWDL	NONE
3 HYDROSTATIC TEST	SIMULATE OCEAN BURIAL	PRESSURIZE IN AUTOCLAVE AT 10 000 psf FOR 2 WEEKS	UO <sub>2</sub> MICROSPHERE STAND-IN	ONE 10-W, ONE 50-W T111 SHELL ONLY	DWDL	NONE
4 SHEAR TEST	SIMULATE SHEAR HANDLING ACCIDENT	LOAD IN SIMPLE SHEAR AT 1000 LB FOR 1 HOUR	UO <sub>2</sub> MICROSPHERE STAND-IN	ONE 10-W, ONE 50-W T111 SHELL ONLY	DWDL	NONE
5 VIBRATION TEST	VERIFY CAPSULE INTEGRITY IN LAUNCH AND SHIPPING ENVIRONMENTS	PERFORM 3-AXIS RANDOM AND SINUSOIDAL CREEP TESTS; NOTE RESONANCES	Sm <sub>2</sub> O <sub>3</sub> COMPLETE	USE PROP. COMPATIBILITY UNITS	MDAC ENVIRONMENTAL LAB	VIBRAPHOR
6 ACCELERATED LIFE TEST	VERIFY CAPSULE INTEGRITY FOR ACTUAL 20-YEAR OPERATION	TEST AT ELEVATED TEMPERATURES IN VACUUM; CONDUCT POSTMORTEM	PuO <sub>2</sub> AND Pm <sub>2</sub> O <sub>3</sub>	ONE 50-W FOR EACH FUEL	DWDL	INDUCTION FURNACE
7 BURIAL TEST	VERIFY CAPSULE INTEGRITY FOR SOIL BURIAL	PLACE ELECTRICALLY HEATED CAPSULES IN SOIL FOR 3 MONTHS	NONE	ONE 10-W, ONE 50-W T111 SHELLS + Pt	DWDL	NONE
8 THERMOCYCLING TEST	VERIFY MATERIAL COMPATIBILITY DURING EXTREME OPERATING CONDITIONS	CYCLE FROM -180° TO +180°C FOR 3 MONTHS AT 12 CYCLES PER DAY (LUNAR EXTREMES)	Sm <sub>2</sub> O <sub>3</sub> COMPOSITE STAND-IN	USES PROP. COMPATIBILITY UNITS	DWDL	TUBE FURNACES AND VACUUM PUMP
9 LAUNCH EXPLOSION TEST	SIMULATE EXPLOSIVE OVER-PRESSURE, FLYING DEBRIS, AND CHEMICAL ENVIRONMENT OF LAUNCH EXPLOSION	RUPTURE ROCKET PROPELLANT AND LIQUID OXYGEN TANK; IGNITE MIXTURE ABOVE DUMMY SYSTEM CONTAINING HEATERS	UO <sub>2</sub> MICROSPHERE STAND-IN	TWO 10-W, TWO 50-W COMPLETE UNIT	MDAC ASTROPPOWER LAB	MOTION PICTURE COVERAGE
10 THERMAL SHOCK TESTS	SIMULATE QUENCH IN WATER AND LIQUID PROPELLANT	HEAT TO 980°C AND QUENCH IN WATER AND LIQUID NITROGEN	UO <sub>2</sub> MICROSPHERE STAND-IN	ONE 10-W, ONE 50-W COMPLETE UNIT	DWDL	RF PLASMA TORCH
11 CORROSION TEST	VERIFY SHELL INTEGRITY IN SEA WATER ENVIRONMENT	TEST BARE CAPSULES IN SEA WATER AND SALT SPRAY ENVIRONMENTS FOR SELECTED PERIODS OF TIME	UO <sub>2</sub> MICROSPHERE STAND-IN	USES UNITS FROM HYDRO STAT TESTS	DWDL OR MSD ENVIRONMENTAL LAB. SANTA MONICA	RESISTANCE STRAIN GAGES, SALT SPRAY CHAMBER
12 IMPACT TESTS	VERIFY FUEL CONTAINMENT FOR EARTH IMPACT ON GRANITE	IMPACT ON GRANITE AT TERMINAL VELOCITIES AND DIFFERENT ANGLES	Sm <sub>2</sub> O <sub>3</sub> COMPLETE STAND-IN	USES PROP. COMPATIBILITY UNITS	MDAC AEROPHYSICS LAB. EL SEGUNDO	LIGHT GAS GUN, MOTION PICTURE COVERAGE
13 REENTRY HEATING TESTS	VERIFY ABLATOR CAPABILITY FOR REENTRY PROTECTION	SIMULATE REENTRY HEATING, PRESSURE, AND ENTHALPY TRANSIENTS FOR EARTH ORBITAL AND LUNAR RETURN	Sm <sub>2</sub> O <sub>3</sub> STAND-IN	USES UNITS FROM PROP. COMPATIBILITY	MDAC/ST LOUIS OR NASA/AMES OR AEDC	THERMOCOUPLES, PYROMETRY AND MOTION PICTURE COVERAGE
			UO <sub>2</sub> MICROSPHERE STAND-IN	NINE 10-W, NINE 50-W COMPLETE UNITS		
14 PROPELLANT COMPATIBILITY TEST	VERIFY HEATER COMPATIBILITY WITH BOOSTER PROPELLANT FUELS	HOLD HEATERS IN PROXIMITY OF VARIOUS ROCKET BOOSTER FUELS FOR 2 DAYS EACH	Sm <sub>2</sub> O <sub>3</sub> COMPLETE STAND-IN	ONE 10-W, ONE 50-W	DWDL	NONE
			NONE	THREE 10-W, THREE 50-W T111 SHELL Pt + ABL + INS		

TABLE 26  
ACCEPTANCE TESTS

Test description	Objectives	Requirements	Fuel form	Specimens	Facility	Special instrumentation
1. Radiation tests	Obtain dose rates	Measure radiation	PuO <sub>2</sub> and Pm <sub>2</sub> O <sub>3</sub>	All fueled capsules	DWDL	Thermal luminescence dosimeters and calorimeters
2. Thermal tests	Verify power output	Measure heat generation rate				

1. Puncture tests - Tests to demonstrate that the heaters will be invulnerable to handling puncture accidents will be based on the ORNL structural Class III safety requirements (ref. 4) and reference 70. The heaters (one of each power level) will be dropped to impinge at 31 ft/sec upon a 1/8-in.-diam steel pin with a full radius hardened to RC 65  $\pm$ 5. If the final design is nonsymmetric with regard to its major axes, several orientations must be tested.

2. Crush tests - One of each power-level heater will be loaded along its weakest axis at 2000 lb for 1 hour (ORNL Class III requirement). The capsules will then be examined for failure.

3. Shear tests - One heater for each power level will be loaded in simple shear at 1000 lb and held for 1 hour. Examination for failure will follow; the permissible shear stress level follows ORNL Class III specifications.

4. Hydrostatic tests - One heater for each power level will be placed in an autoclave at 10 000 psi and held for 2 weeks. Periodic inspections for deformation and/or failure will be made. The pressure level of 10 000 psi corresponds to an ocean burial depth of about 22 000 ft.

5. Accelerated life tests - One 10- and one 50-W heater for each fuel form (<sup>147</sup>Pm<sub>2</sub>O<sub>3</sub> and <sup>238</sup>PuO<sub>2</sub>) will be held in a vacuum at normal peak operating temperatures long enough to simulate a 20-year operating history. The capsules will be disassembled, examined, leak-checked, and smear-checked after an equivalent of 8 years of normal operation. They will then be reassembled and tested for the remaining lifetime.

6. Vibration tests - One heater for each power level will be hard-mounted and vibrated in three orthogonal axes. The frequency spectrum will be scanned and any resonances noted. The vibrations will meet or exceed the requirements of 12 hours at 0.018 in. double amplitude and 150 cps on each axis (ref. 70).

7. Burial tests - Analysis performed to date indicates that, when buried in soil, the temperature of the primary capsule will be so low that no significant corrosion occurs. However, qualification tests will be performed by placing an electrically heated 10- and 50-W capsule shell in two different soils of low thermal conductivity, and corrosive characteristics determined over a 3-month period with weekly inspections.

8. Thermal cycling tests - One 10- and one 50-W heater with stand-in fuel will be thermalcycled from  $-180^{\circ}$  to  $+180^{\circ}\text{C}$  ( $-292^{\circ}$  to  $+356^{\circ}\text{F}$ ) for 3 months at 12 cycles/day. This test is designed to simulate thermal changes during operation in lunar extremes.

9. Launch explosion tests - The launch pad abort situation, including explosive overpressure and flying debris, will be simulated. Two capsules of each power level will be mounted on an aluminum and titanium structure of a normal spacecraft panel size and type to produce a debris environment comparable to a launch abort situation. This dummy system will be attached under a rocket propellant and a liquid oxygen tank for the test. The tank will be ruptured and the explosive mixture ignited. The sequence will be filmed with Fastax motion picture film.

10. Thermal shock tests - One heater of each power level will be heated rapidly with an RF plasma torch to  $1800^{\circ}\text{C}$  ( $3272^{\circ}\text{F}$ ) maximum reentry impact and launch pad fire temperature, and quenched either in water or liquid nitrogen. These tests simulate reentry quench in water or launch pad abort quench in the booster propellant. Sectioning and macrographs of the structure materials will be made for postmortem analysis.

11. Corrosion tests - One bare capsule for each power level will be tested in sea water and salt spray environments at elevated temperatures to simulate a 10 half-life history for both  $\text{Pm}_2\text{O}_3$  and  $\text{PuO}_2$  fuel forms. Examinations for material degradation will be made at selected intervals.

12. Impact tests - The purpose of these tests is to verify capsule and ablator integrity during separation shocks, and to verify capsule fuel containment at reentry impact velocities and temperatures. A total of 30 capsules will be heated and impacted at various angles on granite. All power levels and fuel forms will be represented. The tests will be performed using the light-gas gun at MDAC's Aerophysics Laboratory in El Segundo, California. Motion picture coverage and post-test analysis will be included.

13. Reentry heating tests - The purpose and requirements of these tests are to verify:

a. the ablator capability to withstand steep angle reentry thermal shock combined with mechanical erosion; and simulate  $-90^{\circ}$  lunar return trajectory as closely as possible (peak heat rate  $\approx 5000 \text{ Btu/ft}^2\text{-sec}$ , peak stagnation point pressure  $\approx 12 \text{ atm}$ , peak enthalpy  $\approx 26\,000 \text{ Btu/lb}$ ).

b. the ablator capability to withstand thermal chemical ablation in the worst-case trajectory--a shallow angle ( $-5.2^{\circ}$ ) lunar return (peak heating  $\sim 800 \text{ Btu/ft}^2\text{-sec}$ , integrated heat  $\sim 100\,000 \text{ Btu/ft}^2$ ).

c. the insulation capability of the ablator to prevent point-of-failure temperatures for the capsule shell and fuel in a worst-case trajectory--earth orbital decay (peak heating  $\sim 250 \text{ Btu/ft}^2\text{-sec}$ , integrated heat  $\sim 50\,000 \text{ Btu/ft}^2$ ).

Ten 10-W and ten 50-W heaters will be tested in an electric-arc wind tunnel at representative flow conditions. Instrumentation will include thermocouples for internal temperature measurement, optical pyrometers for surface temperature measurement, and motion picture coverage. Weight loss measurement will be carefully made after the test.

14. Propellant compatibility tests - To verify that the heater materials are compatible with rocket booster propellants, two heaters will be held in proximity to a number of fuels for several days, and an inspection made for signs of corrosion.

15. Acceptance tests - These tests will establish that the capsules meet accepted power performance and radiation safety levels. All fueled heaters will be measured with thermal luminescence dosimeters. Radiation levels must meet accepted standards required by the customer. Also, power generation of the capsules will be measured with calorimeters to ensure proper design performance.

### Safety Analysis Report

A final safety analysis report will be prepared which will contain all safety-related results, qualifications, and requirements for use of the selected radioisotope heaters. The report will provide criteria to establish guidelines for use of the heaters for a given mission, and will specify in detail the mission-oriented information required to complete the safety analysis and documentation for the intended application. An outline of the Preliminary Safety Analysis Report is presented in the Safety Analysis Report section.

### Program Management and Reports

Continued technical and management direction will be given to each task at the appropriate level of effort. Liaison with the customer program monitors will be maintained. Coordination meetings will be scheduled to review program status and exchange technical information. Formal briefings will be held as required to report on program progress.

Reports. - Informal letter reports will be submitted monthly. A draft of the final report will be submitted at the end of the program, after which the report will be printed and distributed as directed by the contract.

Monthly progress reports: A monthly letter report will be submitted within 10 days after the end of each reporting period. These reports will be brief, informal, and in narrative form; they will include a quantitative description of overall progress; identification of current problems which may impede performance; proposed corrective action; and a discussion of work to be performed during the next reporting period.

Final report: A final report which documents and summarizes the results of the contract work will be prepared. Copies of the final draft will be submitted to the customer for review and approval by the program monitors. Upon notification of acceptance of the approval copy (nominally assumed to require 30 days) reproducibles will be prepared and submitted together with a required number of copies.

### Program Plans and Schedule

Results of this study show that two heater sizes and two types of fuel will meet the majority of identified applications and mission requirements. Using these results as guidelines, program elements and options are presented here for the development of flight- and safety-qualified heaters. This is followed by a program schedule, milestones, and costs for each of the options.

Recommended program and options. - Program options are presented for development of safety- and flight-qualified radioisotope heaters. The programs are presented in the order recommended.

Option 1: The first option recommends a program for the development, testing, and qualification of a set of radioisotope heaters consisting of a 10-W  $^{147}\text{Pm}_2\text{O}_3$  cermet, a 10-W  $^{238}\text{PuO}_2$  bare microspheres, a 50-W  $^{147}\text{Pm}_2\text{O}_3$  cermet, and a 50-W  $^{238}\text{PuO}_2$  bare microspheres.

Industrial test facilities would be utilized. Plutonia bare microspheres were chosen over a plutonia cermet because the cermet fuel form will probably not be available prior to completion of phases II and III.

Option 2: The second option is presented in recognition of the fact that it may be more advantageous from a budgetary point of view to spread development and qualification work over a longer period of time. The recommended program under this option would be to first develop the 10-W promethia cermet heater followed in sequence by a 10-W plutonia heater, a 50-W promethia heater, and finally a 50-W plutonia heater. Although a complete program, as outlined in option 1, it would extend over 3 fiscal years (28 months). Industrial test facilities would be utilized.

Option 3: The third option is identical to option 1, but tests such as aerodynamic drag, dynamic pressure, thermal stress, steep-angle reentry, launch explosion, and impact would be performed at Government-furnished test facilities at Government expense.

Option 4: The fourth option is a minimum-cost version of option 3. That is, Government test facilities would be utilized, and the minimum development test program described previously under Prototype Hardware Development and Development Tests would be substituted for the complete test program.

Options 5, 6, 7, and 8: In these options, a single heater size and single fuel form would be developed as follows: Option 5 would provide a 10-W promethia heater; option 6, a 10-W plutonia heater; option 7, a 50-W

promethia heater, and option 8, a 50-W plutonia heater. Government test facilities and a minimum development test program would be utilized for these options

All options would include a complete series of qualification tests.

Program schedule and milestones. - A tentative schedule for phases II and III has been prepared for planning and budget purposes, based on DWDL's current best estimates of the work required to accomplish the program objectives, (fig. 55). This schedule is based on option 1. Milestones for phases II and III are shown in table 27.

Program option budgetary costs. - Budgetary costs for the options are presented below, with a brief summary of the items used in determining these costs.

Costs: \$10<sup>6</sup>

Option 1	1.42
Option 2	1.81
Option 3	1.30
Option 4	1.12
Option 5	0.69
Option 6	0.67
Option 7	0.82
Option 8	0.74

TABLE 27

PHASES II AND III PROGRAM MILESTONES

Task	Months after ATP
1. Complete final design	2
2. Initiate fabrication of test hardware	2
3. Complete development of test program	8
4. Complete licensing and documentation	10
5. Complete fabrication of flight-type hardware	12
6. Complete fabrication of test hardware	15
7. Complete qualification test program	17
8. Complete safety analysis report	17
9. Complete draft of final report	18

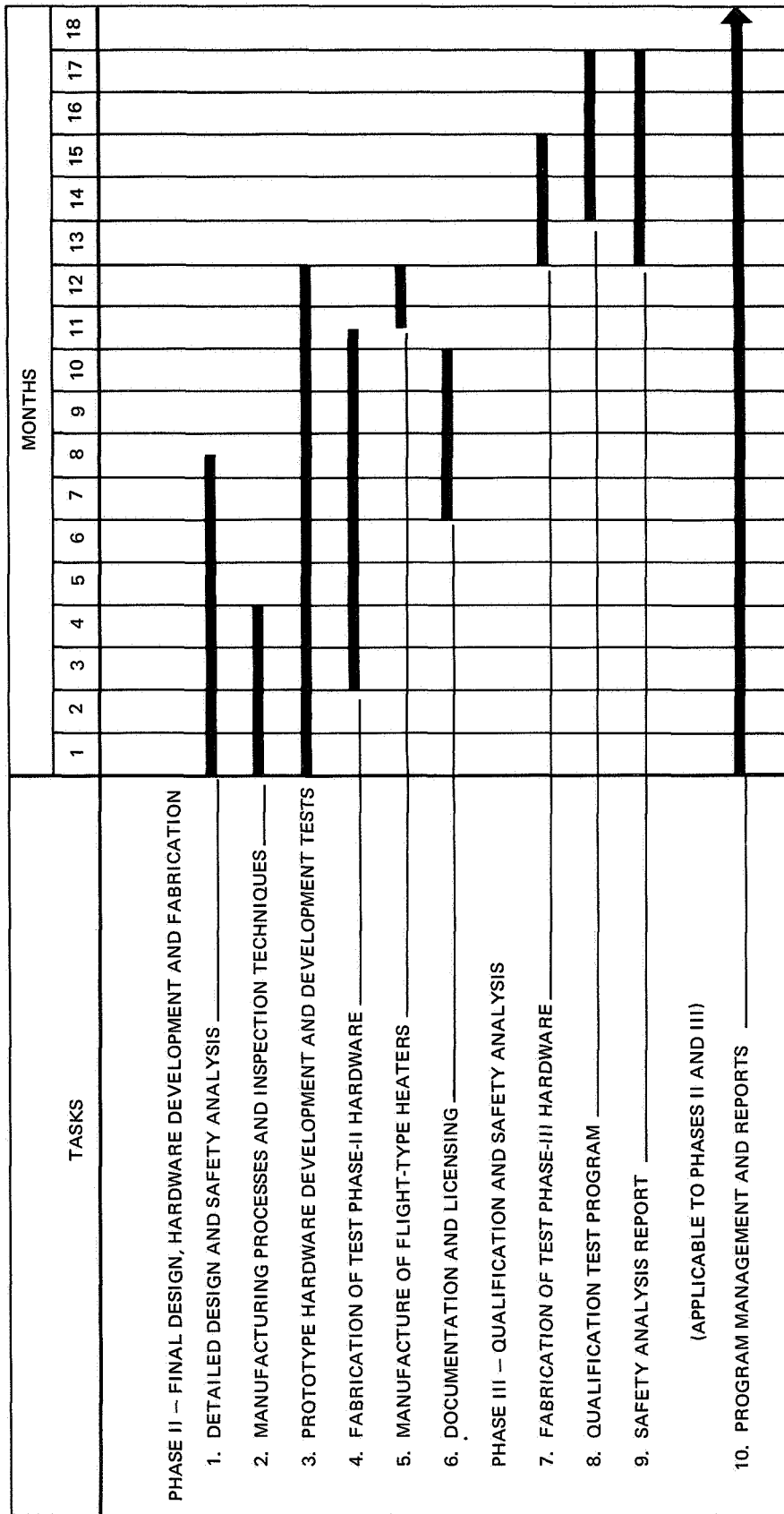


Figure 55. Phases II and III Task Schedule



Basis for budgetary cost data: The following are major items considered in determining the above cost data:

1. Option 1

- a. Design engineering, labor
- b. Manufacturing processes development, labor
- c. Fabrication of development and qualification hardware, labor
- d. Performance of a complete development test program. These tests were discussed under Prototype Hardware Development and Development Tests.
- e. Complete qualification tests as discussed under Qualification and Acceptance Test Programs.
- f. Safety and design analysis, labor
- g. Material and hardware requirements, (plutonia bare microspheres and promethia powder to be government furnished).
- h. Program management, labor

(All tests to be performed at industrial facilities.)

2. Options 2 through 8

Cost data for these options were formulated by adjusting costs according to the program scope of each option.

Engineering labor costs represent about 50% of the total costs, and material costs about 30%.

## SAFETY ANALYSIS REPORT

A primary goal of this program is to develop and qualify radioisotope heaters so that extensive analysis and documentation efforts are not required to secure flight approval for each specific mission. This approach is feasible with regard to safety reporting if the following approach is used: Three documents, (1) reference design, (2) accident model, and (3) safety analysis reports will be prepared to include a range of mission profiles for which the capsules are qualified. A fourth document, mission profile checklist, will be prepared. Its purpose is to ensure that a specific mission utilizing heaters is within the qualified mission envelope. NASA mission integrators will complete the checklist for a planned mission. If all items fall in the qualified range, the integrators can assume flight-safety approval and/or submit the

completed checklist to the appropriate reviewing authority. If some items do not fall in the qualification range, these areas are clearly defined and qualification can be expeditiously completed and sent to the Interagency Safety Evaluation Panel and the Space Council for special review.

An outline of the preliminary safety analysis report to be completed during phase II is presented in table 28. The qualification and flight safety approval philosophy presented above has been included.

TABLE 28  
SAFETY ANALYSIS REPORT OUTLINE

- |     |   |
|-----|---|
| I.  | Introduction                                      |
| A.  | System description (summary)                      |
| 1.  | Qualified mission profile envelope-summary        |
| 2.  | Qualified vehicles, systems                       |
| 3.  | Normal nuclear system disposition                 |
| a.  | Sea   |
| b.  | Land  |
| B.  | Safety criteria                                   |
| 1.  | Prelaunch phase                                   |
| 2.  | Launch Phase                                      |
| 3.  | Preorbit phase                                    |
| 4.  | Orbital phase                                     |
| 5.  | Postorbital phase                                 |
| a.  | Escape  |
| b.  | Reentry envelope                                  |
| C.  | Application of probabilistic philosophy to system |
| II. | Normal mission evaluation                         |
| A.  | Prelaunch handling                                |
| 1.  | Radiation protection (shielding, handling)        |
| 2.  | Fire protection                                   |
| 3.  | Impact prevention                                 |
| 4.  | Criticality control                               |
| B.  | Flight safety                                     |
| 1.  | Safety systems                                    |

TABLE 28. - Continued  
SAFETY ANALYSIS REPORT OUTLINE

2. Radiation protection
3. "Nominal" mission (definition and limits)
- C. Ultimate disposition
  1. Mission duration/ orbital lifetime  
(residual nuclear material)
  2. Reentry mode
  3. Reentry history for mission profile envelope
    - a. Trajectory calculation
      - (1) Model(s) used
      - (2) Satellite input assumptions
        - (a) Attitude
        - (b) Stability
        - (c) Drag coefficient - ballistic parameter
      - (3) Structure disassembly sequence- effect on trajectory
      - (4) Analytical results
        - (a) Velocity vs altitude
        - (b) Altitude vs time
    - b. Heating rates
      - (1) Model(s) used
      - (2) Input assumptions
      - (3) Analytical results
        - (a) Heating rate vs altitude
        - (b) Effect on structure - disassembly altitudes
        - (c) Effect of heat shield
        - (d) Sensitivity of results to input assumptions
    - c. Nuclear source behavior
      - (1) Temperature vs altitude
      - (2) Disassembly mode
        - (a) Intact reentry
        - (b) Dispersed reentry

TABLE 28. - Continued  
SAFETY ANALYSIS REPORT OUTLINE

	(3) Test program results
d.	Effects of reentered nuclear material
	(1) Nature and probability of interactions
	(a) Direct radiation ( $\gamma$ , $\eta$ , $\beta$ )
	(b) Skin exposure ( $\alpha$ , $\beta$ )
	(c) Internal exposure ( $\alpha$ , $\beta$ )
	(2) Extent of interactions
	(3) Dose distributions ( probable number of exposures vs dose)
4.	Comparison of consequences and safety criteria
D.	Summary of normal mission safety
III.	Accident source evaluation
A.	General
	1. Reference to AMD
	2. By phase of operation
B.	Summary of nuclear system response to accident-induced environments
	1. Booster propellant conflagration; Saturn IB, Saturn V and Titan III M (overpressure and temperature profile)
	2. Overtemperature
	3. Impact
	4. Corrosion
	5. Reentry
	6. Other
C.	Prelaunch accidents
	1. Summary tabulation
	(a) Nature
	(b) Probability
	(c) Environment

TABLE 28. - Continued  
SAFETY ANALYSIS REPORT OUTLINE

- 2. Analysis and evaluation
  - (a) Effect of environments on nuclear source
  - (b) Supporting experimental and analytical data
  - (c) Definition of resulting source term
- D. Launch accidents
  - 1. Summary tabulation
    - (a) Nature
    - (b) Probability
    - (c) Environment
  - 2. Analysis and evaluation
- E. Preorbital accidents
  - 1. Summary tabulation
    - (a) Nature
    - (b) Probability
    - (c) Environment
  - 2. Analysis and evaluation
- F. Orbital Phase accidents
  - 1. Summary tabulation
    - (a) Nature
    - (b) Probability
    - (c) Environment
  - 2. Analysis and evaluation
- G. Postorbital accidents
  - 1. Summary tabulation
    - (a) Nature
    - (b) Probability
    - (c) Environment
  - 2. Analysis and evaluation
- H. Summary- tabulation of accident consequences to be evaluated

TABLE 28. - Concluded  
SAFETY ANALYSIS REPORT OUTLINE

IV. Accident severity

A. Summary of transport and dose models (including probability of interaction)

1. Atmospheric release (pad accident, postreentry burial)
  - (a) Transport/diffusion models
  - (b) Inhalation and/or ingestion models
  - (c) Direct radiation
2. Marine release
3. Reentry (dispersed)
4. Reentry (intact)
5. Applicable biological effects data

B. Prelaunch accidents

1. Consequences
  - (a) Dose distributions for accident (including dose and accident probability)
  - (b) Comparison with safety criteria, injury levels
2. Countermeasures and/or safety systems

C. Launch accidents

D. Preorbital accidents

E. Orbital accidents

F. Postorbital accidents

G. Other accidents

V. Summary

A. Overall flight consequences

(Severity and dose probability as a function of mission time)

B. Comparison with safety criteria

C. Multiple-flight applications

1. Cumulative consequences (normal)
2. Cumulative failure probabilities (accident)
3. Cumulative consequences (accident)

VI. References

## CONCLUSIONS AND RECOMMENDATIONS

Results show that the following primary objectives of the phase I study have been met:

1. Identify potential applications for small (1-to 50-W) radioisotope heaters in manned spacecraft systems. - The survey of manned spacecraft and launch vehicles identified more than 37 application areas requiring from 180 to 300 heaters ranging in size from less than 1 to over 100 W. Radioisotope heaters would not have been considered for all of these applications, either because electric heaters would perform just as well, or because of complexity and/or size. However, many of the identified applications such as viewports, heat for base thermal requirements, structural cold spots, and standby fuel cell heat would have seriously considered and quite probably used radioisotopes heaters if they had been available. The applications presented in table 1 are, undoubtedly, not complete--even within the manned spacecraft area. Unmanned spacecraft applications were not surveyed; when this is accomplished, many more applications will be identified.
2. Develop a radioisotope heater design that will meet the selected safety criteria and have a high probability of being safety and flight-qualified. - Detailed safety and design analyses of the reference heater designs that have evolved from this study show that these designs have a high probability of surviving all mission phases, operations, and environments. The material, configurations, and fabrication techniques are (or are near) the state of the art. The reference heater designs presented in this report ensure safe handling by both experienced and inexperienced personnel, and impose no special requirement on the on-board astronauts performing their normal duties on board the spacecraft. The heaters have been designed to present an insignificant probability of injurious radiation dose as a result of a credible accident or incorrect handling.
3. Develop an optimum group of radioisotope heaters that will meet the requirements of a maximum number of applications and mission times of from 14 days to 5 years. - Results of the optimization studies completed for the phase I study conclude that two heater sizes, 10 and 50 W, using two radioisotope fuels, promethia and plutonia, will meet the applications and mission requirements identified. The results of this analysis indicate that well over 100 applications in the 20- to 25-W range would be required to justify production of a third heater size. Optimization analyses further show that only a small weight penalty is incurred by using uniform heaters having the same outer dimensions for both the promethia and plutonia fuels. All material thicknesses are the same from the structural shell outward. The weight penalty costs are small when compared to the additional cost of fabricating and qualifying two different heater sizes for one power level. Also, an important consideration is the interchangeability of promethia and plutonia heaters that the uniform size approach permits, since only one mounting arrangement is required for each power level.

4. Develop program plans and budgetary cost estimates for phases II and III. - Based on the results of phase I, a recommended program plan and a number of alternative program plans were developed. The recommended plan outlines a complete program for development, test, fabrication, and qualification of two heater sizes using two fuel forms. The alternative programs take into consideration cost and schedule constraints. Any one of the programs, however, will result in qualified radioisotope heaters.

The ability to utilize decay heat from radioisotopes to maintain space components within specified temperature limits was determined in the preliminary design of thermal control systems for ALSEP mission components; reference heater designs were combined with controllable heat pipes to keep electronic components on the lunar surface within temperature limits, despite the large temperature variations from lunar day to lunar night.

This design study has shown that it is entirely feasible to develop a group of small radioisotope heaters that will meet a large number of manned spacecraft component applications. Completion of such a development program will greatly reduce the time between mission requirement identification and ultimate mission qualification.

Also, the availability of flight-qualified radioisotope heaters will enable systems engineers to consider their use with the same degree of confidence as they now give electrical heaters. This gives them a degree of flexibility of design and selection not now available.

#### Areas Requiring Additional Analyses or Tests

During phase I, many areas were identified where additional analyses and/or tests are required. Those considered most important are listed below; these are studies or investigations that must be performed prior to breezing of the final design:

1. Spot-check confirmation of physical, mechanical, and thermal properties of the selected heater materials under simulated environmental conditions.

2. Development-test:

- a. Aerodynamic tests on models of the reference designs.

- b. High-temperature rupture or burst.

- c. Fabricated techniques:

- (1) Welding

- (2) Forming methods



(3) Shapes and types

(4) Bonding of material

3. Impact tests and reentry ablation tests to confirm the reference designs and materials selection.

4. Blast debris probability analysis, design, and test.

In addition, there are analysis and development tests that are not essential to development of the reference designs, but are desirable for a complete understanding of the design requirements, and to ensure optimum designs. Following is a partial list of those analyses or tests that fall into this category:

1. Detailed design and analysis of alternate concepts to determine:

- a. Reentry heating and impact condition.
- b. Fabrication complexity.
- c. Development, qualification, and production costs.
- d. Growth and flexibility.
- e. Weight and volume.
- f. Component and mission integration problems.

2. Aerodynamic tests on alternate concepts.

### Recommendations

DWDL recognizes that of the two radioisotope fuels selected, only  $^{238}\text{PuO}_2$  bare microspheres has been considered to be a flight-qualified fuel at the present time. However, DWDL strongly recommends that the  $^{147}\text{Pm}_2\text{O}_3$  cermet fuels be considered for use on missions of up to approximately 2 years. Promethium should be considered to supplement rather than replace plutonia. Both fuels should be developed and qualified in improved fuel forms in order to handle the expected spectrum of uses. Available data on promethium, although more meager than that on plutonium, indicate that promethium will be biologically safer than plutonium. Promethium, of course does not have the helium buildup problem that must be contended with in plutonium. One to two kW of promethium per year is available from existing facilities, provided adequate storage facilities are made available to allow for aging. This would be more than adequate to meet the requirements of thermal heaters developed under this program.

It has been established that radioisotope heaters would have been considered for many space applications had they been available. In fact, the NASA/MSC requirement for a heater for the ALSEP seismic experimental

package was firmed up immediately subsequent to the commencement of the present study. The EASEP heater is being developed by AEC/DID for an early Apollo mission. The reliability of radioisotope heaters is recognized, and the ability to design them with a high probability of being safe under all credible accident conditions and environments has been shown. Therefore, it is strongly recommended that phases II and III be initiated without undue delay, and funded at the level required to produce qualified heaters. Any one of the eight program options discussed under Program Plans and Budgetary Cost Estimates will result in flight- and safety-qualified radioisotope heaters. DWDL believes that option 1 would prove most cost-effective and have the lowest risk factor. But DWDL also recognizes that budget considerations may require the selection of one of the other options. In any case, the need for developing a group of small radioisotope heat sources for space component thermal applications is apparent.

## Appendix A

### HEATER DESIGN EVOLUTION

As the phase I study progressed, many heater configurations were considered. Figures A-1 through A-12 present what are termed baseline designs; ie. original configurations used in the initial analyses. The reference heater designs evolved from these. Figure A-13 presents four types of spherical heater concepts. Table A-1 presents a weight comparison of the baseline and spherical heater designs.

Figures A-1 through A-6 represent the original baseline designs for 10- and 50-W heaters using promethia and plutonia cermets, and bare-microsphere fuels. The designs using plutonia microspheres (figs. A-3 and A-4) had a void-to-volume ratio of about 1.2. In order to be consistent with the plutonia cermet fuels, the heaters were redesigned to have a void-to-volume ratio equal to about 1. This change is reflected in figures A-7 and A-8.

Since the outer dimensions of the plutonia heaters are quite close, it appeared advantageous to standardize all heaters of the same power level, ie. use the same size components from the structure member outward. These changes are reflected in figures A-9 through A-12.

Spherical radioisotope heaters appeared to be a promising alternative configuration on the basis of weight, ease of analysis, potential fabrication techniques, and potential reduction in qualification costs. These designs are presented in figure A-13.

(DIMENSIONS IN INCHES)

69-773

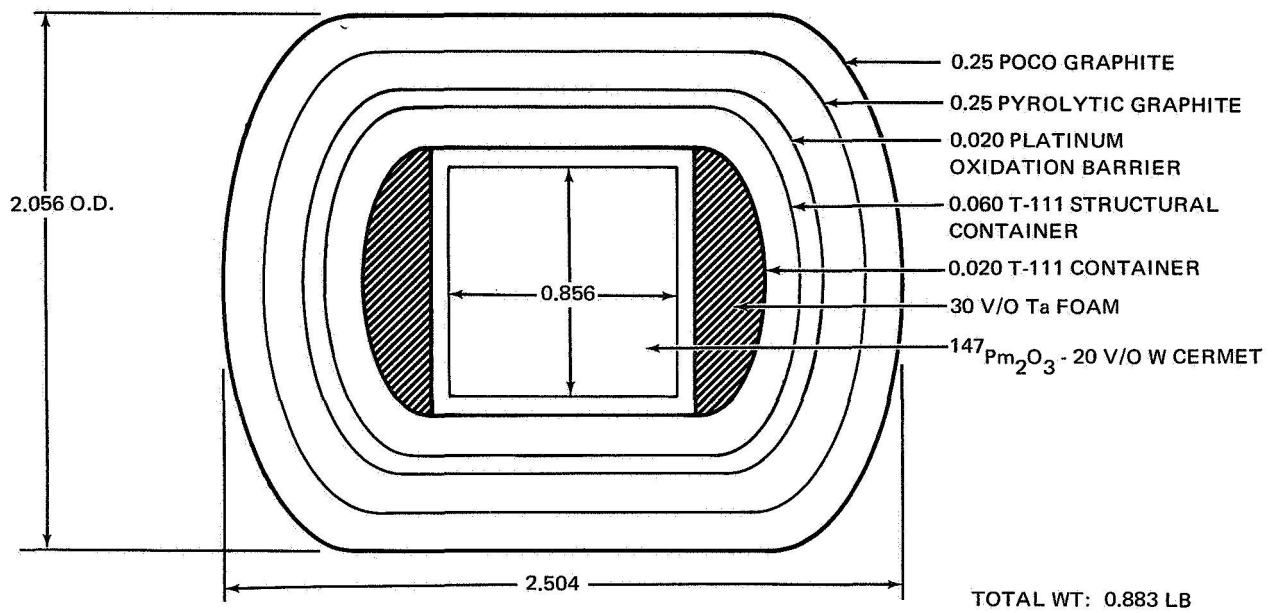


Figure A-1.  $^{147}\text{Pm}_2\text{O}_3$  Capsule, Model PMC-10-1

69-779

(DIMENSIONS IN INCHES)

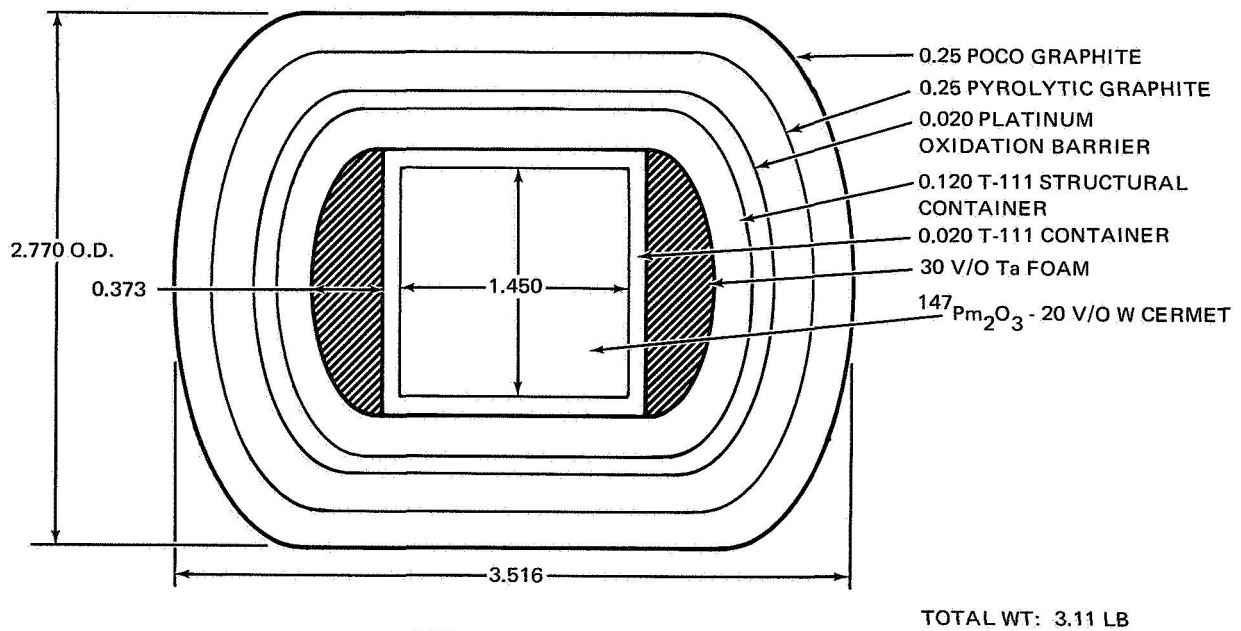
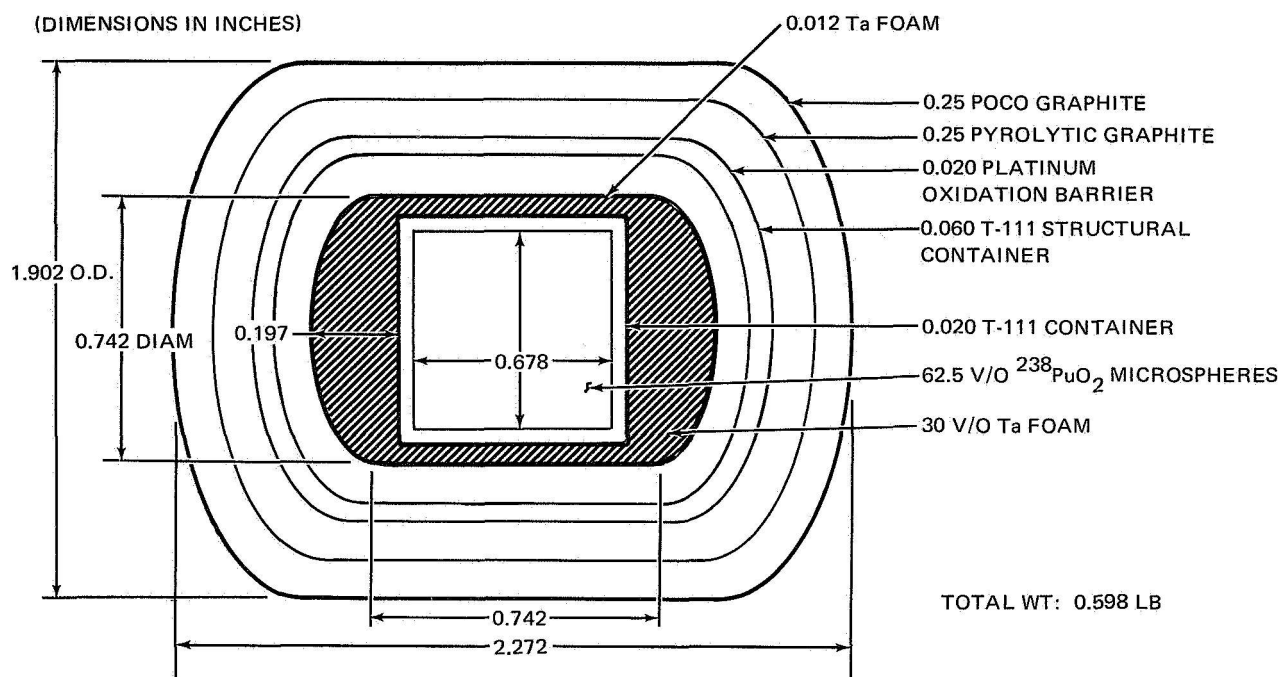
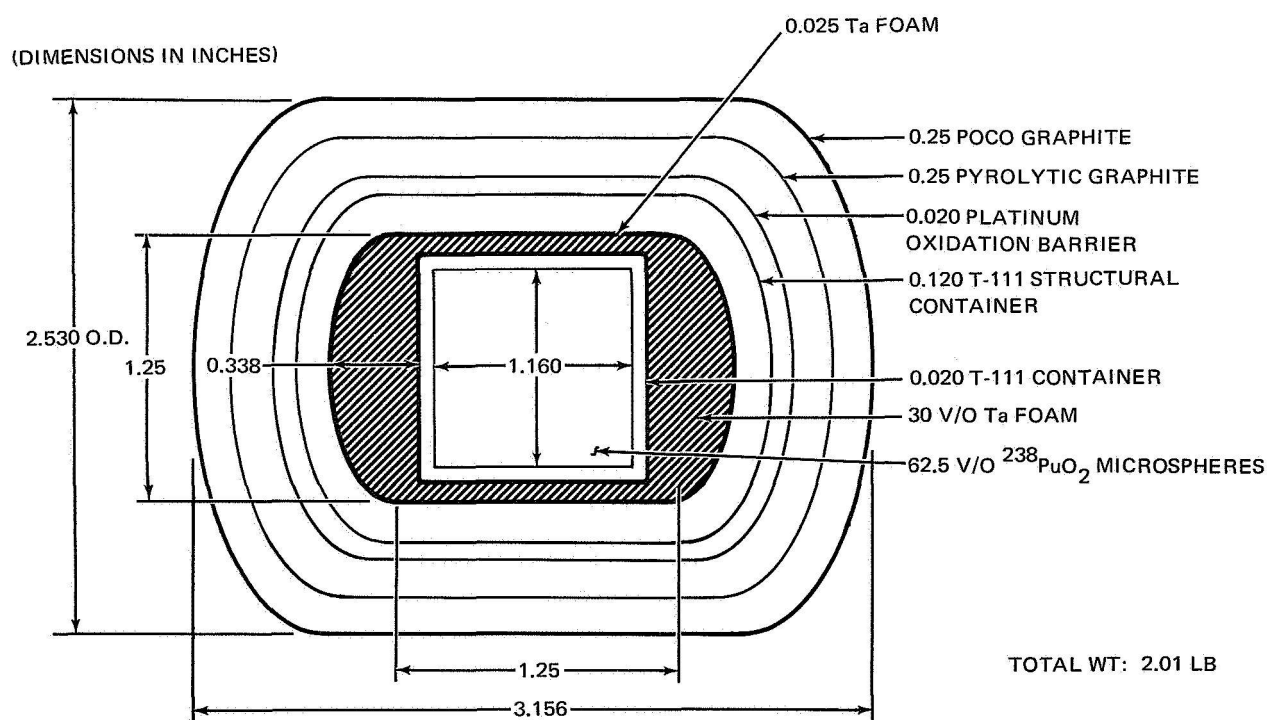


Figure A-2.  $^{147}\text{Pm}_2\text{O}_3$  Capsule, Model PMC-50-1

69-774

Figure A-3.  $^{238}\text{PuO}_2$  Bare Microspheres, Model PUM-10-1

69-781

Figure A-4.  $^{238}\text{PuO}_2$  Bare Microspheres, Model PUM-50-1

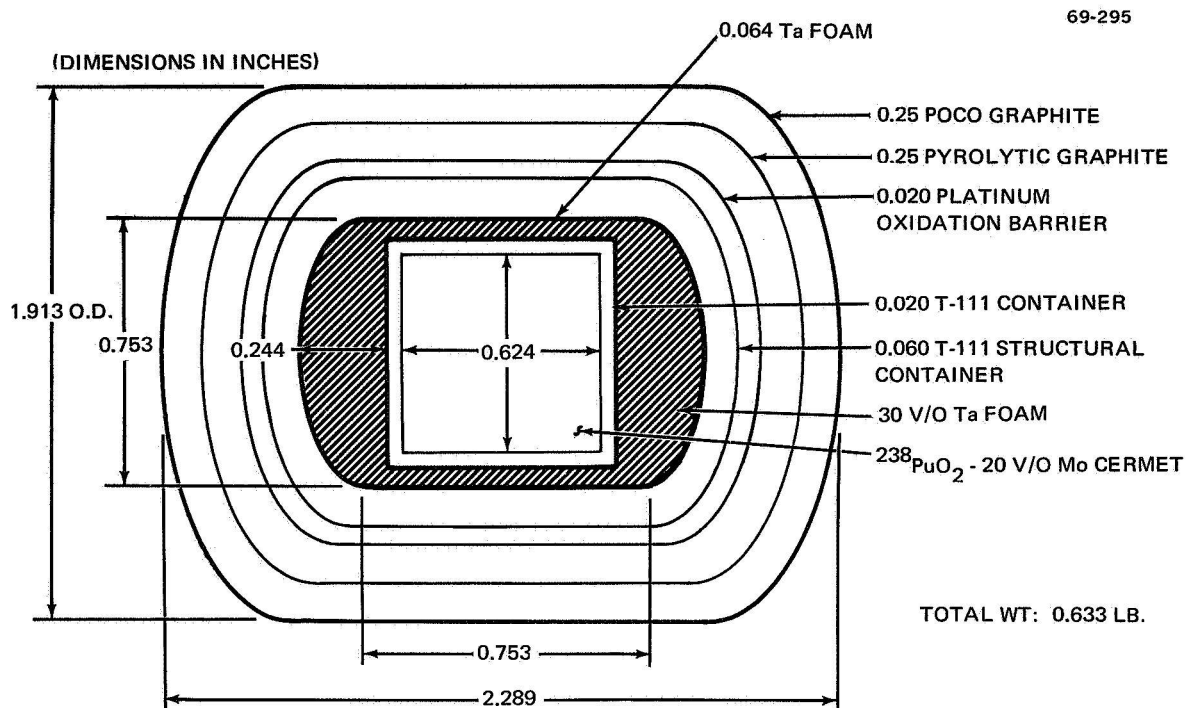


Figure A-5.  $^{238}\text{PuO}_2$  Cermet, Model PUC-10-1

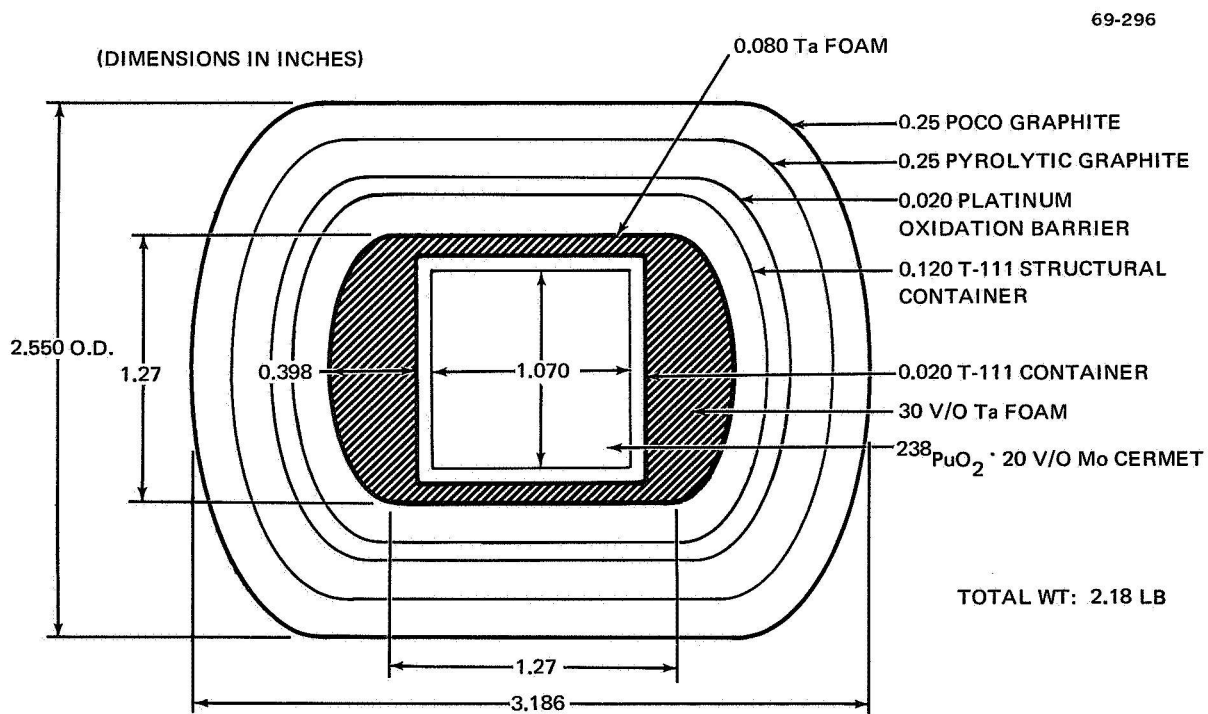
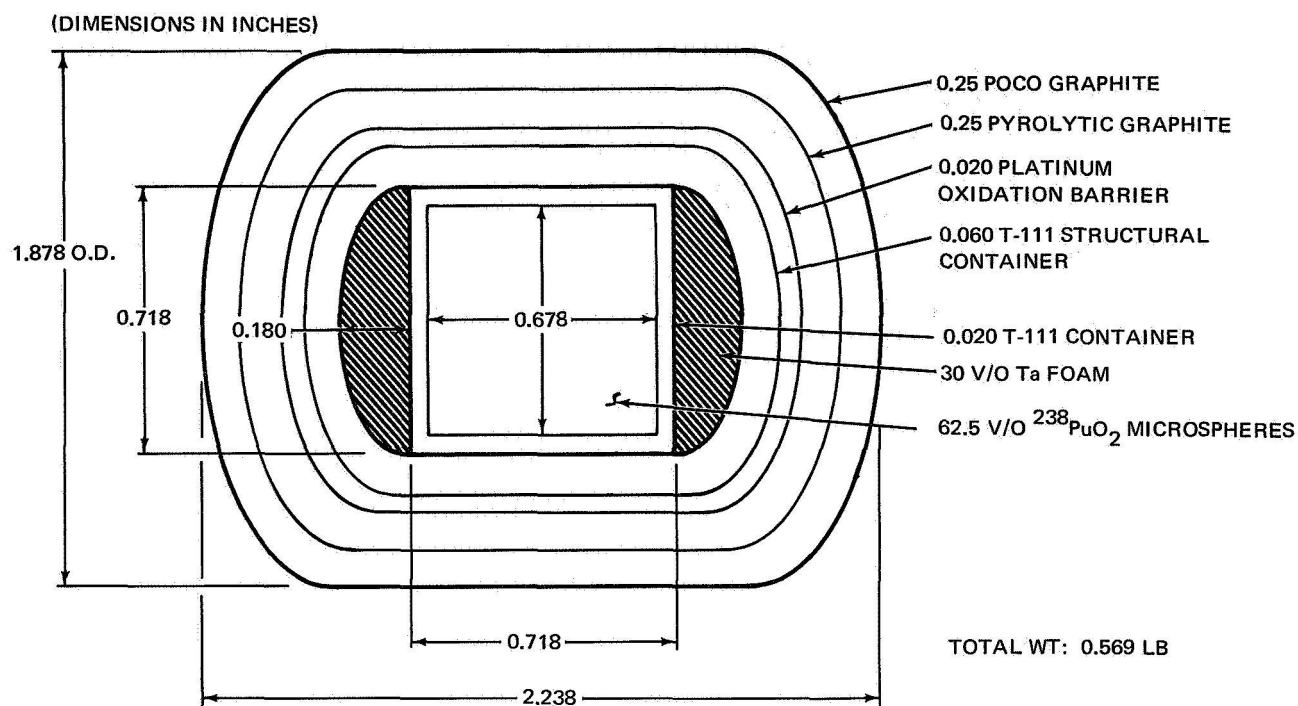
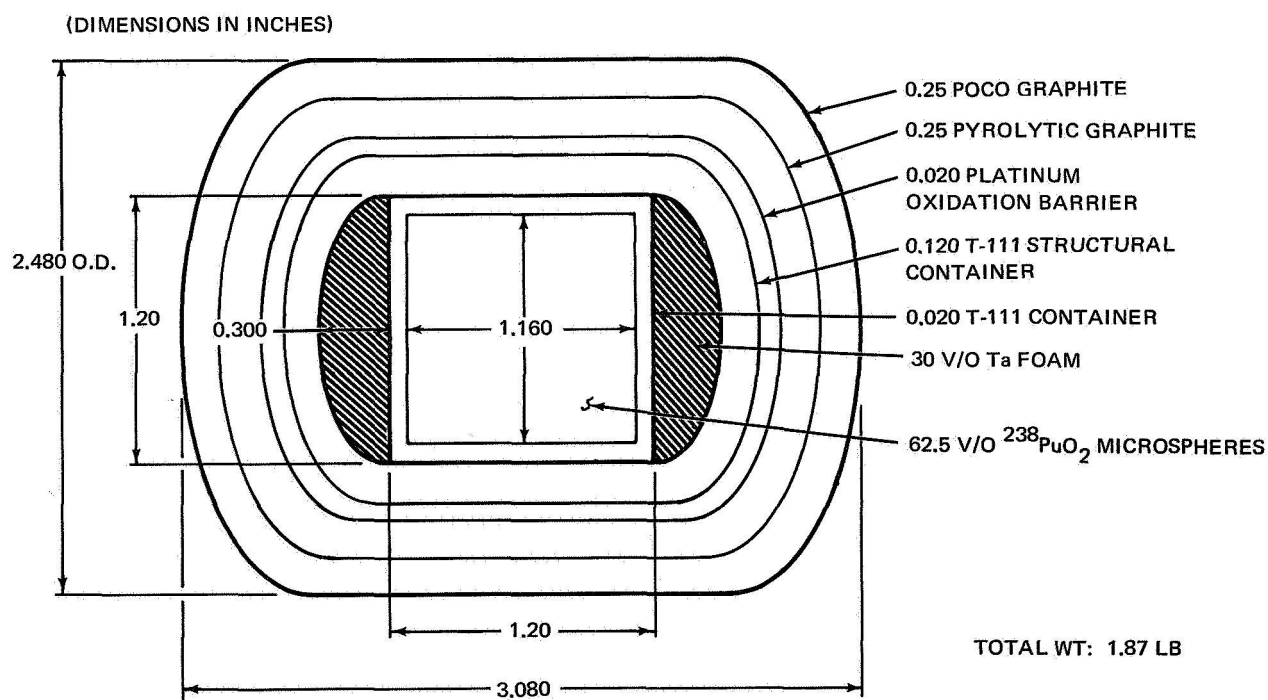
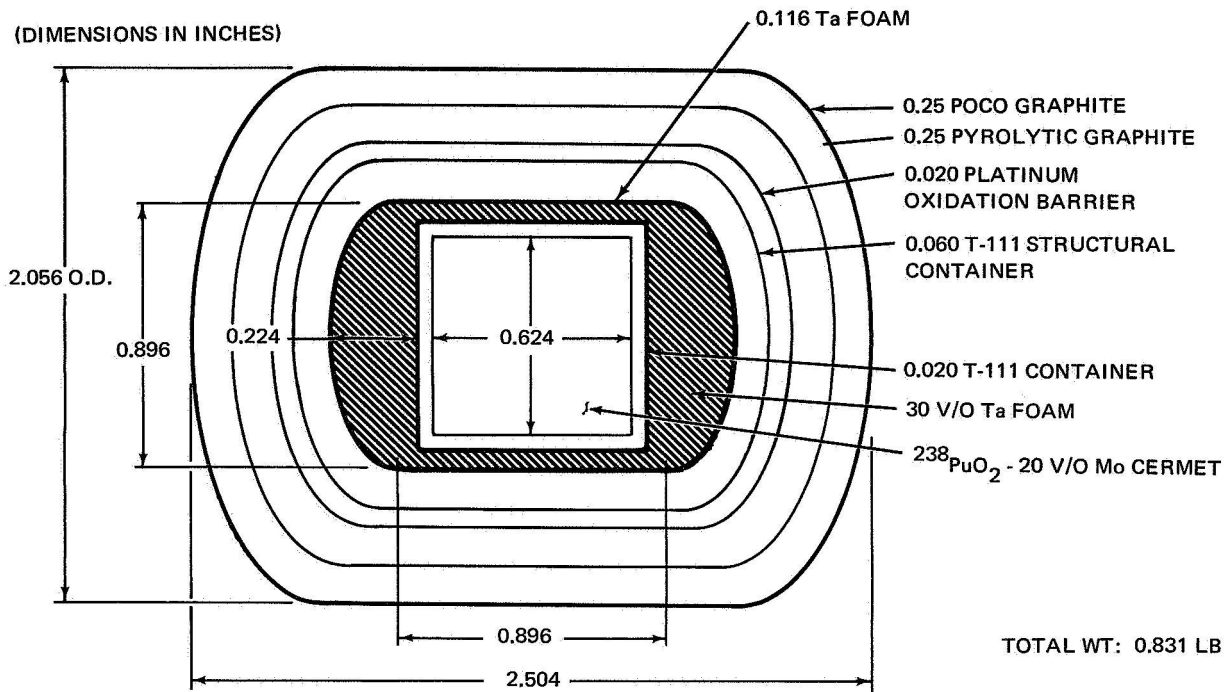


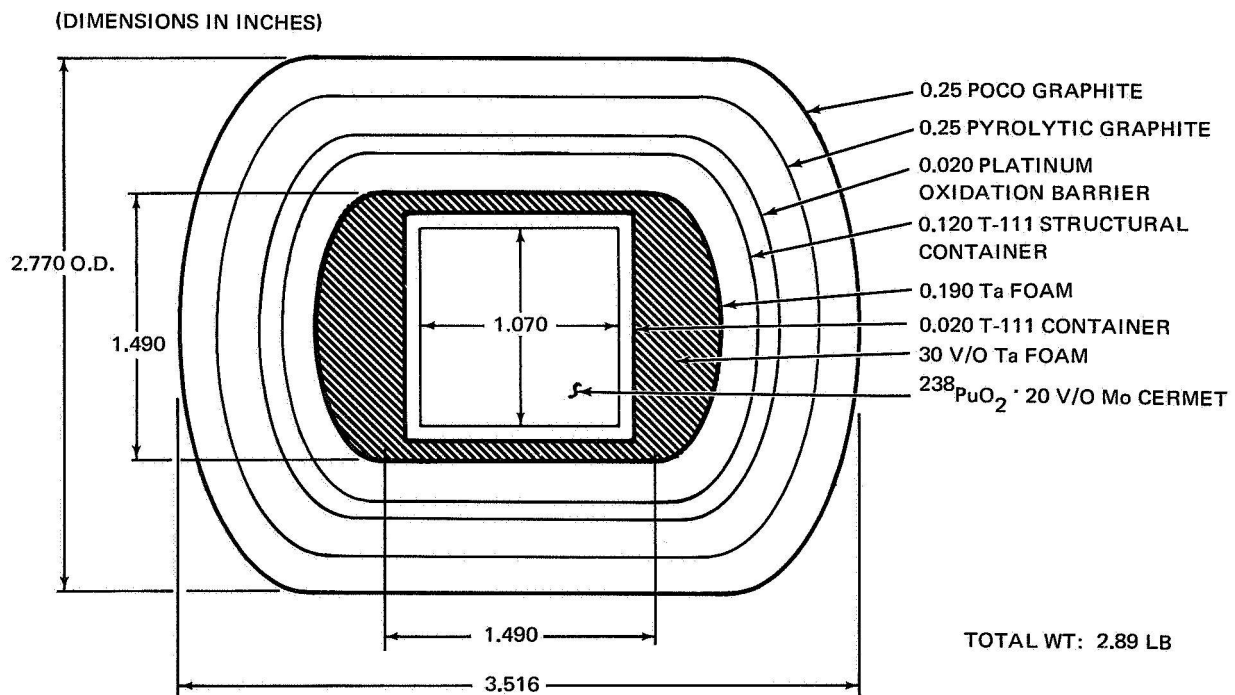
Figure A-6.  $^{238}\text{PuO}_2$  Cermet, Model PUC-50-1

Figure A-7.  $^{238}\text{PuO}_2$  Bare Microspheres, Model PUM-10-2Figure A-8.  $^{238}\text{PuO}_2$  Bare Microspheres, Model PUM-50-2

69-299

Figure A-9.  $^{238}\text{PuO}_2$  Cermet, Model PUC-10-2

69-300

Figure A-10.  $^{238}\text{PuO}_2$  Cermet, Model PUC-50-2



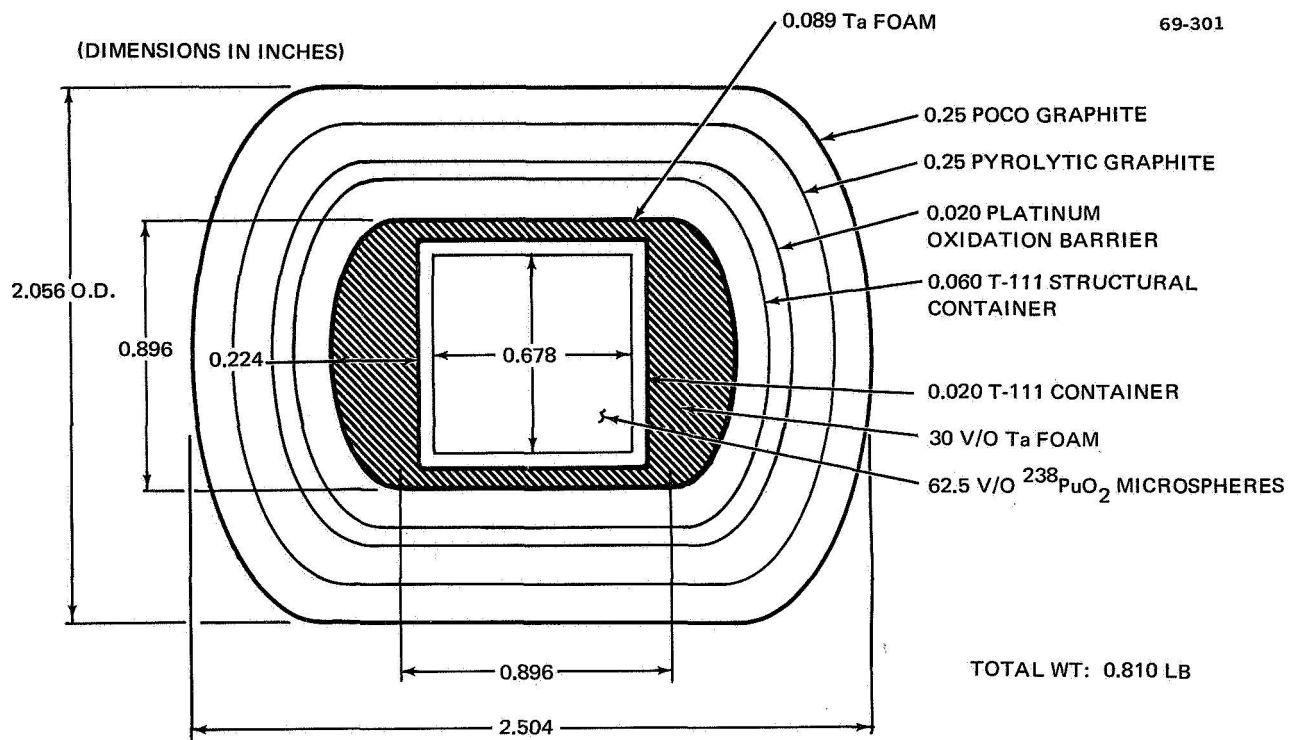


Figure A-11.  $^{238}\text{PuO}_2$  Microspheres, Model PUM-10-3

69-302

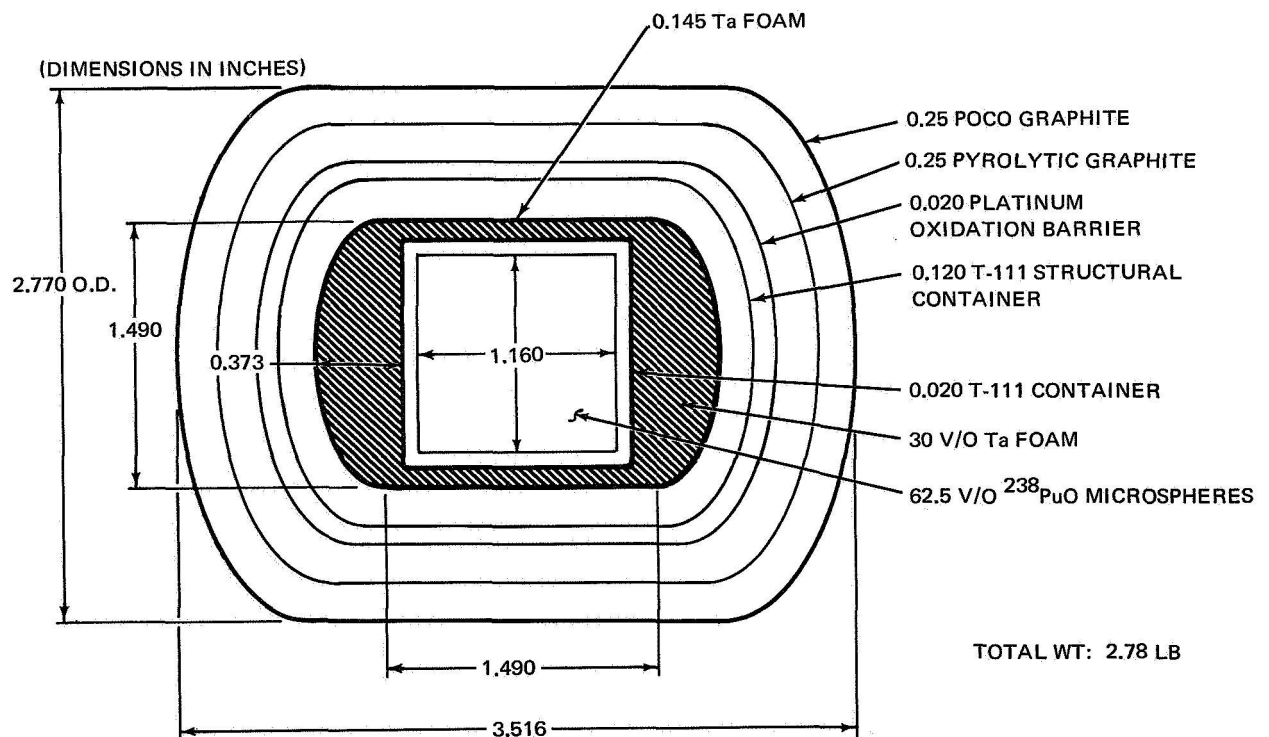


Figure A-12.  $^{238}\text{PuO}_2$  Microspheres, Model PUM-50-3

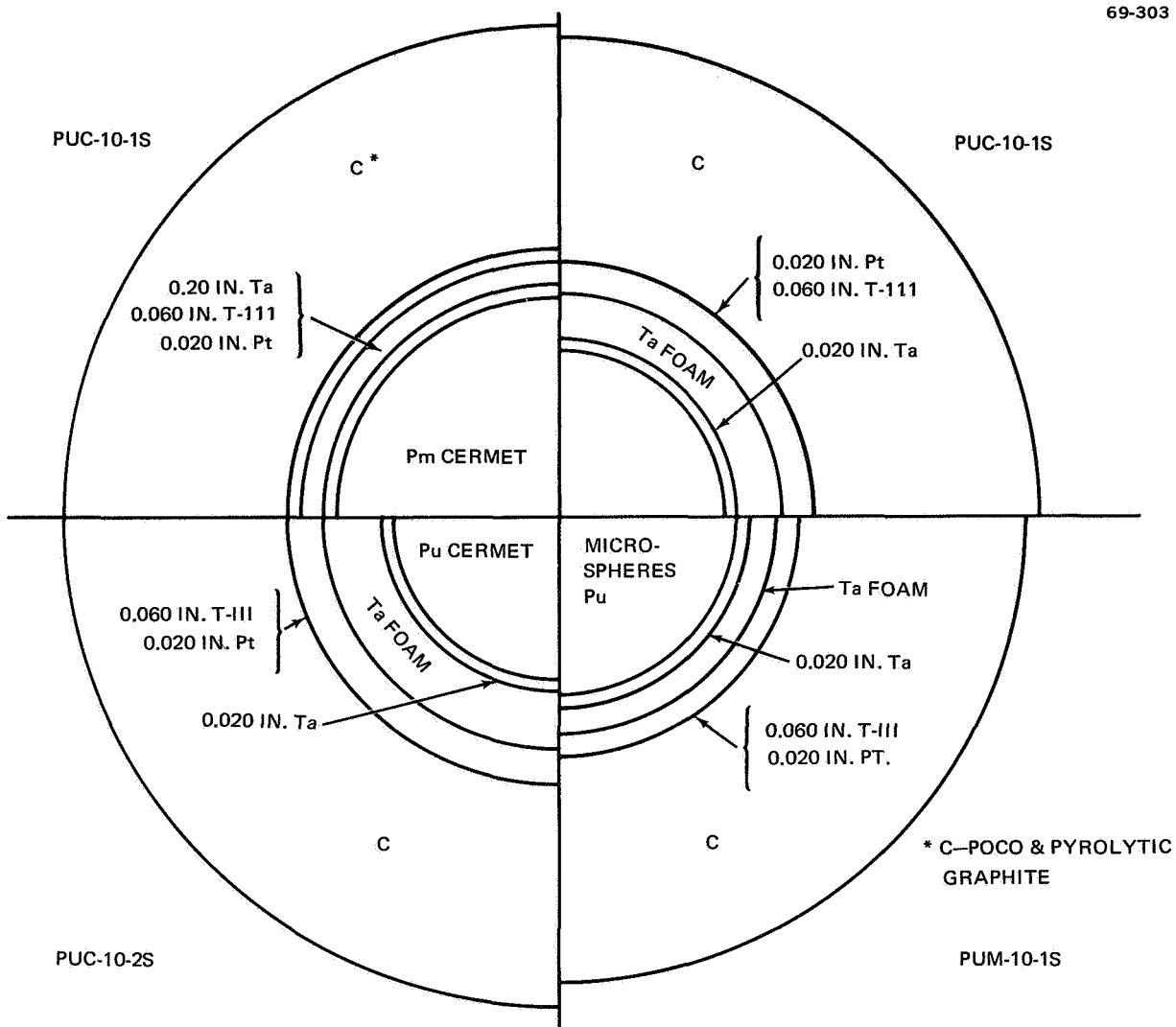


Figure A-13. Spherical Heaters

TABLE A-1  
HEATER WEIGHT COMPARISON

Heater concept	Weight (lb)
PMC-10-1	0.883
PMC-50-1	3.11
PUM-10-1	0.598
PUM-50-1	2.01
PUC-10-1	0.632
PUC-50-1	2.18
PUM-10-2	0.569
PUM-50-2	1.87
PUC-10-2	0.831
PUC-50-2	2.89
PUM-10-3	0.810
PUM-50-3	2.78
PMC-10-1S	0.750
PUC-10-1S	0.597
PUM-10-1S	0.525
PUC-10-2S	--
PMC-50-1S(not shown)	2.56
PUC-50-1S(not shown)	2.086



## Appendix B

### DRAG COEFFICIENT SUMMARY

A study was made of the drag coefficients for the different proposed design shapes in the various flow regimes encountered during reentry. The basic shapes considered were:

1. Flat-faced cylinder (reference and alternate C designs)
2. Rounded-end cylinder (alternate D design)
3. Sphere (alternate E)
4. Cube (alternate A)
5. Rectangular parallelepiped (alternate B)

#### Flat-Faced Cylinder and Rounded-End Cylinder

There are four basic flight orientations for a cylindrical shape: side-on (axis normal to flow), end-on (axis in the direction of flow), random tumbling, and end-over-end tumbling (in a plane parallel to flow).

The probable mode of reentry is the side-on or broadside orientation. It is this orientation which is usually used in reentry analyses of cylindrical designs. It is shown in reference 71 that side-on spinning results in a slightly higher but representative surface heating among tumbling modes which affects uniform surface heating.

In hypersonic flow, the drag in the high-altitude free molecule flow is higher than the drag in continuum flow. Figure B-1 shows the variation of the drag coefficient for a cylinder side-on in rarefied flow plotted as a function of molecular speed ratio,  $s$  (where  $s = V_\infty / \sqrt{2RT_\infty}$ ). Until recently, it was thought that this curve approached 2.0 as  $s \rightarrow \infty$ , since most bluff shapes have a  $C_D$  of about 2.0 at high-speed ratios in free-molecule flow (ref. 72). Recent measurements by Maslach and Shaaf (ref. 73), Maslach et al. (ref. 74) and Coudeville et al. (ref. 75), indicate that free-molecule drag at high-speed ratios (or Mach numbers) is higher than 2.0--probably around 2.8. This is shown by the data correlation in figure B-2. For all bluff shapes, the free-molecule drag becomes constant for hypersonic flow ( $M > 5$  or  $s > 4$ ) and does not decrease further as  $s \rightarrow \infty$ . The trend of the data in figure B-2 appears to bear this out.

The side-on drag variation in the transition regime has been investigated by Maslach and Shaaf (ref. 73) and Maslach et al. (ref. 74). The results

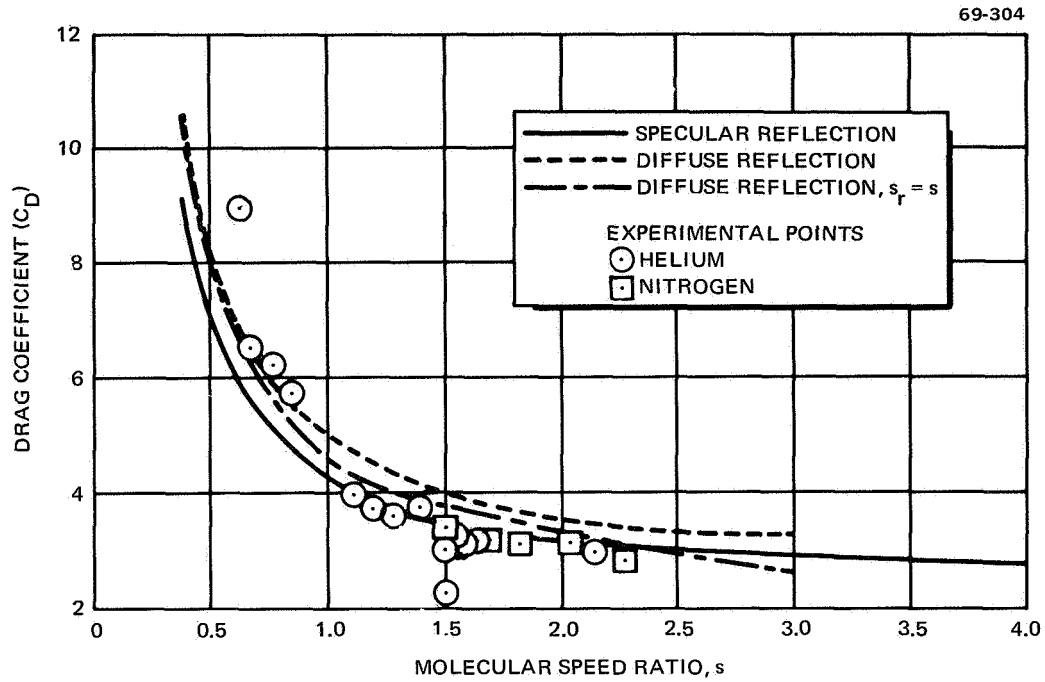


Figure B-1. Comparison of Drag Coefficient of Cylinder for Specular and Diffuse Reflection

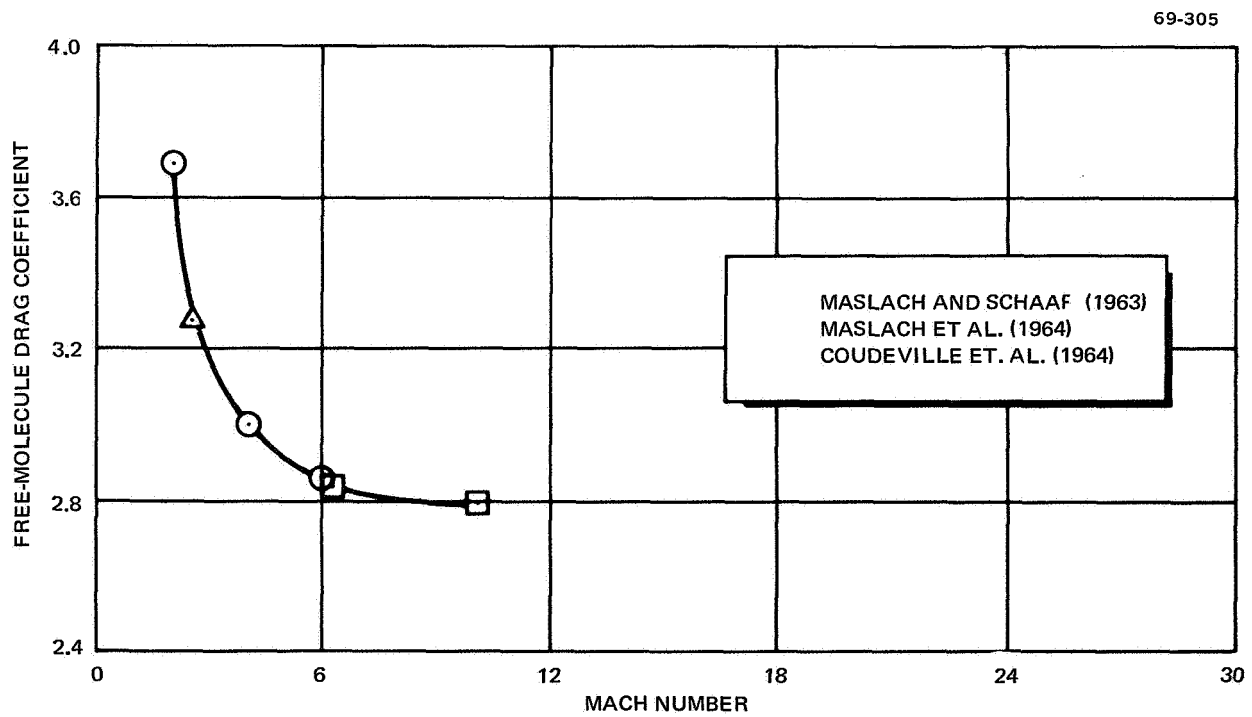


Figure B-2. Side-On Cylindrical Drag Vs Mach No. in Free-Molecule Flow

for Mach 6 and 10 are correlated in figure B-3. These data indicate that  $C_D \approx 2.8$  in free-molecule flow and that  $C_D \approx 1.5$  in continuum flow at values of Knudsen number around 0.01.

These data may be accurately described by the equation,

$$C_D = 1.5 + \left( \frac{2.8 - 1.5}{2} \right) \left[ 1 + \operatorname{erf} \left( \frac{\log_{10} kn + 0.36}{0.8} \right) \right] \quad (B-1)$$

This equation is solved by the RESTORE computer code along the trajectory. The numerical constants must be input.

The value of  $C_D$  calculated as  $kn \rightarrow 0.01$  is higher than predicted by Newtonian theory (1.5 compared to 1.3) for continuum flow. Measurements of crossflow drag in transonic flow indicate agreement with theory at the highest Mach numbers measured (ref. 76). For the side-on cylinder calculations, a transition from  $C_D = 1.5$  at Mach 18 to  $C_D = 1.25$  at Mach 16 was assumed since in this range the Knudsen number drops from 0.01 to the curve for a cylinder with  $L/D = 1.25$  shown in figure B-4 for  $0 < M < 16$ . This curve is a composite fit to the data given in references 76 and 77. Note that the  $L/D$  ratio has a strong effect for Mach numbers below 5. In hypersonic flow, no  $L/D$  effect is evident.

Around  $M = 0.5$ , Reynolds numbers effects become important for diameters on the order of 2 or 3 in. These effects have been thoroughly investigated for an infinite cylinder, perhaps best of all in references 77 and 78 (see also ref. 76). Basically, when  $Re$  exceeds  $2 \times 10^5$ , the flow which at low  $Re$  tends to separate from the body at around  $90^\circ$  from the stagnation point, will follow the body contour around to the aft end, thereby increasing the base pressure. This is a marked characteristic of a rounded body; a sharp-cornered body will separate the flow even at high  $Re$ .

When the velocity of a cylinder (side-on) exceeds about  $M = 0.4$ , however, the drag again rises sharply to the value given in figure B-4. This indicates that for  $0 \leq M \leq 0.4$ ,  $C_D$  should be a function of  $Re$  alone; above a Mach number of 0.4, the drag should be a function of  $M$  alone. Consequently, a tabular approximation of the indicated curve in figure B-4 was used in the reentry analysis for  $0.5 \leq M \leq 16$ . Below  $M = 0.4$ , a tabular approximation to the indicated curve in figure B-5 was used. For  $0.4 < M < 0.5$ , a transition between the two tables is made.

Figure B-5 was constructed from data presented in Hoerner (ref. 76), and references 77, 78, and 79. The sharp drop in drag at  $Re = 3 \times 10^5$  is evident. Also, the strong dependence in the  $L/D$  ratio at low  $Re$  is seen by comparing the curves for  $L/D = \infty$  and  $L/D = 1.25$ . No measurements have been made at high  $Re$  for cylinders with end effects (low  $L/D$  ratios), so that a dependence on  $L/D$  at high  $Re$  is uncertain. The range of data for an infinite cylinder at high  $Re$  is indicated by the shaded band in figure B-5. The lower bound of this band is used in the present calculations, since the values can be expected to be lower for  $L/D = 1.25$ . For the 2- to 3-in. diam heaters, the condition at impact corresponds to the point  $Re \approx 6 \times 10^5$  and  $C_D = 0.25$ . The  $2\sigma$  confidence limit on this value is taken to be 0.10, since this ranges to the upper bound on data for the infinite cylinder and to the lower bound on data for a sphere.

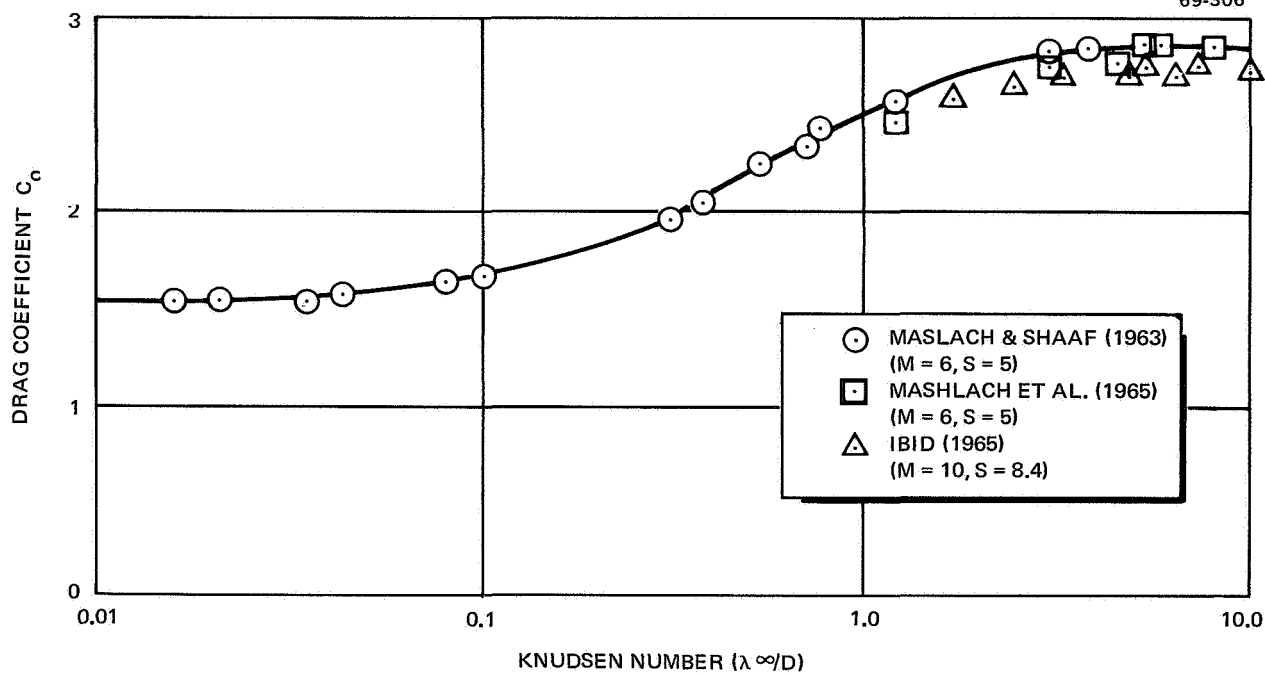


Figure B-3. Drag Coefficient for a Cylinder in Crossflow Vs Knudsen No.

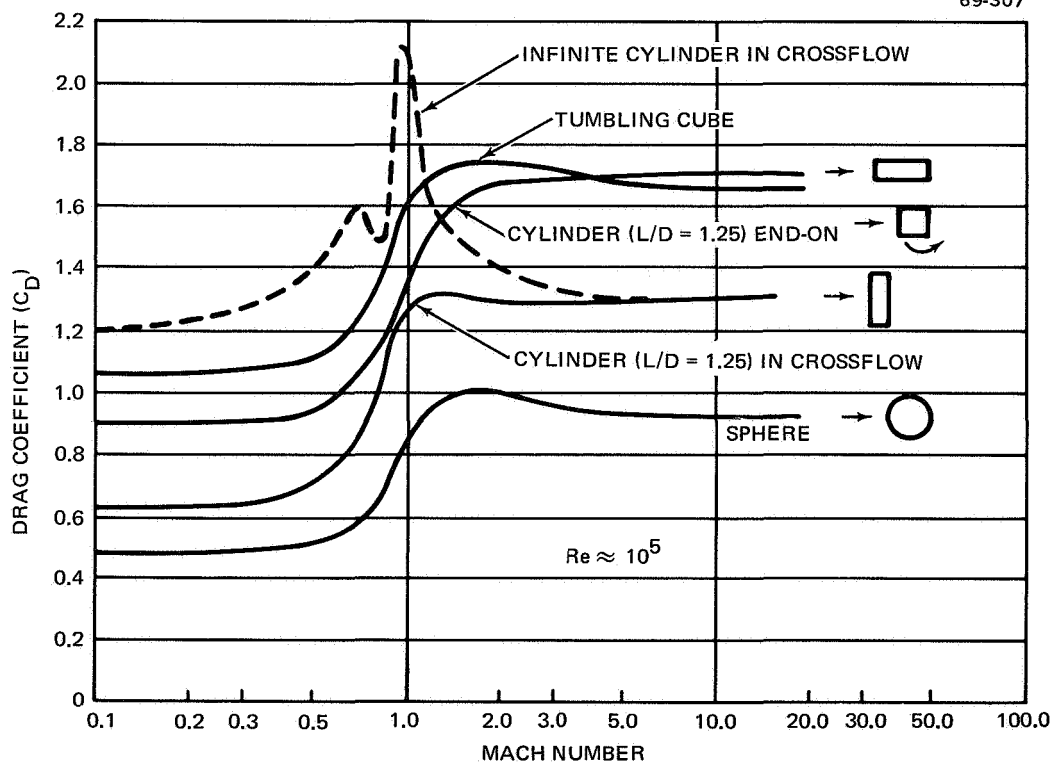


Figure B-4. Transonic Drag Coefficients for Different Shapes



For an end-on cylinder, the drag is no better defined than for side-on. Modified Newtonian theory assumes that the flow lines in hypersonic flow follow the contour of the body. For a flat-ended cylinder, the pressure would then be uniform over the face and the predicted drag would be

$$C_{ps} = 2 - \rho_{\infty}/\rho \quad (\text{ref. 76}) \quad (\text{B-2})$$

where  $\rho_{\infty}/\rho$  is the density ratio across a normal shock. A comparison of theory and experiment (ref. 80) is shown in figure B-6 for end-on cylinders of varying bluntness. Note that theory becomes inaccurate for flat-nosed bodies. An independent measurement (ref. 81) for flat-faced cylinders at Mach numbers up to 14 indicated that the drag is about 0.91 times the theoretical value, in good agreement with the data in figure B-6. Consequently, the drag for a flat-faced cylinder is taken in the present study to be

$$C_D = 2 - 1.6 \frac{\rho_{\infty}}{\rho} \quad (\text{B-3})$$

which is the theoretical equation normalized to fit the experimental data and to meet the boundary condition that  $C_D = 2$  as  $\rho_{\infty}/\rho \rightarrow 0$  in free-molecule flow.

For a cylinder with rounded ends, the drag approaches that for a sphere as the hemispherical shape is approached. For the elliptical ends of the alternate D design, the drag is taken to be that for a spherical segment with a radius of twice the cylinder radius (bluntness ratio  $X_B/R_B$  of 0.5). Thus, values of 2.0 in free-molecule flow and about 1.2 (fig B-6) in continuum flow were assumed. Variation of drag in the transition regime is assumed to follow the equation form for a sphere or hemisphere discussed below.

In transonic flow, the drag for a flat-faced cylinder end-on is given in Hoerner (ref. 76) and in Marks Handbook (ref. 82). The results are shown in figure B-4, for an  $L/D$  of 1.25. The results have been modified in the present study to account for ablation at the edges and on the face. The major portion of ablation occurs just after peak heating, since the oxygen flux to the surface peaks at that time. This corresponds to the time when the body decelerates and the Mach number drops rapidly. Therefore, the above equation is used until  $M = 16$ , just below which the drag drops to 1.2 corresponding to a blunt, convex shape (or elliptical ends). At about Mach 1, the drag is assumed to drop smoothly to about  $0.7 \pm 0.2$ . At high  $Re$  and below  $M = 4$ , the drag for the rounded-end alternate D is assumed to drop to about  $0.25 \pm 0.10$  for the same reason as for the side-on cylinder. The flat-ended cylinder, however, will have an ablated, rounded front-face for end-on but the aft edges will still be sharp. Therefore, there should be little or no change with  $Re$  in the range  $10^5$  to  $10^6$  for the reference and alternate C designs.

These drag coefficients are based on the actual frontal area of the particular orientation. If the cylinder is tumbling, the drag coefficient is a linear combination of the side-on and end-on drag coefficients according to the equations

$$C_D A_S = 0.589 (C_D)_S A_S + 0.25 (C_D)_E A_E \quad (\text{B-4})$$

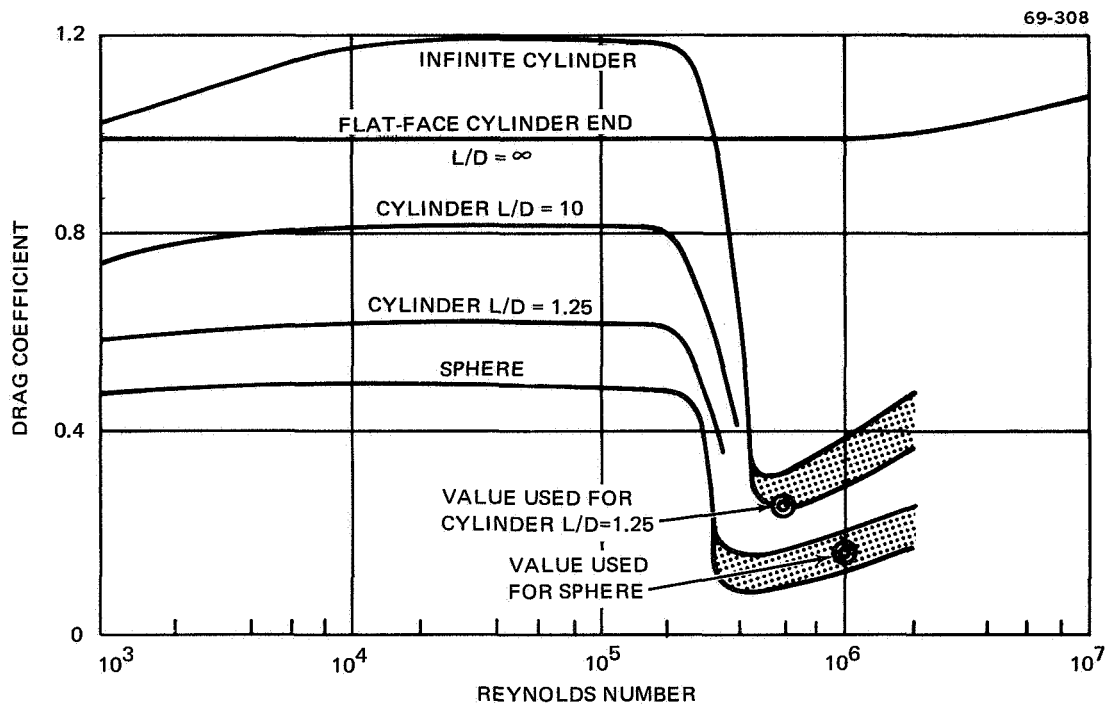


Figure B-5. Drag Coefficient for Cylinders and Spheres Function of Reynolds No. at Low Mach Numbers

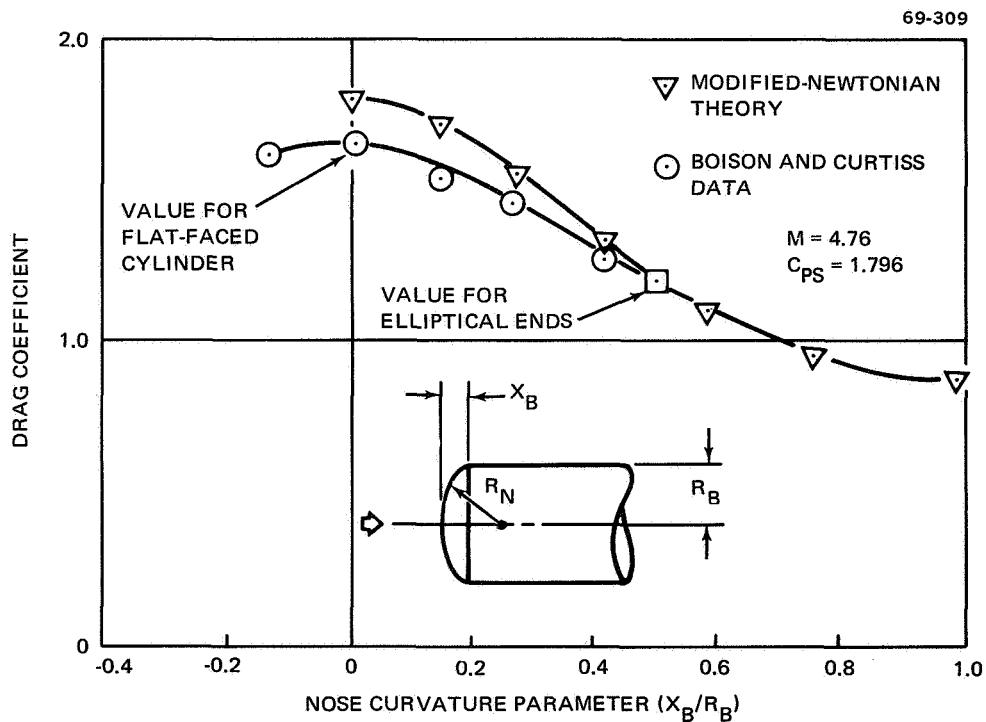


Figure B-6. Drag Coefficients of Spherical Segments

for random tumbling, and

$$C_D A_S = 0.4244 \left[ (C_D)_S A_S + (C_D)_E A_E \right] \quad (\text{ref.} \quad (B-5)$$

for end-over-end tumbling. Subscript E pertains to end-on, and S to side-on.

### Sphere

The drag coefficient of a sphere is relatively well defined (ref. 76). In hypersonic flow, the data, primarily from Masson, Morris, and Bloxsom (ref. 83) have been correlated at Atomics International by the equation

$$C_D = 0.92 + 1.08 \exp \left( - \frac{\rho \omega / \rho}{10 \text{ kn}} \right), \quad (B-6)$$

which is used in the present study. Note that, according to this equation,  $C_D = 2.0$  in free-molecule flow and  $= 0.92$  in continuum flow ( $\text{kn} \rightarrow 0$ ).

The curve presented in figure B-4 is used in transonic flow (ref. 76). At  $M < 0.8$ , the curve of  $C_D$  vs  $\text{Re}$  is used where the mean value in the data band is selected at the appropriate value of  $\text{Re}$ . This point is found to be  $C_D = 0.15 \pm 0.05$  at  $\text{Re} \approx 10^6$ .

### Cube or Rectangular Parallelepiped

The only drag data in transonic flow pertinent to a cubic shape appears to be that given in Hoerner (ref. 76) for a tumbling (at random) cube. The resulting curve is shown in figure B-4, where drag is based on the flat-face area. Some modifications were made in the present study to account for ablation at the edges by lowering this curve to meet the conditions  $C_D = 1.2$  for  $2 \leq M \leq 15$ , and  $C_D = 1.0$  for  $M < 2$ .

Above  $M = 15$ , drag is assumed to rise to 1.8 at  $M = 16$ . Above  $M = 16$ , drag is assumed to follow the same relationship as for an end-on, flat-faced cylinder. Judging from the data for an infinitely long block with a square cross-section (ref. 78), this should be the same drag variation as for the cube oriented with the flat face normal to flow. Therefore, trajectory calculations for the cube may be considered appropriate for the two most likely orientations--random tumbling and flat-face first. Edge-on will result in a higher drag coefficient (based on frontal area) in subsonic flow (refer. 78).

Data given for an infinitely long block with rectangular cross-section in reference 78 indicate that the drag of the alternate B design could be measurably lower if the capsule orients small face first. No quantitative data for the actual shape are available in the  $\text{Re}$  range of interest. Therefore, the drag for this latter design is assumed to be the same as for a cube in tumbling modes; stable modes were not analyzed.

In conclusion, it is found that the heaters will impact a Reynolds numbers where the flow adheres to a rounded body. This increases the base pressure, thereby sharply reducing the drag. Higher drag is achieved by using sharp-cornered shapes. Ablation could severely round off the front corners if oriented in a stable mode, but sharp corners aft will ensure separation of flow. Tumbling modes are not expected to reduce the sharp edges to the extent where no advantage is gained. Experimental data are needed for cubes and flat-ended cylinders with rounded corners.

## Appendix C

### REENTRY MODEL

The computer program is written in FORTRAN and integrates the differential equations of motion of a point-mass moving through the earth's atmosphere. The point-mass is subjected to the forces of atmospheric drag and gravity while moving relative to a rotating oblate earth in an air atmosphere with properties that are a function of altitude alone. The integration technique used is an Adams-Moulton predictor-corrector method.

Initial values of weight-to-area position, flight angle, velocity, and heading are input to the code referenced to a specified initial altitude. The drag coefficient may be a specified tabular function of time, altitude, mach number, Reynolds number,  $\log_{10}$  of the Knudsen number, or  $\log_{10}$  of the modified (including the compressibility) Knudsen number. In addition, drag may be calculated according to the equation.

$$C_D = C_I + C_2 \frac{\rho \infty}{\rho} \quad (C-1)$$

for a flat-face body, and

$$C_D = C_I + \left[ 1 + \operatorname{erf} \left( \frac{\log_{10} \text{Kn} - C_3}{C_4} \right) \right] \quad (C-2)$$

for a sphere or a cylinder in crossflow.

Aerodynamic heating along the trajectory is calculated using the equations and methods presented in reference 84. These are the Fay and Riddell (ref. 85) equations modified and correlated for satellite reentry by Detra and Hidalgo (ref. 86). Although these equations are not strictly valid for reentry velocities in excess of 26 000 ft/sec, they give approximate heating values for lunar return velocities (about 36 000 ft/sec) and were so used in the present study.

In addition to the equation form, note that only convective heating was considered, assuming equilibrium chemistry for dissociation and recombination of molecules in the boundary layer. Radiative heating is small at lunar return velocities for small bodies of the type considered here (ref. 87). However, the bodies do pass through flow regimes where nonequilibrium flow effects can cause significant heating reductions. This occurs when the characteristic time for chemical recombination of dissociated air atoms is much shorter than the time required for the atoms to diffuse across the boundary layer. If the surface is noncatalytic to recombination, the heat of dissociation is lost. Graphite can be expected to have a surface catalycity on the order of oxides. These materials are shown in reference 88 to

experience heating reductions of up to 30% in a wind tunnel under certain conditions. Extrapolations to reentry conditions indicate that overall heating will be reduced on the order of 10% or 15% (ref. 88).

Graphite oxidation is computed throughout the trajectory. The equation used was the one developed in reference 89 assuming an oxygen-diffusion controlled process and using the Reynolds analogy for boundary layer mass flow (mass flow proportional to heat flow). This equation is

$$\frac{dm}{dt} = \frac{0.2 q_{cw}}{H_s - H_{540}} \quad (\text{lb of O}_2/\text{ft}^2) \quad (\text{C-3})$$

where  $dm/dt$  is the mass flux of oxygen,  $q_{cw}$  is the cold-wall heat rate, and  $H_s$  and  $H_{540}$  are the air enthalpies at the stagnation temperature and at  $540^\circ\text{R}$  respectively. This equation agrees well with the relationship given by Bartlett (ref. 90).

This flux is integrated along the trajectory. The total depth of graphite is then determined by multiplying by the heat of combustion (2970 Btu/lb of  $\text{O}_2$ ) and dividing by the graphite density.

Transpiration cooling was not taken into account because, for graphite, these effects are small (ref. 90). However, at higher velocities combined with low pressure where combustion may occur in the boundary layer, heat reduction due to mass addition may be an important effect and should be included.

## Appendix D

### THERMAL ANALYSIS MODELS

#### Thermal Analyzer Program (TAP-3)

The TAP-3 code (ref. 91) used at DWDL to simulate POCO-pyrolytic graphite ablaters facilitates the solution of multidimensional transient and steady-state problems in heat transfer. It can also be used for any problem in which the physical system can be represented by an equivalent electrical network. At present, the maximum size of the network which can be accommodated is 500 capacitors and 999 conductors.

A variety of auxiliary functions are included. For example, thermal radiation paths between elements of the network are computed automatically if the surface areas and effective view factors are given. Thermal properties, internal heat generation rates, and boundary temperatures may be specified as fixed values, tabular functions, or algebraic functions of any other parameter in the system. This makes possible the solution of problems involving ablation, phase changes, etc. However, there is no provision for a continuous surface recession rate; nodes must be lumped together one or more at a time. In addition, there is no direct provision for the effects of mass transfer cooling.

The code is not linked to any specific geometry or set of geometries and is, therefore, quite flexible. Calculations of areas and volumes associated with the nodal network may be done through the algebraic function specification mentioned above.

The time step used by the code must be sufficiently small to avoid divergence in the calculation process. The formula for finding the maximum stable time step,  $\Delta t_{st}$ , is

$$\Delta t_{st} = \frac{C}{\sum_i Y_i} \quad (D-1)$$

where  $C$  is the capacitance of a given node and  $Y_i$  are the admittances of the heat-flow paths by which the given node is connected to other nodes in the network. This formula is applied before each iteration to each node having a nonzero capacity, and the least value found is used as the  $\Delta t$  for that iteration. It is important for the user to make preliminary estimates of the values of  $\Delta t_{st}$  while selecting the nodal network in order to avoid the construction of a network involving very small values of  $\Delta t_{st}$  and, therefore, requiring lengthy machine running times.

## Charring Ablator Code, STAB 2

The STAB 2 code was developed by D. M. Curry of NASA/MSC and is documented in reference 92. The code is presently operational at DWDL and was used to generate some of the data in the report.

A description of the analytical model used, and a complete listing of the program together with instructions for coding, are presented in reference 92. Basically, the code simulates the transient one-dimensional thermal performance of a charring-ablator heat-protection system exposed to a hyper-thermal environment. The system is considered to consist of (1) an ablation material, and (2) a backup structure of up to 12 materials. The ablating material is further considered to consist of three distinct regions: char, reacting, and virgin material. Thermal properties of all materials are temperature-dependent, with the properties of the charring material also being state-dependent. A maximum of 50 nodes in the ablator and 10 nodes in each backup material is possible.

The code offers a number of desirable features: (1) the equations solved are stable, even for relatively large time increments, because of the "backward time step" difference formulation employed; (2) machine running time is relatively short, and multiple cases may be run; (3) the input required is not complex; (4) a wide variety of boundary conditions may be specified; (5) the code includes options for radiative as well as convective heating, mass transfer cooling through injection into the boundary layer (including the capability of specifying the molecular weight of the injectant), and surface recession rates as a function of surface temperatures; and (6) the equations are devised in terms of a moving boundary coordinate system so that surface recession may be handled in a continuous manner without the need of throwing away nodes.

The code is limited in that a one-dimensional geometrical model must be used. Also, there is presently no provision in the code for simulation of convective cooling during the latter phase of the reentry trajectory.

### Heater Model Used for Side-On Spinning Orientation

The cross-axial spinning orientation is such that heating rates may be assumed to be independent of the angle,  $\theta$ , conventionally used in cylindrical coordinates. Since the thermal properties are independent of  $\theta$ , so are the temperatures. If the assumption is made that end effects may be neglected, then the temperatures are functions of only the radial distance,  $r$ , from the capsule center line, and a rather simplified thermal model is possible. The complete nodal network employed to simulate the side-on spinning flight orientation appears in figure D-1. The material and thickness of each layer of the capsule are given. A unit depth out of the plane of the paper was used in the calculation of element volumes and capsule surface area.

By means of TAP-3, thermal behavior of this model during various reentry trajectories was simulated; aerodynamic heating, oxidation heating, internal heat generation, and both radiative and convective cooling were



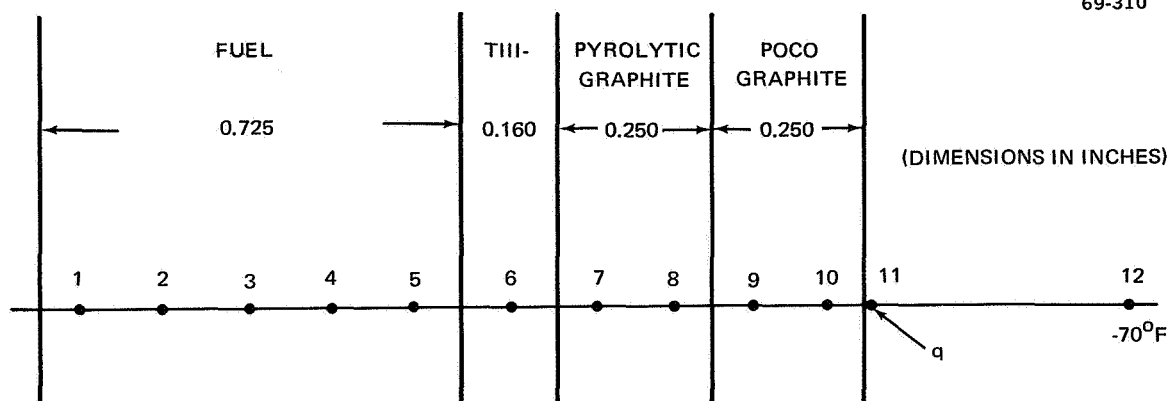


Figure D-1. Nodal Network to Simulate Side-On Spinning Orientation

included in the analysis. The temperature dependence of all thermal properties was included. No provision was made in the analysis for the effects of recession of the POCO graphite surface or for heat blockage due to mass injection into the boundary layer.

#### Heater Model Used for Side-On Nonspinning Orientation

The side-on nonspinning orientation requires somewhat more involved analysis than does the side-on spinning case in that the heating rates, and therefore the temperatures, are functions of the angle,  $\theta$ , conventionally used in cylindrical coordinates. The approach used was to neglect axial dependence of heating rates, temperatures, and properties. Next, a circular section of unit was "lifted" from the capsule. Due to symmetry considerations, it was necessary to analyze only one-half of the resulting unit-depth circular disk. The complete nodal network used to simulate the 50-W promethium capsule with POCO-pyrolytic graphite ablator appears in figure D-2; the composition and thickness of each layer are given.

Thermal behavior of this model during various reentry trajectories was analyzed using TAP-3. The effects of convective cooling at lower altitudes were included in the analysis as was the direction-dependent thermal conductivity of pyrolytic graphite; however, no allowance was made for heat blockage effects arising from mass injection nor was provision made for recession of the POCO graphite surface.

#### Heater Model Used for End-On Orientation

The end-on flight orientation which was analyzed using the TAP-3 heat transfer code involves rather complex geometry. The outer surface of the reference heater is in the shape of a flat-ended right circular cylinder, while all layers except the POCO graphite are in the shape of cylinders with heads

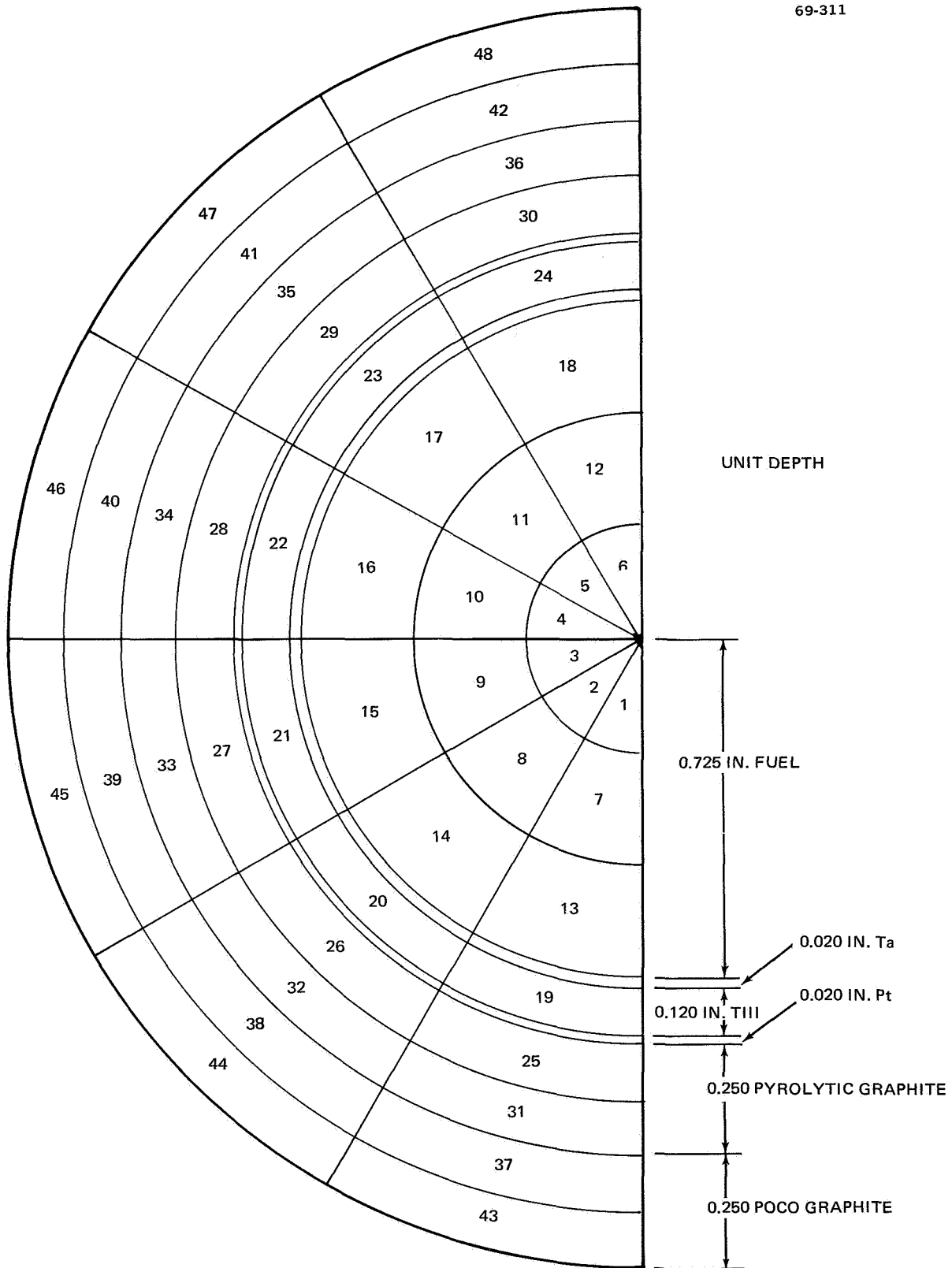


Figure D-2. Nodal Network for Side-On Nonspinning Model of 50-W  $^{147}\text{Pm}$  Heater, Reference Design

which are roughly semiellipsoidal. The complex shape of the reference heater ends as designed is such as to require extensive analysis. The somewhat simpler model used as a first approximation consists of a multilayered right circular cylinder with multilayered hemispherical heads. The complete node-structure model used to simulate the 50-W promethium baseline heater appears in figure D-3.

It is evident that heating rates, properties, and temperatures are independent of the angle,  $\theta$ , normally used in cylindrical coordinates. Thus, there is no heat transfer in the  $\theta$  direction. This allows consideration of only a cross-section lying in the  $r$ - $z$  plane (of conventional cylindrical coordinates) at any angle  $\theta$ .

Surface-node heating rates used were those corresponding to a flat-ended cylinder. With this correction, the hemispherical end approximation of the capsule design may be expected to yield fairly reliable results, especially in the important region behind the stagnation area of the heater where details of the curvature are less important. However, further analysis using a more accurate model is needed.

#### Heater Model Used for Charring Ablator Analysis

The STAB-2 code was applied to the thermal analysis of a 50-W promethium-cermet-fueled heater with 0.5 in. -thick Narmco 4028 carbon-fiber-reinforced phenolic ablator material. Most of the ablator thermal properties were obtained from reference 93. The side-on nonspinning flight orientation for the earth orbital decay reentry trajectory was investigated.

A one-dimensional infinite-slab model is employed by STAB-2; yet the heater has a cylindrical geometry. In order to correct the model for this geometric difference, thermal admittances and capacitances were appropriately adjusted by dummied the values of thermal conductivity and heat capacity, respectively, as functions of the radial distance. The heater was assumed to consist of an infinite cylinder (i. e. end effects were neglected) composed of concentric layers of fuel, T111-Pt, and ablator.

Injection efficiency was determined by the method in reference 94. Recession rates were calculated by use of the equations in reference 95 in connection with experimental data in reference 96.

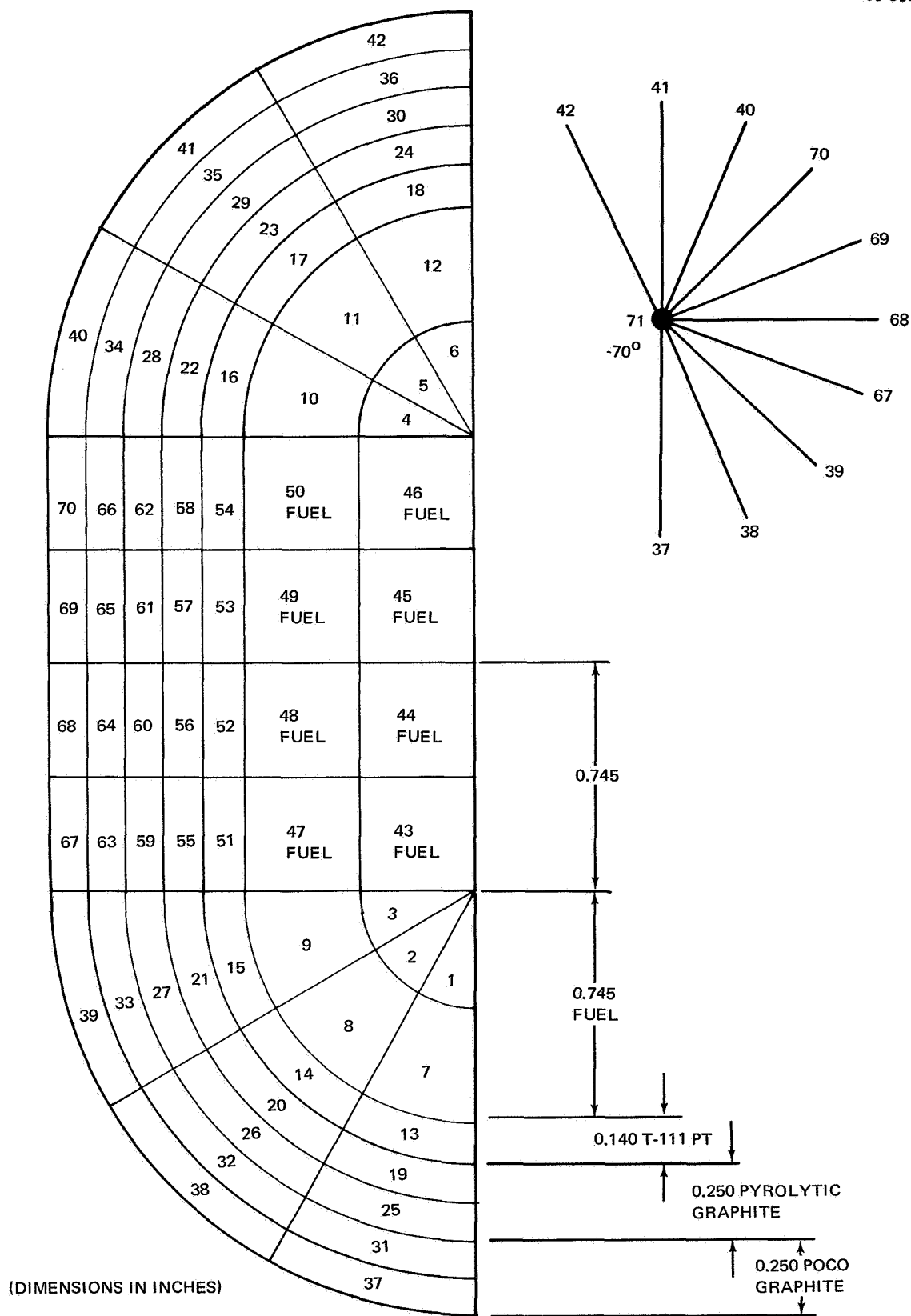


Figure D-3. Nodal Network for End-On Model of 50-W  $^{147}\text{Pm}$  Heater, Reference Design

## Appendix E

### IMPACT STUDIES

Table E-1 summarizes test conditions and results for one segment of a DWDL independent research and development impact testing program. Figures E-1 through E-8 illustrate the simulated heater impact specimens.

Ten simulated 10-W and four simulated 50-W heater specimens were impacted against granite, using the modified light gas gun at the Douglas Aeroballistic Range, El Segundo, California. The specimens consisted of a bronze fuel simulant and tantalum wire springs simulating foam within a T-111 structural shell (0.060 in. thick, 10-W; 120 in. thick, 50-W) surrounded by reinforced, pyrolytic, or phenolic graphite. The specimens were heated to 1500°F in an argon atmosphere and shot end-on, using air pressure, against a granite block. Dual laser beam velocity instrumentation indicated breakup of the graphite before impact. Subsequent calculations show that this could be caused by a combination of thermal stress due to rapid cooling and stress due to differential inertial force (of the light graphite and heavy metal) resulting from air pressure.

TABLE E-1  
SIMULATED HEATER IMPACT TEST

Model no.	Test no.	Power (W)	Insulator	Norm. ablator thick (in.)	OD (in.)	Weight (lb) (not incl graphite)	Config.	Impact temp (°F)	Drive press. (psi)	Velocity (fps)	Helium leak check		Remarks
											Bubbles	Leak rate (std cc/sec)	
01	13	10	Bare	—	.935	0.30	80-505	—	90	420	No	None	Good
02	14	10	Bare	—	.935	0.30	80-505	1318	60	326	Yes	Yes	
04	1	10	RPG	1/4	1.43	0.30	80-1	1235	17	263	No	$2.0 \times 10^{-7}$	
07	2	10	RPG	1/4	1.43	0.30	80-1	1274	26	301	—	—	Broke through weld and end opposite impact.
05	3	10	RPG	1/4	1.43	0.30	80-1	1361	8	158	No	$1.2 \times 10^{-6}$	
03	12	10	RPG	1/4	1.43	0.30	80-1	1378	60	640	—	—	Bad weld—side on impact—ruptured.
09	4	10	Phenol.	1/4	1.43	0.30	80-503	1300	24	308	No	$2.2 \times 10^{-7}$	
10	11	10	Phenol.	1/4	1.43	0.30	80-503	—	60	571	No	$1.8 \times 10^{-5}$	Side on impact—laser indicates graphite bits.
06	8	10	RPG	1/2	1.96	0.30	80-501	1394	60	417	Yes—one spot	—	Laser indicates graphite bits.
08	9	10	RPG	1/2	1.96	0.30	80-501	1336	72	505	Yes—large leaks	—	Laser indicates graphite bits.
21	5	50	RPG	1/4	1.96	1.65	81-1	1322	80	No reading—est. 308	No	$3.2 \times 10^{-5}$	
22	6	50	RPG	1/4	1.96	1.65	81-1	1275	100	371	No	$3.2 \times 10^{-5}$	
23	7	50	Phenol.	1/4	1.96	1.65	81-501	1316	100	Bad reading est. 371	No	$7.1 \times 10^{-4}$	Laser indicates graphite bits; phenol cracked before shot.
24	10	50	Phenol.	1/4	1.96	1.65	81-501	1339	120	320	Yes		No failure evident by eye; gross leakage by bubbles through weld and around outside of end.

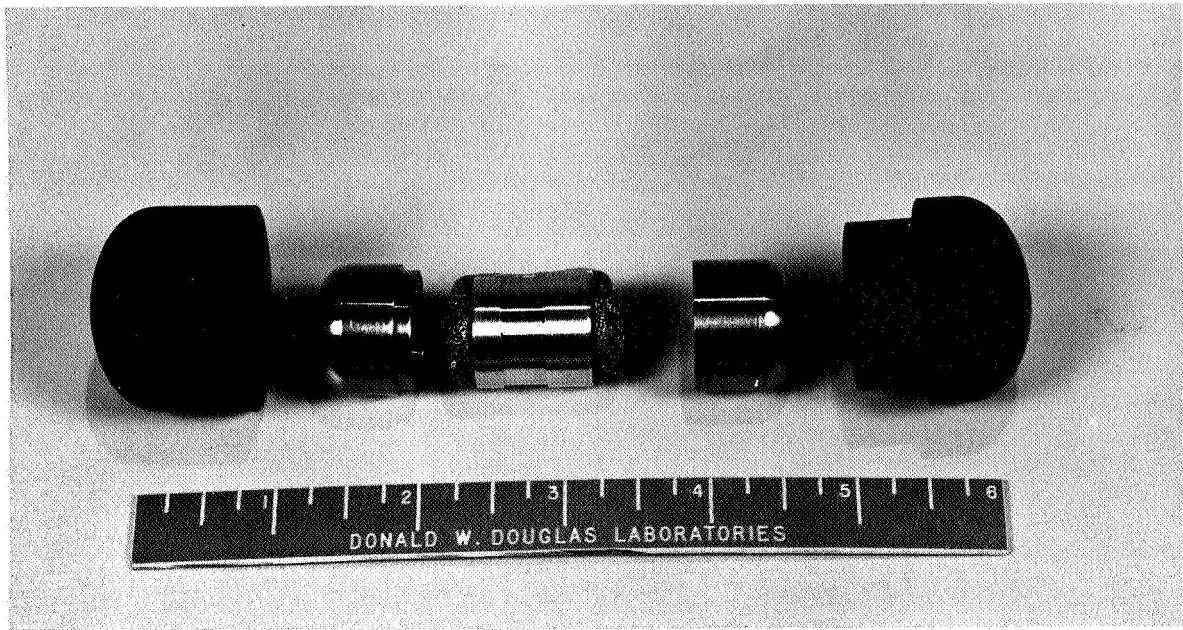


Figure E-1. 10 Watt Simulated Heater Impact Specimen before Assembly, Showing Graphite Insulator, T-III Shell, Ta Foam, and Bronze Fuel Simulant

68-2021

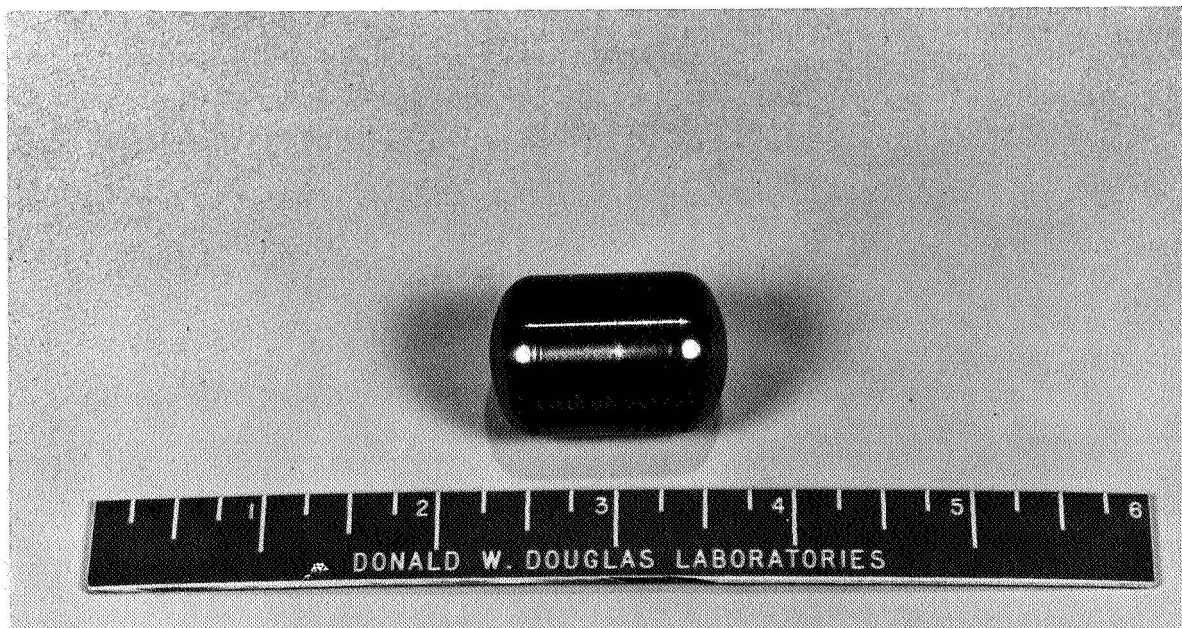


Figure E-2. Electron Beam Welded T-III 10 Watt Simulated Heater Impact Specimen

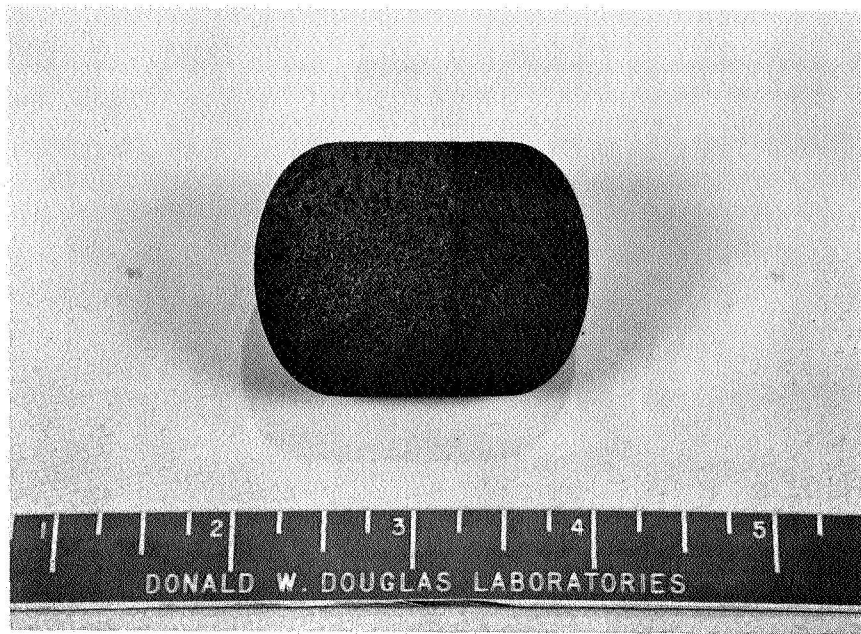


Figure E-3. Complete Graphite Bonded 10-Watt Simulated Heater Impact Specimen

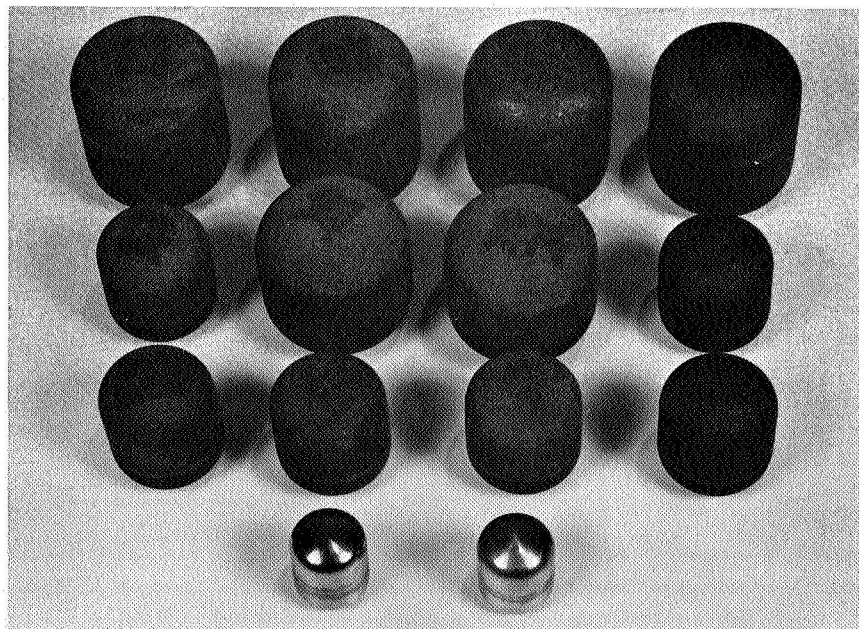


Figure E-4. 4-50 Watt and 10-10 Watt Simulated Heater Impact Specimens before Impact



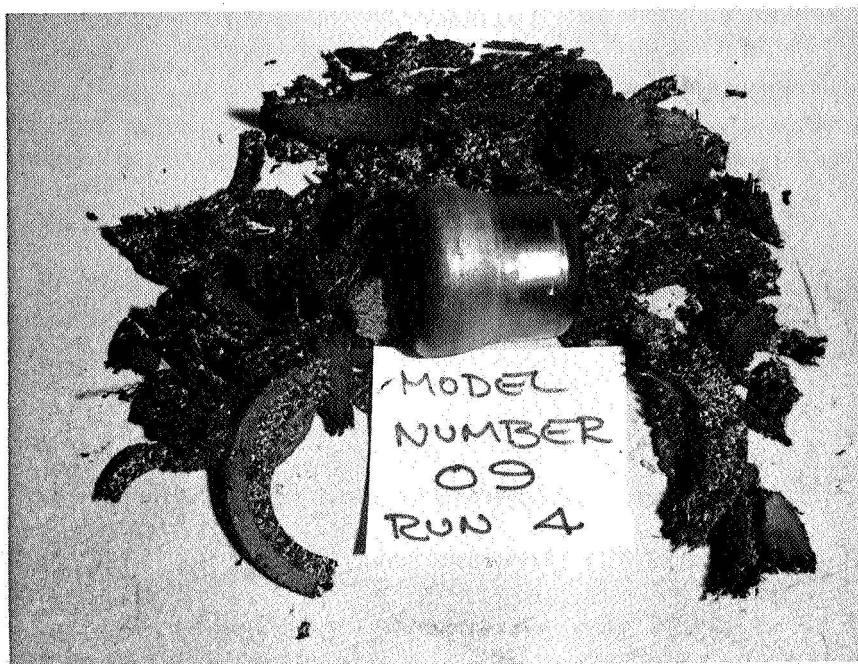


Figure E-5. Model 9 after 308 ft/sec Impact against Graphite



Figure E-6. Model 6 after 417 ft/sec Impact against Graphite

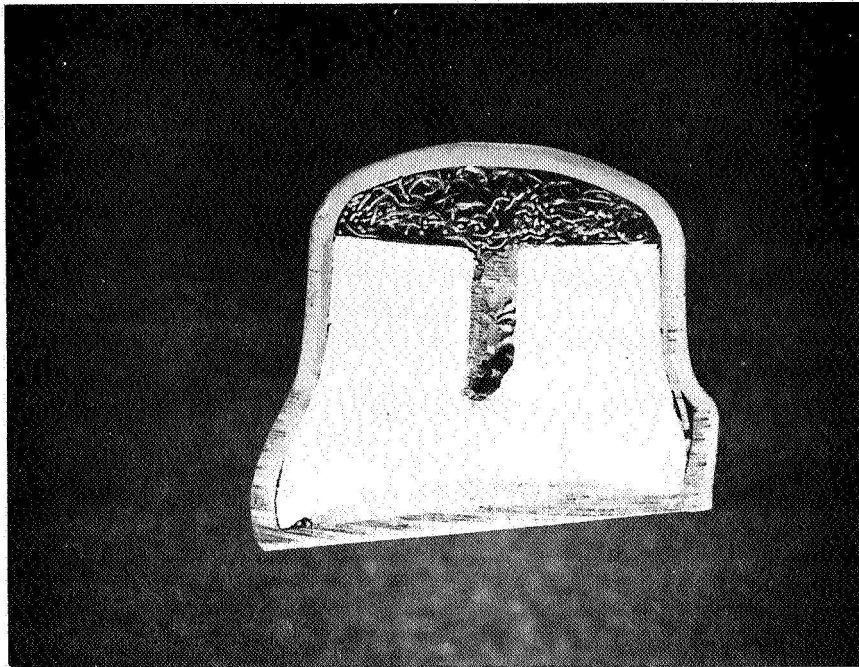


Figure E-7. Longitudinal Section of Model I after Successfully Withstanding 420 ft/sec Impact against Granite

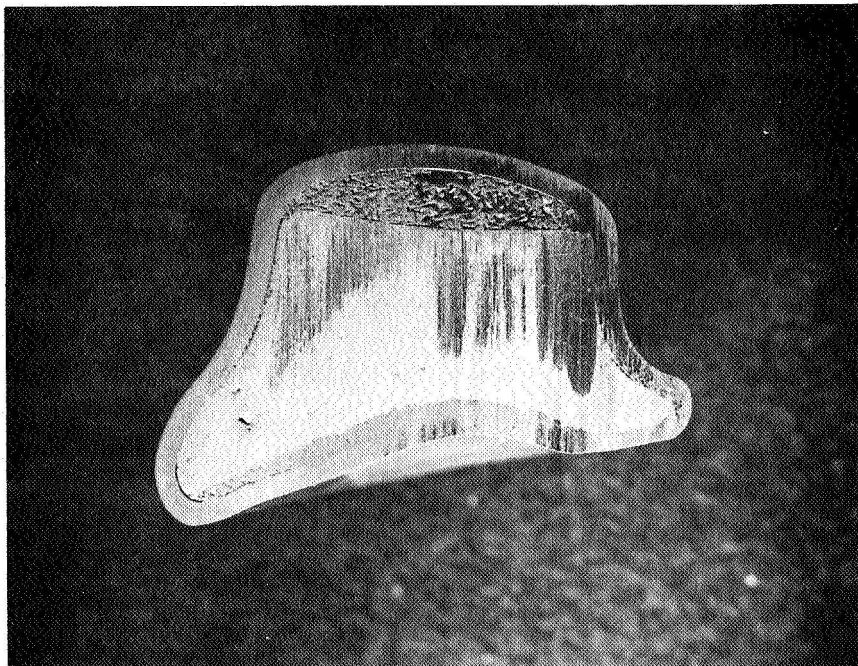


Figure E-8. Longitudinal Section of Model 8 after 505 ft/sec Impact against Granite (This Model Sustained Interfracture Cracks at the Corners of the Impacted End)

## Appendix F

### NEUTRON AND PHOTON SPECTRA

Neutron and photon spectra at 1 meter from reference 10- and 50-W Pm and Pu heaters are presented in Tables F-1 to F-4. These data may be used for system integration analysis such as evaluating radiation detector response and/or the effect of local shielding. These data yield the 1-meter dose ratio specified in the Safety and Design Analysis Section and may be normalized to dose rate and used to evaluate spectral distribution at any point in space. This assumes no spectral shape change with distance, an assumption consistent with accuracy requirements of most system integration analyses. Gamma spectra are based on ISOSHLD output (ref. 46). Neutron spectra are based on spectral data given in the "Plutonium Data Sheets" (ref. 45).

TABLE F-1  
PHOTON FLUX 1 METER FROM Pm<sup>147</sup> HEATER

Photon energy (keV)	<sup>147</sup> Pm - 10 W 60 mils T-111 Photon/cm <sup>2</sup> · sec	<sup>147</sup> Pm - 50 W 120 mils T-111 Photon/cm <sup>2</sup> · sec	Remarks
40 - 50	2.17 x 10 <sup>-2</sup>	5.08 x 10 <sup>-4</sup>	
50 - 70	1.00 x 10 <sup>2</sup>	6.71 x 10 <sup>-2</sup>	
70 - 100	8.40 x 10 <sup>1</sup>	2.97 x 10 <sup>-2</sup>	<sup>146</sup> Pm and <sup>147</sup> Pm bremsstrahlung
100 - 200	5.31 x 10 <sup>2</sup>	2.77 x 10 <sup>1</sup>	
200 - 300	8.40 x 10 <sup>-2</sup>	7.10 x 10 <sup>-2</sup>	
300 - 400	6.51 x 10 <sup>-2</sup>	9.37 x 10 <sup>-2</sup>	
400 - 550	1.00 x 10 <sup>-2</sup>	1.00 x 10 <sup>-2</sup>	
550 - 750	1.93 x 10 <sup>-3</sup>	5.61 x 10 <sup>-3</sup>	
121	7.30 x 10 <sup>2</sup>	3.79 x 10 <sup>1</sup>	<sup>147</sup> Pm gamma
450	5.36 x 10 <sup>2</sup>	1.25 x 10 <sup>3</sup>	<sup>146</sup> Pm gamma
750	7.89 x 10 <sup>2</sup>	2.56 x 10 <sup>3</sup>	<sup>146</sup> Pm gamma

TABLE F-2  
NEUTRON FLUX 1 METER FROM Pu<sup>238</sup> HEATER

Neutron energy (meV)	<sup>238</sup> Pu - 10 W 60 mils - T-111 Neutrons/cm <sup>2</sup> · sec	<sup>238</sup> Pu - 50 W 120 mils - T-111 Neutrons/cm <sup>2</sup> · sec	Remarks
0.4 - 0.7	0.505	2.525	Includes spontaneous fission and (α,η) sources; emission rate = 3 × 10 <sup>4</sup> n/sec · g <sup>238</sup> Pu
0.7 - 1.2	0.349	1.745	
1.2 - 1.8	0.349	1.745	
1.8 - 2.35	0.626	3.130	
2.35 - 2.65	0.747	3.735	
2.65 - 2.9	0.651	3.255	
2.9 - 3.25	0.524	2.620	
3.25 - 3.85	0.302	1.510	
3.85 - 4.6	0.117	0.585	
4.6 - 5.6	0.033	0.165	
5.6 - 6.8	0.016	0.080	
6.8 - 8.7	0.008	0.040	
8.7 - 11.0	0.003	0.015	

TABLE F-3  
PHOTON FLUX 1 METER FROM <sup>238</sup>Pu (NO AGING)  
HEATER

Photon energy (meV)	<sup>238</sup> Pu - 10 W 60 Mils - T-111 Photons/cm <sup>2</sup> · sec	<sup>238</sup> Pu - 50 W 120 Mils - T-111 Photons/cm <sup>2</sup> · sec	Remarks
0.090 - 0.75	2.65	3.46	Contributions from <sup>238</sup> Pu (and F, P.) <sup>239</sup> Pu, <sup>240</sup> Pu <sup>237</sup> U, <sup>236</sup> Pu <sup>241</sup> Pu
0.75 - 0.9	41.09	140.59	Predominantly 0.778 meV from <sup>238</sup> Pu
0.9 - 1.6	0.64	2.49	Predominantly fission products
1.6 - 2.6	0.37	1.52	Predominantly fission products
2.6 - 8.0	0.26	1.09	Predominantly fission products
<u>Pertinent isotopes</u>			
<sup>236</sup> Pu, <sup>237</sup> U, <sup>238</sup> Pu (including fission products), <sup>239</sup> Pu, <sup>240</sup> Pu, <sup>242</sup> Pu			

TABLE F-4  
PHOTON FLUX 1 METER FROM  $^{238}\text{Pu}$  (AGED 6  
YEARS) HEATER

Photon energy(meV)	$^{238}\text{Pu}$ - 10 W 60 mils - T-111 Photons/cm <sup>2</sup> · sec	$^{238}\text{Pu}$ - 50 W 120 mils - T-111 Photons/cm <sup>2</sup> · sec	Remarks
0.09 - 0.75	26.19	53.6	Contributions from all isotopes
0.75 - 0.9	43.5	139.3	Contributions from $^{238}\text{Pu}$ , $^{212}\text{Bi}$ , $^{208}\text{Tl}$
0.9 - 1.61	0.64	2.49	Fission products
1.62	1.01	3.98	$^{212}\text{Bi}$
1.63 - 2.6	0.37	1.51	Fission products
2.61	20.6	84.7	$^{208}\text{Tl}$
2.62 - 8.0	0.26	1.09	Fission products
<u>Pertinent isotopes</u>			
$^{208}\text{Tl}$ , $^{212}\text{Pb}$ , $^{212}\text{Bi}$ , $^{220}\text{Ru}$ , $^{224}\text{Ra}$ , $^{228}\text{Th}$ , $^{232}\text{U}$ , $^{241}\text{Am}$ , $^{237}\text{U}$ , $^{237}\text{N}$ , $^{238}\text{Pu}$ , (including fission products), $^{239}\text{Pu}$ , $^{240}\text{Pu}$ , $^{241}\text{Pu}$ , $^{242}\text{Pu}$			



## Appendix G

### STATISTICAL PROCEDURE

Consider a particular failure mode for a given radioisotope capsule design. Ablator failure during reentry, melting, or stress rupture of structural components are typical examples. The calculated point of failure,  $Q_F$ , is a function of  $n$  input parameters or assumptions,  $a_1, a_2, \dots, a_n$ . In equation form,

$$Q_F = f(a_1, a_2, \dots, a_n) \quad (G-1)$$

For each parameter,  $a_i$ , a standard deviation,  $\sigma_i$ , may be defined with the following characteristics: Assuming a normal frequency (probability density) distribution about a mean or most probable value,  $\bar{a}_i$ , 68.27% of all measurements or calculations of  $a_i$  lie within the range,  $\bar{a}_i \pm \sigma_i$ . Similarly, 95.45% of all measurements or calculations of  $a_i$  lie within the range,  $\bar{a}_i \pm 2\sigma_i$ , and so on (ref. 97, pp. 71-72). The standard deviation is always expressed in the same units of measurements as those of the variable,  $a_i$ .

If we can arrive at a standard or best set of parameter values,  $\bar{a}_1, \bar{a}_2, \dots, \bar{a}_n$ , then the mean or most probable value of  $Q_F$  is

$$\bar{Q}_F = f(\bar{a}_1, \bar{a}_2, \dots, \bar{a}_n) \quad (G-2)$$

A deviation in each parameter from the standard value will then cause a corresponding deviation in  $Q_F$  from the mean. If a standard deviation,  $\sigma_i$ , can be assigned to each parameter,  $a_i$ , then the range of deviation in  $Q_F$ ,  $(\Delta Q_F)_i$ , due to the variation of  $a_i$  within the range,  $\bar{a}_i \pm \sigma_i$ , can be determined by varying each parameter singly. Often, this may be done simply by substituting the maximum and minimum values of the parameter,  $a_i$ ,

$$\begin{aligned} (\Delta Q_F)_i &= f(\bar{a}_1, \bar{a}_2, \dots, \bar{a}_i + \sigma_i, \dots, \bar{a}_n) \\ &\quad - f(\bar{a}_1, \bar{a}_2, \dots, \bar{a}_i - \sigma_i, \dots, \bar{a}_n) \end{aligned} \quad (G-3)$$

Proceeding in this manner for each parameter, the overall standard deviation for  $Q_F$ , namely,  $\sigma_F$ , can be calculated by the law of propagation of errors (ref. 98),

$$\sigma_F = 1/2 \sqrt{(\Delta Q_F)_1^2 + (\Delta Q_F)_2^2 + \dots + (\Delta Q_F)_n^2} \quad (G-4)$$

Assuming normal frequency distributions for each parameter, it follows that the distribution of  $Q_F$  will be normal with the mean value,  $\bar{Q}_F$ , and standard deviation,  $\sigma_F$ .

The strict mathematical derivation is somewhat more restrictive. Assuming that  $f(a_1, a_2, \dots, a_n)$  can be expanded in a Taylor's series, and neglecting products of errors in comparison with the errors themselves,

$$dQ_F = \frac{\partial f}{\partial a_1} da_1 + \frac{\partial f}{\partial a_2} da_2 + \dots + \frac{\partial f}{\partial a_n} da_n \quad (G-5)$$

which is also the expression for the total derivative. For small increments about the mean reference case,  $\Delta Q_F = \bar{Q}_F - Q_F$  and  $a_i = \bar{a}_i - a_i$ , equation (G-5) may be written

$$\Delta Q_F = \frac{\partial f}{\partial a_1} \Delta a_1 + \frac{\partial f}{\partial a_2} \Delta a_2 + \dots + \frac{\partial f}{\partial a_n} \Delta a_n \quad (G-6)$$

Defining  $A_i = \partial a_i$ ,  $A_i$  is called the influence coefficient of the parameter,  $a_i$ . If  $A_i$  can be considered constant in the interval,  $\sigma_i = \Delta a_i$ , the general law for propagation of errors yields

$$\sigma_F = \sqrt{A_1^2 \sigma_1^2 + A_2^2 \sigma_2^2 + \dots + A_n^2 \sigma_n^2}, \quad (G-7)$$

which corresponds to equation (G-4) if  $f$  is linear with the  $a_i$  axis in the interval,  $\Delta a_i$ , for  $i = 1, 2, \dots, n$ .

Although not treated in the textbooks, there is no reason a priori why equation (G-4) cannot be applied to cases where  $f$  is not linear as specified. The basic principles are the same. Statistical analyses have been conducted in which  $f$  was not linear with every parameter axis (ref. 99). The procedure was to find the functional relationship of  $f$  by appropriate variance of the input parameter,  $a_i$ , and so determine the maximum deviation in  $f$  within the range,  $\bar{a}_i - \sigma_i$  to  $\bar{a}_i + \sigma_i$ . This yielded values of  $(\Delta Q_F)_i$  to use in equation (G-4).

The influence coefficients,  $A_i$ , are important since they identify which parameters have the strongest effect on  $Q_F$ . On the other hand, if an influential parameter is also known accurately, its standard deviation is small and the corresponding deviation or uncertainty in  $Q_F$  may be small. Thus,  $(\Delta Q_F)_i$  is the significant quantity denoting each parameter's total influence on  $\sigma_F$ . Reduction in standard deviation for those parameters ranked highest in values of  $(\Delta Q_F)_i$  effects the most efficient reduction in the uncertainty level for  $Q_F$ .

Thus far, the discussion has focused on the point of failure. The major objective of evaluation of the safety of a capsule design in specific hazardous environments also involves analytical modeling of the capsule behavior and, possibly, the environment. In general, the model yields a worst (from the



standpoint of failure) analytical value,  $Q_A$ . This quantity, in turn, is a function of  $m$  input parameters or assumptions. The difference between the two quantities,  $Q_F$  and  $Q_A$ , may be defined as the margin or excess,

$$Q_E = Q_F - Q_A \quad (G-8)$$

In order that failure not occur,  $Q_E$  must be greater than zero. Further, the probability that failure will not occur is equal to the probability that  $Q_E$  is greater than zero (written  $P(Q_E > 0)$ ).

Since there exist uncertainties in the values of the parameters involved in the calculation of  $Q_A$ , as well as in  $Q_F$ , it follows that corresponding uncertainties exist in  $Q_E$ . These uncertainties, along with  $\bar{Q}_E$ , are involved in the calculation of  $P(Q_E > 0)$ . See Figure G-1.

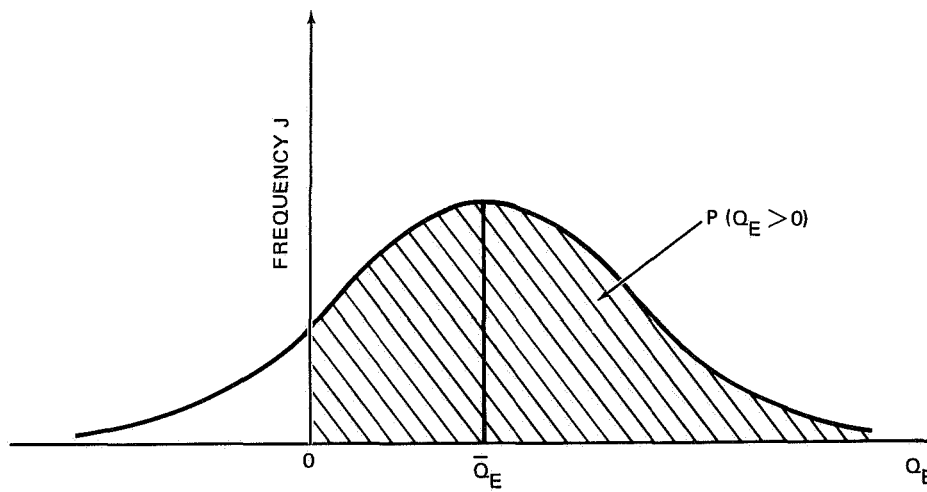


Figure G-1. Normal Frequency Distribution for  $Q_E$

The equation expressing the frequency as a function of  $Q_E$  is, for a normal distribution (ref. 100),

$$v = \frac{1}{\sigma_E \sqrt{2\pi}} \times \exp \left[ \frac{-(Q_E - \bar{Q}_E)^2}{2 \sigma_E^2} \right] \quad (G-9)$$

Thus

$$P(\text{nonfailure}) = \int_{Q_E=0}^{\infty} \frac{1}{\sigma_E \sqrt{2\pi}} \exp \left[ \frac{-(Q_E - \bar{Q}_E)^2}{2 \sigma_E^2} \right] d Q_E \quad (G-10)$$

To facilitate the evaluation of this integral, it is useful to make the abscissa transformation

$$\xi = \frac{Q_E - \bar{Q}_E}{\sigma_E} \quad (G-11)$$

From this definition, it follows that

$$d\xi = \frac{1}{\sigma_E} \times dQ_E \text{ or } dQ_E = \sigma_E d\xi \quad (G-12)$$

Also,

$$\xi = - \frac{\bar{Q}_E}{\sigma_E} \quad \text{for } Q_E = 0 \quad (G-13)$$

Equation (G-10) may then be written

$$P(\text{nonfailure}) = \frac{1}{\sigma_E \sqrt{2\pi}} \int_{\xi = -\frac{\bar{Q}_E}{\sigma_E}}^{\infty} \exp\left(-\frac{\xi^2}{2}\right) \sigma_E d\xi \quad (G-14)$$

By reason of symmetry, the integration limits may be reversed and the signs changed without invalidating the equality. Thus,

$$P(\text{nonfailure}) = \frac{1}{\sqrt{2\pi}} \int_{-\infty}^{\xi = \frac{Q_E}{\sigma_E}} \exp\left(-\frac{\xi^2}{2}\right) d\xi \quad (G-15)$$

The expression on the right hand side of equation (G-15) has the form of the cumulative normal distribution integral which may be evaluated using standard probability tables (probability vs  $\bar{Q}_E / \sigma_E$ ). Such tables may be found in reference 101, p. 229. For a greater number of decimal places and for more extended tabular values, the Tables of Normal Probability Functions (ref. 102) may be used. In this reference, the tables are appropriate for

$$\frac{1}{\sqrt{2\pi}} \int_{-x}^x \exp\left(-\frac{\xi^2}{2}\right) d\xi$$

instead of for the integral above. However, the desired values may be obtained from these tables by noting that

$$1 - \int_{-x}^x = 2 \int_{-\infty}^x \quad (G-16)$$

or

$$\int_{-\infty}^x = -1/2 \int_{-x}^x + 1/2 \quad (G-17)$$

The statistical procedure just outlined yields a quantitative probability of nonfailure for each failure mode of a given radioisotope capsule design. Assuming that each failure mode is independent of the others, the overall probability of nonfailure is simply the product of all nonfailure probabilities,

$$P_{\text{tot}} = P_1 P_2 P_3 \dots P_k, \quad (G-18)$$

where

$P_{\text{tot}}$  is the probability of overall nonfailure,  
 $P_i$  is the nonfailure probability for failure mode  $i$  ( $1 \leq i \leq k$ )  
 $k$  is the total number of failure modes.

Equation (G-18) follows from the probability multiplication rule for sequential (independent) events. However, many radioisotope failure modes are not mutually independent. Consider that the probability of nonfailure on earth impact is affected by ablator failure or nonfailure. Also, parameters which affect one failure mode often affect another. If these cross-influence effects can be incorporated in calculation of the individual failure mode probabilities, then equation (G-18) can be used as before to compute the overall probability of nonfailure. Quite often, the product of probabilities of dependent events is greater than for independent events. Assumption of independent failure modes is therefore usually conservative and acceptable for a first cut, if appropriately qualified.

When quoting probabilities of nonfailure, it is important to note that a probability of 99.9%, for example, does not mean that one capsule out of one thousand will fail. Rather, it is a measure of the reliability or confidence limit on the results. The procedure is sufficient to distinguish between probabilities as high as six or seven 9's (ref. 99). An ideally safe design has a reliability on the order of 99.999% or better. For comparison, the average component reliability of the recent Apollo 8 mission was about 99.9999%.

In many applications, it is often desirable to use the probabilistic treatment to optimize a mission or system condition or parameter, or to find the value of minimum or maximum safety. For example, by taking selected mission reentry angles, the overall probability of nonfailure can be determined as a function of reentry angle. From this, conditions of minimum and maximum safety are pinpointed. This could lead to provisions for avoiding minimum safety conditions.



## Appendix H

### SMALL PARTICLE FALLOUT

Two kinds of fallout are usually considered in safety assessments: local and worldwide. More accurately, large particles and small particles are considered separately because the fallout processes are quite different in the two cases. Large particles are brought to earth primarily by gravitational forces (ref. 103). Small particle fallout is dominated by dynamic atmospheric processes (ref. 104,105). In many instances, attention is restricted to the smaller particles because the nuclides of interest are relatively innocuous unless taken into the body. Particles large enough to fall out quickly due to gravitational forces are above the respirable range.

Radiation doses which may result from small particle fallout are determined by the magnitude and duration of ground-level airborne concentrations, the quantity of activity deposited on the earth's surface, and the deposition rate (ref. 106).

Fallout predictions have been based on a simple three-region stirred reservoir model of the atmosphere (ref. 107). A "mean residence time" for each region (mesosphere, stratosphere, and troposphere) is chosen on the basis of available data, and reasonable values are calculated for ground level activity concentrations in air, deposition rates, and total activity deposited.

Current fallout predictions such as those made by the U. S. Weather Bureau for the SNAP 9A incident and by the Federal Radiation Council for past weapons tests (ref. 108) are much more accurate than the simple stirred reservoir model would permit. A vast quantity of fallout data has been accumulated and compiled to facilitate predictions (ref. 109). It has been possible to establish the importance of many factors and to express this importance quantitatively in many instances.

In the Machta model (ref. 110), the atmosphere is viewed as consisting of the several regions. Materials move very rapidly from the "lower polar stratosphere" to the troposphere where it can affect people. A release to this region results in maximum concentrations and minimum decay time. Releases to the "upper polar stratosphere" reach the troposphere a little more slowly and produce slightly lower concentrations.

Relative deposition rates are presented in figure H-1. This shows the concentrations reaching peaks in the spring and illustrates the importance of seasonal variation. The importance of the release location is also evident.

The area under each of the curves in figure H-1 represents 1 year. Taking the mean residence time of particulate matter in the troposphere as 1 month gives the peak deposition rate as 0.133/month (from a lower polar

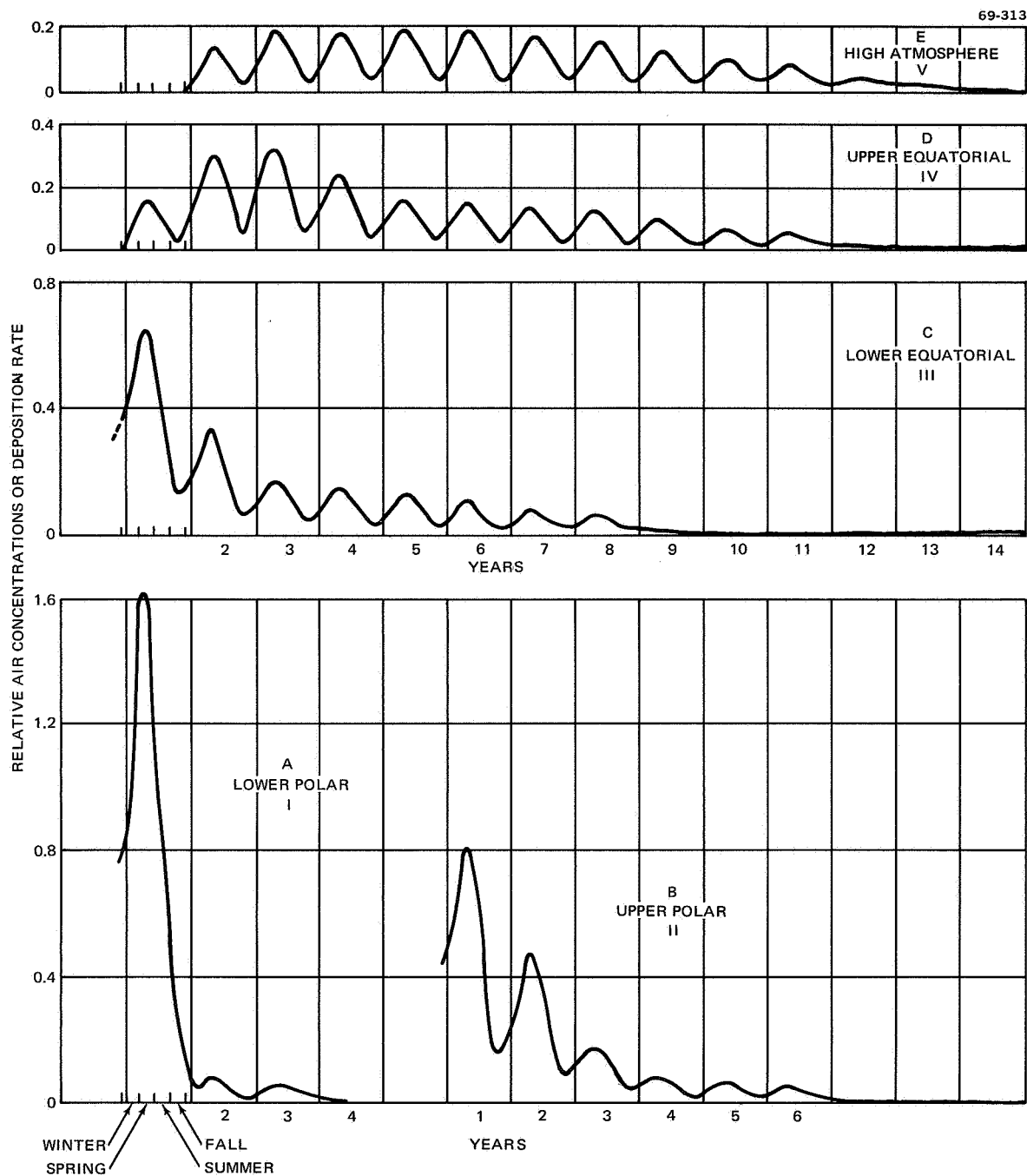


Figure H-1. Deposition Rate Vs Time

stratosphere release). It follows that the peak troposphere inventory is 0.133 of the total release. The mass of the atmosphere (essentially all in the troposphere) is

$$10\,332 \text{ (kg/m}^2\text{)} \times 5.101 \times 10^4 \text{ (m}^2\text{)} = 5.28 \times 10^{18} \text{ (kg)} \quad (\text{H-1})$$

Taking the air density as  $1.3 \text{ (kg/m}^3\text{)}$  gives an effective volume of

$$5.28 \times 10^{18} \text{ (kg)} / 1.3 \text{ (kg/m}^3\text{)} = 4.06 \times 10^{18} \text{ (m}^3\text{)} \quad (\text{H-2})$$

Thus, the release of 1 Ci to the lower polar stratosphere would result in a peak concentration, averaged over the entire earth, of

$$0.133 \text{ (Ci)} / 4.06 \times 10^{18} \text{ (m}^3\text{)} = 3.3 \times 10^{-20} \text{ (Ci/m}^3\text{)} \quad (\text{H-3})$$

Radioactive material would not be uniformly distributed; it would be confined largely to one hemisphere. Further, most of the activity would be in the band between  $30^\circ$  and  $90^\circ$ . The actual peak concentration would be higher than the world average concentration by a factor of 3.

The release of 1 Ci to the lower polar stratosphere would result in a peak concentration of  $10^{-19} \text{ (Ci/m}^3\text{)}$ . Similarly, a 1-Ci release to the mesosphere produces a peak tropospheric concentration of  $5.5 \times 10^{-21} \text{ (Ci/m}^3\text{)}$ . This peak occurs in both hemispheres. The variation with time is illustrated in figure H-2 for the lower polar stratosphere.

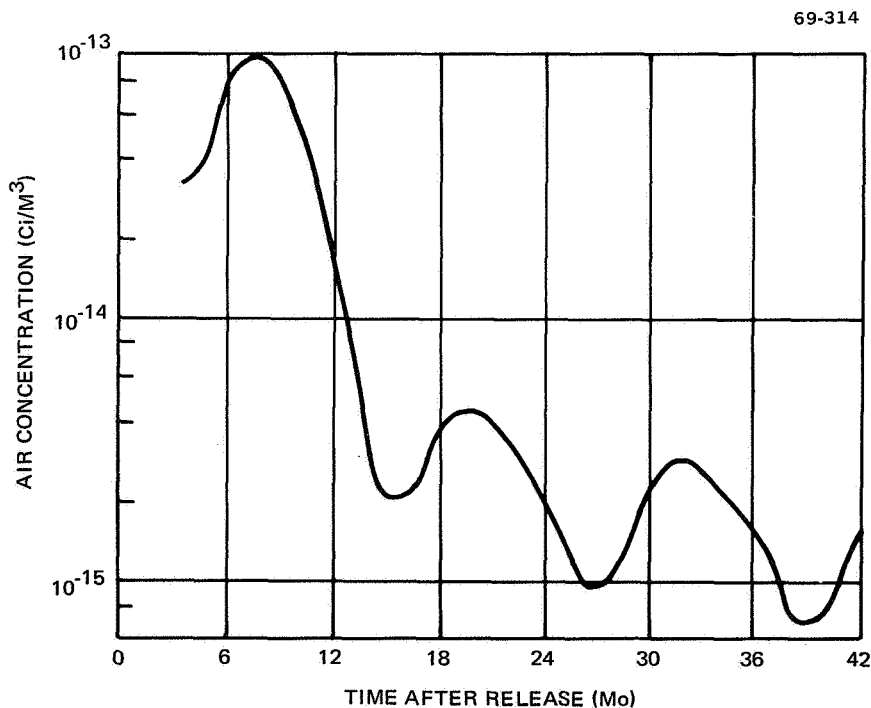


Figure H-2. Tropospheric Air Concentration from a Megacurie Release to the Lower Polar Stratosphere  
(No radiological delay)





## Appendix I

### GROUND RELEASE ANALYSIS

There is uncertainty associated with the volatilization of solids in the atmosphere, but an empirical modification of the classic Langmuir equation can give reasonable estimates. The evaporation rate ( $\text{gm cm}^{-2} \text{ sec}^{-1}$ ) is

$$R = 44.5 P \sqrt{M/T} \quad (\text{I-1})$$

where P is the vapor pressure in atmospheres, M the molecular weight, and T the temperature in °F. For Pu at 1275°F,

$$\begin{aligned} R &= 44.5 \times 10^{-16} \sqrt{238/1275} \\ &= 2 \times 10^{-15} (\text{gm cm}^{-2} \text{ sec}^{-1}) \end{aligned} \quad (\text{I-2})$$

Vapor pressure data is given in figure I-1.

If the fuel is in the form of 100- $\mu$ -radius particles, at 3.5 W/cc the fuel volume must be 14.3 cc and the surface area about 4300  $\text{cm}^2$ . Thus, the release rate would be about  $8.6 \times 10^{-12}$  (gm/sec) which is  $1.45 \times 10^{-10}$  (Ci/sec) or  $5.25 \times 10^{-7}$  (Ci/hr).

Formal techniques for estimating atmospheric dispersion and inhalation doses are available. The Pasquill dispersion model (refs. 111, 112, 113) for a point release gives the concentration in the plume for the continuous release of Q (Ci/sec) as

$$X = \frac{Q}{\pi \sigma_y \sigma_z u} \exp \left[ -\frac{Y^2}{2 \sigma_y^2} - \frac{Z^2}{2 \sigma_z^2} \right] \quad (\text{I-3})$$

where  $\sigma_y$  and  $\sigma_z$  are standard deviations in the crosswind and vertical directions, respectively, u is windspeed (m/sec), and Y and Z are crosswind and vertical distances from the plume centerline (m). Actually, since the concentration has been doubled for ground reflection, only one value of Z is permissible: the effective release height. Standard deviations vary with downwind distance and are described by the empirical relationships (refs. 111 through 113).

The quantity inhaled per unit time is the concentration multiplied by the breathing rate which is about  $3.5 \times 10^{-4} \text{ m}^3/\text{sec}$  for the standard man (ref. 114).

$$q = 3.5 X t \times 10^{-4} \dots (\text{Ci}) \quad (\text{I-4})$$

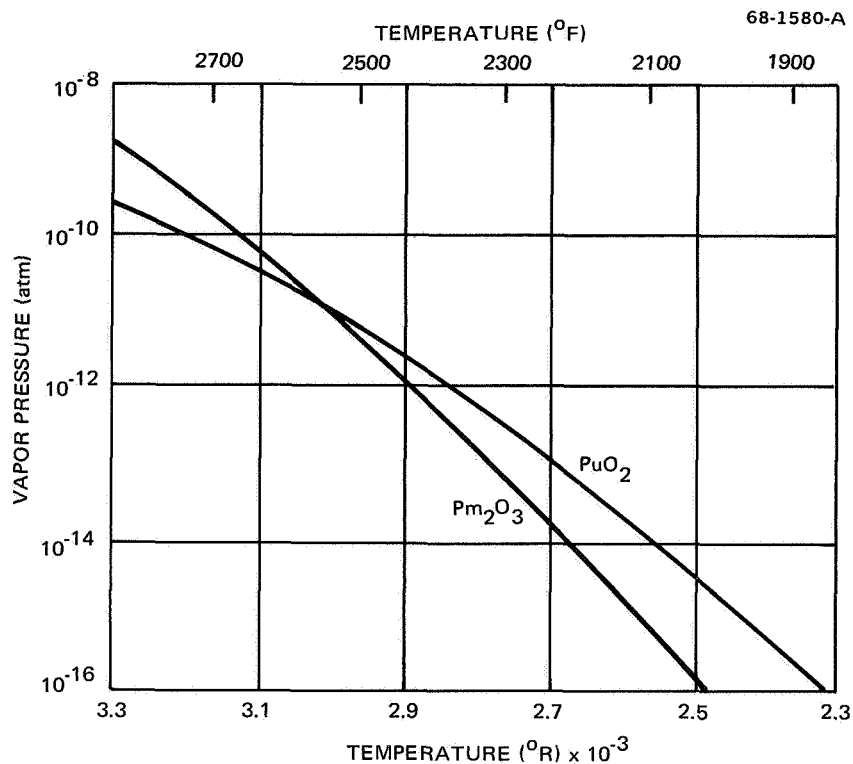


Figure I-1. Isotope Fuel Vapor Pressures

The dose is directly proportional to the quantity inhaled;  $^{238}\text{Pu}$  gives  $2 \times 10^8$  (rem/Ci) and  $^{147}\text{Pm}$  gives  $7 \times 10^4$  (rem/Ci).

Maximum doses occur from a ground level point release. Dose is directly proportional to the quantity released and inversely proportional to the wind-speed. For total release ( $Q_t$ ) of  $1.43 \times 10^{-5}$  Ci of  $^{238}\text{Pu}$ , the dose is  $D = X/Q$ . The dose is the same for total release of 0.041 Ci of  $^{147}\text{Pm}$ . Doses received at locations directly downwind from ground level point releases of these magnitudes is given in figure I-2 for 1 m/sec windspeeds.

Figure 39 assumes no vertical rise of the released radioisotope with the fireball. This most likely will occur and will reduce the maximum possible dose and hazardous distance. For elevated release, Type A weather conditions allow the most isotope to reach ground levels; consequently, this yields the highest possible dose. A "virtual point source distance" is used to account for the initial cloud volume. In this case, the virtual source distance is 700 meters. The maximum dose which occurs is 180 rem, 300 meters downwind. The dose is less than the reactor siting dose guide of 75 rem at distances of 800 meters or more downwind, as illustrated in figure I-3.

Therefore, doses from a 100% release (especially of  $^{238}\text{Pu}$ ) to a launch abort fireball are high enough to justify control measures, but they are not of catastrophic proportions.

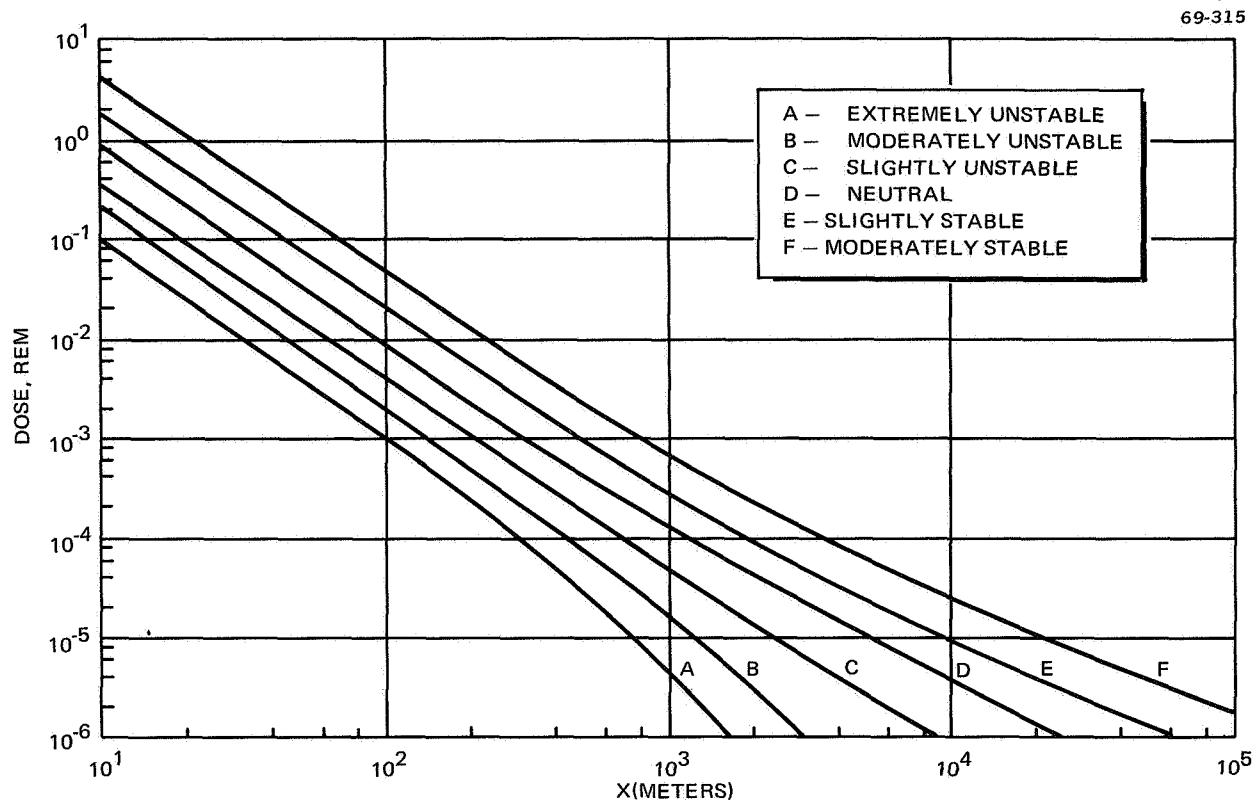


Figure I-2. Lung Dose from the Release of  $1.43 \times 10^{-5}$  Ci  $^{238}\text{Pu}$  or 0.014 Ci  $^{147}\text{Pm}$   
Under Various Meteorological Conditions with a 1 m/sec Windspeed

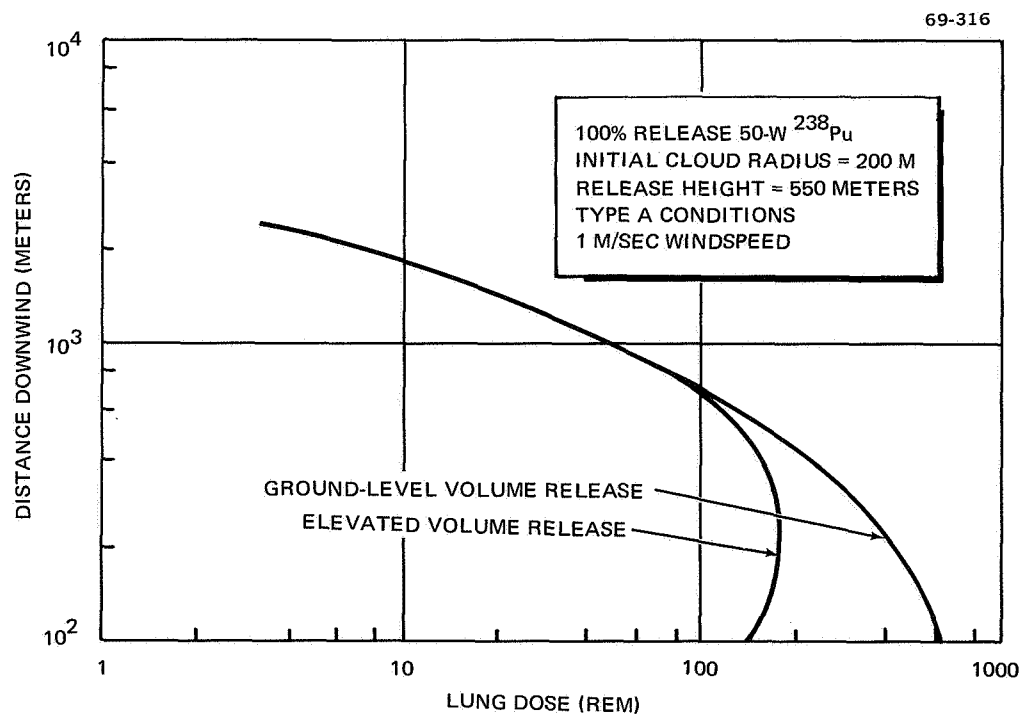


Figure I-3. Maximum Dose from Elevated Volume Release



## Appendix J

### CALCULATION OF MAXIMUM PERMISSIBLE CONCENTRATIONS AND ISOTOPE DISPERSION IN SEAWATER

The International Commission on Radiological Protection (ICRP) has calculated MPC\* and MPBB\*\* values considering various organs as critical (refs. 115 and 116). The ICRP work is the basis for the National Academy of Sciences MPC<sub>s</sub> recommendations (refs. 117 and 118). The MPC problem has been considered in some detail by various investigators (refs. 119 through 125 ). The purpose here is to briefly summarize the basis and give the values for radioisotopes <sup>147</sup>Pm and <sup>238</sup>Pu.

The ICRP has calculated MPC<sub>w</sub> values based on irradiation of the GI tract. Assuming that all protein in the diet of those exposed consists of sea-food which has fully concentrated the radionuclide, the maximum permissible concentration for seawater is

$$\text{MPC}_s = \text{MPC}_w \frac{\left( \begin{array}{c} \text{volume of} \\ \text{water} \\ \text{consumed} \end{array} \right)}{\left( \begin{array}{c} \text{volume of} \\ \text{protein} \\ \text{consumed} \end{array} \right) \left( \begin{array}{c} \text{concentration} \\ \text{factor} \end{array} \right)}$$

or  $\text{MPC}_s = \text{MPC}_w \frac{V_w}{V_P F}$  (J-1)

The standard man consumes approximately 10 times more water than protein; therefore,

$$\frac{V_w}{V_P} = 10$$

$$\text{MPC}_s = \frac{10}{F} \text{MPC}_w \dots \text{GI tract limited} \quad \text{(J-2)}$$

\* Maximum permissible concentration; subscripts a, w, and s denote air, drinking water, and sea water, respectively.

\*\* Maximum permissible body burden.

For the radioisotopes of interest, the concentration factor, F, is 20 for Sr-90; 50 for Cs-137;  $10^3$  for Ce-144, Pm-147, Pu-238 and Cm-244; and  $10^4$  for Co-60 and Po-210 (ref. 118). Therefore, the maximum permissible concentration in seawater is much lower than the drinking water limit.

For nuclides where organs other than the GI tract are limiting, neither the  $MPC_w$  nor the seafood concentration factor is used directly. Rather, the radionuclide is assumed to be chemically affiliated with a carrier material so the activity per unit mass of carrier is invariant. If some quantity ( $I$ ) of carrier is taken into the body each day, a fraction ( $f_w$ ) is deposited in the organ of interest; the quantity of carrier material ( $I_b$ ) in the organ varies as

$$\frac{dI_b}{dt} = I f_w - \lambda_b I_b \quad (J-3)$$

where  $\lambda_b$  is the biological elimination (decay) constant. If each gram of carrier is associated with R ( $\mu Ci$ ) of the activity of interest, activity in the organ ( $q'$ ) varies as

$$\frac{dq'}{dt} = I f_w R - \lambda_b q' - \lambda_R q' \quad (J-4)$$

The effective decay constant ( $\lambda_e$ ) is the sum of biological ( $\lambda_b$ ) and radiological ( $\lambda_R$ ) decay constants,

$$\frac{dq'}{dt} = I f_w R - \lambda_e q' \quad (J-5)$$

at equilibrium

$$\frac{dI_b}{dt} = \frac{dq'}{dt} = 0 \quad (J-6)$$

$$I f_w - \lambda_b I_b = I f_w - \lambda_e q' / R \quad (J-7)$$

$$\frac{q'}{I_b} = \frac{\lambda_b}{\lambda_e} R \left( \frac{\mu Ci}{gm} \right) \quad (J-8)$$

$$R = \frac{q'}{I_b} \frac{\lambda_e}{\lambda_b} \dots \left( \frac{\mu Ci}{gm} \right) \quad (J-9)$$

The quantity, R, is the activity ( $\mu Ci$ )-per-gram carrier. Therefore, if  $q'$  is the maximum permissible organ burden,

$$q' = (MPBB) f_2 \quad (J-10)$$

where  $f_2$  is the fraction of the body burden in the organ, the activity concentration in sea water is the  $MPC_s$ .

$$R = \frac{MPC_s}{I_e} = \frac{q'}{I_b} \frac{\lambda_e}{\lambda_b} = \frac{q'}{I_b} \frac{T_B}{T_e} \quad (J-11)$$

The biological and effective half-lives are  $T_B$  and  $T_e$  respectively; thus

$$MPC_s = q' \frac{I_e}{I_b} \frac{T_B}{T_e} \dots \text{GI tract not limiting} \quad (J-12)$$

$$\left( \begin{array}{c} \text{Ocean} \\ \text{maximum} \\ \text{permissible} \\ \text{concentration} \end{array} \right) = \left( \begin{array}{c} \text{Maximum} \\ \text{permissible} \\ \text{organ} \\ \text{burden} \end{array} \right) \frac{\left( \begin{array}{c} \text{Carrier} \\ \text{concentration} \\ \text{in ocean} \end{array} \right) \left( \begin{array}{c} \text{Biological} \\ \text{half-life} \end{array} \right)}{\left( \begin{array}{c} \text{Quantity of} \\ \text{carrier in} \\ \text{organ} \end{array} \right) \left( \begin{array}{c} \text{Effective} \\ \text{half-life} \end{array} \right)}$$

This calculation also yields  $MPC_s$  values which are generally much smaller than the corresponding  $MPC_w$  values. The two  $MPC_s$  formulas yield values which roughly correspond to the  $MPC_w$  and  $MPC_a$  values in that continuous exposure could produce maximum permissible body burdens or maximum permissible GI tract doses. The  $MPC_s$  values are more conservative than the more familiar limits because biological concentration is considered in terms of the sea water limit. Plants and animals that live in fresh water and/or on land are capable of concentration of radionuclides, but such phenomena are not reflected in the  $MPC_a$  and  $MPC_w$  values.

Despite the relative conservatism of the derived  $MPC_s$  values, certain modifying or adjustment factors are suggested which further reduce these limits. One such adjustment (s) is merely a correction for the use of inappropriate  $q'$  or  $MPC_s$  values. The  $q'$  and  $MPC_w$  values given directly by the ICRP are for occupationally exposed people. For exposure of small groups of people who are not radiation workers, limits are reduced by a factor of 10 ( $s = 1/10$ ). For the irradiation of populations, it was recommended that the limits be reduced by a factor of 30 or 100 ( $s = 1/30$  or  $s = 1/100$ ). The factor of 100 applies only to the  $q'$  and  $MPC_w$  values obtained using the gonads or whole body as the critical organ. More recent ICRP recommendations (ref. 126) do not include this factor for exposure of populations but call for identification of a most sensitive group, which is appreciably more difficult. Thus, for present purposes, it may be of value to include the "populations" values based on the older recommendations.

In addition to using the correct base values, some dose apportionment has been suggested. First, it is suggested that only some fraction ( $N_d$ ) of the permissible dose should come from the sea water contamination;  $N_d$  values of 1/3 and 1/2 have been used. Second, only a fraction ( $N_s$ ) of the total ocean contamination should come from a particular source. The National Research

Council suggested an  $N_s$  value of 1/3 for nuclear ships, and a value of 0.1 has been suggested for nuclear space power units. A "correction" factor tending to increase  $MPC_s$  values has been proposed to account for the fact that it is very rare for all the protein in a diet to come from the sea. Protein fraction factors ( $1/N_p$ ) of 2 and 3 have been suggested, but a value of 1 was used by the NRC and others. The more conservative "adjustment" factors give

$$N_d N_s / N_p = 1/30 \quad (J-13)$$

Thus, the adjusted  $MPC_s$  values are

$$^aMPC_s = MPC_w / 3F_3 \dots \text{GI tract limiting} \quad (J-14)$$

and

$$^aMPC_s = q' I_e T_B / 30 I_b T_e \dots \text{GI tract not limiting.} \quad (J-15)$$

The  $MPC_s$  values calculated in this manner are so different in radiological significance from the  $MPC_a$  and  $MPC_w$  values that they probably merit a different name.  $MPC_s$  values for Pm and Pu are given in table J-1.

TABLE J-1  
ADJUSTED MAXIMUM PERMISSIBLE CONCENTRATIONS  
IN SEA WATER ( $\text{Ci}/\text{m}^3$ ) \*

Radio-isotope	Critical organ - $MPC_s$ - Bone			GI tract - $MPC_s$		
	Continuous occupational	Small group	Populations	Continuous occupational	Small group	Populations
$^{147}\text{Pm}$	$2 \times 10^{-6}$	$2 \times 10^{-7}$	$7 \times 10^{-8}$	$7 \times 10^{-7}$	$7 \times 10^{-8}$	$2 \times 10^{-8}$
$^{238}\text{Pu}$	$2 \times 10^{-9}$	$2 \times 10^{-10}$	$7 \times 10^{-11}$	$10^{-7}$	$10^{-8}$	$3 \times 10^{-9}$
*Unadjusted values are a factor of 30 higher						

Returning to the subject of water dispersal, sea water is not quiescent; radioactivity released in a small volume will soon be dispersed through a much larger volume. Where there is no current, and dispersion is isotropic, the concentration at R meters from the release point is

$$X = \frac{Q}{(2\pi)^{3/2} \sigma^3} \exp \left\{ -\frac{R^2}{2\sigma^2} \right\} \quad (J-16)$$



One measure of the hazard is obtained by comparing the concentration to a maximum permissible values calculated in table J-1. Any dose estimate would be more nearly proportional to the integrated time-concentration product

$$TID = \int_0^{\infty} X dt \quad (J-17)$$

If a depth constraint (D) is assumed in the vertical, the integrated concentration from a Q Curie release is

$$TID = \frac{Q}{2 \sqrt{2\pi} DAR} \quad (J-18)$$

where A is the diffusion velocity. For A = 0.01 m/sec, and a 75-meter mixing depth, this becomes

$$TID = 0.27 Q/R \quad (J-19)$$

For 100% release from a 50-W heater, this gives

$$TID_1 = 400/R \text{ (Ci-sec/m}^3\text{)} \dots {}^{238}\text{Pu} \quad (J-20)$$

$$TID_2 = 3.4 \times 10^4/R \text{ (Ci-sec/m}^3\text{)} \dots {}^{147}\text{Pm} \quad (J-21)$$

This is illustrated in figure J-1.

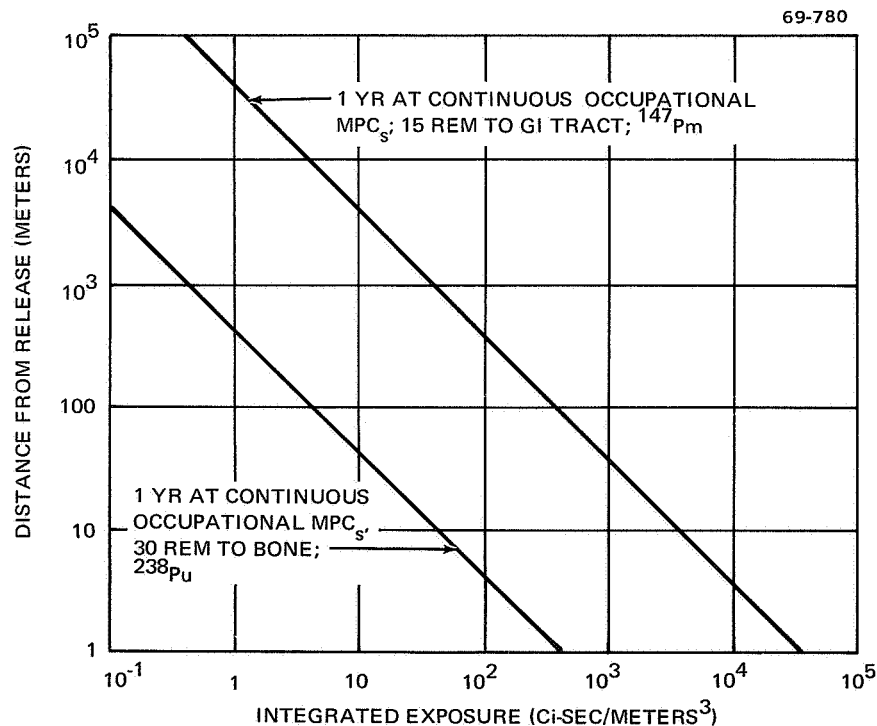


Figure J-1. Integrated Exposure from 100% Release to Sea Water of 50 W of Radioisotope



## REFERENCES

1. Holmen, R. E.: Saturn IB/S-IVB Lifetime Extension Study. MDAC Report DAC-56682, Jul. 1968.
2. Holmen, R. E.: WACS Electronic Subsystem Installation Study. MDAC Report DAC-56690, Sep. 1968.
3. Holmen, R. E.: Saturn V/S-IVB Stage Synchronous Orbit Capability Study. MDAC Vol. II Final Report, DAC-56584, Jul. 31, 1967.
4. Hoff, K. W., et al.: Radioisotope Source Safety Testing. ORNL-4092, May 1967.
5. Kite, F. D.; and Bader, B. E.: Pad-Abort Thermal Flux Model for Liquid Rocket Propellants. SC-RR-66-577, Nov. 1966.
6. DIN: 6300-300, SNAP 27 Safety Report; Vol 11, Accident Model Report. General Electric Co., Philadelphia, Pennsylvania, Jul. 1968.
7. SC-DC-65-1918, Study of the Chemical Integrity of Radioisotope Containment Materials in Launch Abort Environments. TRW Systems, Redondo Beach, California, Dec. 1965.
8. His, K.; and Van Valkenburg, E.: Solar Power Subsystems for Apollo Lunar Experiments Package. Final Report, Volume II Technical Report, BSR 2228, The Bendix Corporation, Jan. 1968.
9. Koelle, H. H.; ed.: Handbook of Astronautical Engineering. 1st edition. New York: McGraw-Hill Book Company, 1961. pp. 3-70, 3-71.
10. Jolley, C. E.; and Read, J. C.: The Effects of Space Environments on Insulation of Teflon TFE and FEP Resins. NP-13615, 1962.
11. Nuclear Reactor Chemistry. Second Conference, Oct. 10-12, 1961, pp. 28-29, TID-7622.
12. Bowen, P. H.; and Hickam, W. H.: Outgassing Characteristics of Dry Lubricant Materials in a Vacuum. Machine Design, Jul. 4, 1963, pp. 119-124.
13. Dahl, R. E.: Study of Reactor Graphite Combustion. Trans. Amer. Nucl. Soc. Vol. 5, No. 1, 1962. p 128.

14. Hove, J. E.; and Riley, W. C., eds.: *Ceramics for Advanced Technologies*. New York: John Wiley & Sons, Inc. 1965.
15. *Pyrolytic Graphite Engineering Handbook*. General Electric Metallurgical Production Department, Jul. 1963.
16. Adams, E. W.: *Analysis of Quartz and Teflon Shields for a Particular Reentry Mission*. Heat Transfer and Fluid Mechanics Institute, 1961.
17. Blair, G. R.: *Materials for Use in a Space Environment*. SAMPE 11th National Symposium and Exhibit, 1967. pp. 265-277.
18. Lyons, C. S.; and Lawson, D. D.: *Ablative Characteristics of Reinforced Plastics in Nozzles and Thrust Chambers for Varying Environments. Applications of Plastic Materials in Aerospace*. Chemical Engineering Progress Symposium Series, No. 40, Vol. 59, 1963.
19. Brennan, W.; Lum, D.; and Riley, M. W.: *High-Temperature Plastics*. New York: Reinhold Publishing Company, 1962.
20. Anon.: *Modern Plastics Encyclopedia for 1968*. Vol 45, No. 1A, Sep. 1967.
21. Anon.: *Space Environmental Effects on Materials and Components*. Vol. 1, Elastomers and Plastic Materials. Appendix B. Plastics. Army Missile Command, Redstone Arsenal. RSIC-150, Vol. 1, App. B. April 1, 1964.
22. Katz, I.; and Goldberg, J.: *Elevated Temperature Properties of Reinforced Plastics*. *Materials Methods*, Nov. 1956, pp. 130-133.
23. Jaffe, L. D.; and Rittenhouse, J. B.: *Behavior of Materials in Space Environments*. JPL-TR-32-150, 1961.
24. Greene, R. B. et al.: *Technical Report Reentry Systems Environmental Protection (RESEP) Task 4, Refractory Materials Development, Volumes I and II*, SAMSO-TR-68-54 (March, 1968) SECRET RD.
25. Timoshenko, S.; and WoinoswkyOKrieger, S.: *Theory of Plates and Shells*, McGraw-Hill Book Co., Inc., 1959.
26. Singer, F. E.: *Strength of Materials*, 2nd ed., Harper & Rowe Publications, 1962.
27. McClintock, F. A.; and Argon, A. S.: *Mechanical Behavior of Materials*. Addison-Wesley Publications, 1966.
28. Bickel, M. B.; and Ruiz, C.: *Pressure Vessel Design and Analysis*. MacMillan, 1967.
29. Easton, C. R.: *Design Considerations for Space Power Capsules Buried in Soil*. Douglas Paper 4699, Nov. 1967.

30. Robinson, R. A. et al.: Brayton-Cycle Radioisotope Heat Source Design Study, Phase 1 (Conceptual Design) Report. ORNL-TM-1691 Del. Aug. 1967.
31. Anon.: Nickel and Nickel Alloys. The International Nickel Co., Inc. 1947. p. D-27, D-29.
32. Uhlig, H. H., ed.: Corrosion Handbook. New York: John Wiley and Sons, Inc. 1948.
33. Young, R. S., ed.: Cobalt. New York: Reinhold Publishing Corporation, 1960.
34. Anon.: Argonne National Laboratory Annual Report for 1962, Metallurgy Division, ANL-6677 pp. 156-157.
35. Vallee, M.: Contribution a l'Etude de l'Oxydation du Cobalt et de Son Protoxyde dans l'Air aux Temperatures Eleves. Doctoral Thesis, CEA-R-2424, 1964. pp. 10-11.
36. Kubose, D., et al.: Measurement of Sea Water Corrosion of SNAP Container Alloys Using Radioactive Tracer Techniques. USNRDL-TR-1092, Oct. 10, 1966.
37. Kubose, D. A.; and Cordova, H. I.: Electrochemical Corrosion Studies of SNAP Container Materials. USNRDL-TR-1036, Jun. 7, 1966.
38. Mikhail, S. Z.; and Kubose, D. A.: Corrosion of Fuel Capsules by Sea Water. USNRDL (to be published).
39. Irradiation Effects on Reactor Structural Materials. Hanford Laboratories Quarterly Progress Report. HW-78760, Aug. 15, 1963.
40. Army Gas - Cooled Reactor Systems Program Quarterly Progress Report. IDO-28621, Feb. 15, 1964.
41. Kubose, D. A.; and Cordova, H. I.: Corrosion Studies of Haynes 25 Alloy in Sea Water Using Electrochemical Techniques. USNRDL-TR-67-64. May 16, 1967.
42. Irradiation Effects on Reactor Structural Materials. Hanford Laboratories Quarterly Progress Report. HW-77281, May 15, 1963.
43. Savannah River Laboratory Isotopic Power and Heat Sources Quarterly Progress Report. Part 1 - Cobalt 60. DP-1105-1. May, 1967.
44. Grove, G. R.: Data Sheets: Plutonium-238 Fuels, Mount Laboratory, Miamiaburg, Ohio, Jul. 1, 1967.
45. Matlack, G. M.; and Metz, G. F.: Radiation Characteristics of Pu<sup>238</sup>, LA-3696, Oct. 11, 1967.

46. Engle, R. L.; Greenborg, J.; and Hendrickson, M. M.: ISOSHLDA Computer Code for General Purpose Isotope Shielding Analysis. BNWL-236, Battelle-Northwest, Richland, Washington Jun. 1966.
47. Kite, F. D.; and Bodeo, D. E.: Pad-Abort Thermal Flux Model for Liquid Rocket Propellants. SC-PR-66-577, Nov. 1966.
48. Ottinger, R. S.; and Von Nice, L. J.: Second Quarterly Progress Report Booster Rocket Attitude Abort Program for Period Ending January 4, 1966. SC-CR-66-2015, Jan. 1966.
49. DIN: 6300-300, SNAP-27 Safety Report, Volume 11, Accident Model Document, Jul. 24, 1968.
50. SC-DC-65-1918, Study of the Chemical Integrity of Radioisotope Containment Materials in Launch Abort Environments. Summary Technical Report, Phase 1. (TRW Systems, Redondo Beach, Calif.) Dec. 1965.
51. SC-CR-2656, Study of the Chemical Integrity of Radioisotope Containment Materials in Launch Abort Environments. (TRW Systems, Redondo Beach, Calif.) Jun. 1967.
52. Anno, G. H.; and Schoutens, J. E.: Conceptual Probabilistic Methods of Analyzing Hazards of a Large (25kWt) Radioisotope Space Power Source, DAC-60944, Jan. 1968.
53. Williams, David C.: SC-RR-68-441, Vaporization of PuO<sub>2</sub> in a Launch Pad Abort Fireball, Aug. 1968.
54. Rohrman, C. A.: Characteristics of Radioisotope Heat Sources. BNWL-680, 1968.
55. Pardue, W. M.; Smith, R. A.; Houston, M. D.; Lozier, D. E.; Browning, M. F.; and Robereskin, M.: Summary Report on Development Program for Fabrication of Composite Fuel Form of <sup>238</sup>PuO<sub>2</sub>. BMI-1849.
56. Spiedel, Edward O.; Kizer, Donald E.; and Keller, Donald L.: Preparation and Properties of UO<sub>2</sub>, UN and UC Cermet Fuels. BMI-1842, Jun. 1968.
57. Space Electric Power Program Space Nuclear Systems Divisions, BNWL 986 C92G, Quarterly Progress Report, Oc., Nov., Dec., 1968, (Feb. 1969).
58. Plutonium 238 Space Electric Power Fuel Development Program, LA-4068-MS, Jul. 1 - Sep. 30, 1968.
59. Mound Laboratory Isotropic Power Fuels Programs, Oct. - Dec. 1968.
60. Plutonium-238 Space Electric Power Fuel Development Program, LA-4089-MS.

61. Hill, B. S.: Samaria-Tungsten Cermet Impact Tests. SC-DR-68-295. Jun. 1968.
62. Metals Handbook, Vol. 1, 8th Edition, 1961.
63. Materials Engineering, Materials Selection, 1968-69.
64. Rare Metals Handbook, Clifford A. Hampel, 1961.
65. Thermophysical Properties at High Temperature, Vol. 1, Thermophysical Properties Center, Purdue University, 1967.
66. Corrosion Handbook, Uhly, 1968.
67. Union Carbide Vendor Data, 1963.
68. Union Carbide Vendor Data, 1964.
69. Barsell, A. W.: Safety Analysis for a 4-W  $^{147}\text{Pm}$  Isomite Miniature Radioisotope Thermionic Converter. MDAC Report DAC-60771, Oct. 1968.
70. Barsell, A. W.; Montgomery, L. D.; and Arnold, J. E.: Thermal Behavior of SNAP Reactor Fuel Elements During Atmospheric Reentry, NAA-SR-11502 (Mar. 1965).
71. Stalder, J. R.; and Zurick, V. J.: Theoretical Aerodynamic Characteristics of Bodies in a Free-Molecule Flow Field. NACA TN-2423 (Jul. 1951).
72. Maslach, G. J.; and Schaaf, S. A.: Cylinder Drag in the Transition from Continuum to Free-Molecule Flow. The Physics of Fluids 6, No. 3, p.315 (Mar. 1963).
73. Maslach, G. J., et al.: Recent Experimental and Theoretical Extensions of Nearly Free Molecular Flow. Rarefied Gas Dynamics, Volume 1, p 433, Academic Press, New York, 1965
74. Coudeville, H., et al.: Drag Measurements in Slip and Transition Flow. Rarefied
75. Hoerner, S. F.: Fluid-Dynamic Drag. Published by the Author 1965.
76. Gowen, F. E.; and Perkins, E. W.: Drag of Circular Cylinders for a Wide Range of Reynolds Numbers and Mach Numbers. NACA TN 2960 Jun. 1953.
77. Delany, N. K.; and Sorenson, N. E.: Low Speed Drag of Cylinders of Various Shapes. NACA TN-3038, Nov. 1953.
78. Knudsen, J. G.; and Katz, D. L.: Fluid Dynamics and Heat Transfer. Engineering Research Bulletin 37, Univ. of Michigan, Ann Arbor, 1953.

79. Boison, J. C.; and Curtiss, H. A.: An Experimental Investigation of Blunt Body Stagnation Point Velocity Gradient. ARS Journal 29, Feb. 1959, p. 130.
80. Stoney, W. E. Jr.; and Swanson, A. G.: Heat Transfer Measured on a Flat-Face Cylinder in Free Flight at Mach Numbers up to 13.9. NACA RM-L-57 E 13 Jun. 1957.
81. Marks, L. S.; and Baumeister, T.: Mechanical Engineers Handbook, 11-82, McGraw-Hill Book Co., Sixth Edition, New York, 1958.
82. Masson, D. J.; Morris, D. N.; and Bloxsom, D. E.: Measurements of Spheres Drag from Hypersonic Continuum to Free-Molecule Flow. Reprint from Rarefied Gas Dynamics, Talbot, L., ed., Academic Press, 1961, pp. 643-666.
83. Elliott, R. D.: Methods for Predicting Aerodynamic Heating Rates to High-Velocity Bodies in the Upper Atmosphere. NAA-SR-11704, Jan. 1966.
84. Fay, J. A.; and Riddell, F. R.: Theory of Stagnation Point Heat Transfer in Dissociated Air. J. Aerospace Sciences 25, Feb. 1958, p. 73.
85. Detra, R. W.; and Hidalgo, H.: Generalized Heat Transfer Formulas and Graphs for Nose Cone Reentry into the Atmosphere. ARS Journal 31, Mar. 1961, p. 318.
86. SNAP-27 Safety Report. General Electric Missile and Space Div., DIN-6300-300, Jul. 1968.
87. Arnold, J. E.; and Barsell, A. W.: Experimental Investigation of the Thermochemical Behavior of SNAP Fuel Material in a Hyperthermal Wind Tunnel. NAA-SR-12082, Jun. 1967.
88. Barsell, A. W.; Montgomery, L. D.; and Arnold, J. E.: Thermal Behavior of SNAP Reactor Fuel Elements During Atmospheric Reentry. NAA-SR-11502, Mar. 1966.
89. Bartlett, E. P.: Effective Heat of Ablation of Graphite. AIAA Journal 2, Jan. 1964, p. 171.
90. Dray, B. J.: Thermal Analyzer Program (TAP) Users Manual--Fortran II Version. NAA-SR-TDR 11812, Jan. 1966.
91. Curry, D. M.: An Analysis of a Charring Ablation Thermal Protection System. NASA TN D-3150, Dec. 1965.
92. Wilson, R. G.: Thermophysical Properties of Six Charring Ablators from 140° to 700°K and Two Chars from 800° to 3000°K. NASA TN D-2991, Oct. 1965.
93. Adams, M. C.: Recent Advances in Ablation. ARSJ 29:625-632, 1959.



94. Bartlett, E. P.: Effective Heat of Ablation of Graphite. AIAAJ. 2:171-173, Jan. 1964.
95. Katsikas, C. J., et al.: Ablation Handbook: Entry Materials Data and Design. AFML-TR-66-262, Nov. 1966.
96. Spiegel, M. R.: Statistics. Schaum's Outline Series (Schaum Publishing Co., New York) 1961.
97. Sherwood, T. K.; and Reed, C. E.: Applied Mathematics in Chemical Engineering. (McGraw-Hill Book Co., Inc., New York) 1957.
98. Barsell, A. E.; Montgomery, L. D.; and Arnold, J. E.: Thermal Behavior of SNAP Reactor Fuel Elements During Atmospheric Reentry. NAA-SR-11502 (Apr. 1966).
99. Dixon, W. F.; and Massey, F. J. Jr.: Introduction to Statistical Analysis. (McGraw-Hill Book Co., Inc., New York) 1957.
100. Crow, E. L.; Davis, F. A.; and Maxfield, M.: Statistics Manual. (Dover Publications, Inc., New York) 1960.
101. National Bureau of Standards, Tables of Normal Probability Functions, Applied Math., Series 23 (U. S. Government Printing Office, Washington, D. C.) Jun. 5, 1953.
102. Willis, C. A.: The External Radiation Field Hazard from the Fall-out of Ablation Particles from SNAP Reactors. NAA SR MEMO 10774, Feb. 1965.
103. Machta, L.: Worldwide Radioactive Fallout from Nuclear Tests - Part I. Nuclear Safety, 4, 4, Jun. 1963, p. 103.
104. Machta, L.: Worldwide Radioactive Fallout from Nuclear Tests - Part II. Nuclear Safety, 5, 1, Fall, 1963, p. 95.
105. Knapp, H. A.: The Effect of Deposition Rate and Cumulative Soil Level on the Concentration of Strontium-90 in U. S. Milk and Food Supplies. TID-13945, Oct. 1961.
106. Dobry, T. J.: SNAP 9A Radioisotope - Fueled Generator, Final Safety Analysis for Transit Mission. MND-P-2775-2 (Secret RF), Mar. 1963.
107. Federal Radiation Council, Revised Fallout Estimates for 1964-1965 and Verification of the 1963 Predictions, FRC-6, Oct. 1964.
108. Hardy, E. P. Jr.; and Rivera, J.: Health and Safety Laboratory Fallout Program Quarterly Summary Report. HASL-158, Apr. 1965.
109. Machta, L.; List, R. J.; and Telegadas, K.: Updating the Radioactive Fallout Picture to 1965. Statement for the Public Hearings of the Joint Committee on Atomic Energy on FRC Protective Action Guides, Jun. 1965.

110. Pasquill, F.: Atmospheric Diffusion. D. Van Nostrand Company Ltd. London 1962.
111. Hilsmeier, W. F.; and Gifford, F. A. Jr.: Graphs for Estimating Atmospheric Dispersion. Atomic Energy Commission Report ORO 545, Jul. 1962.
112. Slad, D. H., Editor: Meteorology and Atomic Energy 1968. Atomic Energy Commission Report TID-24190. Jul. 1968.
113. Recommendations of the International Commission on Radiological Protection, Report of Committee II on Permissible Dose for Internal Radiation (1959). Pergamon Press. London, 1959.
114. Report of Committee II on Permissible Dose for Internal Radiation (1959), ICRP Publication 2. (Pergamon Press, London) 1959.
115. Recommendations of the International Commission on Radiological Protection (As Amended 1959 and Revised 1962), ICRP Publication 6 (Pergamon Press, London) 1964.
116. Radioactive Waste Disposal from Nuclear Powered Ships, NAS-NRC Publication 658, 1959.
117. Disposal of Low-Level Radioactive Waste into Pacific Coastal Waters, NAS-NRC Publication 985, 1962.
118. Prichard, D. W.: Environmental Factors Affecting the Disposal of Radioactive Waste Materials into Tidal Estuaries and Coastal Bodies of Water. Hearings Before the Special Subcommittee on Radiation of the Joint Committee on Atomic Energy (Government Printing Office, Washington, D. C.)
119. Newcombe, C. L., et al.: Evaluation of Radiation Hazards Associated with Operation of Nuclear-Powered Space Units at Pacific Missile Range. USNRDL-545, Feb. 1962.
120. Radioactive - Waste Disposal in the Ocean, U. S. National Bureau of Standards Handbook 58 (Government Printing Office, Washington, D. C.)
121. Redfield, A. C.; and Walford, L. A.: A Study of the Disposal of Chemical Waste at Sea. National Research Council Report 201, 1951.
122. Schaefer, M. B.: Some Fundamental Aspects of Marine Ecology in Relation to Radioactive Wastes. Health Physics, 6, 3/4, Oct. 1961. p. 97.
123. Pritchard, D. W.: Disposal of Radioactive Wastes in the Ocean. Health Physics, 6, 3/4, Oct. 1961. p. 103.
124. Aten, A. H. W. Jr.: Permissible Concentrations of Radionuclides in Sea Water. Health Physics, 6, 3/4, Oct. 1961. p. 114.
125. The Evaluation of Risks from Radiation, ICRP No. 8 (Pergamon, London) 1966.

## BIBLIOGRAPHY

1. Tetz and Wilson: Reference Behavior and Properties of Refractory Metals. Stanford University Press, 1965.
2. Defense Metals Information Center of Battelle Memorial Institute (DMIC) Report 133.
3. Refractory Metals and Alloys. Vol. II, Metallurgical Society Conference AIME Interscience Publication.
4. DMIC Report 189.
5. Westinghouse T-111 Data Sheets, 1963. (Vendor Data).
6. Reactor Materials Vol. 9, No. 4, Winter 1966-1967.
7. Rice, W. L. R.: TID 11295 (3rd edition) Nuclear Fuels and Materials Development. Jul. 1964.
8. Bartlett, E. S.; Schmidt, F. F.; Howe, J. A.; and Barth, V. D.: Review of Recent Developments Refractory Metals (Cb, Ta, Mo, W). (DMIC), Apr. 22, 1966.
9. Sawyer, T. C.; and Steigerwald, E. A.: Generation of Long Time Creep Data on Refractory Alloys at Elevated Temperature. Jul. 15, 1966. MAS-CR-72044.
10. Westinghouse Electric Corporation Revised Preliminary Data Tantalum Base Alloy T-111. Jan. 15, 1963 (Vendor data sheet).
11. ORNL 3992.
12. Chase <sup>R</sup>Rhenium-Molybdenum. Alloys Rhenium Bulletin No. 2 (Vendor data sheet).
13. Chase <sup>R</sup>Rhenium, Rhenium-Molybdenum, Rhenium-Tungsten Alloys (Vendor data sheet).
14. Ammon, R. L.; and Harrod, D. R.: Strengthening Effects in Ta-W-Hf Alloys. WANL SP-013, Jan. 15, 1966.
15. Stringer, J.: The Oxidation on Tantalum at High Temperatures: Geometrical Effect. Journal of Less Common Metals, 16, 1968, pp. 55-64.

16. Poco Graphite Data Sheets from Aerospace Corporation Reentry Materials Handbook. Jun. 1968.
17. Moon, D. P.; Simon, R. C.; and Favor, R. J.: The Elevated Temperature Properties of Selected-Super Alloys. Battelle Memorial Institute, Columbus Laboratories ASTM Data Series DS7-S1.
18. Raffo, Peter L.: NASA TND-456, Yielding and Fracture in Tungsten and Tungsten-Rhenium Alloys. Lewis Research Center, Cleveland, Ohio, May 1968.
19. Buzzard, Robert J.: High Temperature Creep-Rupture Properties of a Tungsten-Uranium Dioxide Cermet produced from Coated Particles. NASA TMS-1625, Aug. 1968.
20. Sawyer, T. C.; and Steigerwald, E. A.: NASA CR 1115. Generation of Long Time Creep Data of Refractory Alloys at Elevated Temperatures. Aug. 1968.

<p>DAC-63364</p> <p>National Aeronautics and Space Administration. RADIOISOTOPE HEATER DEVELOPMENT PROGRAM. M. W. Hulín June 1969</p> <p>A design study was conducted by the Donald W. Douglas Laboratories for NASA/MSC to develop a family of small radioisotope heaters (1- to 50-W) for use with manned spacecraft components that would meet mission times of 14 days to 5 years. It was determined that two heater sizes, 10- and 50-W, and two isotope fuels, promethia and plutonia, would meet the majority of the identified applications and mission requirements. The design provides high probability of fuel containment under all mission operations and environments.</p>	<p>I. M. W. Hulín II. DAC-63364</p> <p>NASA</p>
<p>DAC-63364</p> <p>National Aeronautics and Space Administration. RADIOISOTOPE HEATER DEVELOPMENT PROGRAM. M. W. Hulín June 1969</p> <p>A design study was conducted by the Donald W. Douglas Laboratories for NASA/MSC to develop a family of small radioisotope heaters (1- to 50-W) for use with manned spacecraft components that would meet mission times of 14 days to 5 years. It was determined that two heater sizes, 10- and 50-W, and two isotope fuels, promethia and plutonia, would meet the majority of the identified applications and mission requirements. The design provides high probability of fuel containment under all mission operations and environments.</p>	<p>I. M. W. Hulín II. DAC-63364</p> <p>NASA</p>

KEY WORDS

Radioisotope  
Nuclear  
Thermal heat  
Space  
Design  
Power  
Development